University of Natural Resources and Life Sciences, Vienna

Department of Food Science and Technology

Institute of Food Technology, Food Biotechnology Lab

Characterization and engineering of pyranose dehydrogenases for applications in carbohydrate conversions

PhD thesis

submitted by

DI Iris Krondorfer

Supervisor: Priv.-Doz. Dr. Clemens K. Peterbauer

Head of institute: Univ.-Prof. Dr. Dietmar Haltrich

Vienna, March 2014

BioToP Biomolecular Technology of Proteins

Abstract

Pyranose dehydrogenase (PDH), a fungal flavin-dependent oxidoreductase, catalyzes the oxidation of a broad variety of sugars substrates. The enzyme is unable to utilize dioxygen as an electron acceptor. Benzoquinones and complexed metal ions naturally present during lignocellulose degradation, the supposed biological function of PDH, are preferred. Like pyranose 2-oxidase and cellobiose dehydrogenase, also members of the glucose-methanol-choline (GMC) oxidoreductase family, PDH represents a promising biocatalyst which can be applied in sugar conversions, organic synthesis or electrochemistry. For this purpose, PDHs from *Agaricus meleagris*, *A. xanthoderma* and *A. campestris* were recombinantly expressed in the methylotrophic yeast *Pichia pastoris*, purified and characterized biochemically. Steady-state kinetic parameters and molecular properties were investigated using UV-Vis spectroscopy, SDS-PAGE and TCA precipitation. Batch lactose conversion experiments and HPLC analysis confirmed the suitability of the enzymes from *A. xanthoderma* and *A. campestris* for the production of lactobionic acid or 2-dehydrolactose, a key intermediate for the production of lactulose. The physiological electron acceptor of PDH is undesirable for an application in food technology, therefore site-saturation mutagenesis libraries of twelve amino acids in the active site of *A. meleagris* PDH were expressed in *Saccharomyces cerevisiae*. High-throughput screening resulted in one position altering oxygen reactivity. Mutant H103Y, produced in *P. pastoris*, showed a five-fold increase in oxygen reactivity. Although carrying a non-covalently linked FAD-cofactor in contrast to the wild-type, mutant H103Y was still catalytically active but to a lower degree. Stopped-flow experiments revealed that only the reductive half-reaction was negatively affected by the mutation. Thermal and chemical denaturation experiments were performed and confirmed the lower stability caused by the non-covalent FAD linkage. This semi-rational approach provides a scaffold for further engineering of PDH towards a highly competent biocatalyst.

Kurzfassung

Das Flavoenzym Pyranose Dehydrogenase (PDH) wird extrazellulär von ligninolytischen Basidiomyceten der Familie *Agaricaceae* produziert und katalysiert die Oxidation einer Vielfalt an Zuckern. Als Elektronenakzeptor dienen Benzochinone oder komplexierte Metallionen, das Enzym reagiert nicht oder nur sehr langsam mit Sauerstoff. Wie Pyranose 2-Oxidase und Cellobiose Dehydrogenase, weitere Mitglieder der Glukose-Methanol-Cholin (GMC) Oxidoreduktase Flavoproteinfamilie, ist auch PDH ein vielversprechender Kandidat für den industriellen Einsatz in Zuckerumwandlungen, der organischen Synthese oder in Biobrennstoffzellen und -sensoren. PDHs aus *Agaricus meleagris*, *A. xanthoderma* und *A. campestris* wurden im Zuge dieser Arbeit rekombinant in der methylotrophen Hefe *Pichia pastoris* exprimiert, aufgereinigt und biochemisch charakterisiert. Mittels UV-Vis Spektroskopie, SDS-PAGE und TCA-Fällung wurden die Steady-state Kinetik und molekulare Eigenschaften der Proteine untersucht. Laktose-Umsetzungen im Labormaßstab zeigten die Eignung von PDH aus *A. campestris* und *A. xanthoderma* für die Produktion von Laktobionsäure und 2-Dehydrolaktose, einem wichtigen Intermediat für die Synthese von Laktulose. Da die physiologischen Elektronenakzeptoren von PDH nicht geeignet sind für den Einsatz in der Lebensmittelindustrie, wurden zwölf Site-saturation Mutantenbibliotheken von *A. meleagris* PDH in *Saccharomyces cerevisiae* exprimiert um Varianten mit erhöhter Sauerstoffreaktivität zu finden. Im Zuge des Screenings zeigte sich dass eine Variante erhöhte Sauerstoffaktivität aufwies, Mutante H103Y wurde in größerem Maßstab in *P. pastoris* exprimiert und gereinigt. Die Charakterisierung ergab eine fünffache Steigerung der Sauerstoffreaktivität, trotz nicht-kovalent gebundenem FAD war die Mutante katalytisch aktiv, wenn auch in schwächerem Ausmaß. Stopped-flow experimente zeigten dass ausschließlich die reduktive Halbreaktion von der Mutation negativ beeinflusst wurde. Die Stabilität der Mutante gegenüber thermischer und chemischer Denaturierung war im Vergleich zum Wildtyp verringert. Der angewandte Engineering-Ansatz bildet eine Grundlage für weitere Verbesserungen von PDH für den Einsatz in der Lebensmittelindustrie.

Contents

Chapter 1. Introduction 1

Literature overview 3

Summary of research 19

Chapter 2. Characterization of pyranose dehydrogenases 25

Pyranose dehydrogenase from *Agaricus campestris* and *Agaricus xanthoderma*: Characterization and applications in carbohydrate conversions 27

Simple and efficient expression of *Agaricus meleagris* pyranose dehydrogenase in *Pichia pastoris* 51

The 1.6 Å crystal structure of pyranose dehydrogenase from *Agaricus meleagris* rationalizes substrate specificity and reveals a flavin intermediate 63

Chapter 3. Engineering of *Agaricus meleagris* pyranose dehydrogenase 79

Engineering of pyranose dehydrogenase for increased oxygen reactivity 81

Agaricus meleagris pyranose dehydrogenase: Influence of covalent FAD linkage on catalysis and stability 95

Chapter 4. Characterization and engineering of GMC oxidoreductases 131

Semi-rational engineering of cellobiose dehydrogenase for improved hydrogen peroxide production 133

Convenient microtiter-plate-based activity assays for flavin-dependent oxidoreductases 145

Acknowledgements 157

Chapter 1. Introduction

Literature overview

Flavoproteins

Flavoproteins are colourful enzymes that carry a FMN (flavin mononucleotide) or FAD (flavin adenine dinucleotide) as a prosthetic group. These enzymes catalyze a broad variety of biochemical reactions and are involved in diverse biological processes (Figure 1). The majority of flavin-dependent enzymes are oxidoreductases but around 10% catalyze non-redox reactions (transferases, lyases, isomerases and ligases) (Macheroux et al, 2011).

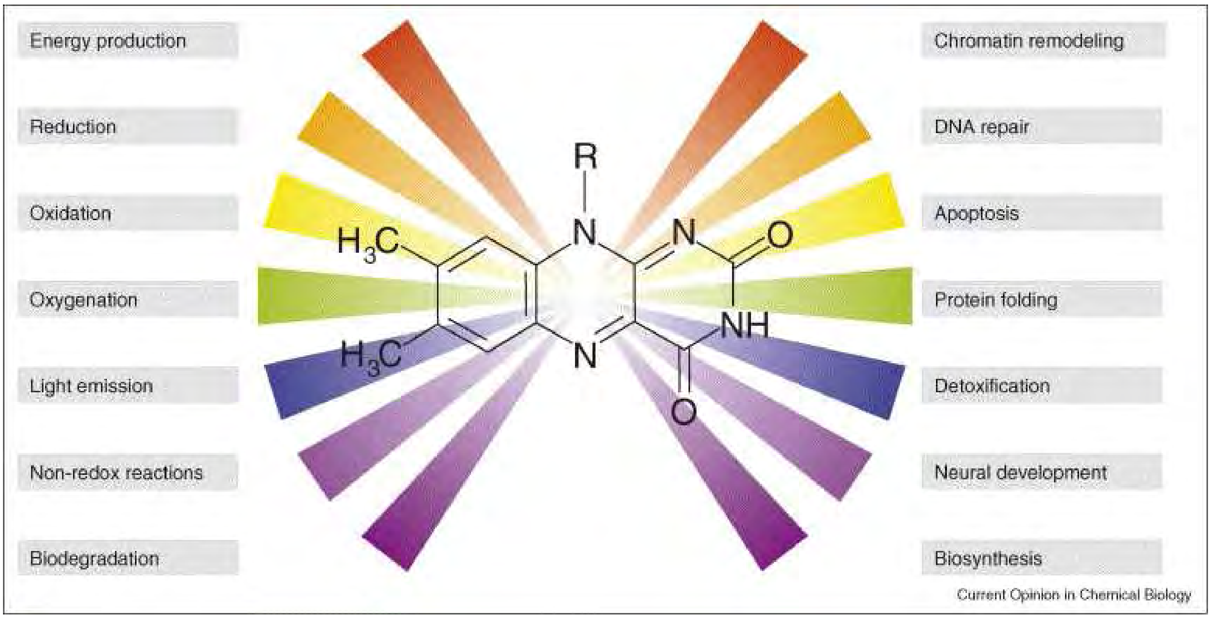
Energy production
Reduction
Oxidation
Oxygenation
Light emission
Non-redox reactions
Biodegradation
Chromatin remodeling
DNA repair
Apoptosis
Protein folding
Detoxification
Neural development
Biosynthesis
R
N
N
O
NH
N
O
H_3C
H_3C
Current Opinion in Chemical Biology

Figure 1: Biological functions of flavoenzymes (Joosten & van Berkel, 2007).

Due to the selectivity, efficiency and controllability of their reactions, flavoproteins are regarded as attractive biocatalysts applied in food, pharmaceutical and fine-chemical industries (Joosten & van Berkel, 2007; Walsh & Wencewicz, 2013). The cofactor FMN consists of a riboflavin moiety (vitamin B_2) and a phosphate group, FAD consists of a riboflavin bound to an ADP (adenosine diphosphate) molecule (Figure 2). The flavin isoalloxazine ring system is the redox-active part of the molecule, the side chain (e.g. the ADP moiety) is not involved in catalysis but serves as an anchor of the molecule to the active site.

The reactions of flavoprotein oxidoreductases can be divided in two half-reactions. In the reductive half-reaction, the FAD isoalloxazine is reduced by the electron donor substrate. In the oxidative half-reaction, the reduced flavin is re-oxidized by an electron acceptor. The reoxidation can occur either by two one-electron transfers or one two-electron transfer (Ghisla & Massey, 1989). Depending on the enzyme, the product is released before the electron acceptor reacts with the free enzyme (ping-pong mechanism) or the electron acceptor reacts with the enzyme-product complex (ternary complex mechanism) (Mattevi, 2006).

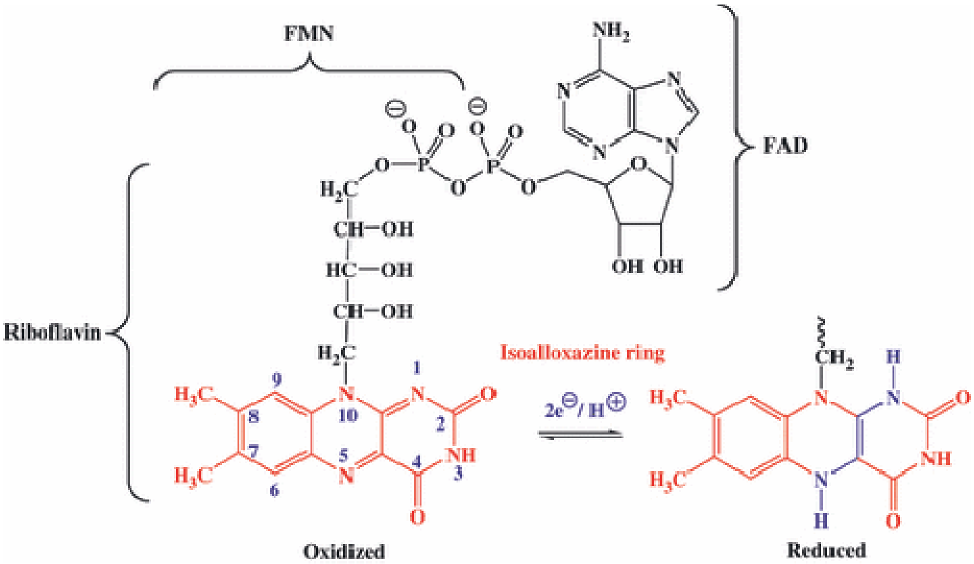

Figure 2: Structure of riboflavin, FMN and FAD (Macheroux et al, 2011).

In the majority of flavoproteins the cofactor is non-covalently linked but an estimated 10 % of all flavoproteins possess a covalent linkage of the cofactor to the polypeptide chain via a histidine, tyrosine, cysteine or threonine. The covalent bond is formed via the C-8 methyl group and/or the C-6 of the isoalloxazine or via a phosphoester bond with a phosphate group. Even a double-covalent linkage (8α-histidyl-6-S-cysteinyl) was discovered. The covalent binding is believed to increase the redox potential and therefore the oxidation power of the enzyme, contribute to protein stability, circumvent unwanted reactions of the cofactor and to enhance the lifetime of the enzyme (Heuts et al, 2009). Incorporation of the cofactor was found to occur via an auto-catalytic process without the aid of specific enzymes (Hassan-Abdallah et al, 2005; Jin et al, 2008).

GMC (glucose-methanol-choline) family of flavoproteins

This family of flavoprotein oxidoreductases, named after three members, includes proteins that share conserved sequence patterns but catalyze quite diverse reactions and are widespread among prokaryotic and eukaryotic organisms (Cavener, 1992). All members with resolved crystal structure have a PHBH (*p*-hydroxybenzoate hydroxylase)-like fold in common and consist of a flavin-binding domain with an ADP-binding βαβ-motif (Rossman fold) and a substrate-binding domain. The latter is not as conserved as the flavin-binding domain, possibly due to the diverse substrate specificity of GMC oxidoreductases ranging from monosaccharides to cholesterol (Kiess et al, 1998; Mattevi, 1998; Zámocký et al, 2004). Members of the GMC family that use sugars as substrate include glucose oxidase (GOx, EC 1.1.3.4), pyranose 2-oxidase (POx, EC 1.1.3.10), the flavodehydrogenase-domain of cellobiose dehydrogenase (CDH, EC 1.1.99.18) and pyranose dehydrogenase (PDH, EC 1.1.99.29) (Peterbauer & Volc, 2010). Three of them will be introduced in more detail.

Pyranose dehydrogenase (PDH)

Pyranose dehydrogenase is a monomeric extracellular glycoprotein of around 75 kDa that carries a covalently bound (8α-N3-histidyl) FAD cofactor (Figure 3) (Tan et al, 2013). PDH was isolated from several members of the family *Agaricaceae* including *Agaricus bisporus, Macrolepiota rhacodes*, *A. xanthoderma*, *A. meleagris* and *A. campestris*, the enzyme generally seems to be limited to litter-decomposing basidiomycetes. As a dehydrogenase, PDH is unable to use dioxygen as an electron acceptor, (organo)metal ions and substituted quinones are preferred (Kujawa et al, 2007; Staudigl et al, 2013; Sygmund et al, 2008; Volc et al, 2001; Volc et al, 1997). For this reason the proposed biological function is a role in lignocellulose degradation by reducing quinone or radical intermediates, or a participation in Fenton's reactions, but the true biological function remains unknown (Giffhorn, 2000; Volc et al, 1985).

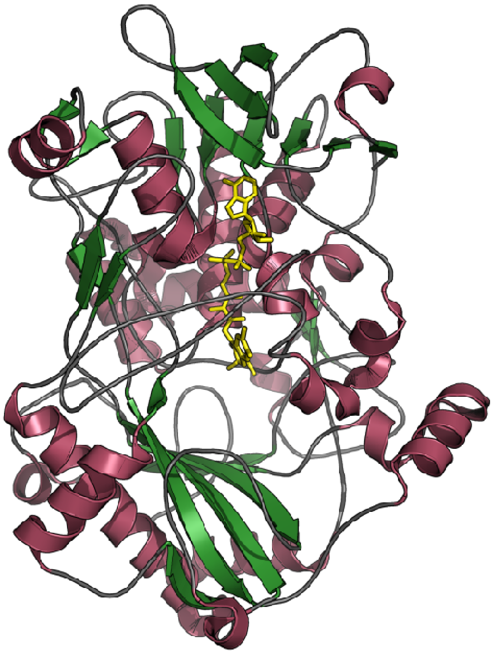

Figure 3: Crystal structure of PDH (Tan et al, 2013). The image was created using PyMol (PDB code 4H7U).

PDH is able to oxidize free, non-phosphorylated mono-, di- and oligosaccharides in pyranose form and glycosides to the corresponding dehydro- and didehydrosugars, the regioselectivity and substrate specificity depend on the source of the enzyme and the conditions of the reaction (Figure 4). Oxidations at C-1, C-2, C-3, C-1,2, C-2,3 and C-3,4 have been observed, double-oxidation occurs when the first oxidation step is nearly complete under excess of electron acceptor (Peterbauer & Volc, 2010; Sedmera et al, 2006).

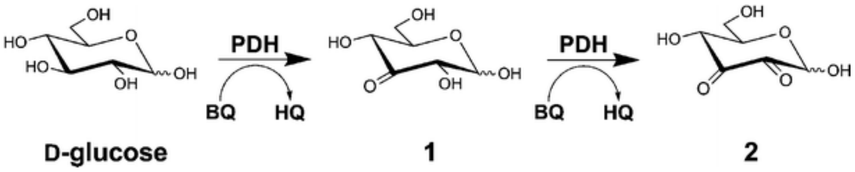

Figure 4: Oxidation of D-glucose to 3-dehydro-D-glucose (1) and 2,3-didehydro-D-glucose (2) and reduction of the electron acceptor 1,4-benzoquinone (BQ) to the hydroquinone (HQ) by PDH from *Macrolepiota rhacodes* (Peterbauer & Volc, 2010; Volc et al, 2001).

Due to the broad substrate spectrum, PDH can be regarded as a versatile biocatalyst for diverse industrial applications. Cheese-whey, the waste-product of cheese manufacturing, contains high amounts of lactose. Tons of whey are discarded each year as effluent and have become an environmental issue, therefore also biotechnological approaches for the valorisation of this by-product are of major importance (González Siso, 1996). PDH from *A. campestris* almost exclusively oxidizes lactose at C-1, the hydrolysis product of the resulting lactobiono-1,5-lactone, lactobionic acid, is used in the cosmetic-, food- and pharmaceutical industry (Gutiérrez et al, 2012). The C-2 oxidation product, 2-dehydrolactose, formed amongst others by PDH from *A. xanthoderma* and *A. meleagris*, represents a key intermediate for the production of lactulose, a prebiotic carbohydrate used against obstipation and hepatic encephalopathy (Schuster-Wolff-Bühring et al, 2010; Staudigl et al, 2013).

The intermediate for the synthesis of the non-cariogenic, prebiotic sweetener D-tagatose, 2-dehydro-D-galactose, can be produced by *A. meleagris* and *A. bisporus* PDH which have a higher affinity for the substrate D-galactose than POx (Sygmund et al, 2008; Volc et al, 1998). In spite of the broad substrate specificity and high affinity for several substrates, one disadvantage of PDH is the utilization of quinones or metal ions as electron acceptor. An application in the (food) industry would lead to high cost and effort in redox mediator regeneration and rigorous product purification. For this reason, O_2 would be a more favourable electron acceptor.

The utilization in biofuel cells and biosensors represents another possible application of PDH. A biofuel cell directly transforms chemical into electrical energy using enzymatic catalysis (Bullen et al, 2006). By wiring PDH with the help of osmium redox polymers to graphite electrodes, amperometric biosensors for the detection of sugars or biofuel cell anodes can be created (Tasca et al, 2007; Zafar et al, 2010). The utilization of the deglycosylated enzyme was shown to improve the electron transfer and current output (Killyéni et al, 2013; Yakovleva et al, 2012). In biofuel cells, *A. meleagris* PDH can be utilized as a bioanode, also in combination with *Myriococcum thermophilum* CDH or the flavodehydrogenase domain of *Corynascus thermophiles* CDH, increasing the output to six electrons from one molecule of D-glucose due to the different oxidation regioselectivity of PDH and CDH (Shao et al, 2013; Tasca et al, 2010). A successful combination with *Glomerella cingulata* glucose dehydrogenase has also been reported (Zafar et al, 2013).

Pyranose 2-oxidase (POx)

POx is a homotetrametric flavoenzyme of 270 kDa carrying a covalently (8α-N3-histidyl) bound FAD cofactor per subunit. The enzyme is presumable intracellularly and occurs in many lignocellulose-degrading basidiomycetes. Its proposed biological function is a participation in lignin degradation by providing hydrogen peroxide (H_2O_2) (Daniel et al, 1994; Danneel et al, 1992; Hallberg et al, 2004; Volc et al, 1985). Interestingly, none of the 76 strains of lignocellulose-degrading basidiomycete fungi screened by Volc and coworkers exhibited simultaneous POx and PDH activity. PDH activity was detected in mainly litter-degrading fungi whereas POx could be found in white-rot fungi like *Trametes sp.* or *Phanerochaete sp.* (Volc et al, 2001).

The reaction catalyzed by POx is the oxidation of aldopyranoses to the corresponding 2-ketoaldose (dehydroaldose), the C-3 position is oxidized only in rare cases. The preferred substrate is D-glucose, also D-galactose, L-arabinose and D-xylose are oxidized but with substantially lower efficiency. Molecular oxygen acts as the electron acceptor resulting in the production of H_2O_2 (Freimund et al, 1998; Kujawa et al, 2006). The high regioselectivity and rather narrow substrate specificity make POx especially interesting for certain industrial applications. The production of rare sugars is one example, 2-keto-D-glucose and 2-keto-D-galactose can be used for the production of D-fructose and D-tagatose in the so-called Cetus process, the formation of by-products can be avoided by using POx (Haltrich et al, 1998; Leitner et al, 1998). Biosensors for the determination of sugars or biofuel cells are other fields of application where the high selectivity of POx is an advantage (Tasca et al, 2007). In this context, the formation of H_2O_2 is detrimental for the enzyme and the redox polymer, therefore a POx with reduced oxygen reactivity would be of great interest for these applications.

Cellobiose dehydrogenase (CDH)

CDH is a monomeric, glycosylated protein of 90-100 kDa which consists of two domains: The catalytically active flavodehydrogenase domain with a non-covalently bound FAD cofactor and a cytochrome domain which contains a heme *b* type as cofactor. These two domains are connected via a flexible polypeptide linker (Cameron & Aust, 2001). CDH is produced extracellularly by white-rot, brown-rot, phytopathogenic and saprophytic basidomycete and ascomycete fungi. Similar to PDH, a role in lignocellulose breakdown and a participation in a Fenton-type reaction are assumed as the physiological functions of CDH (Zamocky et al, 2006). Recently an interaction of CDH with copper-dependent polysaccharide monooxygenases (PMOs) involved in the degradation of cellulose was proposed (Phillips et al, 2011; Sygmund et al, 2012).

The best substrates for CDH are cellobiose and lactose, which are oxidized at the anomeric C-1 to the corresponding lactones and in aqueous solution hydrolyzed to the carboxylic acid. D-glucose or other monosaccharides are rather poor substrates for CDH. Suitable one- or two-electron acceptors are 2,6-dichloroindophenol (DCIP), 1,4-benzoquinone and other (substituted) quinones, complexed metal ions or oxygen, this half-reaction usually takes place at the dehydrogenase domain. The heme-domain can interact with cytochrome c and other one-electron acceptors (Zamocky et al, 2006).

CDH is one of the rare oxidoreductases where a direct electron transfer (DET) is possible between the active site and an electrode surface due to the electron-transferring cytochrome domain. The successful application of CDH in biosensors for the detection of several analytes like lactose, glucose, noradrenalin or catechol or in biofuel cells (as mentioned above also in combination with PDH) was studied extensively (Ludwig et al, 2010; Ludwig et al, 2013). CDH is also suitable for the production of lactobionic acid (Ludwig et al, 2004) or for the production of H_2O_2 in (cotton) bleaching. The latter could replace the conventional method using H_2O_2 and sodium hypochlorite (NaOCl), which is problematic in terms of environmental issues (Pricelius et al, 2009; Pricelius et al, 2011). In this thesis, the rather low oxygen reactivity of CDH was increased for an application in the textile- or paper and pulp industry by means of semi-rational engineering approaches (Sygmund et al, 2013).

Oxygen reactivity in flavoproteins

Oxygen reactivity of flavoproteins is the matter of intensive research but up to date no clear guideline or structural determinant was found (Mattevi, 2006). The supposed molecular mechanism of the oxidative half reaction in flavoprotein oxidases and monooxygenases is illustrated in Figure 5. In the first electron transfer step, a caged radical pair of O_2^- (superoxide) and flavin semiquinone is formed. In oxidases, a subsequent second electron transfer results in the oxidized flavin and hydrogen peroxide. Monooxygenases form a covalent C(4a)-(hydro)peroxyflavin intermediate preceding the catalyzed monoxygenation reaction, the insertion of an oxygen atom into the substrate (Chaiyen et al, 2012). Several oxidases, like POx, are also capable of stabilizing such a covalent intermediate (Sucharitakul et al, 2008).

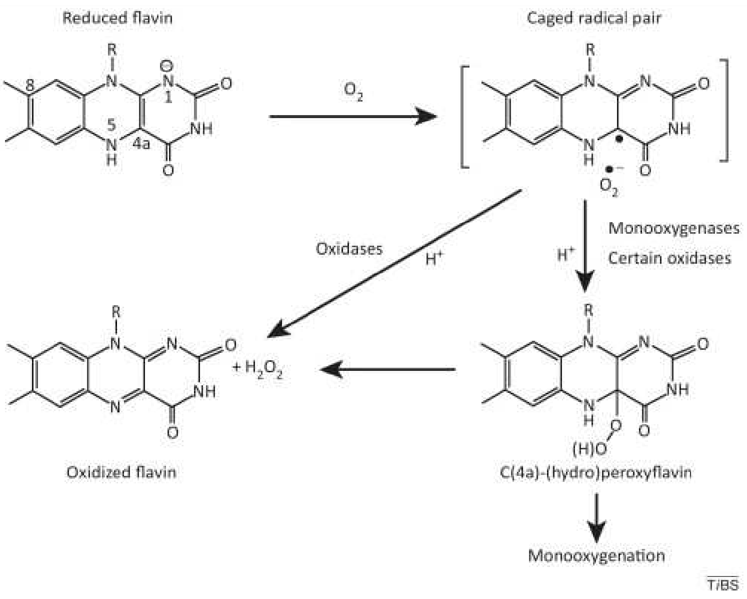
Reduced flavin
Caged radical pair
O2
Oxidases
H+
H+
Monooxygenases
Certain oxidases
+ H2O2
Oxidized flavin
C(4a)-(hydro)peroxyflavin
Monooxygenation
TiBS

Figure 5: Reaction of the reduced flavin with oxygen (Chaiyen et al, 2012).

Several concepts emerged over the last decades about factors determining oxygen reactivity. The exchange of an active site alanine to a glycine in L-galactono-γ-lactone dehydrogenase substantially increased oxygen reactivity, leading to the conclusion that the former, bulkier residue blocked the access of dioxygen to the active site (Leferink et al, 2009). In aryl-alcohol oxidase, phenylalanine 501 is forming a bottleneck in a narrow channel that was identified to guide O_2 to the active site. Surprisingly, mutant F501A showed strongly reduced oxygen reactivity whereas the replacement by a tryptophan resulted in slightly increased oxygen reactivity. The authors supposed that a correct distance of O_2 from the flavin C(4a) was important in this context (Hernández-Ortega et al, 2011). A positive charge in the active site of flavoproteins (a histidine, lysine or the positively charged substrate) seems to influence oxygen reactivity by electrostatically stabilizing the first, rate limiting electron transfer step in glucose oxidase, monomeric sarcosine oxidase, fructosamine oxidase and choline oxidase. In summary, all these findings are often only true for the single case and have to be viewed with care (Gadda, 2012).

Protein engineering

When the number of available X-ray structures of enzymes was slowly growing and the principles of enzymatic catalysis were known, the demand for a technique to elucidate the structure-function relationship emerged. In the early 1980s, site-directed mutagenesis, the systematic exchange of an amino acid in a protein, was reported for the first time and the new field of protein engineering was born (Brannigan & Wilkinson, 2002; Dalbadie-McFarland et al, 1982; Winter et al, 1982). The knowledge gained in mutagenesis studies was used for the design of biocatalysts with desired properties such as higher thermo- or pH-stability, altered substrate specificity or activity in non-physiological environments (Bornscheuer & Pohl, 2001; Brannigan & Wilkinson, 2002). As it is rarely possible to predict the effects of certain mutations, techniques offering a broader variety of more randomly introduced mutations were developed. Directed evolution mimics natural evolution in the lab by selecting a variant with a desired property from a large pool of variants. Variation is generated by random mutagenesis of the whole gene encoding the enzyme or by recombination of gene fragments (Bornscheuer & Pohl, 2001; Tao & Cornish, 2002). For this mutagenesis technique, in-depth understanding of structure and function is not required. Its main limitation lies in the requirement of a high-throughput screening protocol due to the very large library size (Figure 6).

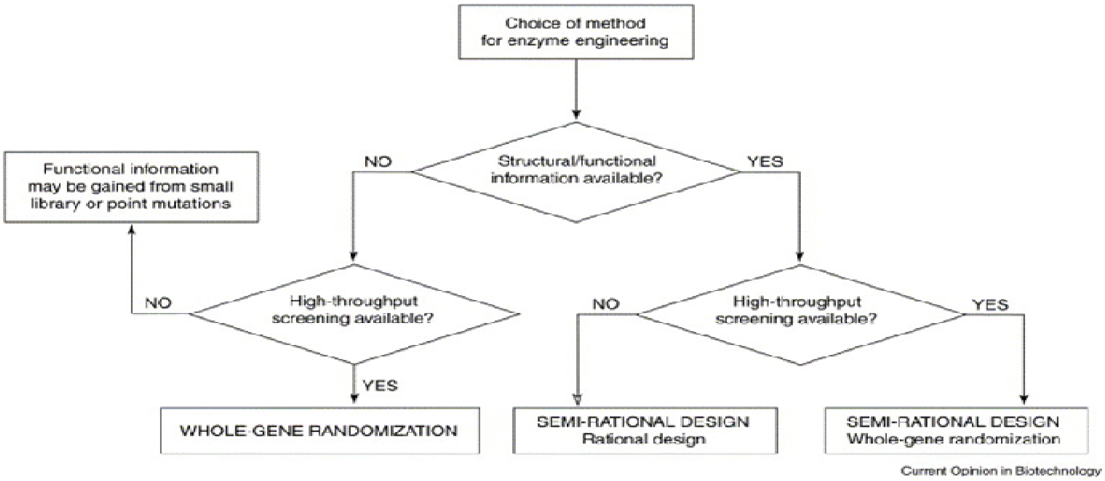
Choice of method for enzyme engineering
Structural/functional information available?
NO
YES
Functional information may be gained from small library or point mutations
NO
High-throughput screening available?
YES
NO
High-throughput screening available?
YES
WHOLE GENE RANDOMIZATION
SEMI-RATIONAL DESIGN Rational design
SEMI-RATIONAL DESIGN Whole-gene randomization
Current Opinion in Biotechnology

Figure 6: Criteria for the choice of the enzyme engineering method (Chica et al, 2005).

A method that combines the advantages of both rational design and directed evolution is site-saturation mutagenesis. This semi-rational approach is based on the exchange of selected amino acids mostly in the active site of an enzyme with all other 19 proteinogenic amino acids to create libraries of variants. The target area of the mutation is chosen based on the structure of the enzyme and/or computational calculations, overcoming the limitation of mutations in parts of the enzyme without any effect. Compared to directed evolution, the library size is smaller and therefore the screening effort on a tolerable level (Chica et al, 2005; Lutz, 2010).

References

Bornscheuer UT, Pohl M (2001) Improved biocatalysts by directed evolution and rational protein design. *Current Opinion in Chemical Biology* **5:** 137-143

Brannigan JA, Wilkinson AJ (2002) Protein engineering 20 years on. *Nature Reviews Molecular Cell Biology* **3:** 964-970

Bullen RA, Arnot TC, Lakeman JB, Walsh FC (2006) Biofuel cells and their development. *Biosens Bioelectron* **21:** 2015-2045

Cameron MD, Aust SD (2001) Cellobiose dehydrogenase - An extracellular fungal flavocytochrome. *Enzyme and Microbial Technology* **28:** 129-138

Cavener DR (1992) GMC oxidoreductases: A newly defined family of homologous proteins with diverse catalytic activities. *Journal of Molecular Biology* **223:** 811-814

Chaiyen P, Fraaije MW, Mattevi A (2012) The enigmatic reaction of flavins with oxygen. *Trends in Biochemical Sciences* **37:** 373-380

Chica RA, Doucet N, Pelletier JN (2005) Semi-rational approaches to engineering enzyme activity: Combining the benefits of directed evolution and rational design. *Current Opinion in Biotechnology* **16:** 378-384

Dalbadie-McFarland G, Cohen LW, Riggs AD, Morin C, Itakura K, Richards JH (1982) Oligonucleotide-directed mutagenesis as a general and powerful method for studies of protein function. *Proceedings of the National Academy of Sciences of the United States of America* **79:** 6409-6413

Daniel G, Volc J, Kubatova E (1994) Pyranose oxidase, a major source of H2O2 during wood degradation by Phanerochaete chrysosporium, trametes versicolor, and Oudemansiella mucida. *Applied and Environmental Microbiology* **60:** 2524-2532

Danneel HJ, Ullrich M, Giffhorn F (1992) Goal-oriented screening method for carbohydrate oxidases produced by filamentous fungi. *Enzyme and Microbial Technology* **14:** 898-903

Freimund S, Huwig A, Giffhorn F, Köpper S (1998) Rare keto-aldoses from enzymatic oxidation: Substrates and oxidation products of pyranose 2-oxidase. *Chemistry - A European Journal* **4:** 2442-2455

Gadda G (2012) Oxygen activation in flavoprotein oxidases: The importance of being positive. *Biochemistry* **51:** 2662-2669

Ghisla S, Massey V (1989) Mechanisms of flavoprotein-catalyzed reactions. *European Journal of Biochemistry* **181:** 1-17

Giffhorn F (2000) Fungal pyranose oxidases: Occurrence, properties and biotechnical applications in carbohydrate chemistry. *Applied Microbiology and Biotechnology* **54:** 727-740

González Siso MI (1996) The biotechnological utilization of cheese whey: A review. *Bioresource Technology* **57:** 1-11

Gutiérrez LF, Hamoudi S, Belkacemi K (2012) Lactobionic acid: A high value-added lactose derivative for food and pharmaceutical applications. *International Dairy Journal* **26:** 103-111

Hallberg BM, Leitner C, Haltrich D, Divne C (2004) Crystal structure of the 270 kDa homotetrameric lignin-degrading enzyme pyranose 2-oxidase. *Journal of Molecular Biology* **341:** 781-796

Haltrich D, Leitner C, Neuhauser W, Nidetzky B, Kulbe KD, Volc J (1998) A convenient enzymatic procedure for the production of aldose-free D-tagatose. *Ann N Y Acad Sci* **864:** 295-299

Hassan-Abdallah A, Bruckner RC, Zhao G, Jorns MS (2005) Biosynthesis of covalently bound flavin: Isolation and in vitro flavinylation of the monomeric sarcosine oxidase apoprotein. *Biochemistry* **44:** 6452-6462

Hernández-Ortega A, Lucas F, Ferreira P, Medina M, Guallar V, Martínez AT (2011) Modulating O 2 reactivity in a fungal flavoenzyme: Involvement of aryl-alcohol oxidase Phe-501 contiguous to catalytic histidine. *Journal of Biological Chemistry* **286:** 41105-41114

Heuts DPHM, Scrutton NS, McIntire WS, Fraaije MW (2009) What's in a covalent bond?: On the role and formation of covalently bound flavin cofactors. *FEBS Journal* **276:** 3405-3427

Jin J, Mazon H, Van Den Heuvel RHT, Heck AJ, Janssen DB, Fraaije MW (2008) Covalent flavinylation of vanillyl-alcohol oxidase is an autocatalytic process. *FEBS Journal* **275:** 5191-5200

Joosten V, van Berkel WJ (2007) Flavoenzymes. *Current Opinion in Chemical Biology* **11:** 195-202

Kiess M, Hecht HJ, Kalisz HM (1998) Glucose oxidase from Penicillium amagasakiense Primary structure and comparison with other glucose-methanol-choline (GMC) oxidoreductases. *European Journal of Biochemistry* **252:** 90-99

Killyéni A, Yakovleva ME, MacAodha D, Conghaile PO, Gonaus C, Ortiz R, Leech D, Popescu IC, Peterbauer CK, Gorton L (2013) Effect of deglycosylation on the mediated electrocatalytic activity of recombinantly expressed Agaricus meleagris pyranose dehydrogenase wired by osmium redox polymer. *Electrochimica Acta* (in press)

Kujawa M, Ebner H, Leitner C, Hallberg BM, Prongjit M, Sucharitakul J, Ludwig R, Rudsander U, Peterbauer C, Chaiyen P, Haltrich D, Divne C (2006) Structural basis for substrate binding and regioselective oxidation of monosaccharides at C3 by pyranose 2-oxidase. *Journal of Biological Chemistry* **281:** 35104-35115

Kujawa M, Volc J, Halada P, Sedmera P, Divne C, Sygmund C, Leitner C, Peterbauer C, Haltrich D (2007) Properties of pyranose dehydrogenase purified from the litter-degrading fungus Agaricus xanthoderma. *FEBS J* **274:** 879-894

Leferink NGH, Fraaije MW, Joosten HJ, Schaap PJ, Mattevi A, van Berkel WJH (2009) Identification of a gatekeeper residue that prevents dehydrogenases from acting as oxidases. *Journal of Biological Chemistry* **284:** 4392-4397

Leitner C, Neuhauser W, Volc J, Kulbe KD, Nidetzky B, Haltrich D (1998) The Cetus process revisited: A novel enzymatic alternative for the production of aldose-free D-fructose. *Biocatalysis and Biotransformation* **16:** 365-382

Ludwig R, Harreither W, Tasca F, Gorton L (2010) Cellobiose dehydrogenase: A versatile catalyst for electrochemical applications. *ChemPhysChem* **11:** 2674-2697

Ludwig R, Ortiz R, Schulz C, Harreither W, Sygmund C, Gorton L (2013) Cellobiose dehydrogenase modified electrodes: Advances by materials science and biochemical engineering. *Analytical and Bioanalytical Chemistry* **405:** 3637-3658

Ludwig R, Ozga M, Zámocky M, Peterbauer C, Kulbe KD, Haltrich D (2004) Continuous enzymatic regeneration of electron acceptors used by flavoenzymes: Cellobiose dehydrogenase-catalyzed production of labtobionic acid as an example. *Biocatalysis and Biotransformation* **22:** 97-104

Lutz S (2010) Beyond directed evolution-semi-rational protein engineering and design. *Current Opinion in Biotechnology* **21:** 734-743

Macheroux P, Kappes B, Ealick SE (2011) Flavogenomics - A genomic and structural view of flavin-dependent proteins. *FEBS Journal* **278:** 2625-2634

Mattevi A (1998) The PHBH fold: Not only flavoenzymes. *Biophysical Chemistry* **70:** 217-222

Mattevi A (2006) To be or not to be an oxidase: challenging the oxygen reactivity of flavoenzymes. *Trends in Biochemical Sciences* **31:** 276-283

Peterbauer CK, Volc J (2010) Pyranose dehydrogenases: Biochemical features and perspectives of technological applications. *Applied Microbiology and Biotechnology* **85:** 837-848

Phillips CM, Beeson WT, Cate JH, Marletta MA (2011) Cellobiose dehydrogenase and a copper-dependent polysaccharide monooxygenase potentiate cellulose degradation by Neurospora crassa. *ACS chemical biology* **6:** 1399-1406

Pricelius S, Ludwig R, Lant N, Haltrich D, Guebitz GM (2009) Substrate specificity of Myriococcum thermophilum cellobiose dehydrogenase on mono-, oligo-, and polysaccharides related to in situ production of H 2O2. *Applied Microbiology and Biotechnology* **85:** 75-83

Pricelius S, Ludwig R, Lant NJ, Haltrich D, Guebitz GM (2011) In situ generation of hydrogen peroxide by carbohydrate oxidase and cellobiose dehydrogenase for bleaching purposes. *Biotechnology Journal* **6:** 224-230

Schuster-Wolff-Bühring R, Fischer L, Hinrichs J (2010) Production and physiological action of the disaccharide lactulose. *International Dairy Journal* **20:** 731-741

Sedmera P, Halada P, Kubátová E, Haltrich D, Přikrylová V, Volc J (2006) New biotransformations of some reducing sugars to the corresponding (di)dehydro(glycosyl) aldoses or aldonic acids using fungal pyranose dehydrogenase. *Journal of Molecular Catalysis B: Enzymatic* **41:** 32-42

Shao M, Zafar MN, Falk M, Ludwig R, Sygmund C, Peterbauer CK, Guschin DA, MacAodha D, Conghaile PÓ, Leech D, Toscano MD, Shleev S, Schuhmann W, Gorton L (2013) Optimization of a membraneless glucose/oxygen enzymatic fuel cell based on a bioanode with high coulombic efficiency and current density. *ChemPhysChem* **14:** 2260-2269

Staudigl P, Krondorfer I, Haltrich D, Peterbauer CK (2013) Pyranose Dehydrogenase from *Agaricus campestris* and *Agaricus xanthoderma*: Characterization and Applications in Carbohydrate Conversions. *Biomolecules* **3:** 535-552

Sucharitakul J, Prongjit M, Haltrich D, Chaiyen P (2008) Detection of a C4a-hydroperoxyflavin intermediate in the reaction of a flavoprotein oxidase. *Biochemistry* **47:** 8485-8490

Sygmund C, Kittl R, Volc J, Halada P, Kubátová E, Haltrich D, Peterbauer CK (2008) Characterization of pyranose dehydrogenase from Agaricus meleagris and its application in the C-2 specific conversion of D-galactose. *J Biotechnol* **133:** 334-342

Sygmund C, Kracher D, Scheiblbrandner S, Zahma K, Felice AKG, Harreither W, Kittl R, Ludwig R (2012) Characterization of the two Neurospora crassa cellobiose dehydrogenases and their connection to oxidative cellulose degradation. *Applied and Environmental Microbiology* **78:** 6161-6171

Sygmund C, Santner P, Krondorfer I, Peterbauer CK, Alcalde M, Nyanhongo GS, Guebitz GM, Ludwig R (2013) Semi-rational engineering of cellobiose dehydrogenase for improved hydrogen peroxide production. *Microbial Cell Factories* **12**

Tan TC, Spadiut O, Wongnate T, Sucharitakul J, Krondorfer I, Sygmund C, Haltrich D, Chaiyen P, Peterbauer CK, Divne C (2013) The 1.6 Å crystal structure of pyranose dehydrogenase from Agaricus meleagris rationalizes substrate specificity and reveals a flavin intermediate. *PLoS One* **8:** e53567

Tao H, Cornish VW (2002) Milestones in directed enzyme evolution. *Current Opinion in Chemical Biology* **6:** 858-864

Tasca F, Gorton L, Kujawa M, Patel I, Harreither W, Peterbauer CK, Ludwig R, Nöll G (2010) Increasing the coulombic efficiency of glucose biofuel cell anodes by combination of redox enzymes. *Biosensors and Bioelectronics* **25:** 1710-1716

Tasca F, Timur S, Ludwig R, Haltrich D, Volc J, Antiochia R, Gorton L (2007) Amperometric biosensors for detection of sugars based on the electrical wiring of different pyranose oxidases and pyranose dehydrogenases with osmium redox polymer on graphite electrodes. *Electroanalysis* **19:** 294-302

Volc J, Denisova NP, Nerud F, Musilek V (1985) Glucose-2-oxidase activity in mycelial cultures of basidiomycetes. *Folia Microbiologica* **30:** 141-147

Volc J, Kubátová E, Daniel G, Sedmera P, Haltrich D (2001) Screening of basidiomycete fungi for the quinone-dependent sugar C-2/C-3 oxidoreductase, pyranose dehydrogenase, and properties of the enzyme from Macrolepiota rhacodes. *Arch Microbiol* **176:** 178-186

Volc J, Kubátová E, Wood DA, Daniel G (1997) Pyranose 2-dehydrogenase, a novel sugar oxidoreductase from the basidiomycete fungus Agaricus bisporus. *Arch Microbiol* **167:** 119-125

Volc J, Sedmera P, Halada P, Přikrylová V, Daniel G (1998) C-2 and C-3 oxidation of D-Glc, and C-2 oxidation of D-Gal by pyranose dehydrogenase from Agaricus bisporus. *Carbohydrate Research* **310:** 151-156

Walsh CT, Wencewicz TA (2013) Flavoenzymes: Versatile catalysts in biosynthetic pathways. *Natural Product Reports* **30:** 175-200

Winter G, Fersht AR, Wilkinson AJ, Zoller M, Smith M (1982) Redesigning enzyme structure by site-directed mutagenesis: tyrosyl tRNA synthetase and ATP binding. *Nature* **299:** 756-758

Yakovleva ME, Killyéni A, Ortiz R, Schulz C, MacAodha D, Conghaile PÓ, Leech D, Popescu IC, Gonaus C, Peterbauer CK, Gorton L (2012) Recombinant pyranose dehydrogenase - A versatile enzyme possessing both mediated and direct electron transfer. *Electrochemistry Communications* **24:** 120-122

Zafar MN, Shao M, Ludwig R, Leech D, Schuhmann W, Gorton L (2013) Improving the current density and the coulombic efficiency by a cascade reaction of glucose oxidizing enzymes. *ECS Transactions* **53:** 131-143

Zafar MN, Tasca F, Boland S, Kujawa M, Patel I, Peterbauer CK, Leech D, Gorton L (2010) Wiring of pyranose dehydrogenase with osmium polymers of different redox potentials. *Bioelectrochemistry* **80:** 38-42

Zamocky M, Ludwig R, Peterbauer C, Hallberg BM, Divne C, Nicholls P, Haltrich D (2006) Cellobiose dehydrogenase - A flavocytochrome from wood-degrading, phytopathogenic and saprotropic fungi. *Current Protein and Peptide Science* **7:** 255-280

Zámocký M, Hallberg M, Ludwig R, Divne C, Haltrich D (2004) Ancestral gene fusion in cellobiose dehydrogenases reflects a specific evolution of GMC oxidoreductases in fungi. *Gene* **338:** 1-14

Summary of research

Oxidoreductases of the glucose-methanol-choline (GMC) family can be applied in a large variety of bioprocesses in the food-, cosmetic-, medical or pharmaceutical industry due to their unique properties. Pyranose dehydrogenase (PDH) is able to oxidize a broad range of carbohydrate substrates at different C-atoms whereas pyranose 2-oxidase (POx) and cellobiose dehydrogenase (CDH) are more specific concerning substrate and oxidation site. Several limitations have to be overcome to provide highly valuable biocatalysts, starting with the substrate specificity of the enzyme or the efficiency of the catalyzed reaction. Therefore the aim of research was the characterization and engineering of these GMC oxidoreductases. The thesis work was part of a project funded by the Austrian Science Fund (FWF) "Oxygen reactivity of pyranose oxidoreductases" (P22094) and the doctoral programme "BioToP" (W1224). Apart from providing fundamental research data on the oxygen reactivity of flavoproteins, the goal of this project was to modify the oxygen reactivity of PDH and POx as well as the reactivity with alternative electron acceptors for applications in the food industry or in biosensors.

PDHs are secreted exclusively by fungi of the family *Agaricaceae* but the catalytic properties of the enzymes are highly heterogeneous. PDHs from *Agaricus campestris* (Ac) and *A. xanthoderma* (Ax) (paper I) and *A. meleagris* (Am) (paper II) were recombinantly expressed in *Pichia pastoris*, purified and characterized with respect to their potential industrial applications. D-glucose turned out to be the preferred substrate for Ac- and AxPDH, AxPDH also oxidizes D-xylose with a nearly equal efficiency. For AmPDH, the favoured substrate is L-arabinose followed by D-glucose. Concerning electron acceptors, a surprisingly strong preference of AcPDH for 1,4-benzoquinone over 2,6-dichloroindophenol (DCIP) and ferrocenium hexafluorophosphate was discovered, whereas the latter was preferred by AxPDH and AmPDH. Batch lactose conversion experiments of Ac- and AxPDH revealed a strong C-1 preference of AcPDH, yielding mainly lactobionic acid. AxPDH catalyzed the oxidation at the C-1 and C-2 in a ratio of 2:1. The C-2 oxidation product, 2-dehydrolactose, represents a key intermediate for the isomerisation to lactulose. In addition to enzyme characteristics, paper II focuses on a simple recombinant expression and purification protocol using a 96-well plate activity pre-screening in order to detect the best expressing clone. AmPDH was produced in 50 L scale in a stirred and aerated bioreactor and purified in a two-step protocol, yielding more than 13 g of pure enzyme. The 1.6 Å crystal structure of AmPDH (paper III) provided a scaffold for sugar docking experiments which confirmed the experimentally determined preference for C-2 and C-3 oxidation with D-glucose as a substrate.

As a dehydrogenase, PDH is unable to use molecular oxygen as an electron acceptor. Alternative acceptors like quinones or complexed metal ions, which are naturally present during lignin degradation, are preferred. In paper IV, semi-rational engineering of twelve active site amino acids of AmPDH towards increased oxygen reactivity is reported. The libraries were expressed in *Saccharomyces cerevisiae* and screened using a high-throughput protocol. Only one mutation was found in variants showing increased oxygen activity: the exchange of histidine 103 to tyrosine, phenylalanine, tryptophan or methionine. Mutant H103Y was produced in *Pichia pastoris* and characterized and revealed a five-fold increase in oxygen reactivity. Although H103 covalently links the cofactor to the protein, the mutant was still catalytically active and carried a tightly but non-covalently bound FAD. The reductive half-reaction was mainly affected by the mutation and was decreased by three orders of magnitude whereas the oxidative half-reaction remained mostly unaffected (paper V). Using electron paramagnetic resonance (EPR) spectroscopy, an anionic semiquinone radical was detected in the resting state of both the mutant and the wild-type protein. The EPR spectrum of variant H103Y suggested a higher mobility of the cofactor in the active site. Furthermore, the stability of AmPDH variant H103Y towards thermal and chemical denaturation was reduced compared to the wild-type protein. These data support the role of covalent flavinylation in tuning the reduction potential and increasing protein stability.

In paper VI, an engineered CDH from *Myriococcum thermophilum* showing enhanced hydrogen peroxide production is described. A semi-rational approach was conducted to enable an application of CDH for biotechnological purposes like cotton bleaching or as a laundry detergent. To facilitate the screening process in protein engineering of flavoproteins, a convenient microtiter-plate based assay based on three redox-dyes was developed (paper VII).

Chapter 2. Characterization of pyranose dehydrogenases

Paper I

Pyranose dehydrogenase from *Agaricus campestris* and *Agaricus xanthoderma*: Characterization and applications in carbohydrate conversions.

Petra Staudigl*, **Iris Krondorfer***, Dietmar Haltrich and Clemens K. Peterbauer

Biomolecules (2013) 3 (3): 535 – 552.

Paper II

Simple and efficient expression of *Agaricus meleagris* pyranose dehydrogenase in *Pichia pastoris*.

Christoph Sygmund, Alexander Gutmann, **Iris Krondorfer**, Magdalena Kujawa, Anton Glieder, Beate Pscheidt, Dietmar Haltrich, Clemens K. Peterbauer and Roman Kittl

Applied Microbiology and Biotechnology (2012) 94 (3): 695 – 704.

Paper III

The 1.6 Å crystal structure of pyranose dehydrogenase from *Agaricus meleagris* rationalizes substrate specificity and reveals a flavin intermediate.

Tien Chye Tan, Oliver Spadiut, Thanyaporn Wongnate, Jeerus Sucharitakul, **Iris Krondorfer**, Christoph Sygmund, Dietmar Haltrich, Pimchai Chaiyen, Clemens K. Peterbauer and Christina Divne

PLoS ONE (2013) 8 (1): e53567. doi:10.1371/journal.pone.0053567.

* The authors contributed equally to this work.

Paper I

Biomolecules **2013**, *3*, 535-552; doi:10.3390/biom3030535

OPEN ACCESS

biomolecules

ISSN 2218-273X

www.mdpi.com/journal/biomolecules/

Article

Pyranose Dehydrogenase from *Agaricus campestris* and *Agaricus xanthoderma*: Characterization and Applications in Carbohydrate Conversions

Petra Staudigl [†], Iris Krondorfer [†], Dietmar Haltrich and Clemens K. Peterbauer *

Food Biotechnology Laboratory, BOKU–University of Natural Resources and Life Sciences Vienna, Muthgasse 11, Vienna 1190, Austria; E-Mails: petra.wuehrer@boku.ac.at (P.S.); iris.krondorfer@boku.ac.at (I.K.); dietmar.haltrich@boku.ac.at (D.H.)

[†] These authors contributed equally to this work.

* Author to whom correspondence should be addressed; E-Mail: clemens.peterbauer@boku.ac.at; Tel.: +43-1-47654-6144; Fax: +43-1-47654-6251.

Received: 28 June 2013; in revised form: 9 August 2013 / Accepted: 11 August 2013 / Published: 16 August 2013

Abstract: Pyranose dehydrogenase (PDH) is a flavin-dependent sugar oxidoreductase that is limited to a rather small group of litter-degrading basidiomycetes. The enzyme is unable to utilize oxygen as an electron acceptor, using substituted benzoquinones and (organo) metal ions instead. PDH displays a broad substrate specificity and intriguing variations in regioselectivity, depending on substrate, enzyme source and reaction conditions. In contrast to the related enzyme pyranose 2-oxidase (POx), PDHs from several sources are capable of oxidizing α- or β-1→4-linked di- and oligosaccharides, including lactose. PDH from *A. xanthoderma* is able to perform C-1 and C-2 oxidation, producing, in addition to lactobionic acid, 2-dehydrolactose, an intermediate for the production of lactulose, whereas PDH from *A. campestris* oxidizes lactose nearly exclusively at the C-1 position. In this work, we present the isolation of PDH-encoding genes from *A. campestris* (Ac) and *A. xanthoderma* (Ax) and a comparison of other so far isolated PDH-sequences. Secretory overexpression of both enzymes in *Pichia pastoris* was successful when using their native signal sequences with yields of 371 $U \cdot L^{-1}$ for AxPDH and 35 $U \cdot L^{-1}$ for AcPDH. The pure enzymes were characterized biochemically and tested for applications in carbohydrate conversion reactions of industrial relevance.

Keywords: pyranose dehydrogenase; heterologous expression; agaricus; lactose conversion; lactobionic acid

---

1. Introduction

Pyranose dehydrogenase (PDH, EC 1.1.99.29) is a monomeric extracellular glycoprotein of around 75 kDa, carrying a covalently bound FAD cofactor (8α-N3-histidyl-FAD) [1]. It is a member of the glucose-methanol-choline (GMC) family together with other sugar oxidoreductases like the catalytically related enzymes glucose oxidase, cellobiose dehydrogenase and pyranose-2 oxidase. PDH was first described in 1997 when it was isolated from the edible basidiomycete fungus *Agaricus bisporus* [2]. Later, the enzyme from other members of the family of *Agaricaceae* like *Macrelepiota rhacodes* [3], *A. xanthoderma* [4] and *A. meleagris* [5,6] was investigated. Recently, the crystal structure of *A. meleagris* PDH (AmPDH) was resolved and revealed a two-domain structure consisting of the ADP-binding Rossman domain and a sugar-binding domain [1].

The biological function of PDH is still not fully clear. As the enzyme is limited to litter-decomposing fungi of the family *Agaricaceae* and is not able to utilize molecular oxygen as electron acceptor, the reduction of quinones and radicals formed during lignin degradation were proposed as its natural role [3]. Other possible functions like a participation in Fenton’s reaction or the defense against antimicrobial (quinone) substances produced by plants were reported [7].

As the production of the enzyme in basidiomycete fungi is quite laborious and time-consuming [2,4,5], approaches for heterologous expression in *Aspergillus nidulans* and *A. niger* [8], *E. coli* and *P. pastoris* [9] were tested. Attempts to solubly express PDH in *E. coli* did not succeed due to the formation of inactive inclusion bodies whereas an expression in *P. pastoris* yielded high levels of recombinant protein with properties equal to the wild-type [9]. Therefore, the methylotrophic yeast was the expression host of choice for the heterologous production of *A. campestris* and *A. xanthoderma* PDH in this study.

The oxidation products of PDH depend on the source of the enzyme, the substrate and the reaction conditions. The enzyme is able to oxidize free, non-phosphorylated sugars in pyranose form, heteroglycosides, disaccharides and glucooligosaccharides at the C-1, C-2, C-3 and also at C-1,2, C-2,3 and C-3,4 atom [2,3,10–14]. The oxidation products of D-glucose and D-galactose, 2-keto-D-glucose and 2-keto-D-galactose, represent industrially relevant intermediates for the production of the high-value sugars D-fructose and D-tagatose [15,16]. An easily available disaccharide lactose, can be oxidized by PDH to the corresponding C-1, C-2 or C-2,3 product. Depending on the source of the enzyme, 2-keto-lactose and lactobionic acid, the hydrolysis product of lactobionolactone, are formed in different ratios. Volc and coworkers screened various *Agaricus sp.* for their PDH oxidation products and observed that *A. campestris* PDH almost exclusively oxidizes lactose at the C-1 position, yielding lactobionic acid, whereas 2-keto-lactose was the main product of *A. xanthoderma* PDH [12]. Lactobionic acid has numerous applications in the pharmaceutical-, cosmetic- and food-industry, such as in organ preservation solutions and macrolide antibiotics, skin care cosmetics or as an acidulant or flavor enhancer in food [17]. The C-2 oxidation product 2-keto-lactose can be used for the production of lactulose, a prebiotic carbohydrate administered against obstipation and hepatic encephalopathy which has beneficial effects on the gastrointestinal microbiota [18]. Here, we describe for the first time the heterologous expression of PDH genes from *Agaricus campestris* and *Agaricus xanthoderma* in the methylotrophic yeast *Pichia pastoris* and present a detailed characterization of both enzymes. Furthermore, we performed comprehensive studies on the conversion of lactose and present a novel alternative for the production of lactobionic acid and 2-dehydrolactose, a key intermediate for the isomerization to lactulose.

2. Results and Discussion

2.1. Expression of Acpdh and Axpdh in P. pastoris

To obtain the PDH-encoding gene from *A. campestris,* different oligonucleotide primers were designed based on conserved regions from already known sequences (accession numbers are given in paragraph 3.8.). PCRs were performed using different forward primers, the anchor primer and first-strand-cDNA as template. Resulting fragments were sequenced and used to design sequence specific primers for identification of the 5'-flanking region by primer walking using the DNA Walking SpeedUp Premix Kit. The nucleotide sequence of the AcPDH cDNA contains an ORF of 1,788 bp encoding a polypeptide of 595 amino acids. Two primers based on the cDNA sequence and containing restriction sites for ligation into the pPICZb vector were designed, and used to re-amplify the cDNA and construct the expression vector under control of the methanol-inducible AOX promoter.

The previously unknown signal sequence and the 5'-flanking region of AxPDH were analogously identified using the DNA Walking SpeedUp Premix Kit and three specific reverse primers (AxTSP1-3). The purified fragments were sequenced, and based on these results, the full-length cDNA could be amplified. The AxPDH encoding cDNA contains an ORF of 1,803 bp encoding a polypeptide of 600 amino acids. The cDNA fragment was re-amplified with two primers containing restrictions sites for ligation into the pPICZb vector. The plasmids were transformed into *E. coli* NEB5α for proliferation. Isolated plasmids were linearized with *SacI* and transformed into the expression host *P. pastoris* and cultivated in 96-well deep well plates and screened for PDH activity. To confirm the results from the first round of screening, a rescreening experiment with multiple parallel determinations was performed. The clones with the highest activity were selected for further studies.

2.2. Multiple Sequence Alignment

To compare the amino acid sequences of the PDHs isolated and characterized so far in our group (*A. meleagris* PDH1 [5,6,9], *A. bisporus* (our unpublished information) *A. campestris* (this work) and *A. xanthoderma* PDH [4]), a multiple sequence alignment was constructed using the MUSCLE algorithm (Figure S1). The PDHs from different sources show a sequence identity between 74% and 78%. From the crystal structure of AmPDH1 [1], His 512 and His 556 were identified as the catalytic pair of major importance for sugar substrate oxidation. These two amino acids and His 103, where the FAD cofactor is covalently bound, are highly conserved among PDHs (Figure S1, highlighted in red). Docking experiments with several electron donors in different oxidation poses revealed that the principal sugar interaction partners are the two catalytic histidines but also Gln 392 and Tyr 510 (Figure S1, highlighted in green). The fact that these amino acids are conserved in all four PDHs supports these findings.

All PDHs are glycoproteins with different degrees of glycosylation. Putative N- and O-glycosylation sites predicted by NetNGlyc 1.0 server and NetOGlyc 3.1 server [19] are highlighted in red and green, respectively.

2.3. Heterologous Protein Production

The cultivation of *P. pastoris* cells expressing the *acpdh*- and *axpdh*-encoding gene was carried out in a 7-L stirred and aerated bioreactor and lasted 187 and 161 h, respectively (Figure 1). The initial glycerol batch phase produced 113 g·L^{-1} and 75 g·L^{-1} wet biomass in 27 h and 25 h (its end was indicated by an increase in dissolved oxygen concentration). The following feed with 50% glycerol was maintained for 17 h and 19 h and resulted in a final biomass of 156 g·L^{-1} and 155 g·L^{-1}, respectively. A methanol feed was initiated for induction, and at the end of this phase, the biomass reached a level of 260 g·L^{-1} and 293 g·L^{-1}. The activity of the extracellular enzyme fraction finally reached 35 U·L^{-1} for AcPDH and 371 U·L^{-1} for AxPDH, while the level of extracellular protein increased to 345 mg·L^{-1} and 350 mg·L^{-1}.

Figure 1. Large scale production of pyranose dehydrogenases (PDHs) in *P. pastoris*. Black circles, wet biomass; grey triangles, extracellular protein concentration; black squares, volumetric activity.

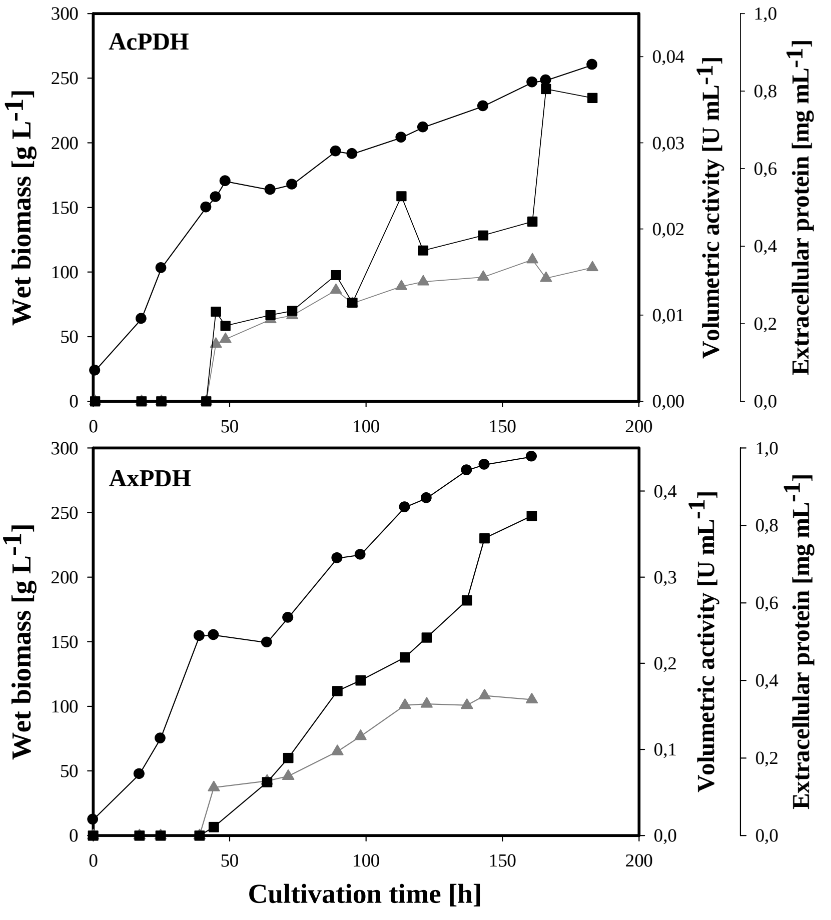

2.4. Purification of Recombinant PDHs

Recombinant AcPDH was purified from the cultivation broth in a four-step protocol (Table 1) including an additional hydrophobic interaction chromatography step (phenyl-source) compared to the three-step purification of AxPDH, which consisted of hydrophobic interaction chromatography, anion exchange chromatography and gel filtration as a polishing step. Before the AcPDH pool was loaded on the phenyl-source column, solid ammonium sulfate was added to a saturation of 40%, similar to the first purification step. Unexpectedly, the protein did not bind to the column in this case, and the whole PDH activity was found in the flow-through. This purification step indeed increased the specific activity from 0.4 U mg^{-1} to 2.8 U mg^{-1} but the flow-through still contained impurities due to the lack of restrictive pooling. Therefore, a subsequent gel filtration step was conducted, resulting in apparent homogeneity for both AcPDH and AxPDH (Figure 2), with final specific activities of 4.9 U mg^{-1} and 16.6 U mg^{-1}, respectively. For AcPDH, two pools with different specific activities were formed due to rather low overall yields. Pool 1 represented the center of the elution peak and all further analyses were performed with this enzyme preparation. The low purification yield for AcPDH corresponds to the fact that PDH accounted only for 0.1% of the total protein in the extracellular fraction, whereas AxPDH accounted for more than 2%. The purification step that decreased the yield most dramatically is the first for both enzymes. As the starting volume for purification after centrifugation was around 4 L in both cases, the calculation of the total activity based on the activity per mL could lead to imprecise results. This is especially true in the case of AcPDH, where the volumetric activity per mL was below the detection limit of the standard ferrocenium/glucose activity assay and only represents an estimate. A reduction of the volume and therefore concentration of the cultivation broth would have been useful for more precise measurements of the initial volumetric activity. The higher degree of glycosylation of AcPDH could also play a disadvantageous role for the purification (Figure 2, Table 2). All concentrated protein pools showed the typical light yellow color of flavoproteins and were stable over several months at 4 °C in 65 mM sodium phosphate buffer pH 7.5.

Table 1. Purification schemes of recombinant PDHs.

Purification step	Total protein [mg]	Total activity [U]	Specific activity [U mg^{-1}]	Purification [-fold]	Yield [%]
AcPDH					
Crude extract	1730	154.4	0.1	1	100
Phenyl sepharose	124.4	27.4	0.2	2.5	18
DEAE sepharose	28.2	21.5	0.4	4.1	14
Phenyl source	5.5	15.2	2.8	31.0	10
Gel filtration pool 1	1.2	5.6	4.9	54.5	4
Gel filtration pool 2	0.4	1.5	3.7	41.9	1
AxPDH					
Crude extract	1226.4	1298.9	1.1	1	100
Phenyl sepharose	109.9	538.6	4.9	4.6	41
DEAE sepharose	40.2	524.9	13.1	12.3	40
Gel filtration	25.8	428.8	16.6	15.7	33

Table 2. Molecular properties of recombinant PDHs.

PDH	Mass SDS-PAGE [kDa]	Mass SDS-PAGE deglyc. [kDa]	Theor. mass [kDa]	Glycan mass [%]	*N*-Glyc sites predicted	*O*-Glyc sites predicted
Ac	98	68	61.8	31	6	3
Ax	73	68	62.3	7	5	0

Figure 2. SDS-PAGE of purified PDHs. M, molecular marker; 1, AcPDH; 2, AcPDH deglycosylated; 3, Ax PDH; 4, AxPDH deglycosylated.

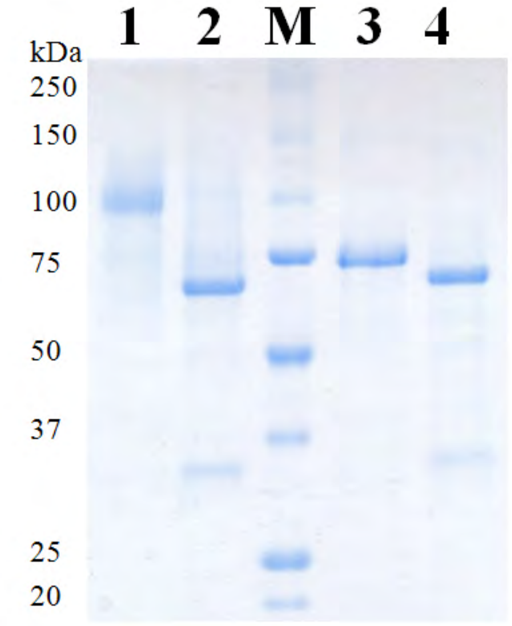

2.5. Molecular Properties

The molecular masses of AcPDH and AxPDH were determined by SDS-PAGE (Figure 2) and native PAGE (Figure 3). AcPDH formed a diffuse band around 98 kDa (Figure 2, lane 1), after deglycosylation with PNGase F under denaturing conditions, a sharp band at 68 kDa could be observed (lane 2). AxPDH showed a band at 73 kDa (lane 4); after deglycosylation, the band shifted to around 68 kDa (lane 5). The high degree of glycosylation of AcPDH compared to AxPDH (Table 2) is also observed in native PAGE (Figure 3). From the migration difference of the glycosylated and deglycosylated protein band in the gel, a glycan mass of 31% for AcPDH and 7% for AxPDH could be calculated (Table 2). The native AxPDH [4] showed a slightly smaller mass on the SDS-PAGE compared to the recombinant protein (around 65 kDa). This is most likely due to a difference in glycosylation in basidiomycete fungi compared to the yeast *P. pastoris*. Whereas proteins in (homo) basidiomycete fungi carry *N*-glycans of the oligomannosidic type (4-9 mannoses), *P. pastoris* tends to produce hyper-mannosylated glycans [20–22]. The NetNGlyc 1.0 server found nine glycosylation motifs in the sequence of AxPDH, five of them putatively glycosylated, and nine for AcPDH with six of them likely to carry a glycan structure. Concerning *O*-glycosylation, NetOGlyc 3.1 server predicted three sites for AcPDH with potential above the threshold and none for AxPDH. The potentially higher degree of *O*-glycosylation of AcPDH compared to AxPDH cannot account for the large difference in glycan mass between the two proteins. The deglycosylation was carried out using PNGase F, which exclusively removes *N*-glycans, and the deglycosylated proteins have a quite similar molecular mass. Furthermore, *O*-glycans in *P. pastoris* mostly consist of up to three, rarely four, mannose units in contrast to hyper-mannosylated *N*-glycans [23]. A substantial over-glycosylation with a comparable glycan content of approximately 30% of protein expressed in *P. pastoris* was also observed for AmPDH [9]. PDH is one of the rare flavoproteins carrying a covalently bound cofactor [24]. Covalent incorporation was proven by the method of Scrutton [25], the flavin associated with the protein gives a fluorescent signal when exposed to UV-light. The positive control (AmPDH), AcPDH and AxPDH showed a bright band under UV-light whereas the negative control glucose oxidase (GOx) from *A. niger* [26] did not give any signal (Figure S2).

Figure 3. Native PAGE of purified PDHs. M, molecular marker; 1, AcPDH; 2, AxPDH.

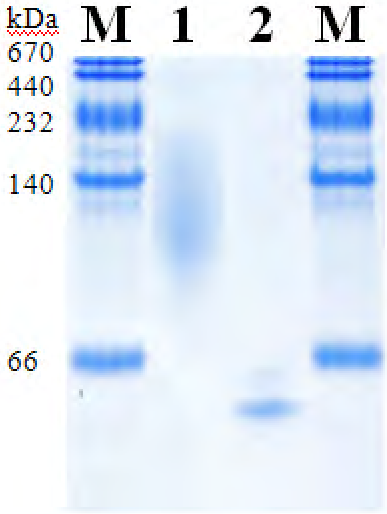

UV-Vis spectra of AcPDH and AxPDH in the oxidized state were recorded; typical flavoprotein absorbance maxima around 450 nm and 340 nm could be observed (Figure S3; AxPDH: data not shown).

2.6. Kinetic Properties

Catalytic constants for selected sugar substrates and electron acceptors were determined and are summarized in Tables 3 and 4. For both enzymes, D-glucose represents the preferred electron donor. This is mainly due to the K_m value, which displays a more than 10 times higher affinity for this substrate compared to e.g., D-galactose. The pentose sugar D-xylose is the second best substrate for Ac and AxPDH. This finding stands in contrast to the catalytic efficiencies of other so-far characterized PDHs like from *Agaricus meleagris* [5] and the native *A. xanthoderma* PDH [4], where L-arabinose and D-galactose are preferred over D-xylose. The catalytic efficiency of AxPDH with D-xylose is more than 75% of the catalytic efficiency for the main substrate D-glucose, whereas for AcPDH it is only 13%. The k_{cat}/K_m-values of AcPDH are in general lower for all sugar substrates. Remarkable here is that the catalytic efficiencies of Ac and AxPDH are similar for lactose but the K_m of AcPDH is 5.5-times lower than the K_m of AxPDH, whereas the k_{cat} behaves the opposite way.

Table 3. Apparent kinetic constants for selected electron donors determined at 30 °C with 0.2 mM ferrocenium hexafluorophosphate as the electron acceptor.

	AcPDH			**AxPDH**		
	K_m [mM]	**k_{cat} [s^{-1}]**	**k_{cat}/K_m [mM^{-1} s^{-1}]**	**K_m [mM]**	**k_{cat} [s^{-1}]**	**k_{cat}/K_m [mM^{-1} s^{-1}]**
D-glucose	0.35 ± 0.06	4.10 ± 0.19	11.7	0.49 ± 0.03	13.02 ± 0.38	26.6
D-galactose	7.13 ± 0.19	5.23 ± 0.53	0.7	4.99 ± 0.16	24.77 ± 2.23	5.0
D-xylose	4.19 ± 0.26	6.37 ± 0.05	1.5	1.44 ± 0.07	29.16 ± 0.25	20.3
L-arabinose	4.23 ± 0.02	3.05 ± 0.04	0.7	4.16 ± 0.58	22.90 ± 2.23	5.5
Lactose	53.16 ± 0.10	3.12 ± 0.17	0.1	293.84 ± 8.00	24.65 ± 0.37	0.1

Table 4. Apparent kinetic constants for selected electron acceptors determined at 30 °C with 25 mM D-glucose as the electron donor.

	AcPDH			**AxPDH**		
	K_m [mM]	**k_{cat} [s^{-1}]**	**k_{cat}/K_m [mM^{-1} s^{-1}]**	**K_m [mM]**	**k_{cat} [s^{-1}]**	**k_{cat}/K_m [mM^{-1} s^{-1}]**
Fc^+PF_6 (pH 8.5)	1.19 ± 0.17	19.92 ± 2.87	16.7	0.03 ± 0.00	22.07 ± 0.05	735.7
1,4-BQ (pH 4)	0.12 ± 0.01	34.82 ± 1.02	302.8	3.25 ± 0.51	12.89 ± 1.56	4.0
DCIP (pH 4)	0.11 ± 0.00	10.56 ± 0.57	96.0	0.09 ± 0.01	7.65 ± 0.66	85.0

Concerning the kinetic constants for the electron acceptors, the two enzymes have quite different preferences (Table 4). For AcPDH 1,4-benzoquinone is the favored substrate whereas AxPDH shows a clear preference for ferrocenium hexafluorophosphate. All PDHs that have been characterized to date show a higher catalytic activity with ferrocenium compared to 1,4-benzoquinone; AcPDH is the first PDH where a clear preference for 1,4-benzoquinone was observed [4,5]. The catalytic efficiencies for DCIP are nearly equal for both PDHs. In general, PDH shows activity only with a limited group of electron acceptors whereas it oxidizes a very broad range of sugar substrates. Many major mono- and oligosaccharide components of lignocellulose can be utilized as substrates, giving evidence for the putative biological function of PDH in lignin degradation [7]. Recently, the molecular mechanism of glucose oxidation by *A. meleagris* PDH was explored using MD simulation; the findings support the experimentally observed promiscuity of PDH concerning sugars [27].

The pH dependence of PDH activity was tested for the electron acceptors ferrocenium hexafluorophosphate and 1,4-benzoquinone with D-glucose as the electron donor (Figure 4). Using 1,4-benzoquinone as the electron acceptor, AcPDH displayed maximum activity at pH 7 (phosphate buffer) and already reached 95% activity at pH 5.5 (citrate buffer). AxPDH showed the highest activity at pH 5.5 (citrate buffer). With ferrocenium hexafluorophosphate, the optimum pH for AcPDH was 8.5 and 9 for AxPDH (borate buffer). Compared to the native AxPDH [4], the pH optimum for ferrocenium hexafluorophosphate is comparable but with 1,4-benzoquinone the native AxPDH exhibited highest activity at pH 2.5 and around 70% activity at pH 8. The recombinant AxPDH showed less than 2.5% activity at pH 2.5. In general, it can be observed that the pH optimum is highly dependent on the electron acceptor used. PDHs from *Agaricus sp.* showed pH optima in the basic region when using ferrocenium hexafluorophosphate whereas with 1,4-benzoquinone the enzymes were more active under acidic conditions and in some cases showed a second maximum in the alkaline region, which could be due to high blank readings caused by the formation of quinhydrone [2,4,5].

Figure 4. pH optima of AcPDH (black squares) and AxPDH (grey triangles) with the electron acceptors ferrocenium hexafluorophosphate and 1,4-benzoquinone; D-glucose as electron donor.

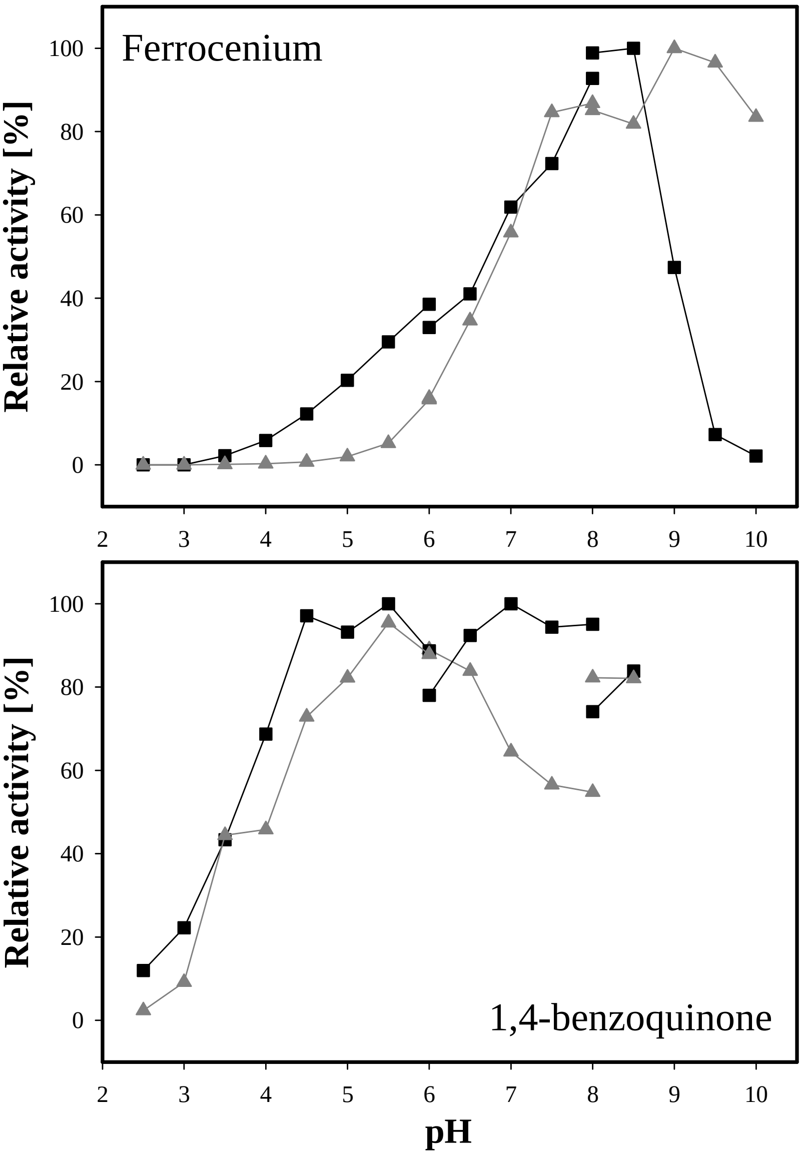

2.7. Batch Carbohydrate Conversion Experiments

Both enzymes were used for the conversion of 25 mM lactose together with equimolar amounts of the electron acceptor 1,4-benzoquinone in 1 mL batch experiments and the reaction products were analyzed by HPLC (Figure 5). Conversions were carried out in water due to interference of buffer salts with the HPLC analysis. 10 U of AxPDH converted lactose to nearly 100% (97%), producing 69% (67%) lactobionic acid and 31% (30%) 2-dehydrolactose (Figure 5a). Due to the fact that the cultivation yield of AcPDH was quite low, only one unit of the purified protein was used for the conversion experiment. Therefore, only 48% of the lactose was converted and yielded 88% (42%)

lactobionic acid and only 12% (6%) 2-dehydrolactose (Figure 5b). These results confirm the preference for C-1 oxidation in AcPDH-catalyzed conversions of lactose (the ratio of C-1 to C-2 oxidation is 7:1), compared to the AxPDH-catalyzed reaction where the ratio of C-1 to C-2 oxidation is only 2:1. C-2,3 oxidation, which can occur when oxidation at C-2 is complete under excess of 1,4-benzoquinone, could not be observed [12]. For industrial use, there is still need for improvement of the conversion yield. Acidification due to spontaneous hydrolysis of lactobionolactone to lactobionic acid slowed down the enzyme activity at the end of the conversion but could be avoided by buffering.

Figure 5. (**a**) HPLC analysis of lactose conversion by AcPDH; (**b**) and AxPDH at 0 h (A), 1 h (B), 3 h (C) and 7 h (D) incubation. Peaks: I, residual salt from enzyme preparation; II, lactobionic acid; III, lactose; IV, 2-dehydrolactose.

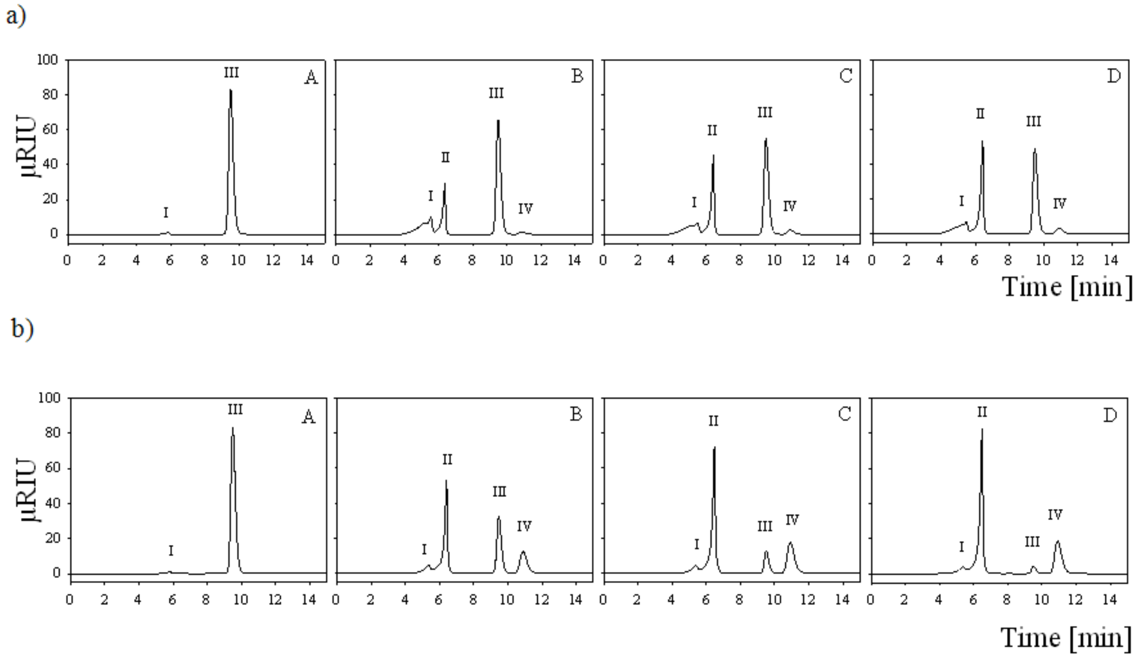

3. Experimental Section

3.1. Chemicals and Microorganisms

All chemicals, sugar standards for HPLC and media components were purchased from Sigma (Steinheim, Germany) unless otherwise stated and were of the highest purity available. Restriction endonucleases, T4 DNA ligase and Phusion High-Fidelity DNA Polymerase were obtained from Fermentas (St. Leon-Rot, Germany) unless otherwise stated and were used according to the manufacturer's instructions. *Agaricus campestris* (strain CCBAS 20649) and *Agaricus xanthoderma* (strain CCBAS 225) were obtained from the Culture Collection of Basidiomycetes of the Academy of Sciences (Prague, Czech Republic). *Escherichia coli* strain NEB5α (New England Biolabs, Ipswich, MA, USA) was used for subcloning, *Pichia pastoris* strain X-33 (Invitrogen, Carlsbad, CA, USA) was used for expression. Ferrocenium hexafluorophosphate and the various substituted quinones were obtained from Aldrich (Steinheim, Germany). Phenyl-Sepharose Fast Flow resin was purchased from Amersham Pharmacia Biotech (Uppsala, Sweden), DEAE Sepharose Fast Flow resin and Sephacryl

S300-HR resin were from GE Healthcare (Chalfont St. Giles, UK). GOx from *Aspergillus niger* was from Sigma.

3.2. Isolation of Genomic DNA and RNA

For DNA- and RNA-isolation, approximately 10 mL liquid Sabouraud medium was inoculated with mycelial fragments from freshly grown malt extract agar plates. The cultivations were performed in petri dishes at 25 °C without shaking over 3 weeks. Mycelia were harvested, squeezed dry between filter paper and shock-frozen in liquid nitrogen. Portions of approximately 100 mg of mycelium were used for DNA- and RNA-isolation. Genomic DNA extraction was performed according to Liu *et al.* [28]. Total RNA was extracted using Trizol reagent (Invitrogen) according to the manufacturer’s instructions. To remove genomic DNA, the samples were incubated with *DNAseI* as recommended by the manufacturer. The isolated mRNA was reverse-transcribed using RevertAid First Strand cDNA Synthesis kit (Thermo Fisher Scientific, Waltham, MA, USA) and the anchor primer (Table S1).

3.3. Cloning and Sequencing of AcPDH Encoding Gene

Nucleic acid amplifications were done using Phusion High-Fidelity Polymerase, GC-Buffer, dNTP mix, oligonucleotide primers (VBC Biotech, Vienna, Austria) and a BioRad C-1000 thermocycler (BioRad, Vienna, Austria). Nucleotide sequences of all primers used in this work are shown in Table S1. To obtain the PDH-encoding gene from *A. campestris* degenerate primers (AcPDHfwd1-3) were designed according to a sequence analysis of conserved regions in *pdh* genes from *A. meleagris* and *A. bisporus* and used for the amplification of cDNA fragments of various lengths. 35 PCR cycles at temperatures of 98 °C (10 s), 57 °C (20 s) and 72 °C (1 min) and an initial denaturation at 98 °C (2 min) and a final extension at 72 °C (7 min), were employed with cDNA as template and “universal” as reverse primer. The amplicons were purified and sequenced by a commercial sequencing service (LGC Genomics, Berlin, Germany). For identification of the 5‘ flanking region, including the native signal sequence, the DNA Walking SpeedUp Premix Kit (Seegene, Seoul, South Korea) was used. Target-specific reverse primers (AcTSP1-3) were designed, genomic DNA was used as template and the PCRs were done according to the manufacturer’s guidelines. The resulting PCR products were purified by using the illustra GFX PCR DNA and Gel Band Purification Kit (GE Healthcare) and sequenced. To obtain full-length cDNA clones a PCR was performed with the primer pair AcPDHfwd and AcPDHrev and cDNA as template. The resulting fragment was cloned into the pJET1.2 vector (Fermentas) according to the instructions in the manual and sequenced.

3.4. Cloning and Sequencing of AxPDH Encoding Gene

To obtain the 5‘- flanking region, including the native signal sequence, the DNA Walking SpeedUp Premix Kit (Seegene) was used. Target-specific reverse primers (AxTSP1-3) were designed according to *A. xanthoderma* PDH gene sequence, genomic DNA was used as template and the PCRs were done according to the manufacturer’s guidelines. The resulting PCR products were purified and sequenced. To obtain full-length cDNA clones a PCR was performed with the primer pair AxPDHfwd and

AxPDHrev and cDNA as template. The amplified sequence was temporarily cloned into the pJET1.2 vector (Fermentas) according to the instructions in the manual and sequenced.

3.5. Construction of Expression Vectors for P. pastoris

The *acpdh* gene (in the pJET1.2 vector) was re-amplified with the primers AcPDHKpnIfwd and AcPDHNotIrev. The re-amplification of the *axpdh* gene was performed using the primer pair AxKpnIfwd and AxNotIrev. The resulting PCR products were digested with *KpnI* and *NotI* and ligated into the equally treated vector pPICZb (Invitrogen). After transformation into chemically competent *E. coli* NEB5α, according to the manufacturer's instructions, the plasmids were proliferated, linearized with *SacI* and transformed into electrocompetent *P. pastoris*, which were prepared according to Lin-Cereghino *et al.* [29]. For selection the Luria Bertani (LB) medium contained 25 µg mL^{-1} Zeocin in case of *E. coli,* while the YPD-medium contained 100 µg mL^{-1}. The resulting colonies were picked and grown in 96-well deep well plates.

3.6. Microscale Screening for High-Producing PDH Transformants

Microscale cultivation and expression in 96-well deep well plates was done according to Weis *et al.* [30] with some modifications. Cells were grown in 250 µL BMD1 (13.4 g·L^{-1} yeast nitrogen base, 0.4 mg·L^{-1} biotin, 10 g·L^{-1} D-glucose, 200 mM potassium phosphate [pH 6.0]) at 25 °C, 385 rpm and 60% humidity for approximately 60 h to reach the stationary growth phase. Induction was started by the addition of 250 µL of BMM2 medium (13.4 g·L^{-1} yeast nitrogen base, 0.4 mg·L^{-1} biotin, 1% methanol, 200 mM potassium phosphate [pH 6.0]) to reach a final concentration of 0.5% methanol. After 70, 82, and 108 h of incubation, 50 µL BMM10 (BMM2 with 5% methanol) were added to maintain inducing conditions. The cultivation was stopped after 130 h by centrifugation of the deep-well plates at 3000 rpm at room temperature for 20 min. PDH activity was measured using 2,6-dichloroindophenol (DCIP, ε520 = 6.8 mM^{-1} cm^{-1}) as electron acceptor and D-glucose as donor. Fifty µL of the supernatant were transferred to the 96-well screening plates and the time-dependent reduction of 300 µM DCIP in 100 mM sodium acetate buffer pH 4 containing 50 mM D-glucose was followed at 520 nm with a PerkinElmer EnSpire plate reader. The reaction was started by addition of 150 µL of the DCIP assay mixture to the screening plate and end-point measurements were carried out after incubation at 30 °C for 2 and 4 h.

3.7. Sequence Analysis

The translated amino acid sequences of the obtained cDNAs were analyzed using the programs Translate, Compute pI/MW and SignalP at http://www.expasy.org/ [31]. A multiple sequence alignment of AmPDH1, AbPDH, AcPDH and AxPDH was created using the MUSCLE algorithm (EMBL-EBI, Cambridgeshire, UK). Sequence identities were determined by BLAST search [32]. Predictions for *N*- and *O*-glycosylation sites were performed on the NetNGlyc 1.0 Server and the NetOGlyc 3.1 Server [19] of the Center for Biological Sequence Analysis (CBS) at the Technical University of Denmark (http://www.cbs.dtu.dk/services/). All predicted *N*- and *O*-glycosylation sites with a threshold above 0.5 except for Asn-Pro-sites were displayed.

3.8. Nucleotide and Protein Sequence Accession Numbers

The NCBI accession numbers for the sequences in this work are: AY53306, AY753308, DQ117577, AAW82996, AAW82997, AAW82998, AAW82999, AAZ94874, AAZ94875 (*A. meleagris* PDHs); AY764148, AAW92124, EKV41672 (*A. bisporus* PDH); AY764147, AAW92123, KF534751 (*A. xanthoderma* PDH); KF534750 (*A. campestris* PDH).

3.9. Recombinant Protein Production in P. pastoris

AxPDH and AcPDH were produced in a 7-L bioreactor (MBR, Wetzikon, Switzerland) with an initial volume of 4 L basal salts cultivation medium, according to the "*Pichia* Fermentation Process Guidelines" (Invitrogen) with slight modifications. After autoclaving the bioreactor, the temperature was set to 30 °C, the pH was adjusted to 5 and maintained by addition of 28% ammonium hydroxide solution during the cultivation. Dissolved oxygen was regulated to 4% by supplying filtered air and adjusting the stirrer velocity (around 800 rpm). Two shaking flasks with 20 mL YPD-Zeocin medium each were inoculated with the colony-PCR-verified *P. pastoris* clones and grown overnight at 30 °C and 120 rpm. The cultures were transferred to two shaking flasks with 200 mL YPD medium each and again grown overnight at 30 °C and 120 rpm. This culture (400 mL) was used to inoculate the bioreactor. After consumption of the glycerol in the batch medium (indicated by an O_2 spike), a feed of 50% glycerol containing 12 mL L^{-1} PTM1 trace salts was initiated with around 20 mL h^{-1} over night. Protein production was induced by changing to a feed of 100% methanol containing 12 mL PTM1 trace elements per liter. The feed rate was adjusted to maintain a dissolved oxygen concentration of around 4%. Samples were taken at least twice a day and biomass wet weight, PDH activity and total protein concentration was determined. The formation of foam was avoided by daily manual addition of approximately 10 mL a 10% antifoam 204 solution (Sigma). When no further increase in the specific activity could be observed, the bioreactor was harvested and the cultivation broth was centrifuged at 4 °C and 6000 rpm in a Sorvall Evolution RC centrifuge (Thermo Fisher Scientific).

3.10. Protein Purification

Solid ammonium sulfate was added to the cultivation supernatants to a saturation of 40%. The crude extracts (approximately 4 L) were applied to a 750 mL phenyl-sepharose FF column (GE Healthcare), and washed with binding buffer (50 mM potassium phosphate, pH 6.5 containing 1.5 M ammonium sulfate). The protein was eluted using a linear gradient from 0–100% elution buffer (50 mM potassium phosphate, pH 6.5) in 1 column volume (CV). Prior to the next purification step, the pooled fractions were desalted using cross-flow filtration (SpectrumLabs, Houston, TX, USA) to a conductivity equal to or less than 2 mS/cm. The pools of desalted fractions were loaded to a 60 mL DEAE sepharose column (GE Healthcare), washed with binding buffer (50 mM BisTris, pH 6) and eluted with a linear gradient from 0–100% elution buffer (50 mM BisTris, 1 M NaCl, pH 6) in 4 column volumes. For AcPDH, the concentrated pool from the anion exchange chromatography was subjected to a second hydrophobic interaction chromatography step using a 70 mL phenyl-source column (GE Healthcare). The purification was conducted similar to the first hydrophobic interaction chromatography step except for the elution of the protein, which was carried out in 5 CV.

The fractions with the highest Ax- and AcPDH activities were pooled and concentrated to a volume of around 2 mL using an Amicon Ultra Centrifugal Filter Unit (EMD Millipore, Billerica, MA, USA). The concentrated pools were applied to a 190 mL Sephacryl S300 gel filtration column (GE healthcare) equilibrated with 50 mM potassium phosphate buffer (pH 7.5) containing 150 mM NaCl. Fractions with the highest purity were pooled, concentrated for buffer exchange (65 mM sodium phosphate buffer, pH 7.5) and stored at 4 °C.

3.11. Enzyme Assay, Molecular Properties

Standard PDH activity was measured by following spectrophotometrically the D-glucose dependent reduction of the ferrocenium ion (Fc+) to ferrocene at 300 nm and 30 °C as described before [4] with modifications: The standard reaction mixture (1 mL) contained 50 µmol sodium phosphate buffer pH 7.5, 0.2 µmol of ferrocenium hexafluorophosphate and 25 µmol D-glucose. Protein concentration was determined using the method of Bradford using a BSA standard curve and a prefabricated assay solution (BioRad). Enzymatic deglycosylation and SDS-PAGE were carried out as described in Sygmund *et al.*, using the Precision Plus Protein Unstained Standard (BioRad) [9]. 1.5–2 µg of the protein samples were loaded in each lane. Native PAGE was performed using 10% and 5% polyacrylamide as the separation and stacking gels, respectively, and Tris-glycine buffer (pH 8.3) as the electrode buffer [33]. 5–10 µg of the protein samples were loaded in each lane. Staining procedure was carried out using Bio-Safe Coomassie (BioRad) according to the manufacturer’s instructions. For determination of molecular weight, HMW Native Marker Kit (GE Healthcare) was used. To proof the covalent linkage of the FAD cofactor an additional SDS-PAGE was performed according to Scrutton [25]. 10 µg of the protein samples were loaded in each lane, the covalently linked FAD was visualized by exposure of the gel to UV-light (λ 302 nm, GelDoc2000, BioRad). As a positive control, recombinant *A. meleagris* PDH was loaded [1]; glucose oxidase from *A. niger* was used as a negative control.

Molecular masses of the proteins were calculated from their migration distances on the SDS-PAGE; the theoretical mass was derived from ExPASy ProtParam tool (http://web.expasy.org/protparam/) [31]. The glycan mass in% was calculated from the difference of the masses of the glycosylated and deglycosylated proteins on the SDS-PAGE.

UV-Vis absorbance spectra of 13 µM AcPDH and AxPDH were recorded in 65 mM sodium phosphate buffer pH 7.5 at room temperature using a U-3000 spectrophotometer (Hitachi, Tokyo, Japan) from 300–700 nm.

3.12. Kinetic Properties

Apparent kinetic constants for electron donors were measured using the standard activity assay with ferrocenium hexafluorophosphate as described above. Kinetic constants for ferrocenium hexafluorophosphate, 1,4-benzoquinone and 2,6-dichloroindophenol were determined using 25 mM D-glucose as electron donor. The observed data were fitted to the Michaelis-Menten equation and kinetic constants were calculated by nonlinear least-squares regression. Using the molecular mass, turnover numbers (k_{cat}) and catalytic efficiencies (k_{cat}/K_m) were calculated. The pH optima with the electron acceptors ferrocenium hexafluorophosphate (0.2 mM) and 1,4-benzoquinone (2 mM) were determined with the following buffers: 100 mM citrate (pH 2.5–6), 100 mM potassium phosphate (pH 6–8) and 100 mM borate (pH 8–10) and 25 mM D-glucose as the electron donor. Activities with 1,4-benzoquinone were not determined above pH 8.5 due to the formation of quinhydrone under basic conditions.

3.13. Batch Conversion Experiments

Small-scale lactose conversions were carried out in 1.5 mL Eppendorf vials containing 25 mM 1,4-benzoquinone, 25 mM lactose monohydrate and 1 U of purified AcPDH or 10 U of purified AxPDH in 1 mL deionized water. The vials were incubated at 30 °C and 400 rpm in a thermomixer, samples were taken in regular time intervals (50 µL). Immediately after sampling, PDH activity was stopped by heating the sample to 99 °C for 3 min. The samples were centrifuged, diluted 1:2 and subjected to HPLC analysis.

3.14. HPLC Analysis of Batch Conversion Products

HPLC analysis of the batch conversion products was performed on a Dionex Summit HPLC system (Thermo Fisher Scientific) fitted with a Shodex RI-101 refractive index detector (Shoko Scientific, Yokohama, Japan) using an Aminex HPX 87-K column (BioRad) with a guard column. Samples and standards were eluted at 80 °C with deionized water (0.5 mL min^{-1}). For the calculation of lactose and lactobionic acid concentrations, standards were included in the run. As there was no standard available for 2-dehydrolactose, the ratio of 2-dehydrolactose to lactobionic acid was estimated by comparing the peak areas.

4. Conclusions

This study demonstrates the successful expression of the PDH-encoding genes from the litter-degrading basidiomycetes *A. campestris* and *A. xanthoderma*, in the eukaryotic host organism *P. pastoris*. Small-scale conversion experiments with lactose as substrate revealed that AcPDH has a strong preference for C-1 oxidation, resulting in the production of lactobionic acid. Compared to AxPDH, which produces mixtures of C-2/C-1 oxidation products in a 1:2 ratio, AcPDH is a very attractive biocatalyst for the production of lactobionic acid. Further research towards a better expression yield is required for industrial applications/purposes.

Acknowledgments

The authors thank Cindy Lorenz for technical assistance and performing the HPLC analysis. This work was supported by the Austrian Science Fund FWF (grant P22094 to CKP), IK is a member of the doctoral program BioToP (Biomolecular Technology of Proteins) of the Austrian Science Fund (W1224).

Conflict of Interest

The authors declare no conflict of interest.

References

1. Tan, T.C.; Spadiut, O.; Wongnate, T.; Sucharitakul, J.; Krondorfer, I.; Sygmund, C.; Haltrich, D.; Chaiyen, P.; Peterbauer, C.K.; Divne, C. The 1.6 å crystal structure of pyranose dehydrogenase from *Agaricus meleagris* rationalizes substrate specificity and reveals a flavin intermediate. *PLoS One* **2013**, *8*, e53567.
2. Volc, J.; Kubátová, E.; Wood, D.A.; Daniel, G. Pyranose 2-dehydrogenase, a novel sugar oxidoreductase from the basidiomycete fungus *Agaricus bisporus*. *Arch. Microbiol.* **1997**, *167*, 119–125.
3. Volc, J.; Kubátová, E.; Daniel, G.; Sedmera, P.; Haltrich, D. Screening of basidiomycete fungi for the quinone-dependent sugar C-2/C-3 oxidoreductase, pyranose dehydrogenase, and properties of the enzyme from *Macrolepiota rhacodes*. *Arch. Microbiol.* **2001**, *176*, 178–186.
4. Kujawa, M.; Volc, J.; Halada, P.; Sedmera, P.; Divne, C.; Sygmund, C.; Leitner, C.; Peterbauer, C.; Haltrich, D. Properties of pyranose dehydrogenase purified from the litter-degrading fungus *Agaricus xanthoderma*. *FEBS J.* **2007**, *274*, 879–894.
5. Sygmund, C.; Kittl, R.; Volc, J.; Halada, P.; Kubátová, E.; Haltrich, D.; Peterbauer, C.K. Characterization of pyranose dehydrogenase from *Agaricus meleagris* and its application in the C-2 specific conversion of D-galactose. *J. Biotechnol.* **2008**, *133*, 334–342.
6. Kittl, R.; Sygmund, C.; Halada, P.; Volc, J.; Divne, C.; Haltrich, D.; Peterbauer, C.K. Molecular cloning of three pyranose dehydrogenase-encoding genes from *Agaricus meleagris* and analysis of their expression by real-time RT-PCR. *Curr. Genet.* **2008**, *53*, 117–127.
7. Peterbauer, C.K.; Volc, J. Pyranose dehydrogenases: Biochemical features and perspectives of technological applications. *Appl. Microbiol. Biotechnol.* **2010**, *85*, 837–848.
8. Pisanelli, I.; Kujawa, M.; Gschnitzer, D.; Spadiut, O.; Seiboth, B.; Peterbauer, C. Heterologous expression of an *Agaricus meleagris* pyranose dehydrogenase-encoding gene in *Aspergillus* spp. and characterization of the recombinant enzyme. *Appl. Microbiol. Biotechnol.* **2010**, *86*, 599–606.
9. Sygmund, C.; Gutmann, A.; Krondorfer, I.; Kujawa, M.; Glieder, A.; Pscheidt, B.; Haltrich, D.; Peterbauer, C.; Kittl, R. Simple and efficient expression of *Agaricus meleagris* pyranose dehydrogenase in *Pichia pastoris*. *Appl. Microbiol. Biotechnol.* **2012**, *94*, 695–704.
10. Volc, J.; Sedmera, P.; Halada, P.; Přikrylová, V.; Daniel, G. C-2 and C-3 oxidation of D-glc, and C-2 oxidation of D-gal by pyranose dehydrogenase from *Agaricus bisporus*. *Carbohydr. Res.* **1998**, *310*, 151–156.
11. Volc, J.; Sedmera, P.; Halada, P.; Prikrylová, V.; Haltrich, D. Double oxidation of D-xylose to D-glycero-pentos-2,3-diulose (2,3-diketo-D-xylose) by pyranose dehydrogenase from the mushroom *Agaricus bisporus*. *Carbohydr. Res.* **2000**, *329*, 219–225.
12. Volc, J.; Sedmera, P.; Kujawa, M.; Halada, P.; Kubátová, E.; Haltrich, D. Conversion of lactose to β-D-galactopyranosyl-(1→4)-D-arabino-hexos-2-ulose-(2-dehydrolactose) and lactobiono-1,5-lactone by fungal pyranose dehydrogenase. *J. Mol. Catal. B Enzym.* **2004**, *30*, 177–184.
13. Sedmera, P.; Halada, P.; Peterbauer, C.; Volc, J. A new enzyme catalysis: 3,4-dioxidation of some aryl β-D-glycopyranosides by fungal pyranose dehydrogenase. *Tetrahedron. Lett.* **2004**, *45*, 8677–8680.

14. Sedmera, P.; Halada, P.; Kubátová, E.; Haltrich, D.; Přikrylová, V.; Volc, J. New biotransformations of some reducing sugars to the corresponding (di)dehydro(glycosyl) aldoses or aldonic acids using fungal pyranose dehydrogenase. *J. Mol. Catal. B Enzym.* **2006**, *41*, 32–42.
15. Haltrich, D.; Leitner, C.; Neuhauser, W.; Nidetzky, B.; Kulbe, K.D.; Volc, J. A convenient enzymatic procedure for the production of aldose-free D-tagatose. *Ann. N. Y. Acad. Sci.* **1998**, *864*, 295–299.
16. Leitner, C.; Neuhauser, W.; Volc, J.; Kulbe, K.D.; Nidetzky, B.; Haltrich, D. The cetus process revisited: A novel enzymatic alternative for the production of aldose-free D-fructose. *Biocatal. Biotransform.* **1998**, *16*, 365–382.
17. Gutiérrez, L.F.; Hamoudi, S.; Belkacemi, K. Lactobionic acid: A high value-added lactose derivative for food and pharmaceutical applications. *Int. Dairy J.* **2012**, *26*, 103–111.
18. Schuster-Wolff-Bühring, R.; Fischer, L.; Hinrichs, J. Production and physiological action of the disaccharide lactulose. *Int. Dairy J.* **2010**, *20*, 731–741.
19. Julenius, K.; Mølgaard, A.; Gupta, R.; Brunak, S. Prediction, conservation analysis, and structural characterization of mammalian mucin-type o-glycosylation sites. *Glycobiology* **2005**, *15*, 153–164.
20. Berends, E.; Ohm, R.A.; de Jong, J.F.; Rouwendal, G.; Wösten, H.A.B.; Lugones, L.G.; Bosch, D. Genomic and biochemical analysis of N glycosylation in the mushroom-forming basidiomycete *Schizophyllum commune*. *Appl. Environ. Microbiol.* **2009**, *75*, 4648–4652.
21. Gemmill, T.R.; Trimble, R.B. Overview of N- and O-linked oligosaccharide structures found in various yeast species. *Biochim. Biophys. Acta* **1999**, *1426*, 227–237.
22. Wilson, I.B.; Zeleny, R.; Kolarich, D.; Staudacher, E.; Stroop, C.J.; Kamerling, J.P.; Altmann, F. Analysis of asn-linked glycans from vegetable foodstuffs: Widespread occurrence of lewis a, core alpha1,3-linked fucose and xylose substitutions. *Glycobiology* **2001**, *11*, 261–274.
23. Duman, J.G.; Miele, R.G.; Liang, H.; Grella, D.K.; Sim, K.L.; Castellino, F.J.; Bretthauer, R.K. O-mannosylation of *Pichia pastoris* cellular and recombinant proteins. *Biotechnol. Appl. Biochem.* **1998**, *28*, 39–45.
24. Heuts, D.P.H.M.; Scrutton, N.S.; McIntire, W.S.; Fraaije, M.W. What's in a covalent bond? On the role and formation of covalently bound flavin cofactors. *FEBS J.* **2009**, *276*, 3405–3427.
25. Scrutton, S. Identification of Covalent Flavoproteins and Analysis of the Covalent Link. In *Methods in Molecular Biology: Flavoprotein Protocols*; Chapman, K., Reid, A., Eds.; Humana Press Inc.: Totowa, NJ, USA, 1999; Volume 131, pp. 181–193.
26. Hecht, H.J.; Kalisz, H.M.; Hendle, J.; Schmid, R.D.; Schomburg, D. Crystal structure of glucose oxidase from *Aspergillus niger* refined at 2.3 å resolution. *J. Mol. Biol.* **1993**, *229*, 153–172.
27. Graf, M.M.; Bren, U.; Haltrich, D.; Oostenbrink, C. Molecular dynamics simulations give insight into D-glucose dioxidation at C2 and C3 by *Agaricus meleagris* pyranose dehydrogenase. *J. Comput. Aided Mol. Des.* **2013**, *27*, 295–304.
28. Liu, D.; Coloe, S.; Baird, R.; Pedersen, J. Rapid mini-preparation of fungal DNA for PCR. *J. Clin. Microbiol.* **2000**, *38*, 471.
29. Lin-Cereghino, J.; Wong, W.W.; Xiong, S.; Giang, W.; Luong, L.T.; Vu, J.; Johnson, S.D.; Lin-Cereghino, G.P. Condensed protocol for competent cell preparation and transformation of the methylotrophic yeast *Pichia pastoris*. *BioTechniques* **2005**, *38*, 44–48.

30. Weis, R.; Luiten, R.; Skranc, W.; Schwab, H.; Wubbolts, M.; Glieder, A. Reliable high-throughput screening with *Pichia pastoris* by limiting yeast cell death phenomena. *FEMS Yeast Res.* **2004**, *5*, 179–189.
31. Artimo, P.; Jonnalagedda, M.; Arnold, K.; Baratin, D.; Csardi, G.; de Castro, E.; Duvaud, S.; Flegel, V.; Fortier, A.; Gasteiger, E.; *et al.* Expasy: Sib bioinformatics resource portal. *Nucleic Acids Res.* **2012**, *40*, W597–W603.
32. Altschul, S.F.; Madden, T.L.; Schäffer, A.A.; Zhang, J.; Zhang, Z.; Miller, W.; Lipman, D.J. Gapped blast and psi-blast: A new generation of protein database search programs. *Nucleic Acids Res.* **1997**, *25*, 3389–3402.
33. Laemmli, U.K. Cleavage of structural proteins during the assembly of the head of bacteriophage t4. *Nature* **1970**, *227*, 680–685.

© 2013 by the authors; licensee MDPI, Basel, Switzerland. This article is an open access article distributed under the terms and conditions of the Creative Commons Attribution license (http://creativecommons.org/licenses/by/3.0/).

Supplemental Figure 1. Multiple sequence alignment of PDH protein sequences using the MUSCLE algorithm. Black shaded areas indicate homology, grey shaded areas indicate amino acids with similar properties. Amino acids discussed in the text and predicted glycosylation sites are marked in red and green.

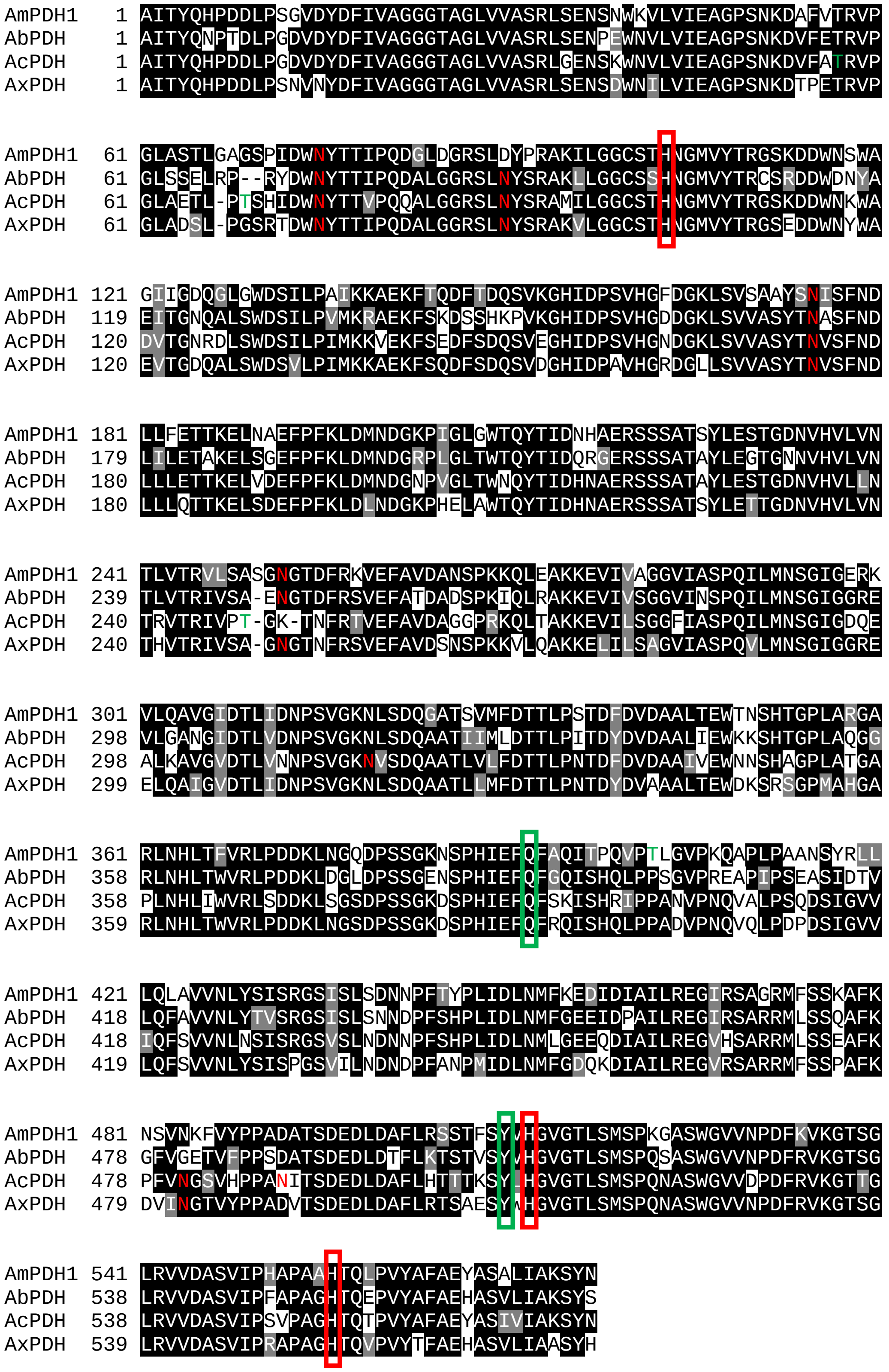

```
AmPDH1   1 AITYQHPDDLPSGVDYDFIVAGGGTAGLVVASRLSENSNWKVLVIEAGPSNKDAFVTRVP
AbPDH    1 AITYQNPTDLPGDVDYDFIVAGGGTAGLVVASRLSENPEWNVLVIEAGPSNKDVFETRVP
AcPDH    1 AITYQHPDDLPGDVDYDFIVAGGGTAGLVVASRLGENSKWNVLVIEAGPSNKDVFATRVP
AxPDH    1 AITYQHPDDLPSNVNYDFIVAGGGTAGLVVASRLSENSDWNILVIEAGPSNKDTPETRVP

AmPDH1  61 GLASTLGAGSPIDWNYTTIPQDGLDGRSLDYPRAKILGGCSTHNGMVYTRGSKDDWNSWA
AbPDH   61 GLSSELRP--RYDWNYTTIPQDALGGRSLNYSRAKLLGGCSSHNGMVYTRCSRDDWDNYA
AcPDH   61 GLAETL-PTSHIDWNYTTVPQQALGGRSLNYSRAMILGGCSTHNGMVYTRGSKDDWNKWA
AxPDH   61 GLADSL-PGSRTDWNYTTIPQDALGGRSLNYSRAKVLGGCSTHNGMVYTRGSEDDWNYWA

AmPDH1 121 GIIGDQGLGWDSILPAIKKAEKFTQDFTDQSVKGHIDPSVHGFDGKLSVSAAYSNISFND
AbPDH  119 EITGNQALSWDSILPVMKRAEKFSKDSSHKPVKGHIDPSVHGDDGKLSVVASYTNASFND
AcPDH  120 DVTGNRDLSWDSILPIMKKVEKFSEDFSDQSVEGHIDPSVHGNDGKLSVVASYTNVSFND
AxPDH  120 EVTGDQALSWDSVLPIMKKAEKFSQDFSDQSVDGHIDPAVHGRDGLLSVVASYTNVSFND

AmPDH1 181 LLFETTKELNAEFPFKLDMNDGKPIGLGWTQYTIDNHAERSSSATSYLESTGDNVHVLVN
AbPDH  179 LILETAKELSGEFPFKLDMNDGRPLGLTWTQYTIDQRGERSSSATAYLEGTGNNVHVLVN
AcPDH  180 LLLETTKELVDEFPFKLDMNDGNPVGLTWNQYTIDHNAERSSSATAYLESTGDNVHVLLN
AxPDH  180 LLLQTTKELSDEFPFKLDLNDGKPHELAWTQYTIDHNAERSSSATSYLETTGDNVHVLVN

AmPDH1 241 TLVTRVLSASGNGTDFRKVEFAVDANSPKKQLEAKKEVIVAGGVIASPQILMNSGIGERK
AbPDH  239 TLVTRIVSA-ENGTDFRSVEFATDADSPKIQLRAKKEVIVSGGVINSPQILMNSGIGGRE
AcPDH  240 TRVTRIVPT-GK-TNFRTVEFAVDAGGPRKQLTAKKEVILSGGFIASPQILMNSGIGDQE
AxPDH  240 THVTRIVSA-GNGTNFRSVEFAVDSNSPKKVLQAKKELILSAGVIASPQVLMNSGIGGRE

AmPDH1 301 VLQAVGIDTLIDNPSVGKNLSDQGATSVMFDTTLPSTDFDVDAALTEWTNSHTGPLARGA
AbPDH  298 VLGANGIDTLVDNPSVGKNLSDQAATIIMLDTTLPITDYDVDAALIEWKKSHTGPLAQGG
AcPDH  298 ALKAVGVDTLVNNPSVGKNVSDQAATLVLFDTTLPNTDFDVDAAIVEWNNSHAGPLATGA
AxPDH  299 ELQAIGVDTLIDNPSVGKNLSDQAATLLMFDTTLPNTDYDVAAALTEWDKSRSGPMAHGA

AmPDH1 361 RLNHLTFVRLPDDKLNGQDPSSGKNSPHIEFQFAQITPQVPTLGVPKQAPLPAANSYRLL
AbPDH  358 RLNHLTWVRLPDDKLDGLDPSSGENSPHIEFQFGQISHQLPPSGVPREAPIPSEASIDTV
AcPDH  358 PLNHLIWVRLSDDKLSGSDPSSGKDSPHIEFQFSKISHRIPPANVPNQVALPSQDSIGVV
AxPDH  359 RLNHLTWVRLPDDKLNGSDPSSGKDSPHIEFQFRQISHQLPPADVPNQVQLPDPDSIGVV

AmPDH1 421 LQLAVVNLYSISRGSISLSDNNPFTYPLIDLNMFKEDIDIAILREGIRSAGRMFSSKAFK
AbPDH  418 LQFAVVNLYTVSRGSISLSNNDPFSHPLIDLNMFGEEIDPAILREGIRSARRMLSSQAFK
AcPDH  418 IQFSVVNLNSISRGSVSLNDNNPFSHPLIDLNMLGEEQDIAILREGVHSARRMLSSEAFK
AxPDH  419 LQFSVVNLYSISPGSVILNDNDPFANPMIDLNMFGDQKDIAILREGVRSARRMFSSPAFK

AmPDH1 481 NSVNKFVYPPADATSDEDLDAFLRSSTFSYVHGVGTLSMSPKGASWGVVNPDFKVKGTSG
AbPDH  478 GFVGETVFPPSDATSDEDLDTFLKTSTVSYVHGVGTLSMSPQSASWGVVNPDFRVKGTSG
AcPDH  478 PFVNGSVHPPANITSDEDLDAFLHTTTKSYLHGVGTLSMSPQNASWGVVDPDFRVKGTTG
AxPDH  479 DVINGTVYPPADVTSDEDLDAFLRTSAESYWHGVGTLSMSPQNASWGVVNPDFRVKGTSG

AmPDH1 541 LRVVDASVIPHAPAAHTQLPVYAFAEYASALIAKSYN
AbPDH  538 LRVVDASVIPFAPAGHTQEPVYAFAEHASVLIAKSYS
AcPDH  538 LRVVDASVIPSVPAGHTQTPVYAFAEYASIVIAKSYN
AxPDH  539 LRVVDASVIPRAPAGHTQVPVYTFAEHASVLIAASYH
```

Supplemental Table 1 . Oligonucleotide primer sequences (restriction sites are underlined)

Primer Name	**Sequence 5‘→3‘**
Anchor	GGCCACGCGTCGACTAGTACTTTTTTTTT
Universal	GGCCACGCGTCGACTAGTAC
AxTSP1	CCAGTCTGAATTCTCACTGAGGC
AxTSP2	CCACCAGCAACGATGAAGTCGT
AxTSP3	CTGGGTGCTGGTACGTGATGGC
AcTSP1	CACCGCCAGCAACGATGAAG
AcTSP2	ACATCACCAGGCAAATCATCTG
AcTSP3	AGGTGATCGCACTACGTGCAAC
AcPDHfwd1	CTC**(G/T)**TTTC**(C/T)**CTCGCATTA**(C/T)**TAGGC
AcPDHfwd2	TACTGGTCATCGAGGCCGG
AcPDHfwd3	TCAG**(A/G)**TCCTCATGAATTC
AcPDHfwd	ATGGCGAGGTTCAACGCCCGGCTC
AcPDHrev	TTAGTTGTAGCTCTTCGCTATCAC
AcPDHKpnIfwd	TCCTGGGTACCATGGCGAGGTTCAACGCCCGGCT
AcPDHNotIrev	AGGATGCGGCCGCTTAGTTGTAGCTCTTCGCTAT
AxKpnIfwd	GTCAAGGTACCATGTTCCCTCGAGTGGCCG
AxNotIrev	ATAATGCGGCCGCTCAGTGGTAGCTCGCCGCGA
AxPDHfwd	ATGTTCCCTCGAGTGGCCGG
AxPDHrev	TCAGTGGTAGCTCGCCGCGAT
5AcPDH	GAGGCATCGCATCCTTGCGCAG

Supplemental Figure 2. Identification of covalent flavoproteins by SDS-PAGE and fluorescence detection. 1, AmPDH; 2, AcPDH; M, molecular marker; 3, AxPDH; 4, GOx from *A. niger*.

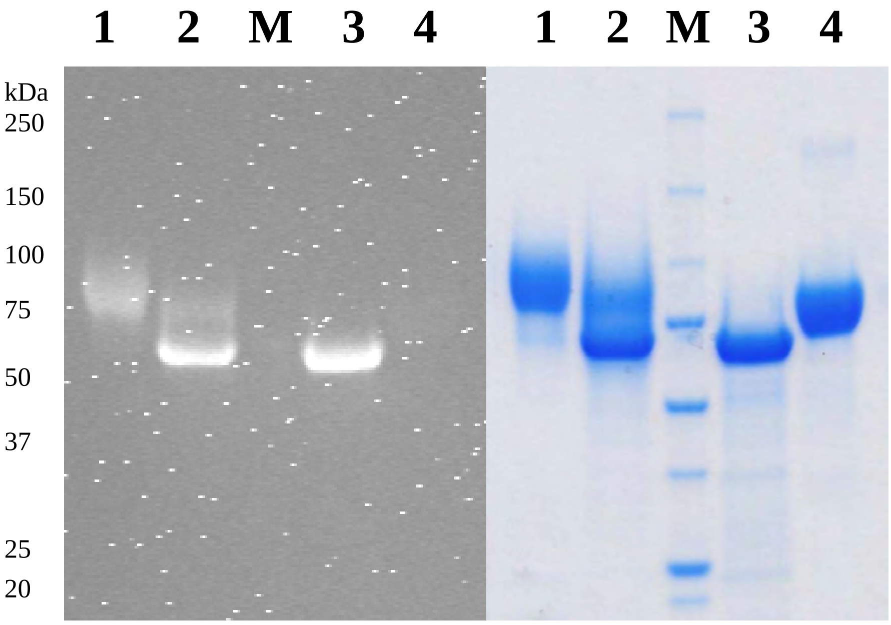
1
2
M
3
4
1
2
M
3
4
kDa
250
150
100
75
50
37
25
20

Supplemental Figure 3. UV-Vis spectrum of oxidized AcPDH.

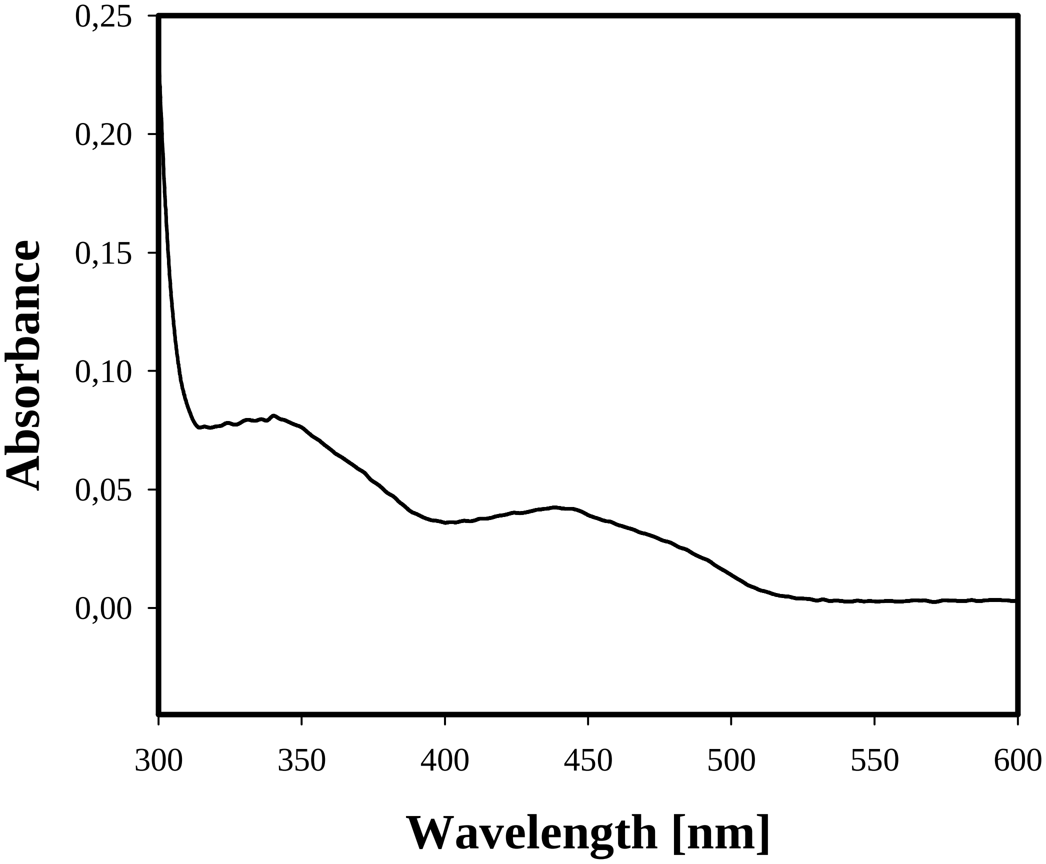

Paper II

Appl Microbiol Biotechnol (2012) 94:695–704
DOI 10.1007/s00253-011-3667-7

BIOTECHNOLOGICALLY RELEVANT ENZYMES AND PROTEINS

Simple and efficient expression of *Agaricus meleagris* pyranose dehydrogenase in *Pichia pastoris*

Christoph Sygmund · Alexander Gutmann · Iris Krondorfer · Magdalena Kujawa · Anton Glieder · Beate Pscheidt · Dietmar Haltrich · Clemens Peterbauer · Roman Kittl

Received: 5 August 2011 / Revised: 24 September 2011 / Accepted: 22 October 2011 / Published online: 13 November 2011
© The Author(s) 2011. This article is published with open access at Springerlink.com

Abstract Pyranose dehydrogenase (PDH) is a fungal flavin-dependent sugar oxidoreductase that is highly interesting for applications in organic synthesis or electrochemistry. The low expression levels of the filamentous fungus *Agaricus meleagris* as well as the demand for engineered PDH make heterologous expression necessary. Recently, *Aspergillus* species were described to efficiently secrete recombinant PDH. Here, we evaluate recombinant protein production with expression hosts more suitable for genetic engineering. Expression in *Escherichia coli* resulted in no soluble or active PDH. Heterologous expression in the methylotrophic yeast *Pichia pastoris* was investigated using two different signal sequences as well as a codon-optimized sequence. A 96-well plate activity screening for transformants of all constructs was established and the best expressing clone was used for large-scale production in 50-L scale, which gave a volumetric yield of 223 mg L^{-1} PDH or 1,330 UL^{-1} d^{-1} in space–time yield. Purification yielded 13.4 g of pure enzyme representing 95.8% of the initial activity. The hyperglycosylated recombinant enzyme had a 20% lower specific activity than the native enzyme; however, the kinetic properties were essentially identical. This study demonstrates the successful expression of PDH in the eukaryotic host organism *P. pastoris* paving the way for protein engineering. Additionally, the feasibility of large-scale production of the enzyme with this expression system together with a simplified purification scheme for easy high-yield purification is shown.

Keywords Pyranose dehydrogenase · *Pichia pastoris* · Heterologous expression · Agaricus · Large scale · Microscale

Introduction

Pyranose dehydrogenase (PDH; pyranose/acceptor oxidoreductase, EC 1.1.99.29) is a flavin-dependent sugar oxidoreductase (Volc et al. 1997, 2001; Kujawa et al. 2007; Sygmund et al. 2008; Morrison et al. 1999). It is an extracellular, glycosylated enzyme mainly found in a relatively narrow group of litter-decomposing fungi belonging to the Agaricaceae (Volc et al. 2001). The biological role of pyranose dehydrogenase in fungi still remains unclear although the enzyme is thought to participate in lignocellulose degradation. The functions suggested for PDH are the reduction of quinones or radical intermediates formed during lignocellulose degradation preventing their repolymerization (Ander and Marzullo 1997) as well as the production of Fenton's reagent via reduction of metal ions (Kerem et al. 1999) which may attack cellulose, xylan, and lignin.

Pyranose dehydrogenase catalyzes the oxidation of free, nonphosphorylated sugars and the transfer of resulting electrons to a number of (substituted) quinones and

Electronic supplementary material The online version of this article (doi:10.1007/s00253-011-3667-7) contains supplementary material, which is available to authorized users.

C. Sygmund · I. Krondorfer · M. Kujawa · D. Haltrich · C. Peterbauer · R. Kittl (✉)
Department of Food Sciences and Technology,
University of Natural Resources and Applied Life Sciences (BOKU), Muthgasse 11,
1190 Vienna, Austria
e-mail: roman.kittl@boku.ac.at

A. Gutmann · M. Kujawa · A. Glieder · B. Pscheidt
Austrian Centre of Industrial Biotechnology (ACIB),
Petersgasse 14,
8010 Graz, Austria

complexed metal ions rather than to molecular oxygen. It exhibits extremely broad sugar substrate specificity, while in contrast only a rather limited number of electron acceptors are used by the enzyme. Unlike other sugar oxidoreductases like cellobiose dehydrogenase or pyranose 2-oxidase, which exclusively oxidize sugars at the C-1 and C-2, respectively, PDH is able to oxidize at C-1 to C-4 with C-2 and/or C-3 predominating, depending on the structure of the sugar (mono-, di-, oligo-saccharide, or glycoside) and the source of the enzyme.

Because of these unique properties, PDH is of interest for a number of technological applications, recently reviewed by Peterbauer and Volc (2010). Among these is the conversion of carbohydrates to interesting products for the food industry, e.g., the conversion of D-galactose to D-tagatose via 2-keto-D-galactose (Giffhorn 2000; Giffhorn et al. 2000). Plain di/tricarbonyl sugars as the main reaction products of PDH could serve as basis for the synthesis of amino sugar moieties of homologues to amino glycoside antibiotics (Reitz and Baxter 1990). The relaxed substrate specificity of PDH makes it an attractive target for further improvements of its reactivity with derivatives of already established substrates such as aromatic glycosides, which may provide new attractive building blocks for synthesis of carbohydrate-based drugs.

A different, very promising application for PDH is its use as anodic biocatalyst in enzymatic biofuel cells, which transform chemical to electrical energy via electrochemical reactions (Barton et al. 2004; Bullen et al. 2006). PDH was successfully “wired” to electrodes using osmium redox polymers and was shown to be suitable for this application (Tasca et al. 2007; Zafar et al. 2010). Apart from being able to provide a second pair of electrons per sugar molecule if double oxidation occurs, PDH’s inactivity with molecular oxygen can be considered an advantage. Unlike in biofuel cells, employing glucose oxidase or pyranose oxidase no harmful H_2O_2 is being formed as a byproduct, avoiding potential oxidative damage to the enzyme or the redox polymer, thereby prolonging the endurance of the biofuel cell. A possibility to increase the power output of a PDH biofuel cell would be to lower the redox potential of the enzyme. This, as well as increasing the activity of PDH with technologically important substrates, could be targeted by protein engineering.

In the past few years, rational and semirational design approaches have shown to be very useful in improving enzyme properties (Lutz 2010). Crucial for success is expression of site-directed mutants or saturation mutagenesis libraries of the target gene with high yields in a genetically easy to manipulate expression host (bacteria and yeasts).

The gene of PDH1 from *Agaricus meleagris* was the first identified and isolated PDH-encoding gene (Kittl et al. 2008) and was recently expressed in *Aspergillus* spp. (Pisanelli et al. 2010). Hereby, we describe for the first time the successful heterologous expression of a PDH gene in the methylotrophic yeast *Pichia pastoris* and the scalability of production and purification of the enzyme on larger scale.

Materials and methods

Chemicals and microorganisms

All chemicals were of the highest purity grade available and were purchased from Sigma (St. Louis, MO, USA) unless stated otherwise. Restriction endonucleases, T4 DNA ligase and DNA-modifying enzymes were obtained from Fermentas unless stated otherwise and were used as recommended by the manufacturer. Nucleic acid amplifications were done employing Phusion High-Fidelity DNA Polymerase (New England Biolabs, Ipswich, MA, USA), dNTP mix, oligonucleotide primers (Invitrogen, Carlsbad, CA, USA), and a GeneAmp PCR System 2700 thermocycler (Applied Biosystems, Foster City, CA, USA). The *pdh1* gene coding for pyranose dehydrogenase from the basidiomycete *A. meleagris* (GenBank accession number AY753307) has been previously isolated and cloned into the pCR Blunt II TOPO vector (Kittl et al. 2008). *Escherichia coli* strain DH5α-T1 was used for subcloning and BL21 DE3 for expression (Invitrogen). *P. pastoris* strain CBS 7435 was used for expression. Ferrocenium hexafluorophosphate and the substituted quinones were from Aldrich (Steinheim, Germany). Phenyl-Sepharose Fast Flow resin was purchased from Amersham Pharmacia Biotech (Uppsala, Sweden) while DEAE Sepharose Fast Flow resin was from GE Healthcare (Chafont St. Giles, UK). PNGaseF was purchased from NewEnglandBiolabs.

Construction of a *pdh1* expression vector for *E. coli*

The *pdh1* gene from *A. meleagris* was amplified from the published plasmid pdh1 in pCR Blunt II TOPO vector (Kittl et al. 2008) using the primers 5pdhN-Nde and 3pdhN-Hind. Nucleotide sequences of all primers used in this work are shown in Table 1. The polymerase chain reaction (PCR) fragment was cut with the restriction enzymes *Nde*I and *Hind*III and ligated into the equally treated expression vector pET21a. The resulting plasmid pET21a*pdh1* was transformed into electrocompetent *E. coli* BL21 DE3 for expression under control of the T7 promoter.

Expression of *pdh1* in *E. coli*

E. coli cells carrying the pET21a*pdh1* plasmid were grown in TB medium (12 gL^{-1} peptone from casein, 24 gL^{-1}

Table 1 Oligonucleotide primer sequences (restriction sites are underlined)

Name	Sequence 5′-3′
5pdhN-Nde	TGCACATATGGCTATCACGTACCAACACC
3pdhN-Hind	CGAATAAGCTTAGTTATAACTCTTTGC
5pdhN-Asc	TCAAGGCGCGCCCGAAACGATGCTGCCTCGAGTGACC
3pdhN-Not	AGATGCGGCCGCTTAGTTATAACTCTTTGCTATCAACG
5pdhS-Eco	ATTCAAGAATTCCGAAACGATG
3pdhS-Not	AGATGCGGCCGCTTAATTG
5alpha-Eco	AAAGAATTCCGAAACGATGAGATTCCC
5alpha-Asc	AAAGGCGCGCCGAAACGATGAGATTCC
3alpha	AGCTTCGGCCTCTCTCTTCTCG
5pdhN-alpha	CGAGAAGAGAGAGGCCGAAGCTGCTATCACGTACCAACACC
5pdhS-alpha	CGAGAAGAGAGAGGCCGAAGCTGCTATCACCTATCAACACC

yeast extract and 4 mL L^{-1} glycerol in 100 mM potassium phosphate buffer, pH 7.5) and induced with two concentrations of IPTG (0.01, 0.10 mM) as well as 0.5% lactose at a 100-mL scale in baffled flasks at 140 rpm and 25 °C overnight. Ten milliliter of the cultures were centrifuged at 4,000×*g* for 10 min at 4 °C, the cell pellets were resuspended in breaking buffer (50 mM potassium phosphate buffer pH 6.5 supplemented with 300 μM PMSF) and broken using a French press. After ultracentrifugation (30,000×*g*, 30 min, 4 °C) the crude extract was tested for enzyme activity and the pellet was analyzed for insoluble PDH. Sodium dodecyl sulfate polyacrylamide gel electrophoresis (SDS-PAGE) was performed on commercial 8–25% acrylamide gels with silver staining of protein bands. Electrophoresis and the staining procedure were done with the PhastSystem (Pharmacia) according to manufacturer's recommendations.

Codon optimization of *pdh1* for expression in *P. pastoris*

The open reading frame of the *pdh1* gene from *A. meleagris* and the *Saccharomyces cerevisiae* α-factor sequence were codon-optimized with the program GeneDesigner from DNA2.0 (https://www.dna20.com/genedesigner2) employing the high-methanol codon usage of *P. pastoris* (Abad et al. 2010), which was calculated based on the genes for alcohol oxidase1 (AOX1), DAS, FLD1, and HbHNL using the DOS program GCUA (http://gcua.schoedl.de). Additionally, mRNA 3′-end processing signals and restriction enzyme recognition sequences (*Eco*RI, *Not*I, *Bgl*II, *Sac*I) were eliminated. The resulting sequences were checked with the program Leto1.0 from Entelechon (www.entechelon.com) for avoiding strong stem-loop structures of the mRNA that were identified by GeneBee (http://www.genebee.msu.ru/). The synthetic gene was ordered from GenScript Corporation (Piscataway, NJ, USA) with the native leader sequence and the flanking restriction sites *Eco*RI and *Not*I. For sequences, see Electronic supplementary material.

Construction of *pdh1* expression vectors for *P. pastoris*

The *pdh1* cDNA and the synthetic gene were amplified with the primer pairs 5pdhN-Asc/3pdhN-Not and 5pdhS-Eco/3pdhS-Not, respectively. Both PCR products were digested with the respective restriction enzymes and ligated into the equally treated vector pPpT2 (Abad et al. 2010; Ruth et al. 2010). Replacement of the α-factor-derived sequence with that of the native signal sequence was done by overlap extension PCR. To this end, the whole α-factor pre–pro leader sequence was amplified with the primers 5alpha-Eco and 3alpha for fusion with the synthetic gene and with 5alphaAsc and 3alpha for fusion with the native gene. These PCR products were finally fused to the corresponding sequences encoding the mature proteins that were amplified with 5pdhS-alpha/3pdhS-Not or 5pdhN-alpha/3pdhN-Not. The resulting PCR products were cut with the respective restriction enzymes and ligated into the equally digested shuttle vector pPpT2. An overview of the constructs is presented in Table 2. After transformation of the constructs into chemically competent *E. coli* DH5α-T1 cells, the plasmids were proliferated, linearized with the respective restriction enzymes, and transformed into electrocompetent *P. pastoris*. Electrocompetent *Pichia* cells were prepared and transformed following the condensed protocol of Lin-Cereghino et al. (2005). For selection, Zeocin was used in a final concentration of 100 μg mL^{-1}. The resulting colonies were picked and grown in 96-well deep well plates.

Microscale cultivation in deep well plates

Microscale cultivation and expression in 96-well deep well plates was done according to Weis et al. (2004) with some

Table 2 Overview of *pdh1* constructs used for expression in *P. pastoris* in deep-well plates

Construct	Leader	Gene	Number of screened transformants	Maximum activity (U mL^{-1})
α-PDH_nat	α-Factor	Native	176	nd
n-PDH_nat	Native	Native	352	0.57
α-PDH_syn	α-Factor	Synthetic	84	nd
n-PDH_syn	Native	Synthetic	252	0.36

nd Not detectable

modifications. Cells were grown in 250 µL BMD1 (1.34% yeast nitrogen base, 4×10^{-5}% biotin, 1% glucose, 200 mM potassium phosphate, pH 6.0) at 28 °C, 320 rpm, and 80% humidity for approximately 60 h to reach the stationary growth phase. BMM2 medium (250 µL; 1.34% yeast nitrogen base, 4×10^{-5}% biotin, 1% methanol, and 200 mM potassium phosphate, pH 6.0) was added so that it gave a final concentration of 0.5% methanol. About 70, 82, and 108 h after the start of the cultivation, 50 µL BMM10 (BMM2 with 5% methanol) were added to keep up induction. After a total of 130 h, the cultivation was stopped. The deep-well plates were centrifuged at 4,000 rpm and 4 °C for 10 min and the supernatants were used for enzyme activity assays in microtiter plates.

Large-scale production of *rec*PDH1 in *P. pastoris*

A fed-batch cultivation was carried out in a 60-L computer-controlled stirred tank reactor (Applikon, Schiedam, The Netherlands) with an initial volume of 40 L fermentation basal salts medium (21 mL L^{-1} H_3PO_4 (85%); 0.93 gL^{-1} $CaSO_4{\cdot}2H_2O$; 14.9 gL^{-1} $MgSO_4{\cdot}7H_2O$; 18.2 gL^{-1} K_2SO_4; 4.13 gL^{-1} KOH; 4% (*v*/*v*) glycerol) supplemented with 4.35 mL L^{-1} PTM1 trace salts (Invitrogen) and 10 mL Antifoam 204 (Sigma, St. Louis, MO, USA).

Temperature, dissolved oxygen (DO), and pH were monitored online by the Bio Controller ADI 1030 (Applikon). Oxygen concentration was regulated to a minimum of 4% and kept constant by supplying sterile-filtered air and adjusting stirrer velocity. Temperature was set to 30 °C and the pH value was regulated to 5 and kept constant by addition of ammonium hydroxide solution. Fifteen 1-L baffled shaking flasks containing 300 mL YPD-Zeocin medium each (10 gL^{-1} yeast extract, 20 gL^{-1} peptone from casein, 4 gL^{-1} glucose, and 25 mg L^{-1} Zeocin) were inoculated with *P. pastoris* strain n-PDH_natCC11 and grown overnight at 30 °C and 150 rpm. This preculture was used for inoculation of the fermenter (10% *v*/*v*).

When the initially added glycerol was consumed completely (indicated by a DO spike after 13.5 h), a glycerol feed (50% glycerol supplemented with 12 mL L^{-1} PTM1 trace salts) was started. Recombinant protein production was induced after 40 h of fermentation by feeding methanol (100% methanol supplemented with 12 mL L^{-1} PTM1 trace salts). The feed rate was adjusted at constant air flow rate and stirrer speed to a DO of 4%. After 180 h of cultivation, the fermenter was harvested, cells were separated from the culture medium by centrifugation at 4,000×*g*, 4 °C for 10 min (Sorvall Evolution RC, Kendro Laboratory Products, Newtown, CT, USA) and the supernatant was recovered as a crude enzyme preparation.

Samples of the fermentation broth were taken periodically; wet biomass was determined by centrifugation (Eppendorf Centrifuge 5424, Hamburg, Germany) for 10 min at 14,000×*g* and weighing of the pellet. PDH activity was measured with the standard assay and soluble protein concentration was determined according to Bradford.

Purification of recombinant PDH1

*rec*PDH1 was purified at room temperature by hydrophobic interaction chromatography and anion exchange chromatography. $(NH_4)_2SO_4$ was added to the crude extract to 30% saturation, clarified by centrifugation and the solution was loaded onto a Phenyl-Sepharose Fast Flow column (8,500 mL; flow rate 330 mL min^{-1}) equilibrated with 50 mM phosphate buffer (pH 6.5, 1.5 M $(NH_4)_2SO_4$). After washing the column with 1 column volume (CV) of the same buffer, *rec*PDH1 was eluted with a linear gradient of starting buffer to 50 mM phosphate buffer (pH 6.5) in 1 CV and fractions were collected.

Fractions with high PDH activity were concentrated and desalted to a conductivity equal to or less than 2 mS cm^{-1} using cross-flow filtration (Microza ultrafiltration module, Pall Austria Filter GmbH, Vienna, Austria). A pool of the fractions containing highest activity was loaded onto a DEAE Sepharose Fast Flow anion exchange chromatography column (500 mL) equilibrated with 50 mM Bis Tris buffer (pH 6) and washed with 1 CV of this buffer. For elution, a linear salt gradient (0–1 M NaCl in 50 mM Bis Tris, pH 6) was run in 10 CV at 10 mL min^{-1}.

Fractions with the highest activities were pooled, concentrated (Vivaflow 50 module, Sartorius AG, Göttingen, Germany), aliquoted, and stored at −30 °C.

Enzyme assay

Pyranose dehydrogenase activity was determined by following spectrophotometrically the D-glucose-dependent reduction of the ferrocenium ion (Fc^+) to ferrocene at 300 nm (ε_{300}=4.3 mM^{-1} cm^{-1}) for 3 min at 30 °C (Kujawa et al. 2007). One unit of PDH activity was defined as the amount of enzyme required for the reduction of 2 µmol of Fc^+ ion per minute.

Molecular properties

The protein concentration was determined by the method of Bradford using a prefabricated assay from Bio-Rad Laboratories (Hercules, CA, USA) and bovine serum albumin as the standard. SDS-PAGE was carried out using Mini-PROTEAN TGX precast gels with a denaturing gradient of 4–20%. Protein bands were visualized by staining with Bio-Safe Coomassie; Dual Color Precision Plus Protein Standard was used for mass determination. All procedures were done according to the manufacturer's recommendations (Bio-Rad).

Enzymatic deglycosylation

Deglycosylation of a 15-µg sample of PDH was performed with peptide/*N*-glycosidase F, which cleaves the bond between *N*-acetyl-glucosamine. All procedures of the enzymatic deglycosylation of PDH with PNGaseF under denaturing conditions were done according to the manufacturer's recommendations.

Kinetic properties

Apparent kinetic constants for D-glucose, D-maltose, L-arabinose, and lactose were measured using the standard ferrocenium assay as described earlier. Kinetic constants for the electron acceptors 1,4-benzoquinone, 2-chloro-1,4-benzoquinone, and Fc^+ hexafluorophosphate were determined with 25 mM glucose as electron donor. The pH dependence of PDH activity with different electron acceptors was determined with the following buffers: 100 mM citrate (pH 2.5–6.0), 100 mM phosphate (pH 6.0–8.0), and 100 mM borate (pH 8.0–9.0). All kinetic constants were calculated by nonlinear least-squares regression, fitting the observed data to the Henri–Michaelis–Menten equation. Turnover numbers (k_{cat}) and catalytic efficiencies (k_{cat}/K_m) were calculated using the molecular mass.

Results

Expression of *pdh1* in *E. coli*

The *E. coli* expression plasmid pET21a*pdh1* was constructed by cloning the nucleotide sequence of mature PDH1 into the pET21a expression vector under control of the T7 promoter. Transformed *E. coli* BL21 (DE3) cultures carrying the plasmid were grown under different inducing conditions. Cultures were harvested 16 h after induction with 0.01 and 0.1 mM IPTG as well as with 0.5% lactose, reaching an OD_{600} of roughly 11. Harvested cells were resuspended in lysis buffer (three times the weight of the wet biomass of the sample) and disrupted using a French press. Disruption efficiencies were compared by measuring total protein concentration of the cleared lysate and varied between 1.1 and 2.0 mg/mL (corresponding to 4.4–8.0 mg of protein per gram of cell paste). Crude extracts were tested for PDH activity using the standard enzyme assay. Unspecific background of a crude extract from an equally treated culture of *E. coli* BL21 (DE3) cells carrying the empty pET21a vector was subtracted from the measurements. No significant PDH activity was measured in any of the cultures. SDS-PAGE analysis of the total soluble proteins of the crude extract showed no band at the expected size (62 kDa) of PDH (data not shown). The insoluble part of the crude extract was tested for the possible existence of inclusion bodies of PDH on an SDS-PAGE gel (data not shown). The majority of insoluble proteins were roughly the size of purified native PDH.

Expression of *pdh1* in *P. pastoris*

Several constructs for extracellular expression of *pdh1* in *P. pastoris* were designed, all of them under control of

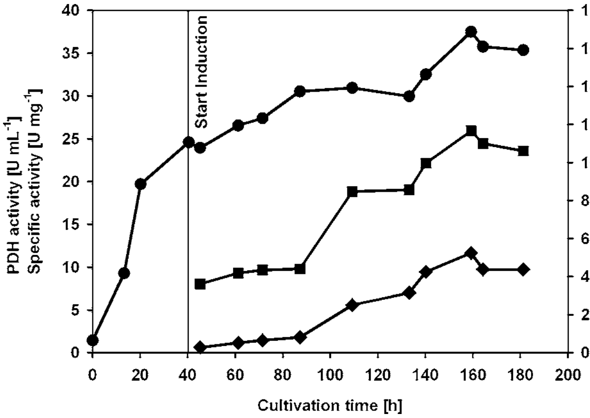

Fig. 1 Large-scale fermentation of *P. pastoris* n-PDH_natCC11. *Circles* wet biomass, *squares* specific activity, *diamonds* volumetric activity. The measurements were done in duplicates and the error was always less than 5%

Table 3 Purification of recombinant PDH1 from *A. meleagris*

	Total activity (U)	Total protein (g)	Volume (L)	Specific activity (U mg^{-1})	Purification (-fold)	Activity yield (%)
Culture supernatant	517,000	22.6	51.5	22.9	1.0	100
Phenyl Sepharose FF	675,000[a]	19	15.4	35.5	1.55	130.6[a]
DEAE Sepharose FF pool 1[b]	48,100	1.1	0.98	43.7	1.90	10.7
DEAE Sepharose FF pool 2	440,000	12.3	1	35.8	1.57	85.1

[a] PDH activity is higher when ammonium sulfate is present

[b] Determination of kinetic constants was done with protein from this fraction

the inducible AOX1 promoter. For extracellular expression with the native signal sequence, the full-length open reading frames of *pdh1* and the gene sequence optimized for expression in *P. pastoris* (*synpdh1*) were cloned into the vector pPpT2 (Abad et al. 2010; Ruth et al. 2010). To test the efficiency of the native leader sequence, it was exchanged to a codon optimized α-factor pre–pro leader peptide of *S. cerevisiae* by overlap extension PCR.

All resulting constructs were transformed into *P. pastoris* strain CBS 7435, cultivated in 96-well deep well plates, and screening for PDH activity (Table 2). On day 6 of the cultivation with approximately 72 h of induction by methanol, supernatants were tested for PDH activity. Constructs with the α-factor leader sequence showed no significant PDH activity. In contrast, constructs with the native leader sequence resulted in *P. pastoris* transformants secreting active recombinant PDH1 (*rec*PDH1). Overall, no significant difference in average activity could be observed when comparing the expression levels of all tested native with synthetic gene constructs. The standard deviation within one group of constructs was always approximately 10%, which shows the uniformity of the 96-well deep well plate screening and proves its suitability for high-throughput screening. To confirm the results from the first round of screening, a rescreening experiment with multiple parallel determinations was performed. The three synthetic gene transformants selected for the rescreen yielded an average volumetric PDH activity of around 0.31 UmL^{-1}. Three native gene transformants showed a slightly lower average PDH activity of 0.28 UmL^{-1} but clone n-PDH_natCC11 had a volumetric activity of 0.47 UmL^{-1}. This clone was selected for large-scale fermentation.

Scale up of *rec*PDH1 production

P. pastoris clone n-PDH_natCC11, expressing extracellular *rec*PDH1, was cultivated on a 50-L scale in a fed-batch fermentation for a total of 181 h (Fig. 1). The initial glycerol batch phase lasted for 13.5 h and its end, i.e., the exhaustion of the carbon source, was indicated by a sharp increase of the dissolved oxygen level. At this time point, a glycerol feed was started to further increase the cell density. After 40 h of cultivation, when the wet biomass had reached 111 gL^{-1}, the glycerol feed was stopped and induction with methanol started by continuously supplying this inducer. Levels of wet biomass reached 159 gL^{-1} during the induction phase and the concentration of soluble protein in the culture supernatant increased from 70 to 440 mg L^{-1}. Volumetric PDH activity in the culture supernatant reached a value of 10,040 UL^{-1} at the time of harvest (corresponding to ~230 mg of *rec*PDH1 per liter) with a specific activity of 22.9 Umg^{-1} total protein.

Purification of recombinant PDH1

*rec*PDH1 was purified by a two-step chromatographic procedure as outlined in Table 3. Hydrophobic interaction chromatography was followed by an anion exchange chromatography step resulting in two pools containing active PDH. Pool 1 represented the center of the elution

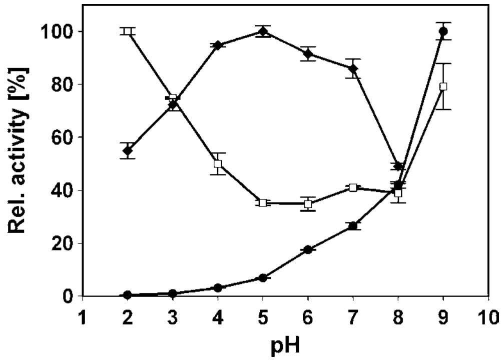

Fig. 2 Effect of pH on the activity of recombinant pyranose dehydrogenase using 25 mM glucose as electron donor and different electron acceptors. Maximum activity measured for each electron acceptor corresponds to 100%. *Empty square* 1,4-benzoquinone, *filled circle* ferrocenium hexafluorophosphate, *filled diamond* 2-chloro-1,4-benzoquinone

Table 4 Apparent kinetic constants of *rec*PDH1 from *A. meleagris* for selected electron acceptor

Substrate		Recombinant PDH1			Native *Am*PDH[a]		
	pH	k_{cat} (s^{-1})	K_m (mM)	k_{cat}/K_m (mM^{-1} s^{-1})	k_{cat} (s^{-1})	K_m (mM)	k_{cat}/K_m (mM^{-1} s^{-1})
1,4-Benzoquinone	4.0	65.4±5.5	1.38±0.28	54.4	76.0±2.3[b]	1.82 ±0.11[b]	57.5[b]
2-Chloro-1,4-benzoquinone	5.0	12.9±1.2	0.62±0.11	20.9	15.1±1.0	0.55±0.11	25.5
Ferrocenium hexafluorophosphate	8.5	130±11	0.16±0.04	812	104±8	0.13±0.03	802

Kinetic data were determined at 30 °C with 25 mM D-glucose as the electron donor

[a] Data from Sygmund et al. (2008)

[b] Measurements were done at pH 3.0

peak and contained a homogenous enzyme preparation as judged by SDS-PAGE. Only 10% of the starting activity could be found in this amber-colored enzyme preparation with a specific activity of 43.6 Umg^{-1} representing a 1.9-fold purification from the culture supernatant. Protein from this pool was used for all further analyses. Since the emphasis of this purification procedure was put on high purification yields, aiming at possible subsequent applications of the enzyme, all other fractions containing PDH with relatively high specific activity were combined in pool 2 resulting in a recovery of 85% with a specific activity of 35.9 Umg^{-1}. In total, 13.4 g of more than 80% pure *rec*PDH1 were obtained.

Catalytic properties

The pH/activity profiles of *rec*PDH1 were measured for the electron acceptors 1,4-benzoquinone, Fc^+ hexafluorophosphate, and 2-chloro-1,4-benzoquinone, using glucose as electron donor (Fig. 2). *rec*PDH1 showed a virtually identical pH behavior compared to the wild-type protein with benzoquinones having their pH optima in the acidic range whereas activity with Fc^+ continually increased with pH in the range of pH 3–9. Apparent kinetic constants for these electron acceptor substrates were determined at those pH values that were previously used for wild-type PDH1 (Table 4). In addition, apparent kinetic constants were determined for selected sugar substrates and compared to those of the wild-type enzyme from *A. meleagris* (Table 5). Catalytic properties of *rec*PDH1 expressed in *P. pastoris* are almost identical to those of the wild-type enzyme (Sygmund et al. 2008).

Molecular properties

The molecular mass of recombinant PDH1 overexpressed in *P. pastoris* was determined to be ~93 kDa by SDS-PAGE (Fig. 3). Deglycoslylation under denaturing conditions using PNGase F reduced the mass of the protein to 64 kDa. This mass corresponds very well to the theoretical molecular mass of 61,967 Da based on the cDNA sequence of mature PDH1. Based on these results, the level of glycosylation of *rec*PDH1 was calculated to be approximately 30%.

Discussion

Production of PDH activity in its natural source, *A. meleagris*, is extremely tedious and time consuming as these cultivations have to be performed in resting shallow cultures for up to 6 weeks. Recently, the PDH1-encoding gene from *A. meleagris* was successfully expressed in

Table 5 Apparent kinetic constants of *rec*PDH1 from *A. meleagris* for selected electron donor substrates

Substrate	Recombinant PDH1			Native *Am*PDH[a]		
	k_{cat} (s^{-1})	K_m (mM)	k_{cat}/K_m (mM^{-1} s^{-1})	k_{cat} (s^{-1})	K_m (mM)	k_{cat}/K_m (mM^{-1} s^{-1})
D-Glucose	37.8±1.1	0.69±0.09	54.8	45.9±0.3	0.82±0.03	57.5
D-Galactose	47.3±3.0	1.07±0.13	44.2	48.5±0.6	1.05±0.05	46.2
D-Xylose	62.4±1.6	1.92±0.14	32.5	43.4±0.8	1.93±0.17	22.9
L-Arabinose	34.7±1.6	0.49±0.05	70.8	37.2±0.6	0.54±0.08	62.1
Lactose	41.0±8.1	128±11.9	0.32	39.6±0.8	134±6.3	0.29

Kinetic data were determined at 30 °C with 0.4 mM ferricenium as the electron acceptor

[a] Data from Sygmund et al. (2008)

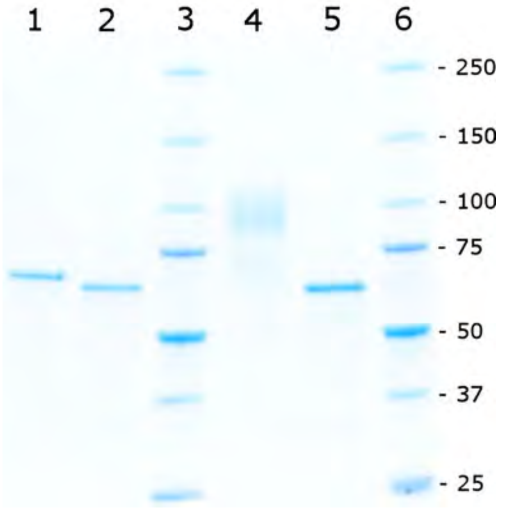

Fig. 3 SDS PAGE analysis of glycosylated and deglycosylated recombinant pyranose dehydrogenase expressed in *P. pastoris* and PDH1 purified from *A. meleagris*. *1* PDH1 from *A. meleagris*, *2* deglycosylated PDH1 from *A. meleagris*, *3* molecular mass marker (Precision Plus Protein Standards, Bio-Rad); *4 rec*PDH1 expressed in *P. pastoris* (purification pool 1), *5* deglycosylated *rec*PDH1 expressed in *P. pastoris* (purification pool 1); *6* molecular mass marker. The gel was stained with Coomassie blue

Aspergillus nidulans and *Aspergillus niger*. By using this approach, the final volumetric activity as well as the space–time yield could be increased significantly with *A. nidulans* as expression host (Pisanelli et al. 2010) compared to production by the natural producer. However, time-consuming transformation protocols and complicated genetic manipulation of *Aspergillus* spp. severely hamper any protein-engineering attempts. Therefore, other microbial expression systems that are better amenable to protein engineering approaches were tested for their ability to produce soluble and active PDH1. Both the prokaryotic host *E. coli* as well as the eukaryotic host *P. pastoris* were selected for expression studies.

The *E. coli* expression construct was designed for expression of PDH1 without *N*-terminal signal peptide. To reduce the possible formation of insoluble recombinant protein cultivation, temperature was lowered to 25 °C and the concentration of the inducer IPTG was varied. Still, PDH1 could only be found as insoluble protein fraction without any enzymatic activity under all tested conditions. One possible reason for the failure of expressing PDH in a prokaryotic system could be the need of glycosylation for correct protein folding as observed previously with other enzymes (Weis et al. 2007). On the other hand, there are examples where random mutagenesis was used to achieve functional expression of fungal proteins in *E. coli* (Sun et al. 2001). A similar strategy could possibly be used for successful expression of PDH1 in *E. coli*. Another key factor that seems to have major impact on PDH expression is the 25-amino acid long signal peptide. As reported earlier, expression levels of PDH1 in *A. nidulans* were much higher compared to the *glaA* signal sequence when its native signal sequence was used (Pisanelli et al. 2010). The same effect was observed in *P. pastoris*, and here it was even more pronounced. No PDH activity could be detected when using the α-factor pre–pro signal sequence although identical constructs containing the native signal sequence showed relatively high expression levels. A similar effect, although less pronounced, was observed for the expression of other proteins in *P. pastoris* before (Colao et al. 2006). A possible reason could be the formation of secondary structures in the mRNA when the α-factor is fused to the *pdh1* gene. However, analysis of the mRNA sequences of the four tested constructs using the program GeneBee (Brodsky et al. 1995) showed that constructs containing the α-factor leader sequence neither have a lower calculated total free energy nor do they form stronger stem–loop structures compared to the sequences with the native signal sequence. The only significant difference with regard to stem–loop formation was between the synthetic gene and the noncodon-optimized sequence. This effect can be explained by the removal of regions capable of forming secondary structures during gene optimization.

A second possible explanation for the failure of expressing PDH1 with the α-factor could be inefficient processing of this signal sequence in combination with the PDH protein sequence. Three proteolytic cleavage steps are necessary to fully process the α-factor pre–pro leader sequence, and especially the efficiency of the last step can be influenced by the amino acids surrounding the cleavage site (Goda et al. 2000; Almeida et al. 2001). Isoleucine and tyrosine at position 2 and 4 of the mature protein can cause steric hindrance to the access of proteases, and thus affect processing of the protein by the Kex2 or the Ste13 protease. Another possible cause for inefficient processing of the protease cleavage sites could be glycosylation close to the *N*-terminus of the protein (Weiss et al. 1998). One possibility to solve this problem is to remove the Glu-Ala repeats by cloning the target gene flush with the Kex2 cleavage site. Another approach could be random mutagenesis in the entire secretion leader, which has been recently reported as a suitable strategy for the functional expression of a foreign laccase in yeast (Maté et al. 2010). Expression levels of both constructs with the native signal sequence in 96-well deep well cultivations were similar and in the range of 0.3 $\mathrm{U\,mL^{-1}}$. Because of this relatively high and uniform expression level the, 96-well deep well cultivations can be used to screen for mutated enzymes produced by semirational design approaches. The use of the optimized synthetic gene did not increase the expression level; indeed, the highest volumetric activity was achieved by a transformant, n-PDH_natCC11, with native *pdh1* sequence. A large-scale laboratory fermentation of clone n-PDH_natCC11 was performed to obtain large amounts of homogenous protein for protein crystallography and fast kinetic studies as well as to demonstrate the feasibility of industrial scale production of PDH for biotechnological applications. The 50-L fermentation resulted in a volumetric activity of 10,040 UL^{-1} or 1,330 $\mathrm{UL}^{-1}\ \mathrm{d}^{-1}$ in space–time yield. This is a 28-fold improvement of the space–time yield compared to the wild-type producer and a 1.6-fold improvement compared to *A. nidulans* expression yields (Pisanelli et al. 2010). The cultivation yielded 223 mg L^{-1} of recombinant protein, which corresponds to 52% of total extracellular protein. Because of the high specific activity (22.9 Umg^{-1}) of PDH in the culture supernatant, the previously established purification protocol (Sygmund et al. 2008) was changed to a two-step procedure with focus on fast high-yield purification. This represents another major advantage over expression in *Aspergillus* spp. where the presence of a large number of secreted proteins considerably reduces purification yields. The purification resulted in an apparently pure protein preparation with a specific activity of 43.7 Umg^{-1} that was used for the subsequent biochemical characterization of the enzyme. To show that recombinant PDH1 can be purified in very high yields with this simple purification protocol for biotechnological applications, where a purity of the target protein of 80% is sufficient, other fractions with high specific activity were pooled resulting in a recovery of 85% of the initial activity and 12.3 g of PDH1. For applications where higher purity is required, the activity yield of 10.7% of pool 1 might be too low and then an additional purification step would be necessary. The specific activity of recombinant PDH1 obtained with *P. pastoris* is about 20% lower compared to wild-type PDH1. A possible reason for the reduced specific activity might be the higher degree of glycosylation of recPDH1 expressed in *P. pastoris* (30% compared to 7%), or inactive, not correctly folded protein that could not be separated from the active form. In contrast to *S. cerevisiae*, hyperglycosylation is not common for proteins expressed in *P. pastoris*. The high degree of glycosylation of PDH1 is a hint that the transit from the endoplasmic reticulum to the Golgi apparatus might be a bottleneck for the expression. The kinetic properties are essentially identical to those measured for the wild-type enzyme isolated from its natural source *A. meleagris*.

This study demonstrates the successful expression of PDH in the eukaryotic host organism *P. pastoris* and thus offers the possibility to easily produce and screen for genetically engineered PDH variants paving the way for future protein engineering. Additionally the feasibility of large-scale production of the enzyme using this expression system together with a simplified purification scheme for easy high-yield purification is shown.

Acknowledgments This work was supported by the Austrian Science Fund (FWF) (grant P22094 to CP) and IK is part of the doctoral program BioTop (Biomolecular Technology of Proteins), FWF W1224.

Open Access This article is distributed under the terms of the Creative Commons Attribution Noncommercial License which permits any noncommercial use, distribution, and reproduction in any medium, provided the original author(s) and source are credited.

References

Abad S, Nahalka J, Bergler G, Arnold SA, Speight R, Fotheringham I, Nidetzky B, Glieder A (2010) Stepwise engineering of a *Pichia pastoris* D-amino acid oxidase whole cell catalyst. Microb Cell Fact 9:24

Almeida MS, Cabral KS, De Medeiros LN, Valente AP, Almeida FCL, Kurtenbach E (2001) cDNA cloning and heterologous expression of functional cysteine-rich antifungal protein Psd1 in the yeast *Pichia pastoris*. Arch Biochem Biophys 395 (2):199–207

Ander P, Marzullo L (1997) Sugar oxidoreductases and veratryl alcohol oxidase as related to lignin degradation. J Biotechnol 53 (2–3):115–131

Barton SC, Gallaway J, Atanassov P (2004) Enzymatic biofuel cells for implantable and microscale devices. Chem Rev 104 (10):4867–4886

Brodsky LI, Ivanov VV, Kalaidzidis IL, Leontovich AM, Nikolaev VK, Feranchuk SI, Drachev VA (1995) GeneBee-NET: an Internet based server for biopolymer structure analysis. Biokhimiya 60(8):1221–1230

Bullen RA, Arnot TC, Lakeman JB, Walsh FC (2006) Biofuel cells and their development. Biosens Bioelectron 21(11):2015–2045

Colao M, Lupino S, Garzillo A, Buonocore V, Ruzzi M (2006) Heterologous expression of *lcc1* gene from *Trametes trogii* in *Pichia pastoris* and characterization of the recombinant enzyme. Microb Cell Fact 5(1):31

Giffhorn F (2000) Fungal pyranose oxidases: occurrence, properties and biotechnical applications in carbohydrate chemistry. Appl Microbiol Biotechnol 54(6):727–740

Giffhorn F, Köpper S, Huwig A, Freimund S (2000) Rare sugars and sugar-based synthons by chemo-enzymatic synthesis. Enzyme Microb Technol 27(10):734–742

Goda S, Takano K, Yamagata Y, Katakura Y, Yutani K (2000) Effect of extra N-terminal residues on the stability and folding of human lysozyme expressed in *Pichia pastoris*. Protein Eng 13(4):299–307

Kerem Z, Jensen KA, Hammel KE (1999) Biodegradative mechanism of the brown rot basidiomycete *Gloeophyllum trabeum*: evidence for an extracellular hydroquinone-driven fenton reaction. FEBS Lett 446(1):49–54

Kittl R, Sygmund C, Halada P, Volc J, Divne C, Haltrich D, Peterbauer CK (2008) Molecular cloning of three pyranose dehydrogenase-encoding genes from *Agaricus meleagris* and analysis of their expression by real-time RT-PCR. Curr Genet 53 (2):117–127

Kujawa M, Volc J, Halada P, Sedmera P, Divne C, Sygmund C, Leitner C, Peterbauer C, Haltrich D (2007) Properties of pyranose dehydrogenase purified from the litter-degrading fungus *Agaricus xanthoderma*. FEBS J 274(3):879–894

Lin-Cereghino J, Wong WW, Xiong S, Giang W, Luong LT, Vu J, Johnson SD, Lin-Cereghino GP (2005) Condensed protocol for competent cell preparation and transformation of the methylotrophic yeast *Pichia pastoris*. Biotechniques 38(1):44–48

Lutz S (2010) Beyond directed evolution—semi-rational protein engineering and design. Curr Opin Biotechnol 21(6):734–743

Maté D, García-Burgos C, García-Ruiz E, Ballesteros AO, Camarero S, Alcalde M (2010) Laboratory evolution of high-redox potential laccases. Chem Biol 17(9):1030–1041

Morrison SC, Wood DA, Wood PM (1999) Characterization of a glucose 3-dehydrogenase from the cultivated mushroom (*Agaricus bisporus*). Appl Microbiol Biotechnol 51(1):58–64

Peterbauer CK, Volc J (2010) Pyranose dehydrogenases: biochemical features and perspectives of technological applications. Appl Microbiol Biotechnol 85(4):837–848

Pisanelli I, Kujawa M, Gschnitzer D, Spadiut O, Seiboth B, Peterbauer C (2010) Heterologous expression of an *Agaricus meleagris* pyranose dehydrogenase-encoding gene in *Aspergillus* spp. and characterization of the recombinant enzyme. Appl Microbiol Biotechnol 86(2):599–606

Reitz AB, Baxter EW (1990) Pyrrolidine and piperidine aminosugars from dicarbonyl sugars in one step. Concise synthesis of 1-deoxynojirimycin. Tetrahedron Lett 31(47):6777–6780

Ruth C, Zuellig T, Mellitzer A, Weis R, Looser V, Kovar K, Glieder A (2010) Variable production windows for porcine trypsinogen employing synthetic inducible promoter variants in *Pichia pastoris*. Syst Synth Biol 4(3):181–191

Sun L, Petrounia IP, Yagasaki M, Bandara G, Arnold FH (2001) Expression and stabilization of galactose oxidase in *Escherichia coli* by directed evolution. Protein Eng 14(9):699–704

Sygmund C, Kittl R, Volc J, Halada P, Kubátová E, Haltrich D, Peterbauer CK (2008) Characterization of pyranose dehydrogenase from *Agaricus meleagris* and its application in the C-2 specific conversion of D-galactose. J Biotechnol 133(3):334–342

Tasca F, Gorton L, Kujawa M, Patel I, Harreither W, Peterbauer CK, Ludwig R, Nöll G (2007) Increasing the coulombic efficiency of glucose biofuel cell anodes by combination of redox enzymes. Biosens Bioelectron 25(7):1710–1716

Volc J, Kubátová E, Wood DA, Daniel G (1997) Pyranose 2-dehydrogenase, a novel sugar oxidoreductase from the basidiomycete fungus *Agaricus bisporus*. Arch Microbiol 167(2–3):119–125

Volc J, Kubátová E, Daniel G, Sedmera P, Haltrich D (2001) Screening of basidiomycete fungi for the quinone-dependent sugar C-2/C-3 oxidoreductase, pyranose dehydrogenase, and properties of the enzyme from *Macrolepiota rhacodes*. Arch Microbiol 176(3):178–186

Weis R, Luiten R, Skranc W, Schwab H, Wubbolts M, Glieder A (2004) Reliable high-throughput screening with *Pichia pastoris* by limiting yeast cell death phenomena. FEMS Yeast Res 5(2):179–189

Weis R, Gaisberger R, Gruber K, Glieder A (2007) Serine scanning—a tool to prove the consequences of N-glycosylation of proteins. J Biotechnol 129(1):50–61

Weiss HM, Haase W, Michel H, Reiländer H (1998) Comparative biochemical and pharmacological characterization of the mouse 5HT5A 5-hydroxytryptamine receptor and the human-β2-adrenergic receptor produced in the methylotrophic yeast *Pichia pastoris*. Biochem J 330(3):1137–1147

Zafar MN, Tasca F, Boland S, Kujawa M, Patel I, Peterbauer CK, Leech D, Gorton L (2010) Wiring of pyranose dehydrogenase with osmium polymers of different redox potentials. Bioelectrochemistry 80(1):38–42

Paper III

The 1.6 Å Crystal Structure of Pyranose Dehydrogenase from *Agaricus meleagris* Rationalizes Substrate Specificity and Reveals a Flavin Intermediate

Tien Chye Tan[1,2]☯, Oliver Spadiut[1]☯, Thanyaporn Wongnate[3], Jeerus Sucharitakul[4], Iris Krondorfer[5], Christoph Sygmund[5], Dietmar Haltrich[5], Pimchai Chaiyen[3], Clemens K. Peterbauer[5], Christina Divne[1,2]*

1 School of Biotechnology, KTH Royal Institute of Technology, Stockholm, Sweden, **2** Department of Medical Biochemistry and Biophysics, Karolinska Institutet, Stockholm, Sweden, **3** Department of Biochemistry and Center of Excellence in Protein Structure and Function, Faculty of Science, Mahidol University, Bangkok, Thailand, **4** Department of Biochemistry, Faculty of Dentistry, Chulalongkorn University, Bangkok, Thailand, **5** Food Biotechnology Laboratory, BOKU University of Natural Resources and Life Sciences, Vienna, Austria

Abstract

Pyranose dehydrogenases (PDHs) are extracellular flavin-dependent oxidoreductases secreted by litter-decomposing fungi with a role in natural recycling of plant matter. All major monosaccharides in lignocellulose are oxidized by PDH at comparable yields and efficiencies. Oxidation takes place as single-oxidation or sequential double-oxidation reactions of the carbohydrates, resulting in sugar derivatives oxidized primarily at C2, C3 or C2/3 with the concomitant reduction of the flavin. A suitable electron acceptor then reoxidizes the reduced flavin. Whereas oxygen is a poor electron acceptor for PDH, several alternative acceptors, *e.g.*, quinone compounds, naturally present during lignocellulose degradation, can be used. We have determined the 1.6-Å crystal structure of PDH from *Agaricus meleagris*. Interestingly, the flavin ring in PDH is modified by a covalent mono- or di-atomic species at the C(4a) position. Under normal conditions, PDH is not oxidized by oxygen; however, the related enzyme pyranose 2-oxidase (P2O) activates oxygen by a mechanism that proceeds *via* a covalent flavin C(4a)-hydroperoxide intermediate. Although the flavin C(4a) adduct is common in monooxygenases, it is unusual for flavoprotein oxidases, and it has been proposed that formation of the intermediate would be unfavorable in these oxidases. Thus, the flavin adduct in PDH not only shows that the adduct can be favorably accommodated in the active site, but also provides important details regarding the structural, spatial and physicochemical requirements for formation of this flavin intermediate in related oxidases. Extensive *in silico* modeling of carbohydrates in the PDH active site allowed us to rationalize the previously reported patterns of substrate specificity and regioselectivity. To evaluate the regioselectivity of D-glucose oxidation, reduction experiments were performed using fluorinated glucose. PDH was rapidly reduced by 3-fluorinated glucose, which has the C2 position accessible for oxidation, whereas 2-fluorinated glucose performed poorly (C3 accessible), indicating that the glucose C2 position is the primary site of attack.

Citation: Tan TC, Spadiut O, Wongnate T, Sucharitakul J, Krondorfer I, et al. (2013) The 1.6 Å Crystal Structure of Pyranose Dehydrogenase from *Agaricus meleagris* Rationalizes Substrate Specificity and Reveals a Flavin Intermediate. PLoS ONE 8(1): e53567. doi:10.1371/journal.pone.0053567

Editor: Luis Eduardo Soares Netto, Instituto de Biociencias - Universidade de São Paulo, Brazil

Received October 16, 2012; **Accepted** November 29, 2012; **Published** January 9, 2013

Copyright: © 2013 Tan et al. This is an open-access article distributed under the terms of the Creative Commons Attribution License, which permits unrestricted use, distribution, and reproduction in any medium, provided the original author and source are credited.

Funding: The authors acknowledge support to CD and TCT from the Swedish Research Council Formas, the Swedish Research Council VR, and the Carl Tryggers Foundation. PC acknowledges research support by the Thailand Research Fund (BRG5480001) and the Faculty of Science, Mahidol University. CKP thanks the Austrian Science Fund (FWF) for financial support (grant P22094). IK is part of the doctoral program BioTop (Biomolecular Technology of Proteins; Austrian Science Fund FWF W1224). The funders had no role in study design, data collection and analysis, decision to publish, or preparation of the manuscript.

Competing Interests: The authors have declared that no competing interests exist.

* E-mail: divne@biotech.kth.se

☯ These authors contributed equally to this work.

Introduction

Pyranose dehydrogenase (PDH; *pdh1* gene; pyranose:acceptor oxidoreductase; EC 1.1.99.29; sequence UniProt: Q3L245_9AGAR [1]) from the litter-decomposing fungus *Agaricus meleagris* (synonym *Leucoagaricus meleagris, Agaricus praeclaresquamosus, California fungus*) is an extracellular, monomeric flavin-dependent oxidoreductase, with one flavin adenine dinucleotide (FAD) prosthetic group covalently bound per polypeptide chain [2].

Like several other fungal sugar oxidoreductases, *Am*PDH belongs to the glucose-methanol-choline (GMC) oxidoreductase family [1]; and as the fungal pyranose 2-oxidase from *Trametes multicolor* (*Tm*P2O), *Am*PDH produces aldoketose or diketose derivatives from non-phosphorylated sugars [2]. PDH transcription is up-regulated during limiting oxygen supply, suggesting that PDH may substitute for oxidases under oxygen-deprived conditions [1]. PDHs can be differentiated from P2Os based on: *i)* PDH is a glycosylated, extracellularly secreted enzyme, whereas P2O is non-glycosylated and located in the hyphal periplasmic space; *ii)* PDH is rather inert towards oxygen, while P2O is a typical flavoprotein oxidase; and *iii)* PDH oxidizes D-glucose at both the C2 and C3 position, whereas P2O is strictly regioselective for the glucosyl C2 position [3–6].

Interestingly, the two enzymes PDH and P2O, which catalyze closely related reactions, appear to be mutually exclusive. Of all fungal strains screened for P2O and PDH activity, they were found to express either PDH or P2O, but never both [7]. Moreover, the enzyme requirement of a particular fungus appears to be coupled to the macroscopic substrate. Volc and co-workers showed that P2O is expressed mainly by wood-decaying white-rot fungi (e.g., *Phanerochaete*, *Trametes etc.*), while PDH expression is limited to the *Agaricales* [7], which are typical litter-degrading fungi that live in forest and grassland soil and are the primary decomposers of residual plant material (leaves, needles, twigs, bark, grass) in the uppermost soil layer. It should be noted that P2O-encoding genes were also found and experimentally confirmed in some members of the genus *Aspergillus*, which does not degrade lignocellulose, notably in species where a glucose 1-oxidase (GOX) is absent [8].

At present, the biologically relevant function of PDH is not clear. One possible role of PDH would be the reduction of quinone compounds or reactive radical species generated during lignin depolymerization, possibly to prevent re-polymerization or to prevent exposure of the cell to toxic quinones. A similar role has been suggested for basidiomyceteous P2O and cellobiose dehydrogenase (CDH) for wood-degrading fungi [9–11]. Although *A. meleagris* feeds mainly on lignocellulose-rich forest litter like straw or bark, and compact wood is usually not degraded [12], one may hypothesize that PDH performs a similar function in litter-decomposing fungi to that of CDH. The ability of PDH to oxidize at comparable activities a wide range of carbohydrates present in wood, *e.g.*, D-xylose, L-arabinose D-glucose, D-galactose, cellobiose, and others [13,14], together with its up-regulation once easily metabolizable carbohydrates are depleted from the medium, strongly support a role in the degradation process.

The fungus *A. meleagris* carries three genes that putatively encode pyranose dehydrogenases, *pdh1*, *pdh2* and *pdh3*. The latter two genes are transcribed on a much lower level than *pdh1* [1], and the PDH protein isolated and characterized from cultures of *A. meleagris* in previous studies [2,13,15] also corresponds exclusively to *pdh1*. The product of *pdh1*, *Am*PDH, is a glycoprotein with a molecular mass of 66.5 kDa and an estimated 7% glycan content [2]. The FAD cofactor displays typical absorption peaks at 371 nm and 464 nm for the oxidized enzyme, whereas the reduced enzyme lacks the 464 nm peak [2]. The optimal pH stability range is broad (pH 4–10), and the temperature optimum is 63°C under standard assay conditions [16]. The enzyme has a broad electron-donor substrate specificity (Fig. 1), including a range of mono- and oligosaccharides where D-glucose, D-galactose, L-arabinose, and D-xylose are all highly competent electron donors when ferricenium is used as an electron acceptor. Suitable electron acceptors are either complexed metal ions or substituted quinones. Of the electron acceptors tested, ferricenium performs best, followed by 3,5-di-tert-butyl-benzoquinone and 2,6-dichloroindophenol [2].

Regioselectivity in sugar oxidation strictly differs depending on the substrate used. An extensive study by Sedmera and co-workers [13] has shown that PDH is able to oxidize sugar substrates through monooxidation reactions at the C1, C2, C3 positions, or double-oxidations at C1/3, C2/3, or C3/4. Whereas D-glucose is double-oxidized at C2 and C3 to yield 2,3-didehydro-D-glucose, D-galactose (the C4 epimer of glucose) is oxidized exclusively at C2 to give 2-dehydro-D-galactose. Similar to D-galactose, L-arabinose is oxidized at C2 yielding 2-dehydro-L-arabinose. Cellobiose, maltotriose, D-xylose and maltose are all double-oxidized at C2 and C3. The double-oxidation reactions of cellobiose and maltose resulted in the novel compounds 2,3′-didehydrocellobiose and 2,3′-didehydromaltose, respectively. Lactose is oxidized at the reducing-end C1 or C2 position to give lactobionolactone and 2-dehydrolactose [17]. The monosaccharides D-ribose, D-allose (C3 epimer of glucose), D-gulose (C3 epimer of galactose), and D-talose (C2 epimer of galactose) are oxidized exclusively at C1 to the corresponding aldonic acids. Interestingly, *Am*PDH has been shown to perform double-oxidation of a number of aromatic glycosides, of which β-D-glucopyranosides and a β-D-xylopyranoside are converted to novel sugar compounds corresponding to the 3,4-didehydro-β-D-aldopyranoside forms [15]. The reactions carried out by PDHs can be summarized as:

(1) pyranose+acceptor = 2-dehydropyranose (or 1-dehydropyranose or 3-dehydropyranose or 2,3-didehydropyranose)+reduced acceptor

(2) pyranoside+acceptor = 3-dehydropyranoside (or 3,4-didehydropyranoside)+reduced acceptor

Based on its primary structure, PDH belongs to the same flavoenzyme family as the oxygen-activating enzymes *Tm*P2O, *Aspergillus niger* glucose 1-oxidase (*An*GOX), which oxidizes β-D-glucose to D-gluconolactone [18], and *Arthrobacter globiformis* choline oxidase (*Ag*CHO), which oxidizes choline to glycine betaine [19]. Unlike *Am*PDH, the oxidases *Tm*P2O, *Ag*CHO and *An*GOX use molecular oxygen as electron acceptor to generate hydrogen peroxide. Given the structural, functional and mechanistic kinship between these enzymes, the crystal structure of *Am*PDH also gives us the opportunity to identify structural features that may help rationalize the difference in oxygen reactivity, *i.e.*, structural determinants underlying the designation of a GMC enzyme as an oxidase or a dehydrogenase.

Here we report the crystal structure of *Am*PDH (the translated product of *pdh1*), refined at 1.6 Å resolution, featuring a C(4a)-modified flavin ring. Based on the PDH structure, we rationalize the observed pattern of sugar substrate preference and regioselectivity, and discuss the relevance of the flavin adduct species with respect to the biological function of PDH. The surrounding environment of the C(4a)-flavin adduct in PDH is compared with those of related flavoprotein oxidases and monooxygenases.

Results

Activity on 2- and 3-Fluorinated Glucose

When mixing 3-fluoro-3-deoxy-D-glucose (3FG) and *Am*PDH, the reaction mixture monitored at 30 s after mixing was colorless (Fig. 2) showing that *Am*PDH was rapidly reduced, presumably by a hydride moiety at glucose C2. The rate of reduction of PDH by 2-fluoro-2-deoxy-D-glucose (2FG) was significantly slower because the reduction kinetics could be monitored over a period of 1000 s (Fig. 3*a*). Fig. 3*b* shows the reduction kinetics of PDH by 2FG monitored at 463 nm, which is consistent with an observable rate constant (k_{obs}) of 0.0091 s^{-1}.

Oxygen Activity

The absorption spectra of *Am*PDH undergoing oxidation by oxygen at air-saturation over a time period of 15 h are shown in Fig. 4. The reaction proceeded slowly, and the enzyme was still only partially oxidized after 15 h. After 15 h, enzyme denaturation occurred as judged by increased turbidity of the solution. The spectra in Fig. 4 indicate absorption peaks ~370 nm and resolving shoulders around 395 and 495 nm, which are characteristic of a flavin anionic semiquinone.

Overall Structure

The overall structure of *Am*PDH features the classical p-hydroxybenzoate hydroxylase (PHBH)-like fold of members of the GMC oxidoreductase family with two intimately associated domains, an ADP-binding Rossmann domain, and a substrate-

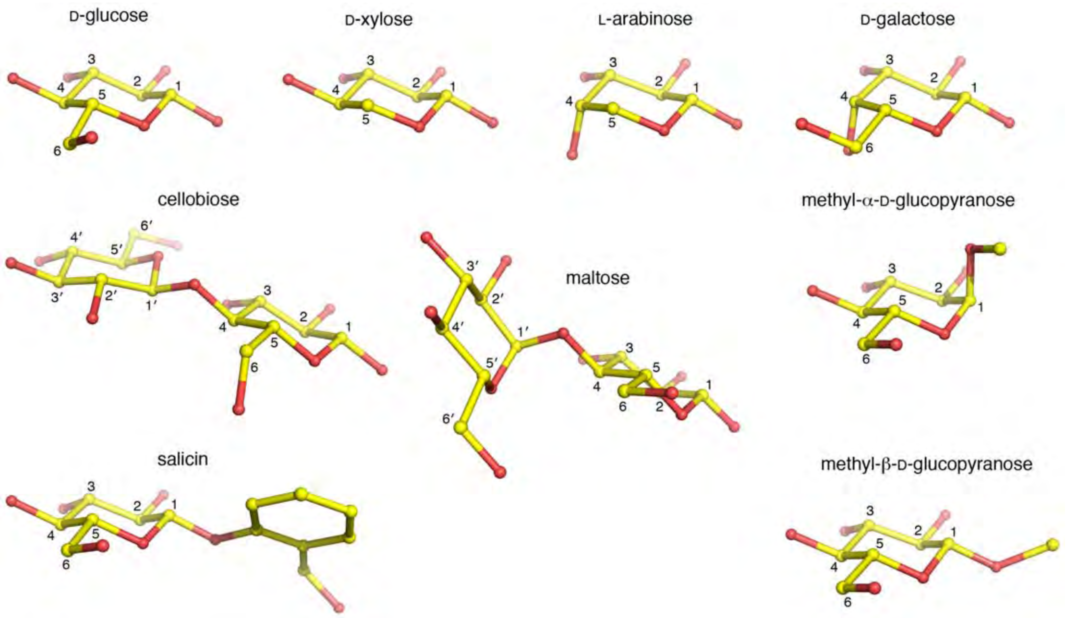

Figure 1. Electron-donor substrates modeled in the active site of *Am*PDH. Carbons are colored yellow and numbered. Apostrophes indicate carbons on the non-reducing end sugar. Hydrogen atoms have been omitted for the purpose of clarity.
doi:10.1371/journal.pone.0053567.g001

binding domain (Fig. 5a). Data collection and model refinement statistics are given in Table 1. The GMC member most structurally similar to PDH returned by the Dali server (DaliLite v.3; http://www.ebi.ac.uk/Tools/dalilite/[20]) is aryl-alcohol oxidase (AAO; PDB code 3FIM [21]) with a root-mean-square distance (r.m.s.d) of 1.6 Å for 544 of 575 aligned Cα atom pairs, and a sequence identity of 38% (Fig. 5b, c). Of the GMC members using carbohydrates as electron-donor substrates, optimized structural alignments with PDH were obtained using the *LSQ_IMPROVE* option in the program *O* [22], giving r.m.s.d. values of 1.5 Å for GOX (PDB code 1CF3 [23], 461 Cα pairs); 1.6 Å for CDH (PDB code 1NAA [24], 387 Cα pairs), and 2.0 Å for P2O (PDB code 3PL8 [6], 313 Cα pairs).

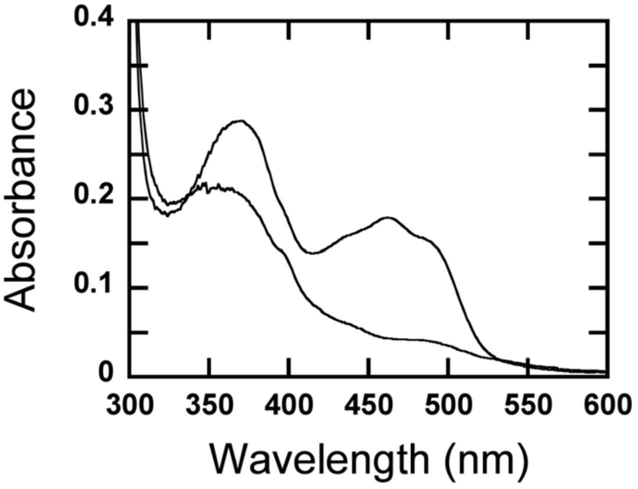

Figure 2. Reduction of oxidized *Am*PDH by 3-fluoro-3-deoxy-D-glucose. The upper spectrum represents the absorption spectrum of the oxidized PDH (20 μM), and the lower spectrum shows the reduced enzyme after incubation with 20 μM 3FG for 30 sec at 25°C. The reduction by 3FG (presumably by a hydride transfer from C2-H) is very rapid and cannot be followed kinetically by manual mixing in an anaerobic cuvette.
doi:10.1371/journal.pone.0053567.g002

Active-Site Structure

Of closely related GMC members that use sugars as electron-donor substrates, three-dimensional structural information exists for two oxidases (P2O and GOX) and two dehydrogenases (PDH and CDH). A structural overlay of PDH with GOX, P2O and CDH (Fig. 6*a, b, c*) highlights the similarities and differences between the enzyme active sites. For the purpose of discussing oxygen reactivity, CHO has been included (Fig. 6*d*). CHO does not oxidize sugar substrates, but its structure has been determined with a covalent C(4a) flavin modification that is probably an artifact introduced during data collection. Although the overall similarity of the active sites is high, some differences are noted (Fig. 6, Table 2): *i)* PDH and GOX contain a His-His catalytic pair, whereas P2O, CDH and CHO use a His-Asn constellation; *ii)* PDH, P2O and CHO are flavinylated (8α-(*N*3)–histidyl–FAD), while GOX and CDH carry non-covalently bound FAD; and *iii)* PDH, GOX and CDH lack a *si*-face N(5) partner, *i.e.*, the side chain close to N(5) that forms hydrogen bonds with the N(5)/O(4) locus, but P2O and CHO contain a Thr and Ser, respectively. Unexpectedly for a flavoprotein dehydrogenase, the flavin ring in *Am*PDH is modified at C(4a) by an unidentified atomic species (*Fig. 7*). The covalently bound atom (probably an oxygen species) is tightly coordinated by the two active site histidines (512 and 556).

Comparison of Flavin C(4a)-Adduct Geometry in Existing Crystal Structures

The C(4a)-modified flavin in *Am*PDH shows an sp^3-hybridized C(4a) atom, and a relatively subtle conformational change compared with a planar isoalloxazine ring (Fig. 7). A detailed analysis of the flavin geometry is provided in Table S1, where the *Am*PDH adduct is compared with the flavin C(4a) adduct of *Ag*CHO (PDB code 2JBV [25]), and the available crystal structures of artificial synthetic isoalloxazine oxygen-nucleophile adducts, O-

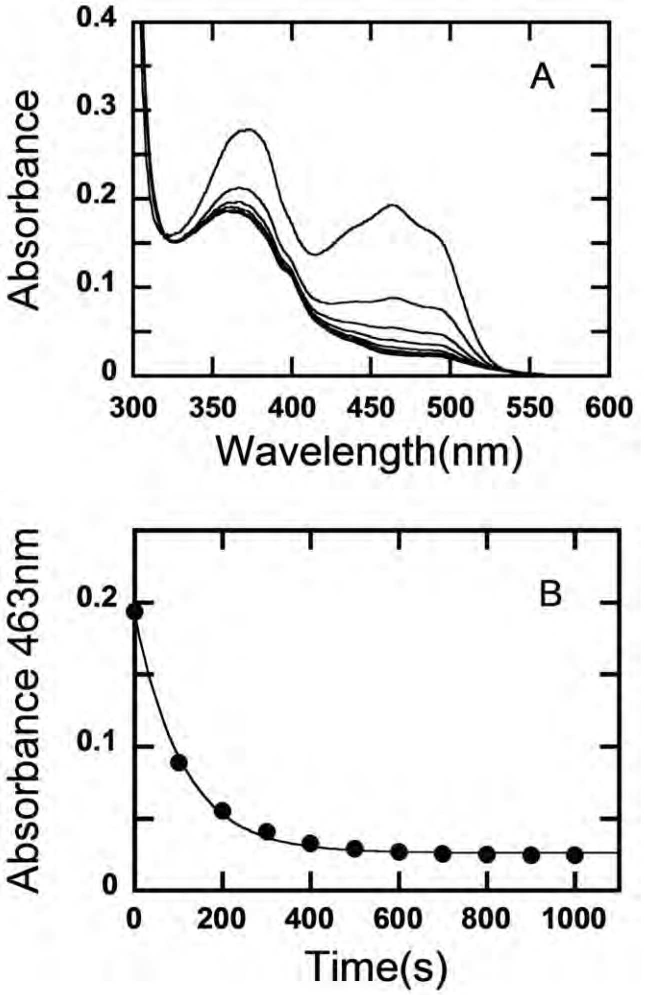

Figure 3. Reduction of oxidized AmPDH by 2-fluoro-2-deoxy-D-glucose. (A) Reduction spectra of PDH (20 μM) reduced by 2FG (20 μM) at 25°C. The top spectrum represents the absorption spectrum of the oxidized PDH. Spectra were recorded at intervals during the reaction. The upper spectrum represents the start of the reaction, and the lowest spectrum the end ($t = 1000$ sec) showing PDH in its fully reduced state. (B) Reduction kinetics of PDH with 2FG was monitored at 463 nm. The reaction kinetics corresponds to a k_{obs} value of 0.0091 sec^{-1}.
doi:10.1371/journal.pone.0053567.g003

adducts [26]. Specifically, the structures of two flavin C(4a)-OH adducts (1AOH, CCDC code 784805; 1BOH, CCDC code 784806) allow a detailed characterization of the adduct geometry. The two flavin OH-adducts, 1AOH and 1BOH, correspond to isoalloxazine and alloxazine (lacking the C7 and C8 methyl groups), respectively. To stabilize the flavin adducts, the (iso)alloxazine rings were modified at N(5) to yield the 5-alkyl flavin analogs prior to adduct formation [26]. As a result, these artificial C(4a) O-adducts are formed at the *si*-face of the flavin rather than the *re*-face observed in the crystal structures of the flavoprotein oxidases, but we do not expect this difference to be of any major importance for a comparison of O-adduct geometry. The substituted C(4a) atoms in 1AOH and 1BOH display sp^3 character with an average value for the bond angles at C(4a) close to 109.5° (expected for a tetrahedral carbon), resulting in a flavin-ring distortion with a small but distinct deviation from planarity [26].

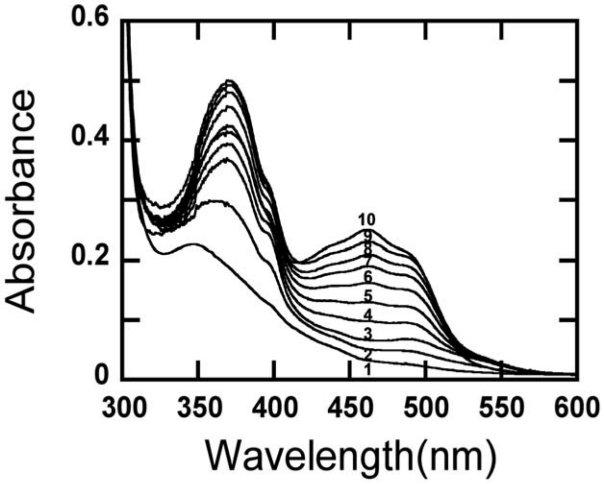

Figure 4. Absorption spectra of reduced *Am*PDH reacting with molecular oxygen. Oxidation of PDH by oxygen at air-saturation as a function of time at 25°C. Line 1: reduced PDH at start of the reaction which lacks the flavin absorption shoulder around 490 nm; line 5, the spectrum of partially oxidized PDH (~40% oxidation); line 10, the absorption spectrum of partially oxidized PDH after the reaction proceeded for 15 h.
doi:10.1371/journal.pone.0053567.g004

For the purpose of analyzing the differences in flavin ring conformation for different O-adducts, we find the dihedral angle N(10)–C(10)–C(4a)–C(4) to be useful in that it provides a measure of the distortion of the pyriminoid ring (the ring that is most affected by O-substitution in the 1BOH, *Am*PDH and CHOx adducts). This torsion angle relates the N(10) atom of the pyrazinoid ring to the C(4) atom of the pyriminoid ring, and a value of ±180° would mean that these atoms are in one plane, and *trans* to each other. The values reported for the two *si*-face O-adducts 1AOH and 1BOH are 174.5° and 139.7° [26]. For *re*-face flavin O-adducts (as those in *Am*PDH and CHO) these values would translate into the counterclockwise rotations of –174.5° and –139.7°.

For *Ag*CHO, Orville and co-workers reported the crystal structure of a trapped flavin C(4a) adduct, as well as density functional theory (DFT) calculations. Based on the DFT calculations, values for the N(10)–C(10)–C(4a)–C(4) angle for the C(4a)–OH, C(4a)–OOH, FAD semiquinone, and $FADH^-$ fall in the range –130° to –156°, whereas the value of this dihedral angle in the *Ag*CHO crystal structure (PDB code 2JBV) is 86°. The observed value of –152° for the N(10)–C(10)–C(4a)–C(4) dihedral angle in the *Am*PDH adduct (Table S1) agrees reasonably well with those generated by DFT calculations [25] and with the synthetic flavin O-adducts [26], but is distinct from the modified flavin in *Ag*CHO. Thus, the adduct geometry in the *Ag*CHO structure differs about 40° from the DFT values for C(4a)–OH/C(4a)–OOH, and 50–90° from those of the synthetic adducts and *Am*PDH. Indeed, this torsion angle emphasizes the fundamentally different conformation of the pyriminoid ring in *Ag*CHO compared with that in *Am*PDH (Fig. 8), and synthetic flavin O-adducts.

Modeling of Monosaccharide Electron-Donor Substrates in the *Am*PDH Active Site

Electron-donor substrates (saccharides) were docked in the *Am*PDH active site to rationalize the observed patterns of substrate specificity and regioselectivity [2,13]. Only substrates for which the activity exceeds 50% of the activity for D-glucose, and with

Table 1. Data collection and crystallographic refinement statistics for *Am*PDH.

Data collection[a]	
Cell constants a, b, c (Å)	51.94, 74.64, 139.29
Space group/molecules per asymmetric unit	$P2_12_12_1$/1
Beamline, λ (Å)	*I*911–5, 0.90772
Resolution range, nominal (Å)	48.7–1.60 (1.70–1.60)
Unique reflections	72,035 (11,811)
Multiplicity	7.3 (7.3)
Completeness (%)	99.7 (99.8)
$<I/\sigma I>$	16.4 (2.6)
R_{sym}[b] (%)	7.5 (84.1)
CC(1/2)[c]	99.9 (80.1)
Crystallographic refinement	
Resolution range (Å)	50–1.60 (1.686–1.600)
Completeness, all % (outer bin)	99.7 (99.8)
R_{factor}[d]/work reflns, all	0.171/69,857
R_{free}/free reflns, all	0.201/2,177
Non-hydrogen atoms	5,017
Mean *B* (Å^2) protein all/mc/sc	15.6/14.5/16.7
Mean *B* (Å^2) solvent/N°. mol.	29.9/541
Rmsd bond lengths (Å), angles (°)	0.016, 1.853
Ramachandran: favored/allowed (%)[e]	97.2/100

[a] The outer shell statistics of the reflections are given in parentheses. Shells were selected as defined in *XDS* [54] by the user.
[b] $R_{sym} = [\Sigma_{hkl} \Sigma_i |I-<I>|/\Sigma_{hkl} \Sigma_i |I|] \times 100\%$.
[c] CC(1/2) = Percentage of correlation between intensities from random half-datasets. Values given represent correlations significant at the 0.1% level [66].
[d] $R_{factor} = \Sigma_{hkl} \mid |F_o|-|F_c| \mid / \Sigma_{hkl} |F_o|$.
[e] As determined by *MolProbity* [62].

doi:10.1371/journal.pone.0053567.t001

experimentally determined site(s) of oxidation, were considered (according to compiled data [13]; Fig. 1). A summary of possible protein-sugar hydrogen bonds for monosaccharide and disaccharide substrates is given in Table S2 and Table S3, respectively. Based on our structural modeling, *Am*PDH should be able to oxidize C1, C2, C3 and C4 of D-glucose and D-xylose [27] (the only difference being that xylose lacks the C6–O6 group) without any obvious problems (Fig. S1 and S2). All oxidation-binding modes generate similar sets of possible hydrogen bonds, which explain the more promiscuous oxidation activity of *Am*PDH compared with *Tm*P2O for these monosaccharides. Single oxidations at C1 and C4 have not been observed experimentally, but should be possible from a purely structural point of view (Fig. S1*a,d* and S2*a,d*). For all sugar-binding modes, the principal interactions are provided by the catalytic histidine pair (His512/His556), the backbone carbonyl oxygen of Tyr510, and the side chain of Gln392. The C6 hydroxyl group does not form any interactions in either of the modeled binding modes. Since the two binding modes, the C2-oxdiation and C3-oxidation modes, generate similar sets of interactions (Fig. S1*b,c*), their difference in kinetics (see above) is difficult to rationalize at the structural level.

Unlike D-glucose and D-xylose, oxidations of L-arabinose (Fig. S3) and D-galactose, the C4 epimer of glucose, (Fig. S4) are highly regioselective reactions, targeting only the C2 position and strongly discriminating against C1, C3 and C4. Thus, for D-galactose, only 2-dehydro-D-galactose is produced [28], and for L-arabinose, which is identical to D-galactose except for the absence of an exocyclic C6–O6 group, only 2-dehydro-L-arabinose [13]. The reason for the observed product outcome is easily rationalized at the structural level using modeling.

When L-arabinose and D-galactose are oriented for oxidation at C2, the axial O4 is easily accommodated in the active site, whereas in all other orientations, *i.e.,* oxidation at C1, C3 and C4, the axial O4 group would experience steric hindrance and generate clashes (qualititatively defined as a distance less than the sum of the van der Waals radii for any two non-bonded atoms, and not participating in short-strong hydrogen bonds or low-barrier hydrogen bonds). In orientation for C1 (Fig. S3*a* and S4*a*) or C3 (Fig. S3*c* and S4*c*) clashes are observed with the aromatic ring of Tyr510 in subsite C, and binding for oxidation at C4 results in equally unfavorable clashes, but with the flavin ring (Fig. S3*d* and S4*d*). In contrast, the C2-oxidation mode enables four possible protein-sugar hydrogen bonds (Fig. S3*b* and S4*b*), and no unfavorable interactions, yielding L-*erythro*-pentos-2-ulose [13] and D-lyxo-hexos-2-ulose [2,28] from L-arabinose and D-galactose, respectively.

Oxidations of PDH by the glucopyranosides methyl-α-D-glucopyranose [29] (methyl-α-D-Glc*p*; Fig. S5) and methyl-β-D-glucopyranose (methyl-β-D-Glc*p*; Fig. S6) are also highly regioselective, favoring oxidation at C3, all of which is substantiated by our modeling (Fig. S5*c* and S6*c*). For oxidation at other positions of methyl-α-D-Glc*p* (Fig. S5*a, b, d*) the axially configured methoxy group will generate clashes with either the flavin ring or the tyrosine 510 ring. In principle, the same applies to methyl-β-D-Glc*p*: in the C1-oxidation mode, the methoxy group experiences steric problems with the flavin ring (Fig. S6*a*), and in the C2-oxidation mode it clashes with Val511 (Fig. S6*b*). Although C4-oxidation has, to our knowledge, not been shown for methyl-β-D-Glc*p*, this nonetheless appears possible from a structural point of view (Fig. S6*d*).

Modeling of Disaccharide and Glucopyranoside Electron-donor Substrates in the *Am*PDH Active Site

For binding of disaccharides or glucopyranosides substituted with large aglycons, we use the subsite-naming convention previously defined for CDH [24,30]. According to this convention, the innermost site where oxidation takes place is referred to as subsite C (indicating that this is the catalytic site), and the second binding site is named B1 ("B" for binding). Longer oligomers would then involve additional subsites, B2, B3 *etc*. The disaccharides cellobiose and maltose consist of two linked glucosyl units, but with different glycosidic linkages: a β(1→4) glycosidic bond in cellobiose, and an α(1→4) linkage in maltose. In both cases, PDH catalyzes single oxidations at C1 and C2 of the reducing-end glucosyl unit, *i.e.,* 1- and 2-oxidation; and at C3 of the non-reducing glucosyl terminus, *i.e.,* 3′-oxidation [13] (positions denoted by an apostrophe refer to positions in the non-reducing end sugar). In addition to the single oxidations, PDH also catalyzes the sequential double-oxidation reactions 1,3′ (C1 oxidation of reducing-end glucosyl and C3 oxidation of non-reducing end glucosyl) or 2,3′ (C2 oxidation of reducing-end glucosyl and C3 oxidation of non-reducing end glucosyl), to yield the 1,3′ or 2,3′-double-oxidation products [2]. The products from 1,3′-double-oxidation reactions are 3′-dehydrocellobionic acid and 3′-dehydromaltobionic acid, and from 2,3′-double-oxidation, products 2,3′-didehydrocellobiose and 2,3′-didehydromaltose are obtained.

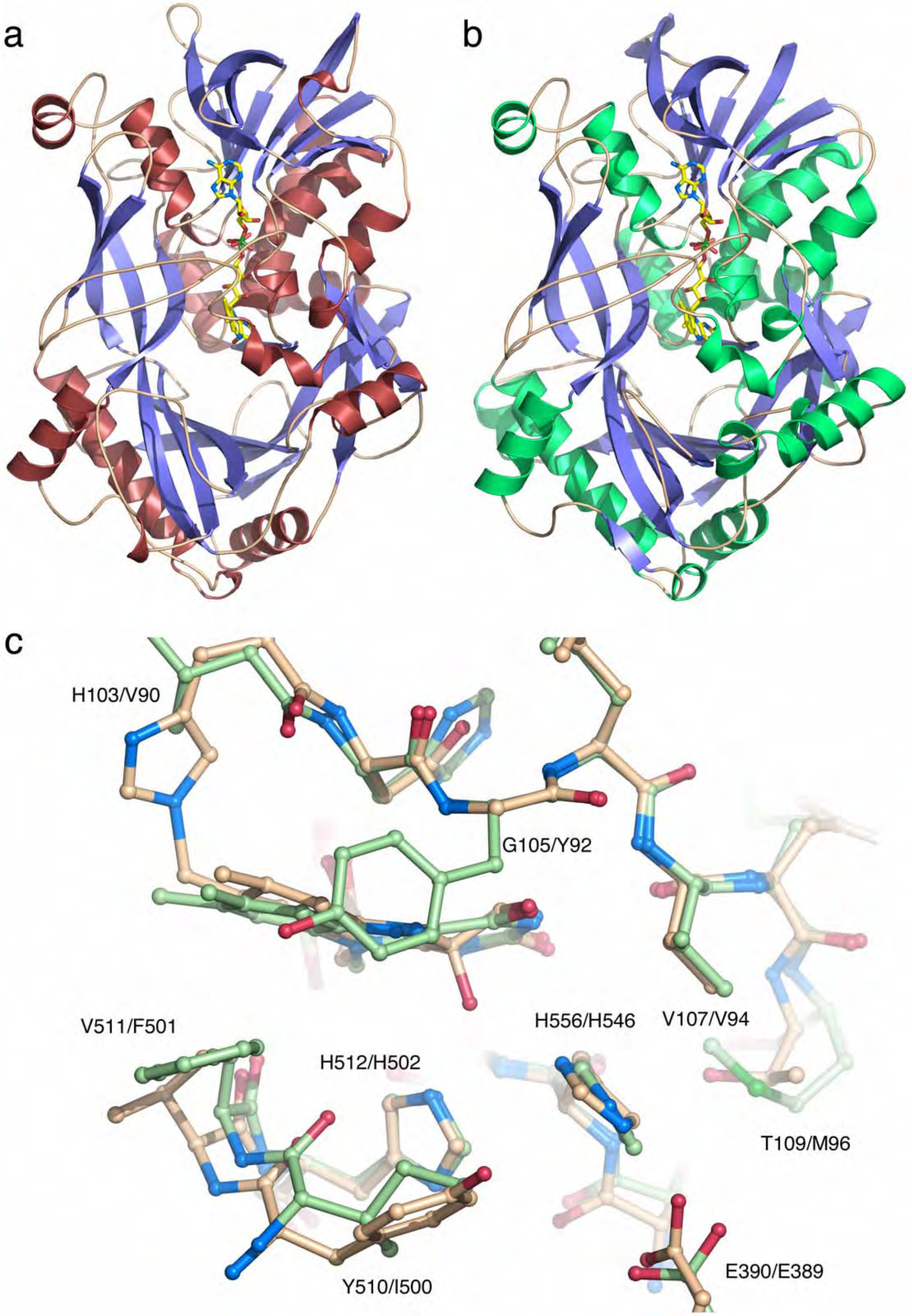

Figure 5. Overall structure of *Am*PDH and similarity to AAO. Ribbon drawing of *Am*PDH (a) and aryl-alcohol oxidase (b), showing α-helices as spirals and β-strands as arrows. The covalently bound flavin cofactor is depicted as a stick model with carbon atoms in yellow. An overlay picture of the active site in *Am*PDH (beige carbon atoms) and AAO (green carbon atoms) is shown in (c).
doi:10.1371/journal.pone.0053567.g005

The product outcome is straightforward to rationalize based solely on structural considerations (cellobiose, Fig. S7; maltose, Fig. S8): favorable interactions are only possible when the C-site sugar unit is oriented for oxidation at C1 or C2 (Fig. S7*a, b* and S8*a, b*). The 3- (Fig. S7*c* and S8*c*) and 2′-oxidations (Fig. S7*d* and S8*d*) are discriminated against due to severe steric clashes

Table 2. Comparison of related GMC dehydrogenases and oxidases.

Enzyme[a] (PDB code)	Physiol. O_2 activity	Catalytic pair	N-N distance catalytic pair (Å)	Physiol. flavin C(4a) adduct	Flavin attachment	*si*-face N(5) partner
*Am*PDH (this work)	No	His512 Nε2, His556 Nδ1	3.5	No, radiation artifact	8α-(*N*3)–histidyl–FAD	Gly105
*Pc*CDH (1KDG [30])	No	His689 Nε2, Asn732 Nδ2	3.3	No	Non-covalent	Gly310
*Tm*P2O (1TT0 [46])	Yes	His548 Nε2, Asn593 Nδ2	4.2	Yes	8α-(*N*3)–histidyl–FAD	Thr169
*Ag*CHO (3LJP [67]; 2JBV [25])	Yes	His466 Nε2, Asn510 Nδ2	4.0	No, radiation artifact	8α-(*N*3)–histidyl–FAD	Ser101[b]
*An*GOX (1CF3 [23])	Yes	His516 Nε2, His559 Nδ1	4.8	No	Non-covalent	Gly108

[a] *Am*PDH, *A. meleagris* pyranose dehydrogenase; *Pc*CDH, *P. chrysosporium* cellobiose dehydrogenase; *Tm*P2O, *T. multicolor* pyranose 2-oxidase; *An*GOX, *A. niger* glucose 1-oxidase; *Ag*CHO; *A. globiformis* choline oxidase.

[b] The *Ag*CHO mutant S101A shows increased efficiency in the oxidative half-reaction [68], stressing that the function of this side chain is different in *Ag*CHO compared with the sugar-oxidizing enzymes.

doi:10.1371/journal.pone.0053567.t002

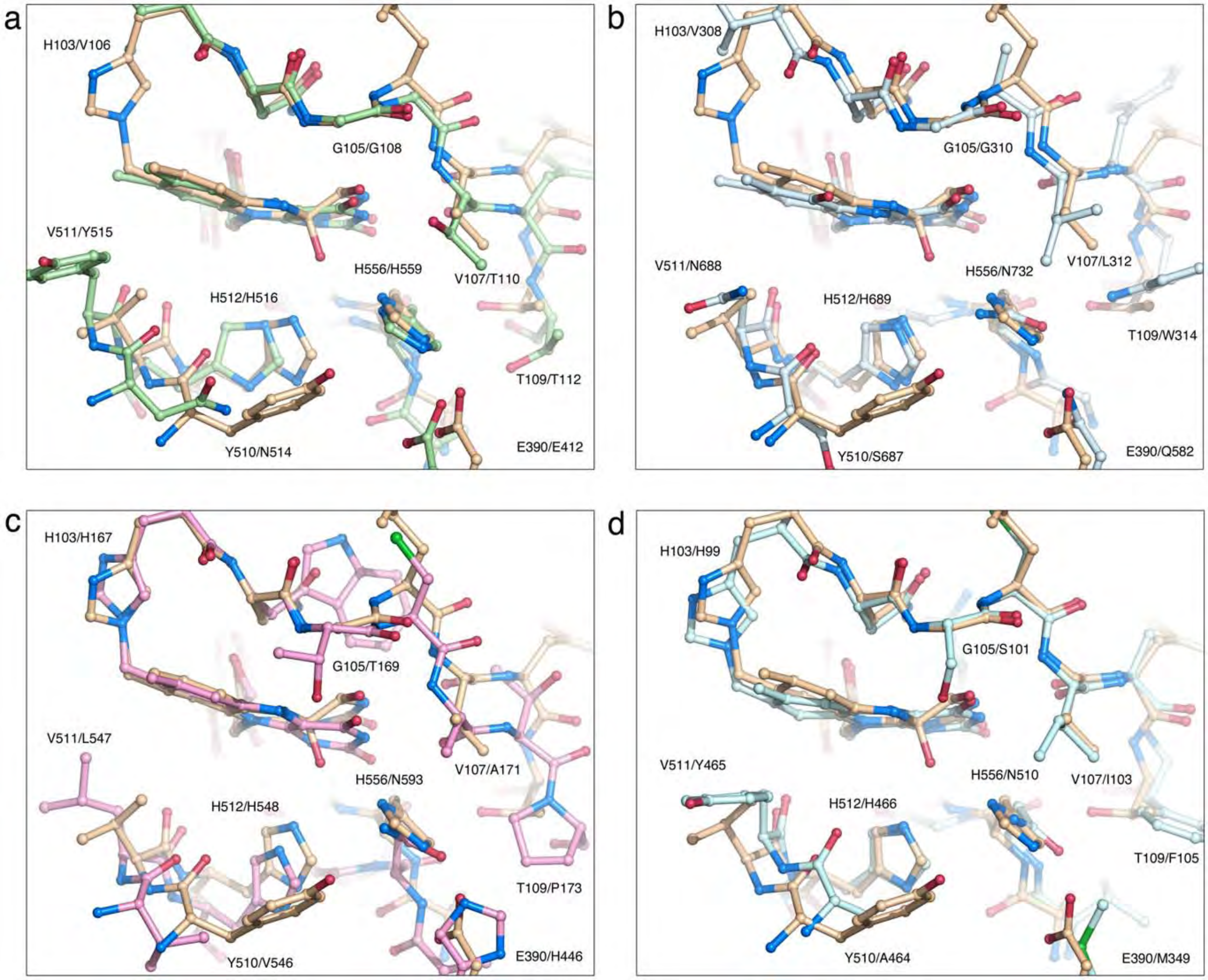
a
H103/V106
G105/G108
V511/Y515
H556/H559
V107/T110
H512/H516
T109/T112
Y510/N514
E390/E412
b
H103/V308
G105/G310
V511/N688
H556/N732
V107/L312
H512/H689
T109/W314
Y510/S687
E390/Q582
c
H103/H167
G105/T169
V511/L547
H556/N593
V107/A171
H512/H548
T109/P173
Y510/V546
E390/H446
d
H103/H99
G105/S101
V511/Y465
H556/N510
V107/I103
H512/H466
T109/F105
Y510/A464
E390/M349

Figure 6. Comparison of *Am*PDH with GOX, CDH, P2O and CHO. Structural superpositioning of the *Am*PDH active site (beige carbon atoms) with those of (a) GOX (PDB code 1CF3 [23]), green carbons; (b) CDH flavoprotein domain (PDB code 1KDG [30]), light blue carbons; (c) P2O (PDB 1TT0 [46]), pink carbons; and (d) CHO (PDB 3LJP [67]), pale cyan carbons. For each equivalent pair, that of AmPDH is given first.

doi:10.1371/journal.pone.0053567.g006

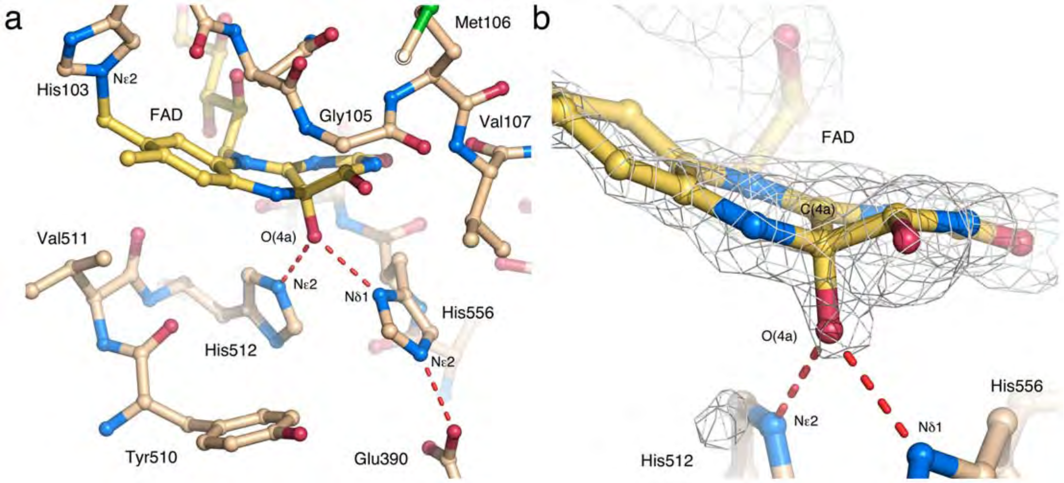

Figure 7. Structural evidence for a flavin C(4a)-adduct. (a) The AmPDH active site showing the relevant amino acids including the catalytic His-His pair. The FAD molecule is covalently linked through the C8M atom to His103 Nε2, and features a modification at the C(4a) locus. The adduct-stabilizing imidazole nitrogens of His512 and His556 are pictured with dashed lines indicating hydrogen bonds. (b) Zoom in at the monoatomic flavin-adduct species, presumably a covalently bound oxygen atom, overlaid by a 5000 K simulated annealing omit electron density map calculated using *PHENIX* [63], contoured at the 3σ level.
doi:10.1371/journal.pone.0053567.g007

incompatible with substrate binding: in the case of 3-oxidation, extreme clashes are observed between the non-reducing end sugar and the Tyr510-Val511 backbone (Fig. S7*c* and S8*c*); and for 2′-oxidation, clashes are formed between the reducing end glucose and Tyr510 (Fig. S7*d* and S8*d*).

In the case of the 3′-oxidation mode for cellobiose (C3 of the non-reducing end glucosyl positioned for oxidation in subsite C; Fig. S7*e*), we observe no possible interactions for the reducing-end glucosyl unit in site B1, however, a minor pivotal rotation of the subsite B1 glucosyl together with a concomitant rotamer shift of the Ser64 side chain generates a possible additional hydrogen bond O1–Ser64 Oγ. In the case of maltose, the 3′-oxidation activity is more difficult to rationalize at the structural level since most positions appear to result in clashes either with the Gly105 or Ser64 backbone in subsite B1 (Fig. S8*e*). The clashes are however not severe, and small adjustments of the protein backbone regions could easily relieve unfavorable energies.

Although the 4′-oxidations of cellobiose (Fig. S7*f*) or maltose (Fig. S8*f*) have not been reported for *Am*PDH, these reaction may be possible from a purely structural point of view. Analysis of the maltose 4′-oxidation mode (Fig. S8*f*) indicates that this mode may be somewhat difficult to accommodate with respect to the Tyr510 ring, which forms a "floor" below the sugar ring positioned for oxidation in subsite C. The steric hindrance does not seem severe, but considering the potentially important role of Tyr510 to ensure optimal induced fit, even minor spatial problems in this region are likely to be incompatible with productive substrate-binding modes. Thus, for the disaccharides cellobiose and maltose, the 1 and 2 positions in the reducing-end glucosyl unit are indeed the only sites easily accessible for oxidation. Moreover, placing the non-reducing end glucosyl unit of cellobiose, or maltose, in subsite C unambiguously shows that only C3 and C4 are possible, *i.e.,* 3′- and 4′-oxidation.

Salicin is a glucopyranoside substituted at O1 with an *ortho*-benzylic alcohol ring present in willow bark and known for its properties as a natural analgesic. In the C1- and C2-oxidation modes (Fig. S9*a, b*), the benzylic ring of salicin forms severe clashes with either the flavin ring or the Tyr510 backbone. Favorable interactions are formed only when the non-reducing end glucose unit is positioned in site C for 3- or 4-oxidation (Fig. S9*c, d*).

Discussion

Electron-donor Substrate Preference

The similarity in electron-donor substrate and active-site structure of *Am*PDH, GOX and P2O offers a framework to study substrate selectivity and regioselectivity. The active site of *Am*PDH is more similar to that of *An*GOX than to *Tm*P2O, however, regioselectivity differs for the sugar substrate: *An*GOX oxidizes exclusively at the glucosyl C1 position, whereas *Am*PDH can perform single oxidations at the endocyclic glucosyl-ring positions C1, C2 and C3, as well as double oxidations at C1/3, C2/3, or C3/4 of various sugars [14] and of certain aromatic glycosides [15]. The active sites of *Am*PDH and *Tm*P2O are also relatively similar, and their substrate preference is partly overlapping for the reductive half-reaction.

Modeling D-glucose in orientation for oxidation at C1, C2, C3 or C4 shows that the principal interactions are provided by the catalytic histidine pair and the backbone carbonyl oxygen of Tyr510 (Table S2; Fig. S1). In agreement with observed activity data [7,28], the C2 and C3 oxidation modes appear very favorable (Fig. S1*b, c*). *Tm*P2O has been shown to strongly favor the D-glucose C2 position for oxidation [4,5]. In addition, our previous crystallographic studies on fluorinated glucose derivatives bound to *Tm*P2O provided a rationale for the discrimination of this enzyme against oxidation at the glucosyl C3 position [6]. With D-glucose as substrate, PDH was previously shown to display a slight preference for C3 over C2 [7,16]. To evaluate the relative preference of *Am*PDH for D-glucose oxidation at C2 or C3, we performed reduction experiments using 3FG (C2 accessible) or 2FG (C3 accessible). Reduction of *Am*PDH by 3FG was considerably faster than by 2FG, showing that C2 is the preferred site of oxidation. Although, theoretically, the fluorine might influence the outcome of site attack, the pattern of regioselectivity for fluorinated and non-fluorinated glucose was consistent in the case of *Tm*P2O indicating that the

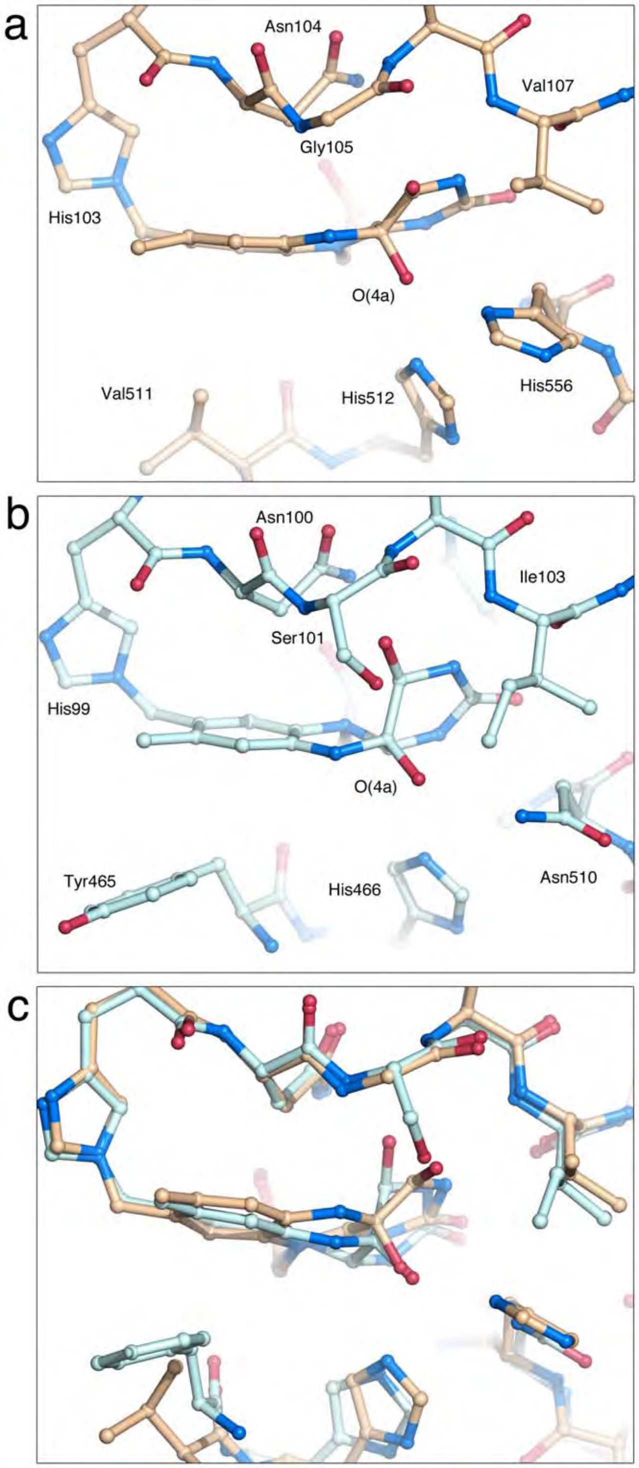

Figure 8. Comparison of the flavin C(4a) adduct in *Am*PDH and CHO. The active site in (a) *Am*PDH (this work; beige carbons) and (b) *Ag*CHO (rerefined model of 2JBV [38], unpublished; light blue carbons) highlighting the modified FAD cofactor. (c) Overlay of the images in (a) and (b). The distortion of the flavin ring accompanying adduct formation is more subtle in *Am*PDH compared with *Ag*CHO.
doi:10.1371/journal.pone.0053567.g008

fluorine does not significantly change the regioselectivity mechanism.

We may conclude that the observed substrate preferences of *Am*PDH can be satisfactorily rationalized by the crystal structure, and that steric clashes are less well tolerated in subsite C than in subsite B1. Subsite B1 is further out from the flavin pocket, and there is likely to be an increased ability for the protein to adjust and reposition loop regions to accommodate different substrates. In this context, it should be noted that only one structural conformer has been determined of *Am*PDH, and ligand-induced conformational changes may, as in the case of *Tm*P2O where regioselectivity is governed by active-site loop movements, recruit other protein groups to offer additional and differential interaction possibilities. However, the temperature factors are typically low for protein backbone atoms in site B1, and the electron density is well defined for all parts of the *Am*PDH active site, indicating that the conformer observed here is heavily dominating the conformational ensemble, at least in the present crystal form and in the absence of ligand. It should also be noted that extensive attempts have been made to capture ligand complexes of PDH using fluorinated glucoses, but without success so far.

Oxygen Reactivity

Due to the potential generation of reactive oxygen species by molecular oxygen, biological redox processes involving oxygen are tightly controlled. The two-electron reduction of O_2 by reduced singlet flavin is a spin-forbidden reaction, and to overcome this barrier, flavoenzymes have developed precisely tuned mechanisms to enable efficient catalysis of the one-electron O_2 reduction reaction [31]. As pointed out recently [32,33], any one single structural determinant in a flavoenzyme is unlikely to be solely and sufficiently responsible for oxygen reactivity. An identical side chain, equivalently positioned and oriented near the flavin, may be important for oxygen activation in one enzyme, but not in another, emphasizing the importance of context-dependent function.

In the case of flavoproteins, formation of a covalent flavin C(4a)-hydroperoxide adduct is one of the means for the enzymes to carry our monooxygenation (monooxygenase) or hydrogen peroxide elimination (oxidase) [34,35]. This flavin species was considered to be limited to the monooxygenase reaction, but was recently reported also for the flavoprotein oxidase *Tm*P2O [36,37]. A flavin C(4a)-adduct has also been detected in a crystalline state of the GMC enzyme choline oxidase [25,38]. In the case of GOX, it has been suggested that the hydroperoxyflavin intermediate is bypassed in the oxygen activation mechanism, and instead, the superoxide anion is stabilized through direct interactions with protonated His516 [39,40].

Suggested determinants of oxygen reactivity include thermodynamic and kinetic considerations, specifically the rate-limiting nature of the first thermodynamically unfavorable one-electron transfer to oxygen; as well as the possible presence of discrete oxygen channels and pockets for oxygen movement and capture [33,39]. In the case of GOX, the positively charged His516 would offer stabilization to the superoxide, thus supporting sufficient rate enhancement of the oxygen reaction, while preventing the risk of accumulating toxic oxygen species [39]. Although these are clearly insightful and important observations, the structural origin of such effects is inherently difficult to assess and remain elusive.

Other studies emphasize the volume restriction of the flavoenzyme active site as a determinant of oxygen reactivity. One study concerns L-galactono-γ-lactone dehydrogenase (GALDH), a member of the *p*-cresol methylhydroxylase family of oxidoreductases [41]. GALDH displays some oxygen activity but performs poorly as an oxidase, however a single Ala→Gly replacement at position 113 was sufficient to convert the enzyme from a very poor oxidase to a highly competent oxidase [42]. This led the authors to suggest that Ala113 acts as a gatekeeper to prevent oxygen binding in wild-type GALDH, whereas the absence of a side chain creates enough space for oxygen to access the flavin ring. The authors provide an extensive analysis of amino-acid occurrences at this position in related enzymes, which implicated that the dehydrogenases feature Ala/Pro/Thr/Ser/Ile/Leu, whereas the oxidases have Gly/Ala/Pro [42].

A comparison of the position of the Ala105 Cβ atom in the enzyme alditol oxidase (PDB code 2VFS [43]) with that of Pro186 Cβ in cholesterol oxidase (type BCO2; PDB code 1I19 [44]) shows that they superimpose within 1 Å, a displacement that is correlated with the precise positioning of the isoalloxazine pyrimidine ring. Thus, the proline ring should be just as efficient in preventing oxygen binding as is the alanine side chain in a dehydrogenase. Moreover, cholesterol oxidase features a second proline (188) opposite to Pro186 which appears to restrict the space for a hypothetical oxygen molecule even further. These observations seriously challenge the assignment of this region as a general determinant of oxygen reactivity, and provide little support for the gatekeeper hypothesis, beyond possibly being relevant for GALDH. Nonetheless, the data mining carried out by Leferink and co-workers highlights the difficulties in generalizing structural determinants of oxygen activity even within a family of highly homologous structures. Recently, site-directed mutagenesis studies of aryl alcohol oxidase have shown the opposite effect when replacing a bulky sidechain (Phe501) with an alanine led to a ~120-fold decrease in the oxygen activity, while the oxygen reactivity was increased ~2-fold by the introduction of a larger Trp side chain [45].

Because of the obvious complexity of context dependency, great care has to be taken when analyzing structure, as well as biophysical and biochemical data. Preferably, enzymes that evolved structurally very similar active sites, but different oxygen reactivity, should be compared to simplify analysis of contextual interaction networks. The GMC family of oxidoreductases includes FAD-dependent oxidoreductases that share a common subunit fold, but represents a spectrum of electron-donor and electron-acceptor substrate specificities. Several members use sugars as electron donors, but display differences in electron-acceptor preference. The enzymes PDH, GOX and P2O represent an interesting triad where the active sites and electron-donor substrate specificities are sufficiently similar, and the oxygen reactivity significantly different, to allow a comparison: *i)* P2O displays oxygen reactivity and stabilizes a flavin C(4a) intermediate; *ii)* GOX displays oxygen reactivity but no flavin C(4a) adduct; and *iii)* PDH has no physiological oxygen reactivity but is able to physically form and stabilize a flavin C(4a) adduct.

As we show here, the oxygen reactivity of PDH is negligible, confirming that this reaction is not likely to be important physiologically and functionally. Notwithstandingly, it is interesting to note that *i)* PDH shows a red anionic flavin semiquinone, and that *ii)* the reduced enzyme forms a stable, long-lived flavin C(4a) adduct with an unidentified mono- or diatomic species under the conditions of the X-ray experiment. At this point, we make no claims that the flavin C(4a) adduct is a functionally relevant intermediate during the oxidative half-reaction of *Am*PDH, but rather, an artifact arising from attack by reactive oxygen species on the C(4a) position during irradiation of the protein crystal. The protein used for crystallization was in the reduced state, making such reactions possible. Presumably, the *Am*PDH preparation was reduced by sugars already inside the cell. The importance of the presence of the adduct species in *Am*PDH lies not in its tentative role, but in its well-defined structure, which provides insight regarding the structural details of this type of flavin intermediate in the active site of the closely related "oxygen-active" GMC members. Thus, this information can be extrapolated to the closely related active sites of GOX (PDB code 1CF3 [23]) and P2O (PDB code 1TT0 [46]) to evaluate possible structural requisites for oxygen reactivity, and activation (*i.e.*, flavin C(4a)-adduct formation and stabilization).

In *An*GOX, His516 has been pointed out as the critical residue for oxygen activation [40,47], however, no spectral evidence has been obtained for a hydroperoxy-flavin intermediate. This histidine is conserved throughout the GMC family and it has been confirmed as the catalytic base in P2O [48]. If this histidine constitutes a general mechanism for oxygen activation, why would GMC members like PDH and CDH show no, or poor ability to activate oxygen? (see comparison in Table 2) The histidine may represent a necessary condition for O_2 activation in the GMC-type flavoprotein oxidases (and possibly others), but is clearly not sufficient. Further comparison of related GMC flavoenzymes shows that neither of the determinants hitherto suggested in the literature is by itself a sufficient condition for oxygen reactivity (Table 2); *i.e.*, the principal histidine of the catalytic pair, protein flavinylation, formation of a flavin C(4a) adduct, or a stabilizing *si*-face N(5) factor.

In contrast to GOX, oxygen activation by *Tm*P2O has been confirmed to proceed *via* a flavin-C(4a)-hydroperoxide intermediate [36]. Indeed, we have shown previously that in order to support formation of a flavin-C(4a)-hydroperoxide intermediate in P2O, a fine-tuned environment around the flavin *re*-face below N(5) is critical for flavin C(4a)-adduct formation since replacing Thr169 by Ser, Ala or Gly effectively abolished C(4a)-hydroperoxy-flavin formation [49]. Similar results have also been observed in an FMN-dependent monooxygenase [50]. Using the reduced FAD specifically labeled at the flavin N(5) in P2O and solvent kinetic isotope effects, it was shown that the bond breakage of the flavin N(5)-H controls the overall process of H_2O_2 elimination [37]. The fine-tuned environment around the flavin N(5) is also important for enzyme flavinylation [51]. Without stabilizing flavin-C(4a)-hydroperoxide, the oxygen-activation mechanism of GOX has been suggested to involve a pre-organized superoxide anion-binding site [40,47]. Based on the *Am*PDH adduct structure, one may conclude that there is definitely enough space in GOX to accommodate this intermediate, ruling out space limitation as a reason for lack of adduct formation in GOX.

An interesting observation is that *Tm*P2O, which is capable of both oxygen reactivity and flavin C(4a)-intermediate stabilization, features a distance of ~4 Å between the side-chain nitrogen atoms of the catalytic pair, *i.e.*, the N–N distance (Table 2). This distance is considerably shorter in the two sugar-oxidizing dehydrogenases that are unable to react with oxygen (~3 Å in PDH and CDH), and longer in *An*GOX (~5 Å), which reacts readily with oxygen but does not form a C(4a)-flavin intermediate. It should be noted that *Ag*CHO also displays an N–N distance of about 4 Å, but due to the uncertain relevance of the crystallographically observed adduct, we refrain from drawing any further conclusions regarding this enzyme.

Although it is too early to speculate on the general mechanistic significance of the N–N distance, undoubtedly, the intimate association of these two active-site side chains in the dehydrogenases leads to closer interaction not only with each other, but also with a hypothetical C(4a) adduct, however without generating steric hindrance or clashes. This is confirmed by the tight association of His512 Nε2 and His556 Nδ1 atoms with the C(4a)-oxygen species in *Am*PDH. At least for these GMC flavoenzymes, the N–N distance probably needs to be precisely controlled to offer the proper magnitude of intermediate stabilization needed for formation and decomposition of the adduct. A long N–N distance would offer no or little stabilization, whereas a very short distance would either abolish adduct formation altogether, or provide too strong stabilization. Clearly, electrostatic interactions [39,52], and space requirements [41,42] are likely to be of general importance for oxygen reactivity and the oxygen reaction mechanism. At least in the case of *Tm*P2O, which makes use of an oxygen-activation mechanism that takes place *via* the collapse of a caged radical pair to form the covalent flavin C(4a) intermediate that eventually leads to H_2O_2 elimination [37], the *si*-face partner (Thr169) constitutes a structural determinant for flavin C(4a) intermediate formation by stabilizing interactions at the flavin N(5)/O(4) locus [49]. A finely tuned interatomic distance between the two nitrogen atoms of the catalytic pair at the *re*-side of the N(5) locus may constitute an additional structural determinant. Drawing on its close structural and functional relationship to the sugar oxidases P2O and GOX, we anticipate that future mutagenesis and kinetic analyses of *Am*PDH, GOX and P2O will advance our understanding regarding oxygen reactivity and oxygen activation for this group of GMC oxidoreductases.

Materials and Methods

Expression and Purification

The *pdh1* gene from *A. meleagris* was heterologously expressed in *Pichia pastoris* under control of the inducible AOX promoter, and *Am*PDH was purified from the culture supernatant of a 60-L fed batch cultivation in principle as previously described [53]. In short, the purification protocol is based on hydrophobic interaction chromatography and anion exchange chromatography. A final step of size exclusion chromatography on a Superdex-75 column (GE Healthcare Life Sciences) equilibrated with 100 mM KH_2PO_4, pH 7.0 buffer containing 100 mM KCl was added to this published protocol to remove minor impurities. Fractions containing *Am*PDH activity were pooled, diafiltrated in 100 mM KH_2PO_4 buffer (pH 7.0) and concentrated.

Re-oxidation of Reduced *Am*PDH

*Am*PDH is isolated mainly as the reduced enzyme. To generate the oxidized enzyme, *Am*PDH was mixed with 1 mM 2,6-dichlorophenol-indophenol (DCIP). The solution was centrifuged at 15,000 rpm for 10 min to remove precipitation of DCIP, and then passed through a gel-filtration column (Sephadex G25) pre-equilibrated with 100 mM NaH_2PO_4 (pH 7.5) to remove DCIP.

Activity of Oxidized *Am*PDH with 2- and 3-Fluorinated Glucose as Electron Donor

To measure the reduction of *Am*PDH by fluorinated glucoses, either 20 µM 3FG or 20 µM 2FG, was added to 20 µM oxidized PDH in 100 mM NaH_2PO_4, pH 7.5 (prepared as above) in an anaerobic cuvette at 25°C. Absorption spectra of the reduction process were monitored at various intervals over a period of 1000 s.

*Am*PDH Reactivity with Oxygen as Electron Acceptor

A solution of oxidized *Am*PDH (23 µM) was reduced with an equal amount of D-glucose to generate the reduced enzyme, and left at air-saturation ($[O_2] = 0.26$ mM) for 15 hrs at 25°C. Absorption spectra of the reduced PDH reacting with 0.26 mM oxygen were recorded.

Deglycosylation and Crystallization

A concentrated preparation of 90 mg *Am*PDH (60 mg/ml) was deglycosylated using a 30:1 mass ratio of *Am*PDH and Jack bean α-mannosidase (Sigma-Aldrich®), specifically, 90 mg PDH and 3.1 mg (68 U) α-mannosidase. The reaction was performed in a solution containing 50 mM sodium acetate (pH 5.5) and 0.4 mM $ZnCl_2$. The sample was incubated overnight at 37°C. Following digestion, the sample was applied onto a Superdex-75 column (GE Healthcare Life Sciences) in 50 mM HEPES (pH 6.5), 150 mM NaCl. Fractions containing *Am*PDH were pooled, diafiltrated in 50 mM HEPES buffer (pH 6.5) and concentrated. The purified protein was screened for crystallization under aerobic conditions using Crystal Screen (Hampton Research). Good quality crystals were obtained from formulation 42 with the addition of 2-methyl-2,4-pentanediol (MPD) [50 mM KH_2PO_4, 5% MPD, and 20% (w/v) polyethylene glycol 8,000], and microseeding. Prior to vitrification in liquid nitrogen, crystals were transferred to a cryo solution containing 50 mM KH_2PO_4, 5% MPD, 35% (v/w) polyethylene glycol 8,000. The crystals belong to space group $P2_12_12_1$ with one molecule in the asymmetric unit and cell dimensions $a = 52.315$ Å, $b = 75.170$ Å, $c = 140.212$ Å. Intensity data were collected to 1.6 Å resolution at beamline *I*911-5 ($\lambda = 0.90772$ Å), MAX-lab, Lund, Sweden. Data were processed and scaled using the *XDS* package [54].

Crystallographic Phasing and Refinement

The *Am*PDH structure was determined by molecular replacement using the fully automated *BALBES* pipeline [55] as implemented in *CCP4i* [56,57], starting with diffraction and sequence data. Automated search model generation in *BALBES* tested five template models: 2JBV, 1CF3, 1GPE, 1JU2, 1KDG; with sequence identities to PDH of 26.1, 27.0, 25.3, 25.3, and 21.5%, respectively. The best Q value after all model calculations (0.5395) was obtained for 2JBV, which resulted in a suggested structure of 82% probability of being correct. After the integrated refinement with *REFMAC5* [58], the initial R/R_{free} values of 0.539/0.538 for this model decreased to 0.448/0.491. Following structure solution, the resulting partially refined model from *BALBES* was submitted for automated model building using the online ARP/wARP web service [59] available at the EMBL Hamburg website (http://www.embl-hamburg.de/ARP). Automatic model building resulted in a nearly complete model of 554 assigned residues (of 577) in eight chains and R/R_{free} values of 0.225 and 0.269, respectively. Refinement was performed using *REFMAC5* [56,58], including anisotropic scaling, calculated hydrogen scattering from riding hydrogen atoms. Individual anisotropic B-factor refinement was performed for all atoms. Atomic displacement parameter refinement was performed using the translation, libration, screw-rotation (TLS) model. Eight TLS groups were defined, as determined by the TLS Motion Determination server, *TLSMD* [60]. Rebuilding and model manipulation were done using O [22] and Coot [61], guided by σ_A-weighted $2F_o$–F_c and F_o–F_c electron-density maps. Model validation was performed using *MolProbity* [62]. The 5000 K simulated annealing omit map shown in Fig. 7 was calculated using *PHENIX* [63]. Data collection and model refinement statistics are given in Table 1.

All pictures showing structures were generated with PyMOL™ [64] (DeLano Scientific LLC, www.pymol.org). The atomic coordinates and structure factors (code 4H7U) for the *Am*PDH model have been deposited with the Protein Data Bank, Research Collaboratory for Structural Bioinformatics, Rutgers (http://www.rcsb.org).

Modeling of Substrates in the *Am*PDH Active Site

To rationalize the observed patterns of substrate selectivity and regioselectivity for *Am*PDH [13], *in silico* modeling analyses were performed using substrates for which *i)* the relative activity is >50% of the activity for D-glucose, and *ii)* the site(s) of oxidation have been determined. The modeled substrates are shown in Fig. 1 and include: D-glucose, D-xylose, L-arabinose, D-galactose, methyl-α-D-glucose, methyl-β-D-glucose, cellobiose, maltose, and salicin [13,14]. Modeling was performed by docking the individual substrates in the *Am*PDH active site using the program *O* [22], and identifying possible hydrogen bonds. The modeling was guided by the known binding modes for C2 and C3 oxidation of D-glucose determined for *Tm*P2O (PDB code 3PL8 [6] and 2IGO [3], respectively). Protein-sugar interactions were considered possible if appropriate hydrogen-bond donor and acceptor atoms are present within a distance of 3.3 Å. The coordinates for carbohydrate structures were retrieved using the HIC-Up database at Uppsala Software Factory (http://xray.bmc.uu.se/usf/), or in the case of salicin, generated from the published coordinates [65].

Supporting Information

Figure S1 Modeling of D-glucose in position for 1-, 2-, 3- and 4-oxidation. The active site in *Am*PDH with D-glucose modeled in orientation for oxidation at (a) C1, (b) C2, (c) C3, and (d) C4. The protein is shown with beige carbon atoms, and the FAD cofactor and sugars in yellow and green, respectively.
(TIF)

Figure S2 Modeling of D-xylose in position for 1-, 2-, 3- and 4-oxidation. The active site in AmPDH with D-xylose modeled in orientation for oxidation at (a) C1, (b) C2, (c) C3, and (d) C4. The protein is shown with beige carbon atoms, and the FAD cofactor and sugar in yellow and green, respectively.
(TIF)

Figure S3 Modeling of L-arabinose in position for 1-, 2-, 3- and 4-oxidation. The active site in AmPDH with L-arabinose modeled in orientation for oxidation at (a) C1, (b) C2, (c) C3, and (d) C4. The protein is shown with beige carbon atoms, and the FAD cofactor and sugar in yellow and green, respectively.
(TIF)

Figure S4 Modeling of D-galactose in position for 1-, 2-, 3- and 4-oxidation. The active site in AmPDH with D-galactose modeled in orientation for oxidation at (a) C1, (b) C2, (c) C3, and (d) C4. The protein is shown with beige carbon atoms, and the FAD cofactor and sugar in yellow and green, respectively.
(TIF)

Figure S5 Modeling of methyl-α-D-glucose in position for 1-, 2-, 3- and 4-oxidation. The active site in AmPDH with methyl-α-D-glucose modeled in orientation for oxidation at (a) C1, (b) C2, (c) C3, and (d) C4. The protein is shown with beige carbon atoms, and the FAD cofactor and sugar in yellow and green, respectively.
(TIF)

Figure S6 Modeling of methyl-β-D-glucose in position for 1-, 2-, 3- and 4-oxidation. The active site in AmPDH with methyl-β-D-glucose modeled in orientation for oxidation at (a) C1, (b) C2, (c) C3, and (d) C4. The protein is shown with beige carbon atoms, and the FAD cofactor and sugar in yellow and green, respectively.
(TIF)

Figure S7 Modeling of cellobiose in position for 1-, 2-, 3-, 2′-, 3′- and 4′-oxidation. The active site in AmPDH with cellobiose modeled in orientation for oxidation at (a) C1, (b) C2, (c) C3, (d) C2′, (e) C3′, and (f) C4′. The protein is shown with beige carbon atoms, and the FAD cofactor and sugar in yellow and green, respectively.
(TIF)

Figure S8 Modeling of maltose in position for 1-, 2-, 3-, 2′-, 3′- and 4′-oxidation. The active site in AmPDH with maltose modeled in orientation for oxidation at (a) C1, (b) C2, (c) C3, (d) C2′, (e) C3′, and (f) C4′. The protein is shown with beige carbon atoms, and the FAD cofactor and sugar in yellow and green, respectively.
(TIF)

Figure S9 Modeling of salicin in position for 1-, 2-, 3- and 4-oxidation. The active site in AmPDH with salicin modeled in orientation for oxidation at (a) C1, (b) C2, (c) C3, and (d) C4. The protein is shown with beige carbon atoms, and the FAD cofactor and sugar in yellow and green, respectively.
(TIF)

Table S1 Geometry of flavin C(4a) O-adducts in known crystal structures.
(DOCX)

Table S2 Computational modeling of monosaccharides in the *Am*PDH active site.
(DOCX)

Table S3 Computational modeling of disaccharides in the *Am*PDH active site.
(DOCX)

Acknowledgments

The authors thank Magdalena Kujawa for help with preparation of *Am*PDH. We also thank the beamline staff scientists at MAX-lab (Lund, Sweden) for support during data collection.

Author Contributions

Conceived and designed the experiments: TCT OS CD PC CKP. Performed the experiments: TCT OS CD TW IK JS CS. Analyzed the data: TCT OS CD PC TW JS. Wrote the paper: CD TCT OS DH CKP PC TW.

References

1. Kittl R, Sygmund C, Halada P, Volc J, Divne C, et al. (2008) Molecular cloning of three pyranose dehydrogenase-encoding genes from *Agaricus meleagris* and analysis of their expression by real-time RT-PCR. Curr Genet 53: 117–127.
2. Sygmund C, Kittl R, Volc J, Halada P, Kubatova E, et al. (2008) Characterization of pyranose dehydrogenase from *Agaricus meleagris* and its application in the C-2 specific conversion of D-galactose. J Biotechnol 133: 334–342.
3. Kujawa M, Ebner H, Leitner C, Hallberg BM, Prongjit M, et al. (2006) Structural basis for substrate binding and regioselective oxidation of monosaccharides at C-3 by pyranose 2-oxidase. J Biol Chem 281: 35104–35115.

4. Prongjit M, Sucharitakul J, Wongnate T, Haltrich D, Chaiyen P (2009) Kinetic mechanism of pyranose 2-oxidase from Trametes multicolor. Biochemistry 48: 4170–4180.
5. Sucharitakul J, Wongnate T, Chaiyen P (2010) Kinetic isotope effects on the noncovalent flavin mutant protein of pyranose 2-oxidase reveal insights into the flavin reduction mechanism. Biochemistry 49: 3753–3765.
6. Tan TC, Haltrich D, Divne C (2011) Regioselective control of β-D-glucose oxidation by pyranose 2-oxidase is intimately coupled to conformational degeneracy. J Mol Biol 409: 588–600.
7. Volc J, Kubatova E, Daniel G, Sedmera P, Haltrich D (2001) Screening of basidiomycete fungi for the quinone-dependent sugar C-2/C-3 oxidoreductase, pyranose dehydrogenase, and properties of the enzyme from *Macrolepiota rhacodes*. Arch Microbiol 176: 178–186.
8. Pisanelli I, Wuhrer P, Reyes-Dominguez Y, Spadiut O, Haltrich D, et al.(2012) Heterologous expression and biochemical characterization of novel pyranose 2-oxidases from the ascomycetes *Aspergillus nidulans* and *Aspergillus oryzae*. Appl Microbiol Biotechnol 93: 1157–1166.
9. Ander P, Marzullo L (1997) Sugar oxidoreductases and veratryl alcohol oxidase as related to lignin degradation. J Biotechnol 53: 115–131.
10. Giffhorn F (2000) Fungal pyranose oxidases: occurrence, properties and biotechnical applications in carbohydrate chemistry. Appl Microbiol Biotechnol 54: 727–740.
11. Volc J, Denisova NP, Nerud F, Musilek V (1985) Glucose 2-oxidase activity in mycelial cultures of basidiomycetes. Folia Microbiol 30: 141–147.
12. Dix NJ, Webster J (1995) *Fungal ecology*. London: Chapman & Hall, UK, p.549.
13. Sedmera P, Halada P, Kubatova E, Haltrich D, Prikrylova V, et al. (2006) New biotransformations of some reducing sugars to the corresponding (di)dehydro(-glycosyl) aldoses or aldonic acids using fungal pyranose dehydrogenase. J Mol Catal B 41: 32–42.
14. Peterbauer CK, Volc J (2010) Pyranose dehydrogenase: biochemical features and perspectives of technological applications. Appl Microbiol Biotechnol 85: 837–848.
15. Sedmera P, Halada P, Peterbauer C, Volc J (2004) A new enzyme catalysis: 3,4-dioxidation of some aryl β-D-glycopyranosides by fungal pyranose dehydrogenase. Tetrahedron Lett 45: 8677–8680.
16. Kujawa M, Volc J, Halada P, Sedmera P, Divne C, et al. (2007) Properties of pyranose dehydrogenase purified from the litter-degrading fungus *Agaricus xanthoderma*. FEBS J 274: 879–894.
17. Volc J, Sedmera P, Kujawa M, Halada P, Kubatova E, et al. (2004) Conversion of lactose to β-D-galactopyranosyl-(1–4)-D-arabino-hexos-2-ulose-(2-dehydrolactose) and lactobiono-1,5-lactone by fungal pyranose dehydrogenase. J Mol Catal B 30: 177–184.
18. Wong CM, Wong KH, Chen XD (2008) Glucose oxidase: natural occurrence, function, properties and industrial applications. Appl Microbiol Biotechnol 78: 927–938.
19. Gadda G (2008) Hydride transfer made easy in the reaction of alcohol oxidation catalyzed by flavin-deoendent oxidases. Biochemistry 47: 13745–13753.
20. Holm L, Park J (2000) DaliLite workbench for protein structure comparison. Bioinformatics 16: 566–567.
21. Fernandez IS, Ruis-Duenas FJ, Santillana E, Ferreira P, Martinez MJ, et al. (2009) Novel structural features in the GMC family of oxidoreductases revealed by the crystal structure of fungal aryl-alcohol oxidase. Acta Crystallogr D Biol Crystallogr 65: 1196–1205.
22. Jones TA, Zou JY, Cowan SW, Kjeldgaard M (1991) Improved methods for building protein models in electron density maps and the location of errors in these models. Acta Crystallogr A 47: 110–119.
23. Wohlfahrt G, Witt S, Hendle J, Schomburg D, Kalisz HM, et al. (1999) 1.8 and 1.9 A resolution structures of the *Penicillium amagasakiense* and *Aspergillus niger* glucose oxidases as a basis for modelling substrate complexes. Acta Crystallogr D Biol Crystallogr 55: 969–977.
24. Hallberg BM, Henriksson G, Pettersson G, Vasella A, Divne C (2003) Mechanism of the reductive half-reaction in cellobiose dehydrogenase. J Biol Chem 278: 7160–7166.
25. Orville AM, Lountos GT, Finnegan S, Gadda G (2009) Crystallographic, spectroscopic, and computational analysis of a flavin C4a-oxygen adduct in choline oxidase. Biochemistry 48: 720–728.
26. Menova P, Eugner V, Cejka J, Dvorakova H, Sanda M, et al. (2011) Synthesis and structural studies of flavin and alloxazine adducts with O-nucleophiles. J Mol Struct 1004: 178–187.
27. Volc J, Sedmera P, Halada P, Prikrylova V, Haltrich D (2000) Double oxidation of D-xylose to D-glycero-pentos-2,3-diulose (2,3-diketo-D-xylose) by pyranose dehydrogenase from the mushroom *Agaricus bisporus*. Carbohydr Res 329: 219–225.
28. Volc J, Sedmera P, Halada P, Prikrylov V, Daniel G (1998) C-2 and C-3 oxidation of D-Glc, and C-2 oxidation of D-Gal by pyranose dehydrogenase from *Agaricus bisporus*. Carbohydr Res 310: 151–156.
29. Volc J, Sedmera P, Halada P, Daniel G, Prikrylova V, et al. (2002) C-3 oxidation of non-reducing sugars by a fungal pyranose dehydrogenase: spectral characterization. J Mol Catal B Enzym 17: 91–100.
30. Hallberg BM, Henriksson G, Pettersson G, Divne C (2002) Crystal structure of the flavoprotein domain of the extracellular flavocytochrome cellobiose dehydrogenase. J Mol Biol 315: 421–434.
31. Massey V (1994) Activation of molecular oxygen by flavins and flavoprotein. J Biol Chem 269: 22459–22462.
32. McDonald CA, Fagan RL, Collard F, Monnier VM, Palfey BA (2011) Oxygen reactivity in flavoenzymes: context matters. J Am Chem Soc 133: 16809–16811.
33. Chaiyen P, Fraaije MW, Mattevi A (2012) The enigmatic reaction of flavins with oxygen. Trends Biochem Sci 37: 373–380.
34. Chaiyen P (2010) Flavoenzymes catalyzing oxidative aromatic ring-cleavage reactions. Arch Biochem Biophys 493: 62–70.
35. Ruangchan N, Tongsook C, Sucharitakul J, Chaiyen P (2011) pH-dependent studies reveal an efficient hydroxylation mechanism of the oxygenase component of p-hydroxyphenylacetate 3-hydroxylase. J Biol Chem 286: 223–233.
36. Sucharitakul J, Prongjit M, Haltrich D, Chaiyen P (2008) Detection of a C4a-hydroperoxyflavin intermediate in the reaction of a flavoprotein oxidase. Biochemistry 47: 8485–8490.
37. Sucharitakul J, Wongnate T, Chaiyen P (2011) Hydrogen peroxide elimination from C4a-hydroperoxyflavin in a flavoprotein oxidase occurs through a single proton transfer from flavin N5 to a peroxide leaving group. J Biol Chem 286: 16900–16909.
38. Quaye O, Lountos GT, Fan F, Orville AM, Gadda G (2008) Role of Glu312 in binding and positioning of the substrate for the hydride transfer reaction in choline oxidase. Biochemistry 47: 243–256.
39. Klinman JP (2007) How do enzymes activate oxygen without inactivating themselves? Acc Chem Res 40: 325–333.
40. Kommoju P-R, Chen Z-W, Bruckner RC, Mathews FS, Schuman Jorns M (2011) Probing oxygen activation sites in two flavoprotein oxidases using chloride as an oxygen surrogate. Biochemistry 50: 5521–5534.
41. Fraaije MW, van Berkel WJH, Benen JA, Visser J, Mattevi A (1998) A novel oxidoreductase family sharing a conserved FAD-binding domain. Trends Biochem Sci 23: 206–207.
42. Leferink NGH, Fraaije MW, Joosten H-J, Schaap PJ, Mattevi A (2009) Identification of a gatekeeper residue that prevents dehydrogenases from acting as oxidases. J Biol Chem 284: 4392–4397.
43. Forneris F, Heuts DPHM, Delvecchio M, Rovida S, Fraaije MW, et al. (2008) Structural analysis of the catalytic mechanism and stereoselectivity in *Streptomyces coelicolor* alditol oxidase. Biochemistry 47: 978–985.
44. Coulombe R, Yue KQ, Ghisla S, Vrielink A (2001) Oxygen access to the active site of cholesterol through a narrow channel is gated by an Arg-Glu pair. J Biol Chem 276: 30435–30441.
45. Hernández-Ortega A, Lucas F, Ferreira P, Medina M, Guallar V, et al. (2011) Modulating O2 reactivity in a fungal flavoenzyme: involvement of aryl-alcohol oxidase Phe-501 contiguous to catalytic histidine. J Biol Chem 286: 41105–41114.
46. Hallberg BM, Leitner C, Haltrich D, Divne C (2004) Crystal structure of the 270 kDa homotetrameric lignin-degrading enzyme pyranose 2-oxidase. J Mol Biol 341: 781–796.
47. Roth JP, Klinman JP (2003) Catalysis of electron transfer during activation of O2 by the flavoprotein glucose oxidase. Proc Natl Acad Sci U S A 100: 62–67.
48. Wongnate T, Sucharitakul J, Chaiyen P (2011) Identification of a catalytic base for sugar oxidation in the pyranose 2-oxidase reaction. Chembiochem 12: 2577–2586.
49. Pitsawong W, Sucharitakul J, Prongjit M, Tan TC, Spadiut O, et al. (2010) A conserved active-site threonine is important for both sugar and flavin oxidations of pyranose 2-oxidase. J Biol Chem 285: 9697–9705.
50. Thotsaporn K, Chenorakhon P, Sucharitakul J, Mattevi A, Chaiyen P (2011) Stabilization of C4a-hydroperoxyflavin in a two-component flavin-dependent monooxygenase is achieved through interactions at flavin N5 and C4a atoms. J Biol Chem 286: 28170–28180.
51. Tan TC, Pitsawong W, Wongnate T, Spadiut O, Haltrich D, et al. (2010) H-bonding and positive charge at the N(5)/O(4) locus are critical for covalent flavin attachement in *Trametes* pyranose 2-oxidase. J Mol Biol 402: 578–594.
52. Gadda G (2012) Oxygen activation in flavoprotein oxidases: the importance of being positive. Biochemistry 51: 2662–2669.
53. Sygmund C, Gutmann A, Krondorfer I, Kujawa M, Glieder A, et al. (2012) Simple and efficient expression of Agaricus meleagris pyranose dehydrogenase in Pichia pastoris. Appl Microbiol Biotechnol 94: 695–704.
54. Kabsch W (1993) Automatic processing of rotation diffraction data from crystals of initially unknown symmetry and cell constants. J Appl Crystallogr 26: 795–800.
55. Long F, Vagin A, Young P, Murshudov GN (2008) BALBES: a Molecular Replacement Pipeline. Acta Crystallogr D Biol Crystallogr 64: 125–132.
56. Winn MD, Ballard CC, Cowtan KD, Dodson EJ, Emsley P, et al. (2011) Overview of the CCP4 suite and cirrent developments. Acta Crystallogr D Biol Crystallogr 67: 235–242.
57. Potterton E, Briggs P, Turkenburg M, Dodson EJ (2003) A graphical user interface to the CCP4 program suite. Acta Crystallogr D Biol Crystallogr 59: 1131–1137.
58. Murshudov GN, Vagin AA, Dodson EJ (1997) Refinement of macromolecular structures by the maximum-likelihood method. Acta Crystallogr D Biol Crystallogr 53: 240–255.
59. Perrakis A, Morris RJ, Lamzin VS (1999) Automated protein model building combined with iterative structure refinement. Nat Struct Biol 6: 458–463.
60. Painter J, Merritt EA (2006) Optimal description of a protein structure in terms of multiple groups undergoing TLS motion. Acta Crystallogr D Biol Crystallogr 62: 439–450.
61. Emsley P, Cowtan K (2004) Coot: model-building tools for molecular graphics. Acta Crystallogr D Biol Crystallogr 60: 2126–2132.

62. Chen VB, Arendall III WB, Headd JJ, Keedy DA, Immormino RM, et al. (2010) MolProbity: all-atom structure validation for macromolecular crystallography. Acta Crystallogr D Biol Crystallogr 66: 12–21.
63. Adams PD, Afonine PV, Bunkóczi G, Chen VB, Davis IW, et al. (2010) PHENIX: a comprehensive Python-based system for macromolecular structure solution. Acta Crystallogr D Biol Crystallogr 66: 213–221.
64. DeLano WL (2002) The PyMOL Molecular Graphics System. DeLano Scientific, Palo Alto, CA, USA.
65. Ueno K (1984) Structure of salicin, $C_{13}H_{18}O_7$. Acta Crystallogr C 40: 1726–1728.
66. Karplus PA, Diederichs K (2012) Linking crystallographic model and data quality. Science 336: 1030–1033.
67. Finnegan S, Agniswamy J, Weber IT, Gadda G (2010) Role of valine 464 in the flavin oxidation reaction catalyzed by choline oxidase. Biochemistry 49: 2952–2961.
68. Finnegan S, Yuan H, Wang Y-F, Orville AM, Weber IT, et al. (2010) Structural and kinetic studies on the Ser101Ala variant of choline oxidase: catalysis by compromise. Arch Biochem Biophys 501: 207–213.

Chapter 3. Engineering of *Agaricus meleagris* pyranose dehydrogenase

Paper IV

Engineering of pyranose dehydrogenase for increased oxygen reactivity.

Iris Krondorfer, Katharina Lipp, Dagmar Brugger, Petra Staudigl, Christoph Sygmund, Dietmar Haltrich and Clemens K. Peterbauer

PLoS ONE (2014) 9 (3): e91145. doi:10.1371/journal.pone.0091145.

Paper V

Agaricus meleagris pyranose dehydrogenase: Influence of covalent FAD linkage on catalysis and stability

Iris Krondorfer, Dagmar Brugger, Regina Paukner, Katharina F. Pirker, Stefan Hofbauer, Paul G. Furtmüller, Christian Obinger, Dietmar Haltrich, Clemens K. Peterbauer

Archives of Biochemistry and Biophysics (2014) submitted.

Paper IV

Engineering of Pyranose Dehydrogenase for Increased Oxygen Reactivity

Iris Krondorfer[1], Katharina Lipp[1,2], Dagmar Brugger[1], Petra Staudigl[1], Christoph Sygmund[1], Dietmar Haltrich[1], Clemens K. Peterbauer[1]*

1 Food Biotechnology Laboratory, Department of Food Science and Technology, University of Natural Resources and Life Sciences, Vienna, Austria, **2** University of Applied Sciences Wiener Neustadt – Campus Tulln, Tulln, Austria

Abstract

Pyranose dehydrogenase (PDH), a member of the GMC family of flavoproteins, shows a very broad sugar substrate specificity but is limited to a narrow range of electron acceptors and reacts extremely slowly with dioxygen as acceptor. The use of substituted quinones or (organo)metals as electron acceptors is undesirable for many production processes, especially of food ingredients. To improve the oxygen reactivity, site-saturation mutagenesis libraries of twelve amino acids around the active site of *Agaricus meleagris* PDH were expressed in *Saccharomyces cerevisiae*. We established high-throughput screening assays for oxygen reactivity and standard dehydrogenase activity using an indirect Amplex Red/horseradish peroxidase and a DCIP/D-glucose based approach. The low number of active clones confirmed the catalytic role of H512 and H556. Only one position was found to display increased oxygen reactivity. Histidine 103, carrying the covalently linked FAD cofactor in the wild-type, was substituted by tyrosine, phenylalanine, tryptophan and methionine. Variant H103Y was produced in *Pichia pastoris* and characterized and revealed a five-fold increase of the oxygen reactivity.

Citation: Krondorfer I, Lipp K, Brugger D, Staudigl P, Sygmund C, et al. (2014) Engineering of Pyranose Dehydrogenase for Increased Oxygen Reactivity. PLoS ONE 9(3): e91145. doi:10.1371/journal.pone.0091145

Editor: Danilo Roccatano, Jacobs University Bremen, Germany

Received January 14, 2014; **Accepted** February 7, 2014; **Published** March 10, 2014

Copyright: © 2014 Krondorfer et al. This is an open-access article distributed under the terms of the Creative Commons Attribution License, which permits unrestricted use, distribution, and reproduction in any medium, provided the original author and source are credited.

Funding: This work was financed by the Austrian Science Fund (FWF; www.fwf.ac.at): Individual Grant P22094 to CKP Doctoral programme BioToP (Biomolecular Technology of Proteins; grant nr. W1224; IK and DB are members). The funders had no role in study design, data collection and analysis, decision to publish, or preparation of the manuscript.

Competing Interests: The authors have declared that no competing interests exist.

* E-mail: clemens.peterbauer@boku.ac.at

Introduction

The flavoenzyme pyranose dehydrogenase (PDH, EC 1.1.99.29), a monomeric, extracellular fungal glycoprotein of around 65 kDa, catalyzes the oxidation of a broad range of mono-, oligosaccharides and glycosides at different sites to the corresponding aldoketose or diketose derivatives. Dependent on the sugar, the source of the enzyme and the reaction conditions, C-1, C-2, C-3 and dioxidations at C-1,2, C-2,3 and C-3,4 can be performed. Unlike the closely related enzyme pyranose 2-oxidase (POx), PDH is unable to utilize O_2 as an electron acceptor, (substituted) quinones and complexed metal ions are used instead [1].

PDH was first isolated from the edible basidiomycete *Agaricus bisporus* and subsequently from other members of the *Agaricaceae* family [2–6]. The fungus *A. meleagris* was found to possess three *pdh*-genes, with *pdh1* being transcribed in higher levels than *pdh2* and *pdh3*, especially in stages of oxygen deprivation [7]. POx- and PDH-encoding genes were found to occur mutually exclusive in Basidiomycetes and have not been detected in one species. Wood-degrading white rot fungi (e.g. *Trametes sp.*, *Phanerochaete sp.*) generally possess POx whereas PDH seems to be limited to the mostly litter-decomposing fungi of the family *Agaricaceae* [3]. The biological function of the enzyme is not clear, due to the narrow range of electron acceptors one role of PDH could be the reduction of reactive radicals and quinone compounds emerging during lignin decomposition to prevent their repolymerization and protect the cell from damage [8–10].

Its substrate promiscuity renders the enzyme a promising biocatalyst for the synthesis of high-value carbohydrate compounds in the pharmaceutical-, cosmetic- and food industry [5,6,11,12]. Removal of the (mostly) undesirable electron acceptors would increase costs of product purification significantly and limit the application of PDH in industrial scale, especially for the production of food ingredients. Despite the disadvantageous effects of the produced hydrogen peroxide, an enzyme with the broad sugar substrate specificity of PDH utilizing O_2 as a nonhazardous electron acceptor could substantially simplify production processes.

The overall structure of PDH shows a typical p-hydroxybenzoate hydroxylase (PHBH)-like fold that is shared by the members of the glucose-methanol-choline (GMC) family of oxidoreductases like POx, glucose oxidase (GOx) or cellobiose dehydrogenase (CDH). PDH consists of a Rossman-domain where the FAD cofactor is covalently bound and a substrate binding domain [13].

Several structural characteristics in flavoprotein oxidases apparently contribute to oxygen reactivity, but a general mechanism why a protein does or does not react with oxygen remains unknown [14]. The chemistry of the reaction with oxygen is believed to start with an initial electron transfer from the reduced flavin to oxygen, which forms $O_2^{\bullet -}$ and flavin semiquinone. In flavoprotein oxidases an immediate second electron transfer occurs, resulting in the reoxidized flavin and H_2O_2.

Monooxygenases and certain oxidases like POx form a transient C(4a)-(hydro)peroxyflavin intermediate [15,16]. In the recently resolved crystal structure of PDH, such a C(4a) adduct is visible as well. Although considered a radiation artifact, it shows that PDH is able to form and stabilize such an adduct [13].

A protonated histidine in the active site of GOx was identified to be crucial for the first and rate-limiting electron transfer step [17,18]. Studies on other flavoprotein oxidases showed a positive charge in the active site to be a general prerequisite [19]. Not only amino acids, like a lysine in monomeric sarcosine oxidase [20], but also a charged substrate like in choline oxidase can fulfill this requirement [21]. Furthermore, a nonpolar site close to the flavin C(4a) in addition to the positive charge seems to maximize these electrostatic effects by desolvation of the active site [19,22]. The accessibility of the active site through tunnels and channels is another important aspect for oxygen reactivity [23–25]. All these observations indicate that the microenvironment of the flavin, especially of the C(4a)N5 locus, and subtle changes therein, are of major importance concerning oxygen reactivity [26].

For this reason a semi-rational approach using site-saturation mutagenesis of twelve amino acids in the active site of *A. meleagris* PDH (AmPDH) was chosen for this work. We show for the first time the expression of site-saturation libraries of AmPDH in *S. cerevisiae* and the high-throughput screening for increased oxygen reactivity using an Amplex Red/horseradish peroxidase based assay. Amino acid substitutions only at position H103 to tyrosine, phenylalanine, tryptophan and methionine showed increased oxygen reactivity. Variant H103Y was produced in 5 L scale and partially characterized in order to gain further insight into the oxygen reactivity of flavoproteins.

Material and Methods

2.1 Chemicals and vectors

All chemicals were of the highest purity available and purchased from Sigma Aldrich (St. Louis, MO), Roth (Karlsruhe, Germany), and VWR (Radnor, PA). Primers were from LGC genomics (Vienna, Austria), restriction endonucleases, T4 DNA ligase and phusion polymerase from Thermo Fisher Scientific Biosciences (St. Leon-Rot, Germany). GoTaq polymerase was obtained from Promega (Madison, WI). The uracil independent and ampicillin resistance-encoding shuttle vector pYES2/CT and the Zeocin resistance-encoding shuttle vector pPICZB were purchased from Invitrogen (Carlsbad, CA).

2.2 Strains and media

P. pastoris strain X33 was purchased from Invitrogen, the protease-deficient *S. cerevisiae* strain BJ5465 from LGC Promochem (Barcelona, Spain) and *Escherichia coli* strain NEB5α from New England Biolabs (Ipswich, MA). YPD plates contained 10 g L^{-1} peptone, 20 g L^{-1} yeast extract, 10 g L^{-1} D-glucose, 20 g L^{-1} agar and 100 mg L^{-1} Zeocin. LB low salt medium contained 10 g L^{-1} peptone from casein, 5 g L^{-1} yeast extract, 5 g L^{-1} NaCl and 25 mg L^{-1} Zeocin. Basal salts medium (Invitrogen) was used for fermentation, containing 0.93 g L^{-1} calcium sulfate, 18.2 g L^{-1} potassium sulfate, 14.9 g L^{-1} magnesium sulfate heptahydrate, 4.13 g L^{-1} potassium hydroxide, 40 g L^{-1} glycerol, 26.7 mL 85% phosphoric acid and 4.35 mL PTM_1 trace salts per liter. SC-dropout plates contained 1.92 g L^{-1} Y1501 (synthetic dropout medium without uracil), 20 g L^{-1} agar, 100 mL L^{-1} 20% D-glucose, 100 mL L^{-1} 10× YNB and 1 mL L^{-1} chloramphenicol. For the preparation of the liquid medium (without agar), D-glucose was replaced by raffinose. SG/R-CAA expression medium [27] contained 5 g L^{-1} casein hydrolysate, 9.67 g L^{-1} $NaH_2PO_4.2H_2O$, 6.77 g L^{-1} $Na_2HPO_4.2H_2O$, 50 mL L^{-1} 10× YNB, 100 mL L^{-1} 20% D-galactose, 100 mL L^{-1} 20% raffinose and 5 mL L^{-1} 20% D-glucose.

2.3 Construction of plasmids for expression in P. pastoris and S. cerevisiae

The internal *Bam*HI restriction site of the *Agaricus meleagris pdh1* gene [7] in the vector pCR Blunt II TOPO (Invitrogen) *pdh1* was removed by site-directed mutagenesis following the *Dpn*I-method [28] using the overlapping mutagenesis primers AmFw/AmRev (Table S1). The PCR-product was purified from an agarose gel, digested with *Dpn*I for 2 h at 37°C to degrade methylated template-DNA, and 5 µL of the PCR product were transformed into chemically competent *E. coli* NEB5α. The presence of the mutation was confirmed by sequencing. The *pdh1* gene was then amplified using the primer pairs Am*Kpn*Ifw/Am*Xba*Irev and Am*Bam*HIfw/Am*Not*Irev. The purified product was digested with the respective restriction endonucleases and ligated into the equally treated vectors pPICZB and pYES2/CT, respectively. The resulting plasmids pPICZB_AmPDH and pYES2/CT_AmPDH were transformed into chemically competent *E. coli* NEB5α (New England Biolabs), proliferated and stored at −20°C.

2.4 Heterologous expression of A. meleagris PDH in S. cerevisiae

Plasmid pYES2/CT_AmPDH was transformed into *S. cerevisiae* BJ5465 using the yeast transformation kit (Sigma) based on the lithium acetate/ss-DNA/PEG method [29]. Transformed cells were plated onto SC-dropout plates and incubated at 30°C for 4 days. Transformants were picked into 96-well deep-well plates (Ritter, Schwabmünchen, Germany) containing 200 µL of SC-dropout minimal medium. As a negative control, transformants carrying the empty vector pYES2/CT were used (four wells per plate in row 8). The plates were sealed with BreatheEasy membranes (Diversified Biotech, Dedham, MA) to avoid evaporation of the liquid. After 48 h incubation at 25°C and 365 rpm, 500 µL of SG/R-CAA expression medium were added to each well, followed by seven days of incubation under the same conditions.

2.5 Site saturation library construction

The plasmid pYES2/CT_AmPDH was used as a template for site-saturation library generation using the overlap extension method [30]. The codon NNK (N = A, G, C, or T and K = G or T) was used to reduce the necessary library size to statistically cover 99% of all possible substitutions [31]. A complementary pair of inner primers was designed for each of the twelve selected positions (Table S1) as well as a pair of outer primers producing overlaps with the vector (RMLN-sense, RMLC-antisense [32]). Two separate PCR reactions were carried out, producing fragment 1 (RMLN-sense and mutagenic reverse-primer) and fragment 2 (mutagenic forward-primer and RMLC-antisense). The two fragments were fused in a third PCR-reaction with the outer (RMLN-sense and RMLC-antisense) primers and the purified PCR-product was transformed to *S. cerevisiae* BJ5465 together with the digested vector pYES2/CT (*Bam*HI, *Not*I) for in-vivo recombination in a 4:1 ratio. The variant libraries were expressed as described above (section 2.4) for the wildtype enzyme with some modifications: As a negative control two wells in row 8 were inoculated with *S. cerevisiae* transformed with the empty vector pYES2/CT, three wells with *S. cerevisiae* transformants expressing a cellobiose dehydrogenase (CDH) gene from *Myriococcum thermophilum* [33] as a positive control for the Amplex Red oxygen screening assay and three wells with transformants expressing wild-type AmPDH.

2.6 High throughput screening assay

One hundred µL of the culture were transferred to a sterile 96-well plate (Greiner, Kremsmünster, Austria) and OD600 was measured. After addition of 100 µL of 30% (v/v) glycerol the plates were stored at −70°C as master plates. The remaining cultures in the deep-well plates were centrifuged for 20 min at 3,000 rpm and room temperature and the screening assay was performed with the supernatant. For each target position 352 clones were screened.

PDH dehydrogenase activity was determined with an assay containing 2,6-dichloroindophenol (DCIP, $\varepsilon_{520} = 6.8\ \text{mM}^{-1}\ \text{cm}^{-1}$) and D-glucose. Fifty µL of the culture supernatant were transferred from the deep-well plate to the 96-well screening plates using the JANUS liquid handling workstation (PerkinElmer, Waltham, MA). The reaction was started by addition of 150 µL of the DCIP assay mixture (300 µM DCIP in 100 mM sodium acetate buffer pH 4 containing 50 mM D-glucose) and the time-dependant reduction of DCIP was followed at 520 nm with an EnSpire plate reader (PerkinElmer). End-point measurements were carried out after 2 h and 4 h incubation at 30°C and the difference in absorbance (ΔAbs) was calculated in relation to wild-type AmPDH. For calculation of the number of active clones all clones with ΔAbs values higher than the negative controls for each screening plate were considered active.

Oxygen reactivity was determined using a fluorimetric assay based on detection of the hydrogen peroxide formed by PDH. *N*-acetyl-3,7-dihydroxyphenoxazine (Amplex Red reagent) and horseradish peroxidase react with hydrogen peroxide and produce highly fluorescent resorufin [34,35] which was measured at 550 nm excitation and 587 nm emission wavelength. The assay in 50 mM sodium phosphate buffer pH 7.4 contained 25 µM Amplex Red reagent, 10 mM D-glucose, 0.1 U mL^{-1} horseradish peroxidase and 100 µL of culture supernatant. The screening plates were incubated at 30°C for 5 h only in the presence of D-glucose, end-point measurements of the fluorescence were carried out immediately after addition of the Amplex Red reagent.

2.7 Rescreening

Aliquots of 5 µL of the best variants from the master plates were used to inoculate 96-well deep-well plates containing 200 µL SC-dropout minimal medium. Five wells were inoculated per clone, in row 6 positive and negative controls were included and the plates were cultivated and screened as described in section 2.5. The clones showing improved oxygen reactivity again were identified by colony-PCR using *Taq* polymerase and the primers RMLN-sense and RMLC-antisense and sequencing of the PCR-product (LGC genomics).

2.8 Heterologous expression of H103Y variant in P. pastoris

The mutation H103Y was introduced to the plasmid pPICZ-B_AmPDH by site-directed mutagenesis as described in section 2.3 using the overlapping primers H103Yfw and H103Yrev. Prior to transformation into electro-competent *P. pastoris* strain X33 the plasmid was linearized with *Pme*I at 37°C for at least 2 h and purified. Transformants were selected on YPD-Zeocin plates and the integration of the gene was verified by colony PCR. PDH variant H103Y was produced in a 7-L fermenter (MBR, Wetzikon, Switzerland) with an initial volume of 4 L basal salts fermentation medium and purified in a 3-step protocol as described before [6]. Fractions of the highest purity were pooled, concentrated and frozen in liquid nitrogen for storage at -30°C. Gel filtration pool 1 was used for all characterizations. Wild-type AmPDH protein was produced and purified as described previously [36]. In contrast to mutant H103Y, AmPDH is present in the reduced state after purification, oxidized enzyme was generated according to [13] except using a Superose 12 column (GE Healthcare, Chalfont St. Giles, UK) and 50 mM potassium phosphate buffer pH 7.5 containing 150 mM NaCl.

2.9 Enzyme assay, molecular properties

PDH activity was measured using the standard assay with ferrocenium hexafluorophosphate as described before [6]. Protein concentrations were determined using the method of Bradford with a pre-fabricated assay (BioRad, Hercules, CA), SDS-PAGE and enzymatic deglycosylation using PNGase F were carried out as described previously [36].

Protein concentrations of the samples in the oxidized state were adjusted to an absorbance at 450 nm of around 0.2 with 65 mM sodium phosphate buffer pH 7.5 and an initial spectrum from 300 to 600 nm was recorded using a U-3000 spectrophotometer (Hitachi, Tokyo, Japan). Precipitation was carried out by mixing the double-concentrated protein solution with 10% (v/v) trichloroacetic acid and 40% (v/v) acetone followed by an incubation on ice for 10 min. The samples were centrifuged at 13,000 rpm for 5 min, spectra of the supernatants were recorded.

2.10 Steady-state kinetics

Apparent kinetic constants for the electron donors D-glucose, D-galactose and lactose were measured using the standard assay with ferrocenium. Kinetic constants for the electron acceptors DCIP, 1,4-benzoquinone and ferrocenium hexafluorophosphate were determined using 25 mM D-glucose as electron donor. The observed data were fitted to the Michaelis-Menten equation and kinetic constants were calculated by nonlinear least-squares regression (Sigma Plot 11, Systat Software, Chicago, IL). Turnover numbers (k_{cat}) and catalytic efficiencies ($k_{\text{cat}}/K_{\text{m}}$) were calculated using the molecular mass.

2.11 O_2 reactivity

The oxygen reactivity of the purified enzymes was determined using a fluorimetric assay with Amplex Red/horseradish peroxidase as described in section 2.6 with some modifications. The assay was carried out in black 96-well plates using 0.5 mg mL^{-1} of the purified enzymes, 50 µM Amplex Red, 25 mM D-glucose, 0.1 U mL^{-1} horseradish peroxidase and 50 mM sodium phosphate buffer pH 7.4. The increase in fluorescence of the wild-type, variant H103Y, two negative controls (assay without enzyme and assay without D-glucose) and an internal standard (2.5 µM hydrogen peroxide) was measured over 60 minutes and the slope per minute was determined. A calibration curve with hydrogen peroxide standards was prepared (Fig. S1) containing 50 µM Amplex Red, 50 mM sodium phosphate buffer pH 7.4 and hydrogen peroxide concentrations from 0–5 µM. Oxygen activity was calculated via the formed hydrogen peroxide per minute and milligram of enzyme by fitting the curve and solving the 3-parameter logarithmic equation.

Results and Discussion

3.1 Expression of PDH in S. cerevisiae

The production of PDH from its native host organism *Agaricus sp.* is laborious and time-consuming [4,5]. Therefore several attempts for heterologous expression of PDH in different organisms like *Aspergillus sp.* [37], *E. coli* and *P. pastoris* [36] were made. Due to glycosylation and solubility issues, PDH could only be sucessfully expressed in eukaryotic systems with *P. pastoris* being the host of choice for large-scale fast and efficient protein expression [36]. For protein engineering and mutagenesis, different requirements have to be considered. Expression of *pdh1* in *P. pastoris* using the constitutive *GAP* promoter yielded only low amounts of recombinant protein (our unpublished information), and using the strong inducible *AOX1* promoter requires repeated feeding with methanol, which is a cumbersome and contamination-prone procedure. Furthermore, vectors available for *P. pastoris* are integrated into the genome, yielding significantly fewer transformant colonies [38]. *S. cerevisiae* can maintain and replicate plasmids and is therefore the most commonly used eukaryotic organism for extensive mutagenesis studies [39]. In addition to higher transformation efficiencies, *S. cerevisiae* is able to perform *in-vivo* overlap-recombination of the vector and a library of inserts, which facilitates fast and simple library construction [40]. Therefore the expression of *A. meleagris pdh1* in *S. cerevisiae* under the control of the *GAL1* promoter in the vector pYES2/CT was established. The native signal sequence of PDH was used for expression in *S. cerevisiae*, as this was successful in other eukaryotic host organisms as well. With a combination of SC-dropout minimal medium as preculture medium to grow the cells to a uniform density and the SG/R-CAA expression medium containing the inducer D-galactose, activity levels high enough to sufficiently distinguish between active and inactive variants could be reached.

3.2 Site-saturation mutagenesis library construction and high-throughput screening

According to the crystal structure of *A. meleagris* PDH (PDB code 4H7U) twelve amino acids immediately surrounding the flavin isoalloxazine C(4a), the site of oxygen activation in flavoenzymes [14,19,41], and interacting with carbohydrate substrates in docking experiments [13] were targeted for site-saturation mutagenesis. Positions T102, H103, N104, G105, M106, Q392, S509, Y510, V511, H512, H556 and Q558 were selected (Fig. 1), and 352 clones were screened per position. Standard PDH activity was monitored with a DCIP-based assay and the libraries were screened for increased oxygen reactivity with an Amplex Red/horseradish peroxidase-based assay via the formed hydrogen peroxide. While the two catalytic histidines H512 and H556 are supposed to play an important role in the interaction of PDH with the sugar substrate and act as catalytic bases, H103 is the amino acid where the FAD cofactor is covalently bound to [13,42]. Substitution of these three histidines resulted in the highest number of inactive variants in the screening using the DCIP/D-glucose assay with only 7.4% (H512), 20.7% (H556) and 7.1% (H103) active clones (Fig. 2), suggesting essential functions for these amino acids. Due to appropriate distances and hydrogen bonding interactions with the sugar both H512 and H556 showed the ability to act as catalytic base in molecular dynamics simulations of the interaction of AmPDH with D-glucose [42]. Graf and coworkers concluded that the two histidines could have similar roles to H502 and H546 in aryl-alcohol oxidase (AAO) [43], the GMC family member that shows the highest structural similarity to PDH, where H502 (H512 in PDH) is of higher importance for catalysis than H546 (H556 in PDH). This is reflected in the number of active variants with 7.4% for H512, which may all be represented by the wild-type amino acid, and 20.7% for H556. In *Trametes multicolor* POx, the equivalent of H556 is N593, indicating that asparagine can fulfill the same or similar functions at this position [44]. It is noteworthy that for H556 no variant with increased oxygen reactivity could be identified. In contrast, a mutation of the corresponding position N700 in *Myriococcum thermophilum* CDH to serine led to higher hydrogen peroxide production [33]. This illustrates that the generation of a favorable micro-environment for oxygen reactivity around the flavin C(4a)N5 locus is complex and cannot readily be achieved with single amino acid exchanges. All other amino acid positions showed a number of active variants higher than 50% except for N104 (28.7%) and G105 (47.3%). The highest variety of amino acids was tolerated at position T102 and V511 with more than 80% active clones. For position T102 this finding is not surprising as the side chain is pointing away from the FAD isoalloxazine but V511 occupies a prominent position in the active site, next to the catalytic histidine H512 (Fig. 1). Molecular dynamic simulation detected hydrogen bonding interaction of the sugar substrate with V511 but only with the backbone and not with the side chain [42]. This could be an explanation for the high tolerance for substitution of this very central amino acid position.

Variants with at least the two-fold oxygen reactivity of the wild-type were chosen for the rescreening. When the increased oxygen reactivity was confirmed in the rescreening, the amino acid exchange was identified by sequencing. All sequenced variants showed a substitution of the amino acid H103 to tyrosine, phenylalanine, tryptophan and methionine and an increase in oxygen reactivity of 2.0–2.6-fold in the screening compared to the wild-type AmPDH. These four amino acids have in common that they are all large to very large, aromatic (except for methionine), uncharged and (rather) hydrophobic [45]. All substitutions were encoded by all possible codons, a confirmation for the reliability of the mutagenesis technique. Due to the fact that the substitution to tyrosine was the most abundant and showed the highest increase in oxygen reactivity, variant H103Y was chosen for further characterization.

3.3 Large scale protein production and purification of PDH variant H103Y

P. pastoris was chosen for the larger scale production of variant H103Y [36]. Variant H103Y was produced by site-directed mutagenesis and plasmid pPICZB_H103Y was transformed to

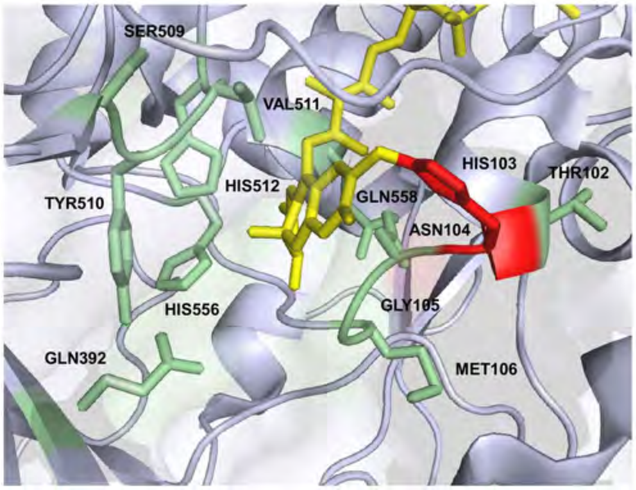

Figure 1. PDH active site. The covalently bound FAD cofactor is shown in yellow, the mutated amino acid positions (green) and HIS103 (red) are highlighted. The image was created using PyMOL (PDB code 4H7U), for clarity a few amino acids were omitted.
doi:10.1371/journal.pone.0091145.g001

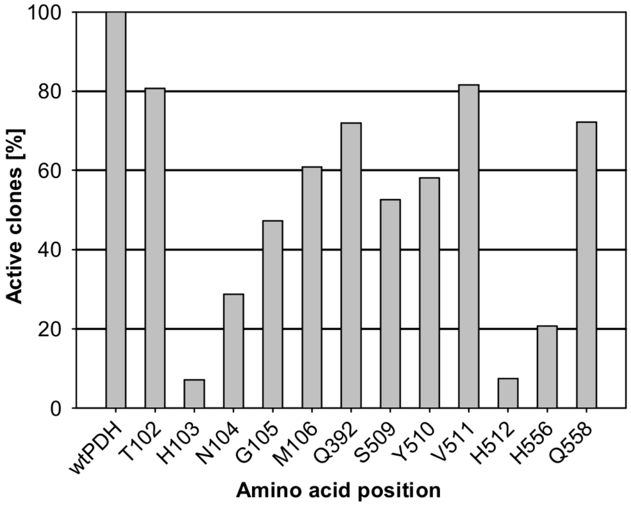

Figure 2. Active clones (in %) of site-saturation mutagenesis target positions. Activity was determined using a screening assay containing 0.3 mM DCIP and 50 mM D-glucose in 100 mM sodium acetate buffer pH 4 at 30°C. Libraries were expressed in *S. cerevisiae*. wt: wild-type *A. meleagris* PDH.
doi:10.1371/journal.pone.0091145.g002

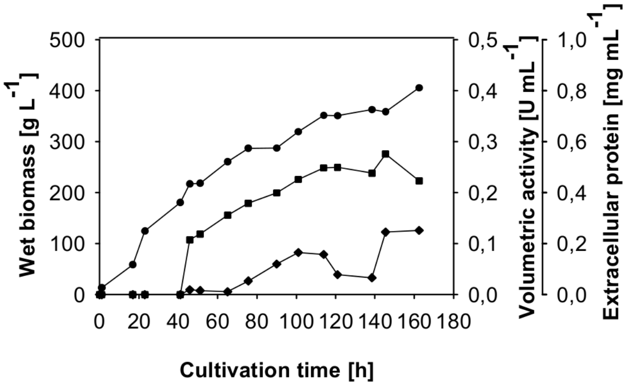

Figure 3. Large scale production of PDH variant H103Y in *P. pastoris*. Fermentation was carried out in a 7 L aerated and stirred bioreactor with 4 L starting volume of basal salts cultivation medium. Circles, wet biomass; squares, extracellular protein; diamonds, volumetric activity.
doi:10.1371/journal.pone.0091145.g003

competent *P. pastoris* X33 cells. A colony-PCR-verified clone of variant H103Y was used for large-scale protein production in a 7-L aerated and stirred bioreactor. During cultivation wet biomass, extracellular protein concentration and volumetric activity were monitored by taking samples in regular time intervals (Fig. 3). A level of wet biomass of 217 g L^{-1} could be obtained after the glycerol batch and fed-batch phase. The fermentation lasted for 163 h in total and a wet biomass of 405 g L^{-1}, 0.45 mg mL^{-1} extracellular protein concentration and 0.13 U mL^{-1} of volumetric PDH activity were reached at time of harvest. The recombinant protein was purified in a 3-step protocol to apparent homogeneity, a hydrophobic interaction chromatography step was followed by anion exchange chromatography and a final gel filtration step (Table 1). The purified protein showed a bright yellow color, gel filtration pool 1 represents the purest enzyme preparation with a yield of 34% which was used for all further analyses. Together with the second pool 70% of the enzyme activity could be recovered. Recombinant wild-type AmPDH was produced in 60 L scale and purified as described in [36].

3.4 Molecular properties

Both the recombinant wild-type AmPDH and variant H103Y showed a broad smear around 90 kDa on SDS-PAGE (Fig. 4). Deglycosylation with PNGase F under denaturing conditions reduced the mass of both enzymes to around 64 kDa, which gives a degree of glycosylation of around 30%. This value is in good agreement with other PDH glycoproteins produced so far in *P. pastoris* [6,36]. The high degree of glycosylation is due to the additon of glycans of the high-mannose type by the yeast [46]. The molecular properties of the mutant appear unchanged in SDS-PAGE compared to the wild-type.

The mutation of H103 to a tyrosine raised the question whether the FAD-cofactor was still covalently attached to the enzyme. The proteins were precipitated with 10% TCA and 40% acetone and spectra of the protein solution before and the supernatant after the treatment were recorded (Fig. 5). Due to the colorless supernatant lacking the flavin peak and the bright yellow protein pellet it could be clearly seen that the wild-type protein did not release the covalently bound FAD. Precipitation of variant H103Y resulted in a bright yellow supernatant with a spectrum typical for free FAD and a colorless protein precipitate. In none of the purification steps described above yellow fractions without PDH activity could be found, confirming that the mutant did not lose FAD during purification. When stored at 4°C, the activity of the mutant remained stable over several weeks, otherwise this would be a sign for weak incorporation of the FAD cofactor. These findings indicate that the variant H103Y carries a tightly but non-covalently bound FAD cofactor.

Comparing the spectra of the unprecipitated proteins, a shift towards blue (hypsochromic shift) of the second flavin peak (around 370 nm) can be observed for the wild-type enzyme. This

Table 1. Purification of PDH variant H103Y.

Purification step	Total protein	Total activity	Specific activity	Purification	Yield
	[mg]	[U]	[U mg^{-1}]	[-fold]	[%]
Crude extract	1440.5	1746.2	1.21	1.00	100
Phenyl sepharose	407.4	1582.2	3.88	3.21	91
DEAE sepharose	209.1	1268.0	6.06	5.01	73
Gel filtration pool 1	**31.3**	**597.6**	**19.09**	**15.78**	**34**
Gel filtration pool 2	49.4	635.7	12.88	10.64	36

doi:10.1371/journal.pone.0091145.t001

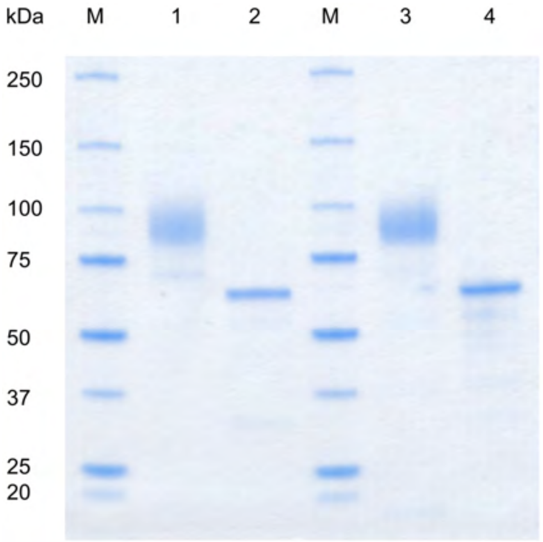

Figure 4. SDS-PAGE. Recombinant *A. meleagris* PDH and variant H103Y were expressed in *P. pastoris* and purified in a two- and three-step protocol. M, molecular marker (Precision Plus Protein Standard, BioRad); 1, wild-type *Am*PDH; 2, wild-type *Am*PDH deglycosylated (PNGase F); 3, *Am*PDH variant H103Y; 4, *Am*PDH variant H103Y deglycosylated.
doi:10.1371/journal.pone.0091145.g004

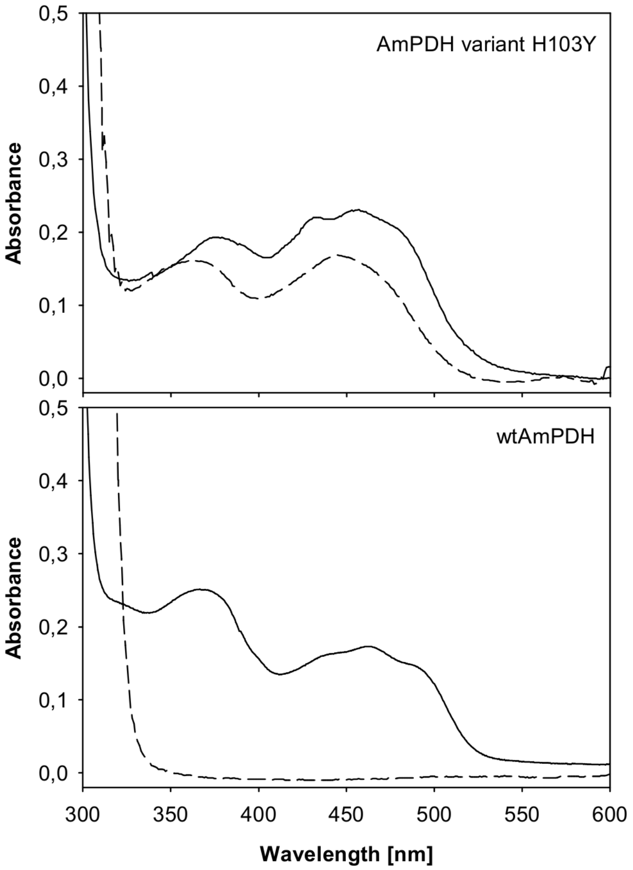

Figure 5. TCA/acetone precipitation of wild-type AmPDH and variant H103Y. Precipitation was carried out using 10% TCA and 40% acetone on ice, spectra of the oxidized proteins before (solid lines) and the supernatants after precipitation are shown (dashed lines).
doi:10.1371/journal.pone.0091145.g005

is typical for an 8α-modified FAD in contrast to the unmodified cofactor of variant H103Y [47]. A covalent bond formation in PDH specific for (the N3 of) H103 can be concluded, which is not possible with a tyrosine at this position. A similar observation was made for vanillyl-alcohol oxidase (VAO) [48].

3.5 Steady-state kinetics

To examine the effect of the mutation, steady-state kinetics for electron donors were determined using ferricenium as the electron acceptor (Table 2). Catalytic efficiencies (k_{cat}/K_m) for the monosaccharides D-glucose and D-galactose are around eight-fold lower for variant H103Y compared to the wild-type due to higher K_m-values and lower turnover numbers (k_{cat}). The mutation also decreased the catalytic efficiency for the disaccharide lactose about three-fold, indicating a negative effect of the mutation on sugar substrate turnover. A disruption of the covalent FAD-linkage leads in most cases to a decrease in reduction potential of the mutant and therefore impaired substrate-mediated flavin reduction [48–50]. AmPDH has a relatively high midpoint potential of +150 mV [51], it is very likely that non-covalent mutant H103Y exhibits a lower potential. A detailed electrochemical characterization of the mutant H103Y is a matter of ongoing studies.

Kinetic constants for electron acceptors were measured with 25 mM D-glucose as the electron donor (Table 3). Catalytic efficiencies of variant H103Y for electron acceptors other than oxygen are generally lower compared to the wild-type protein. For ferrocenium hexafluorophosphate and DCIP variant H103Y showed a lower K_m-value (higher affinity) but also a lower turnover number (k_{cat}) than the wild-type AmPDH. Catalytic efficiencies are reduced around three- and two-fold for these

Table 2. Apparent kinetic constants of recombinant *A. meleagris* PDH and variant H103Y for selected electron donors, determined with 0.2 mM ferricenium as electron acceptor at 30°C.

	AmPDH[a]			H103Y		
	K_m	k_{cat}	k_{cat}/K_m	K_m	k_{cat}	k_{cat}/K_m
	[mM]	[s^{-1}]	[mM^{-1} s^{-1}]	[mM]	[s^{-1}]	[mM^{-1} s^{-1}]
D-glucose	0.69±0.09	37.8±1.1	54.8	3.85±0.35	27.4±0.5	7.1
D-galactose	1.07±0.13	47.3±3.0	44.2	5.29±0.39	28.9±2.1	5.5
Lactose	128±11.9	41.0±8.1	0.32	395.90±16.27	24.7±0.4	0.1

[a] Data from [36].
doi:10.1371/journal.pone.0091145.t002

Table 3. Apparent kinetic constants for selected electron acceptors and oxygen reactivity of recombinant *A. meleagris* PDH and variant H103Y, determined with 25 mM D-glucose as electron donor at 30°C.

	AmPDH			H103Y		
	K_m	k_{cat}	k_{cat}/K_m	K_m	k_{cat}	k_{cat}/K_m
	[mM]	[s^{-1}]	[mM^{-1} s^{-1}]	[mM]	[s^{-1}]	[mM^{-1} s^{-1}]
Fc^+PF_6 (pH 8.5)	0.16±0.04[a]	130±11[a]	812.5	0.10±0.01	26.0±0.9	260.0
1,4-BQ (pH 4)	1.38±0.28[a]	65.4±5.5[a]	47.4	3.64±0.47	13.6±1.1	4.0
DCIP (pH 4)	0.14±0.01	40.7±4.1	290.7	0.02±0.01	2.8±0.5	140.0
O_2 [μM min^{-1} mg^{-1}]	0.095±0.003			0.500±0.033		

[a] Data from [36].

doi:10.1371/journal.pone.0091145.t003

electron acceptors whereas 1,4-benzoquinone showed a nearly twelve-times reduced catalytic efficiency, due to a higher K_m-value of variant H103Y for 1,4-benzoquinone.

Oxygen reactivity was assessed indirectly via the formed hydrogen peroxide in the Amplex Red/horseradish peroxidase fluorimetric assay. To calculate the amount of H_2O_2, a calibration curve was established and a 3-parameter logarithmic function (y = y0+a*ln(x−x0)) turned out to give the best fit ($R^2 = 0.999$). The standard curve showed a slight offset due to background fluorescence (Fig. S1). Wild-type AmPDH produced 0.095 μM of hydrogen peroxide per mg enzyme and minute whereas variant H103Y produced 0.500 μM per mg and minute, representing a 5.3-fold increase in oxygen reactivity (Table 3, Fig. 6). As the fluorimetric assay of the protein samples did not start with identical RFU values (depending on sample handling times and "dead time" of the plate reader), the slope per minute was used for the calculation of the formed hydrogen peroxide. The calibration curve is not linear and flattens off towards higher hydrogen peroxide concentrations, therefore the more than five-fold increase in oxygen reactivity cannot be directly estimated from Figure 6. Due to the still low reactivity of PDH with oxygen, catalytic constants (K_m, k_{cat}) could not be determined.

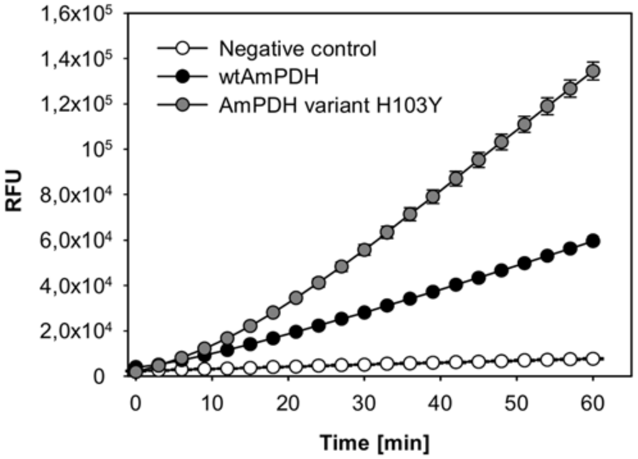

Figure 6. Oxygen reactivity of wild-type AmPDH and variant H103Y. Oxygen reactivity was determined using an Amplex Red/horseradish peroxidase based assay. The assay contained 0.5 mg/mL of the purified enzyme, 50 μM Amplex Red, 25 mM D-glucose, 0.1 U mL^{-1} horseradish peroxidase and 50 mM sodium phosphate buffer pH 7.4. Error bars represent the standard deviation of three repeats.

doi:10.1371/journal.pone.0091145.g006

Position H103 is located on the *si*-side of the flavin isoalloxazine and covalently links the cofactor to the enzyme. A disruption of this covalent bond could lead to an altered arrangement of the FAD isoalloxazine in the active site and create more space or form channels to facilitate O_2 diffusion. In a study of Hernández-Ortega and coworkers [52], the replacement of a phenylalanine located in a narrow oxygen channel of AAO by alanine decreased oxygen reactivity substantially. A substitution with an even bulkier tryptophan resulted in a two-fold increase, suggesting that volume restrictions as determinants of oxygen reactivity should be viewed with care. Only mostly unpolar, uncharged residues (tyrosine, phenylalanine, tryptophan and methionine) were found replacing H103 in oxygen-active clones. This points towards the importance of a nonpolar site near the flavin C(4a), as observed for choline oxidase [22]. As already mentioned in the introduction, in the recently published crystal structure of AmPDH, a C(4a)-adduct on the *si*-side of the isoalloxazine was observed. This observation shows that AmPDH is able to stabilize this oxygen species which is tightly coordinated by the catalytic histidines H512 (Nε2) and H556 (Nδ1). The distance between this catalytic pair is shorter in AmPDH (3.5 Å) than in TmPOx (4.2 Å), which was found to show a physiological C(4a) adduct [13,16]. The shorter distance might lead to an "overstabilization" of the C(4a)-hydroperoxide and limit oxygen reactivity in wild-type AmPDH, the non-covalently bound FAD in AmPDH H103Y variant could create more space and lead to a destabilizing effect, therefore increase oxygen reactivity. Crystallographic data of mutant H103Y would be of interest to support this hypothesis. In summary, the study provides a starting point for engineering efforts with PDH and valuable insight on the catalytic importance of the amino acid environment surrounding the FAD cofactor of PDH. The large distance of position H103 to the C(4a) and the lack of a crystal structure of the H103Y variant make providing a rationale for the increased oxygen reactivity challenging. Further engineering attempts and studies towards increased or altered oxygen reactivity of PDH and other flavoproteins will be required.

Supporting Information

Figure S1 Calibration curve H_2O_2 Amplex Red assay. The curve was fitted with a 3-parameter logarithmic function (y = y0+a*ln(x-x0)). The assay contained the indicated concentration of hydrogen peroxide, 50 μM Amplex Red, 0.1 U mL^{-1} horseradish peroxidase and 50 mM sodium phosphate buffer pH 7.4. Error bars show the standard deviation of six repeats. (TIF)

Table S1 Nucleotide sequences of the primers. Sites of restriction or mutagenesis are indicated in bold letters. N = A, T, G, C; K = G, T.
(DOCX)

Acknowledgments

The authors thank Cindy Lorenz and Michael Graf for technical assistance.

Author Contributions

Conceived and designed the experiments: IK CS DH CKP. Performed the experiments: IK KL PS. Analyzed the data: IK DB CS DH CKP. Wrote the paper: IK DB CKP.

References

1. Peterbauer CK, Volc J (2010) Pyranose dehydrogenases: Biochemical features and perspectives of technological applications. Applied Microbiology and Biotechnology 85: 837–848.
2. Volc J, Kubátová E, Wood DA, Daniel G (1997) Pyranose 2-dehydrogenase, a novel sugar oxidoreductase from the basidiomycete fungus *Agaricus bisporus*. Arch Microbiol 167: 119–125.
3. Volc J, Kubátová E, Daniel G, Sedmera P, Haltrich D (2001) Screening of basidiomycete fungi for the quinone-dependent sugar C-2/C-3 oxidoreductase, pyranose dehydrogenase, and properties of the enzyme from *Macrolepiota rhacodes*. Arch Microbiol 176: 178–186.
4. Kujawa M, Volc J, Halada P, Sedmera P, Divne C, et al. (2007) Properties of pyranose dehydrogenase purified from the litter-degrading fungus *Agaricus xanthoderma*. FEBS J 274: 879–894.
5. Sygmund C, Kittl R, Volc J, Halada P, Kubátová E, et al. (2008) Characterization of pyranose dehydrogenase from *Agaricus meleagris* and its application in the C-2 specific conversion of D-galactose. J Biotechnol 133: 334–342.
6. Staudigl P, Krondorfer I, Haltrich D, Peterbauer CK (2013) Pyranose Dehydrogenase from *Agaricus campestris* and *Agaricus xanthoderma*: Characterization and Applications in Carbohydrate Conversions. Biomolecules 3: 535–552.
7. Kittl R, Sygmund C, Halada P, Volc J, Divne C, et al. (2008) Molecular cloning of three pyranose dehydrogenase-encoding genes from *Agaricus meleagris* and analysis of their expression by real-time RT-PCR. Curr Genet 53: 117–127.
8. Giffhorn F (2000) Fungal pyranose oxidases: Occurrence, properties and biotechnical applications in carbohydrate chemistry. Applied Microbiology and Biotechnology 54: 727–740.
9. Volc J, Denisova NP, Nerud F, Musilek V (1985) Glucose-2-oxidase activity in mycelial cultures of basidiomycetes. Folia Microbiologica 30: 141–147.
10. Ander P, Marzullo L (1997) Sugar oxidoreductases and veratryl alcohol oxidase as related to lignin degradation. Journal of Biotechnology 53: 115–131.
11. Sedmera P, Halada P, Kubátová E, Haltrich D, Přikrylová V, et al. (2006) New biotransformations of some reducing sugars to the corresponding (di)dehydro (glycosyl) aldoses or aldonic acids using fungal pyranose dehydrogenase. Journal of Molecular Catalysis B: Enzymatic 41: 32–42.
12. Volc J, Sedmera P, Kujawa M, Halada P, Kubátová E, et al. (2004) Conversion of lactose to β-D-galactopyranosyl-(1 → 4)-D-arabino-hexos-2-ulose-(2-dehydrolactose) and lactobiono-1,5-lactone by fungal pyranose dehydrogenase. Journal of Molecular Catalysis B: Enzymatic 30: 177–184.
13. Tan TC, Spadiut O, Wongnate T, Sucharitakul J, Krondorfer I, et al. (2013) The 1.6 Å crystal structure of pyranose dehydrogenase from *Agaricus meleagris* rationalizes substrate specificity and reveals a flavin intermediate. PLoS One 8: e53567.
14. Mattevi A (2006) To be or not to be an oxidase: challenging the oxygen reactivity of flavoenzymes. Trends in Biochemical Sciences 31: 276–283.
15. Massey V (1994) Activation of molecular oxygen by flavins and flavoproteins. Journal of Biological Chemistry 269: 22459–22462.
16. Sucharitakul J, Prongjit M, Haltrich D, Chaiyen P (2008) Detection of a C4a-hydroperoxyflavin intermediate in the reaction of a flavoprotein oxidase. Biochemistry 47: 8485–8490.
17. Klinman JP (2007) How do enzymes activate oxygen without inactivating themselves? Accounts of Chemical Research 40: 325–333.
18. Su Q, Klinman JP (1999) Nature of oxygen activation in glucose oxidase from *Aspergillus niger*: The importance of electrostatic stabilization in superoxide formation. Biochemistry 38: 8572–8581.
19. Gadda G (2012) Oxygen activation in flavoprotein oxidases: The importance of being positive. Biochemistry 51: 2662–2669.
20. Zhao G, Bruckner RC, Jorns MS (2008) Identification of the oxygen activation site in monomeric sarcosine oxidase: Role of Lys265 in catalysis. Biochemistry 47: 9124–9135.
21. Gadda G, Fan F, Hoang JV (2006) On the contribution of the positively charged headgroup of choline to substrate binding and catalysis in the reaction catalyzed by choline oxidase. Archives of Biochemistry and Biophysics 451: 182–187.
22. Finnegan S, Agniswamy J, Weber IT, Gadda G (2010) Role of valine 464 in the flavin oxidation reaction catalyzed by choline oxidase. Biochemistry 49: 2952–2961.
23. Leferink NGH, Fraaije MW, Joosten HJ, Schaap PJ, Mattevi A, et al. (2009) Identification of a gatekeeper residue that prevents dehydrogenases from acting as oxidases. Journal of Biological Chemistry 284: 4392–4397.
24. Saam J, Rosini E, Molla G, Schulten K, Pollegioni L, et al. (2010) O2 reactivity of flavoproteins: Dynamic access of dioxygen to the active site and role of a H+ relay system in D-amino acid oxidase. Journal of Biological Chemistry 285: 24439–24446.
25. Baron R, Riley C, Chenprakhon P, Thotsaporn K, Winter RT, et al. (2009) Multiple pathways guide oxygen diffusion into flavoenzyme active sites. Proceedings of the National Academy of Sciences of the United States of America 106: 10603–10608.
26. McDonald CA, Fagan RL, Collard F, Monnier VM, Palfey BA (2011) Oxygen reactivity in flavoenzymes: Context matters. Journal of the American Chemical Society 133: 16809–16811.
27. Bowley DR, Labrijn AF, Zwick MB, Burton DR (2007) Antigen selection from an HIV-1 immune antibody library displayed on yeast yields many novel antibodies compared to selection from the same library displayed on phage. Protein Engineering, Design and Selection 20: 81–90.
28. Li S, Wilkinson MF (1997) Site-directed mutagene sis: A two-step method using PCR and *Dpn*I. BioTechniques 23: 588–590.
29. Gietz RD, Schiestl RH, Willems AR, Woods RA (1995) Studies on the transformation of intact yeast cells by the LiAc/SS-DNA/PEG procedure. Yeast 11: 355–360.
30. Ho SN, Hunt HD, Horton RM, Pullen JK, Pease LR (1989) Site-directed mutagenesis by overlap extension using the polymerase chain reaction. Gene 77: 51–59.
31. Georgescu R (2003) High-throughput tetramethylbenzidine (TMB) screen for peroxidases. Methods Mol Biol 230: 171–176.
32. García-Ruiz E, Maté D, Ballesteros A, Martinez AT, Alcalde M (2010) Evolving thermostability in mutant libraries of ligninolytic oxidoreductases expressed in yeast. Microbial Cell Factories 9.
33. Sygmund C, Santner P, Krondorfer I, Peterbauer CK, Alcalde M, et al. (2013) Semi-rational engineering of cellobiose dehydrogenase for improved hydrogen peroxide production. Microbial Cell Factories 12.
34. Mohanty JG, Jaffe JS, Schulman ES, Raible DG (1997) A highly sensitive fluorescent micro-assay of H2O2 release from activated human leukocytes using a dihydroxyphenoxazine derivative. J Immunol Methods 202: 133–141.
35. Zhou M, Diwu Z, Panchuk-Voloshina N, Haugland RP (1997) A stable nonfluorescent derivative of resorufin for the fluorometric determination of trace hydrogen peroxide: applications in detecting the activity of phagocyte NADPH oxidase and other oxidases. Anal Biochem 253: 162–168.
36. Sygmund C, Gutmann A, Krondorfer I, Kujawa M, Glieder A, et al. (2012) Simple and efficient expression of *Agaricus meleagris* pyranose dehydrogenase in *Pichia pastoris*. Appl Microbiol Biotechnol 94: 695–704.
37. Pisanelli I, Kujawa M, Gschnitzer D, Spadiut O, Seiboth B, et al. (2010) Heterologous expression of an *Agaricus meleagris* pyranose dehydrogenase-encoding gene in *Aspergillus* spp. and characterization of the recombinant enzyme. Appl Microbiol Biotechnol 86: 599–606.
38. Weis R, Luiten R, Skranc W, Schwab H, Wubbolts M, et al. (2004) Reliable high-throughput screening with *Pichia pastoris* by limiting yeast cell death phenomena. FEMS Yeast Research 5: 179–189.
39. Gonzalez-Perez D, Garcia-Ruiz E, Alcalde M (2012) *Saccharomyces cerevisiae* in directed evolution: An efficient tool to improve enzymes. Bioengineered Bugs 3: 172–177.
40. Alcalde M (2010) Mutagenesis protocols in *Saccharomyces cerevisiae* by in vivo overlap extension. Methods in Molecular Biology 634: 3–14.
41. Chaiyen P, Fraaije MW, Mattevi A (2012) The enigmatic reaction of flavins with oxygen. Trends in Biochemical Sciences 37: 373–380.
42. Graf MMH, Bren U, Haltrich D, Oostenbrink C (2013) Molecular dynamics simulations give insight into d-glucose dioxidation at C2 and C3 by *Agaricus meleagris* pyranose dehydrogenase. Journal of Computer-Aided Molecular Design 27: 295–304.
43. Hernández-Ortega A, Lucas F, Ferreira P, Medina M, Guallar V, et al. (2012) Role of active site histidines in the two half-reactions of the aryl-alcohol oxidase catalytic cycle. Biochemistry 51: 6595–6608.
44. Hallberg BM, Leitner C, Haltrich D, Divne C (2004) Crystal structure of the 270 kDa homotetrameric lignin-degrading enzyme pyranose 2-oxidase. Journal of Molecular Biology 341: 781–796.
45. Pommié C, Levadoux S, Sabatier R, Lefranc G, Lefranc MP (2004) IMGT standardized criteria for statistical analysis of immunoglobulin V-Region amino acid properties. Journal of Molecular Recognition 17: 17–32.

46. Gemmill TR, Trimble RB (1999) Overview of N- and O-linked oligosaccharide structures found in various yeast species. Biochim Biophys Acta 1426: 227–237.
47. Kenney WC, Edmondson DE, Seng RL (1976) Identification of the covalently bound flavin of thiamin dehydrogenase. Journal of Biological Chemistry 251: 5386–5390.
48. Fraaije MW, Van Den Heuvel RHH, Van Berkel WJH, Mattevi A (1999) Covalent flavinylation is essential for efficient redox catalysis in vanillyl-alcohol oxidase. Journal of Biological Chemistry 274: 35514–35520.
49. Kujawa M, Ebner H, Leitner C, Hallberg BM, Prongjit M, et al. (2006) Structural basis for substrate binding and regioselective oxidation of monosaccharides at C3 by pyranose 2-oxidase. Journal of Biological Chemistry 281: 35104–35115.
50. Winkler A, Kutchan TM, Macheroux P (2007) 6-S-cysteinylation of bi-covalently attached FAD in berberine bridge enzyme tunes the redox potential for optimal activity. Journal of Biological Chemistry 282: 24437–24443.
51. Tasca F, Gorton L, Kujawa M, Patel I, Harreither W, et al. (2010) Increasing the coulombic efficiency of glucose biofuel cell anodes by combination of redox enzymes. Biosensors and Bioelectronics 25: 1710–1716.
52. Hernández-Ortega A, Lucas F, Ferreira P, Medina M, Guallar V, et al. (2011) Modulating O2 reactivity in a fungal flavoenzyme: Involvement of aryl-alcohol oxidase Phe-501 contiguous to catalytic histidine. Journal of Biological Chemistry 286: 41105–41114.

Supporting Information

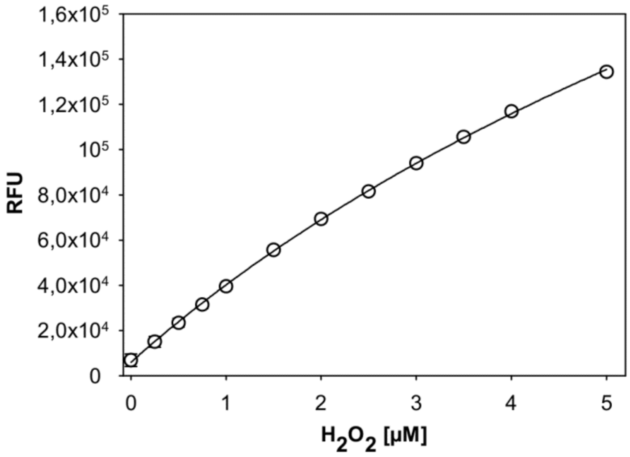

Figure S1. Calibration curve H_2O_2 Amplex Red assay. The curve was fitted with a 3-parameter logarithmic function (y = y0+a*ln(x-x0)). The assay contained the indicated concentration of hydrogen peroxide, 50 µM Amplex Red, 0.1 U mL^{-1} horseradish peroxidase and 50 mM sodium phosphate buffer pH 7.4. Error bars show the standard deviation of six repeats.

Table S1: Nucleotide sequences of the primers. Sites of restriction or mutagenesis are indicated in bold letters. N=A, T, G, C; K=G, T.

Name	Sequence 5’ – 3’
AmKpnIfw	CATAG**GGTACC**ATGCTGCCTCGAGTGACCA
AmBamHIfw	ATTAA**GGATCC**ATGCTGCCTCGAGTGACCA
AmXbarev	CGTGC**TCTAGA**TTAGTTATAACTCTTTG
AmNotIrev	CGTGC**GCGGCCGC**TTAGTTATAACTCTTTG
AmFw	CCTTCGAGTGGCAAGAATTCACCACATATT
AmRev	CACTCGAAGG**GTC**CTGTCCGTTCAGTTTG
AmT102fw	CCTGGGTGGCTGCAGT**NNK**CATAATGGAATGGTG
AmT102rev	CACCATTCCATTATG**MNN**ACTGCAGCCACCCAGG
AmH103fw	GTGGCTGCAGTACT**NNK**AATGGAATGGTGTAC
AmH103rev	GTACACCATTCCATT**MNN**AGTACTGCAGCCAC
AmN104f	GCTGCAGTACTCAT**NNK**GGAATGGTGTACACCCG
AmN104rev	CGGGTGTACACCATTCC**MNN**ATGAGTACTGCAGC
AmG105fw	GCAGTACTCATAAT**NNK**ATGGTGTACACCCGAG
AmG105rev	CTCGGGTGTACACCAT**MNN**ATTATGAGTACTGC
AmM106fw	GTACTCATAATGGA**NNK**GTGTACACCCGAGGTT
AmM106rev	AACCTCGGGTGTACAC**MNN**TCCATTATGAGTAC
AmQ392fw	CCACATATTGAGTTC**NNK**TTTGCACAAATCACC
AmQ392rev	GGTGATTTGTGCAAA**MNN**GAACTCAATATGTGG
AmS509fw	GCGATCTTCAACATTC**NNK**TACGTGCATGGTGT
AmS509ev	ACACCATGCACGTA**MNN**GAATGTTGAAGATCGC
AmY510fw	CTTCAACATTCTCA**NNK**GTGCATGGTGTGGG
AmY510rev	CCCACACCATGCAC**MNN**TGAGAATGTTGAAG
AmV511fw	CAACATTCTCATAC**NNK**CATGGTGTGGGAACG
AmV511rev	CGTTCCCACACCATG**MNN**GTATGAGAATGTTG
AmH512fw	CATTCTCATACGTG**NNK**GGTGTGGGAACGTTG
AmH512rev	CAACGTTCCCACACC**MNN**CACGTATGAGAATG
AmH556fw	CATGCTCCGGCCGCA**NNK**ACTCAACTACCTGT
AmH556rev	ACAGGTAGTTGAGT**MNN**TGCGGCCGGAGCATG
AmQ558fw	GGCCGCACACACT**NNK**CTACCTGTTTACGCA
AmQ558rev	TGCGTAAACAGGTAG**MNN**AGTGTGTGCGGCC
H103Yfw	AATGGAATGGTGTACACCCGAGGTTC
H103Yrev	CCATTCCATT**ATA**AGTACTGCAGCCACCCA

Paper V

Agaricus meleagris pyranose dehydrogenase: Influence of covalent FAD linkage on catalysis and stability

Iris Krondorfer[a], Dagmar Brugger[a], Regina Paukner[a], Katharina F. Pirker[b], Stefan Hofbauer[b], Paul G. Furtmüller[b], Christian Obinger[b], Dietmar Haltrich[a], Clemens K. Peterbauer[a*]

[a] Department of Food Science and Technology, Food Biotechnology Laboratory, BOKU - University of Natural Resources and Life Sciences, Muthgasse 11, 1190 Vienna, Austria.

[b] Department of Chemistry, Division of Biochemistry, BOKU - University of Natural Resources and Life Sciences, Muthgasse 18, 1190 Vienna, Austria.

[*]Corresponding author at: Department of Food Science and Technology, Food Biotechnology Laboratory, BOKU - University of Natural Resources and Life Sciences, Muthgasse 11, 1190 Vienna, Austria. Tel.: +43 1 47654 6144; fax: +43 1 47654 6199.

E-mail: clemens.peterbauer@boku.ac.at

Abstract

Pyranose dehydrogenase (PDH) is a monomeric flavoprotein belonging to the glucose-methanol-choline (GMC) family of oxidoreductases. It catalyzes the oxidation of free, non-phosphorylated sugars to the corresponding ketosugars. The enzyme harbours an FAD cofactor that is covalently attached to His^{103} via an 8α-N(3) histidyl linkage. Our previous work showed that variant H103Y was still able to bind FAD (non-covalently) and perform catalysis but steady-state kinetic parameters for several substrates were negatively affected. In order to investigate the impact of the covalent FAD attachment in *Agaricus meleagris* PDH in more detail, pre-steady-state kinetics and stability of variant H103Y in comparison to the wild-type enzyme were probed using a broad set of techniques. Stopped flow analysis revealed that the mutation slowed down the reductive half-reaction by around three orders of magnitude whereas the oxidative half-reaction was affected only to a minor degree. No alterations in the secondary structure composition could be observed due to the mutation. The existence of an anionic semiquinone radical in the resting state of both the wild-type and variant H103Y was demonstrated using electron paramagnetic resonance (EPR) spectroscopy and suggested a higher mobility of the cofactor due to the non-covalent linkage in the variant H103Y. Temperature-mediated and chemical unfolding showed significant negative effects of the disruption of the FAD bond on thermal and conformational stability. Our results support the role of the covalent FAD linkage in increasing the reduction potential as well as thermal and conformational protein stability.

Keywords

pyranose dehydrogenase; covalent flavinylation; FAD; thermal stability; conformational stability; semiquinone radical

Introduction

Pyranose dehydrogenase (PDH, EC 1.1.99.29) is a monomeric FAD-dependent oxidoreductase and member of the glucose-methanol-choline oxidase (GMC) family. The glycoprotein is around 75 kDa in size and was first isolated from the edible basidiomycete *Agaricus bisporus* [1]. It catalyzes the oxidation of free, non-phosphorylated sugars at different C-atoms to the corresponding keto-derivatives. PDH is unable to utilize oxygen, suitable electron acceptors include ferrocenium hexafluorophosphate, $ABTS^{+\bullet}$, 1,4-benzoquinone or 2,6-dichloroindophenol (DCIP). The biological role of the enzyme is not entirely clear, a participation in lignocellulose degradation or the defense against antimicrobial substances produced by plants seem plausible [2].

An estimated 10 % of all flavoproteins carry a covalently bound cofactor [3]. Pyranose dehydrogenase is one of these rare examples, like the closely related enzyme pyranose 2-oxidase (POx). The two proteins possess the most common type of covalent FAD-linkage, the 8α-histidyl-FAD, connected via the N3 of histidine 103 (PDH) and 167 (POx) [4, 5]. Another possibility of a covalent FAD-linkage, 8α-S-cysteinyl-FAD, is not very widespread. The extremely rare 8α-O-tyrosyl linkage was only found in *p*-cresol methylhydroxylase and 4-ethylphenol methylene hydroxylase [6, 7]. A double-covalent linkage, the 8α-N1-histidyl-6-S-cysteinyl-FAD, was first described in 2005 in the enzyme glucooligosaccharide oxidase [8]. All bicovalent flavoproteins characterized so far belong to the so-called VAO (vanillyl-alcohol-oxidase) family [9].

The formation of the FAD-linkage is believed to mostly occur as an autocatalytic post-translational reaction. The covalent incorporation of the FAD cofactor seems to be possible after folding of the protein in a lock-and-key manner, as shown in VAO and monomeric sarcosine oxidase (MSOX) [10-12]. Recently, a protein was discovered which is required for the covalent flavinylation of a bacterial flavoprotein controlling succinate dehydrogenase activity [13]. By looking at the fold or the sequence of a flavoprotein, one cannot predict a covalent or non-covalent linkage. Interestingly, the majority of flavoproteins carrying a covalently linked cofactor are oxidases, which may be explained by the higher reduction potential due to the covalent linkage and the resulting limitation of suitable electron acceptors other than dioxygen [3]. However, PDH as a flavoprotein dehydrogenase with a covalently linked cofactor and a very high midpoint potential of +150 mV seems to be an exception to this observation [14].

The removal of the covalent FAD-bond in POx, also a member of the GMC flavoprotein family, resulted in a tightly, but non-covalently bound FAD. Mutant H167A showed a decreased turnover rate and lower reduction potential, but no significant structural changes were observed [15]. *A. meleagris* PDH variant H103Y was recently found in a screening of twelve site-saturation mutagenesis libraries of amino acids around the active site to show increased oxygen reactivity. The FAD-cofactor was shown to be bound in a tight, but non-covalent manner. Steady-state kinetics showed that the mutation decreased the catalytic efficiencies towards sugar-substrates as well as electron acceptors by around one order of magnitude [16].

In this study, the PDH variant lacking the covalently linked FAD-cofactor (H103Y) was used to investigate the effect of the non-covalent linkage on catalysis and stability of the protein in more detail. Applied methods included electron paramagnetic resonance (EPR)-, stopped-flow-UV-vis and electronic circular dichroism (ECD)-spectroscopy as well as unfolding experiments by using fluorescence spectroscopy and differential scanning calorimetry (DSC).

Materials and methods

Materials

All chemicals were purchased from Sigma Aldrich (St. Louis, MO), Roth (Karlsruhe, Germany) or VWR (Radnor, PA). *Pichia pastoris* strain X-33 and Zeocin-resistance encoding shuttle vector pPICZB were from Invitrogen (Carlsbad, CA). *Escherichia coli* strain NEB5α was from New England Biolabs (Ipswich, MA).

Site-directed mutagenesis, protein expression and purification

Preparation of plasmids, recombinant expression in *P. pastoris* and purification of pyranose dehydrogenase from *A. meleagris* (AmPDH) and variant H103Y were described in Sygmund et al. 2012 [17] and Krondorfer et al., 2014 [16].

Enzymatic activity

PDH activity was determined using the standard assay with ferrocenium hexafluorophosphate and D-glucose at 30 °C as described before [18]. pH optima of AmPDH and variant H103Y were measured from pH 2.5-6 (100 mM citrate buffer), pH 6-8 (100 mM phosphate buffer) and pH 8-10 (100 mM borate buffer). Protein concentrations were determined using the method of Bradford with a pre-fabricated assay (BioRad, Hercules, CA) or photometrically with a U-3000 spectrophotometer (Hitachi, Tokyo, Japan) using the absorbance at 280 nm and the molar absorption coefficients ($\varepsilon_{\mathrm{AmPDH}}$=67,840 $M^{-1}cm^{-1}$; $\varepsilon_{\mathrm{H103YAmPDH}}$=69,330 $M^{-1}cm^{-1}$).

Electronic circular dichroism spectroscopy

Far UV electronic circular dichroism (ECD) spectra of the wild-type and the mutant enzyme were recorded using a Chirascan CD Spectrophotometer (Applied Photophysics, Leatherhead, UK) in the wavelength range from 180 to 260 nm. The instrument was flushed with nitrogen, the pathlength was 1 mm, spectral bandwidth was set to 3 nm and the scan time per point to 10 s. The protein concentration of both samples was adjusted to 8 µM using 50 mM sodium phosphate buffer, pH 7.5.

Electron paramagnetic resonance (EPR) spectroscopy

Electron paramagnetic resonance (EPR) measurements were carried out on a Bruker EMX continuous wave (cw) spectrometer, operating at X-band (9 GHz) frequencies, equipped with a high sensitivity resonator. EPR measurements were carried out using 50 µl of wild-type AmPDH (650 µM) or H103Y AmPDH (1000 µM). The solutions were transferred into 50 µl capillary tubes (Blaubrand, Wertheim, Germany) for EPR measurements at room temperature. EPR spectra were recorded using 2 mW microwave power (MWP), 100 kHz modulation frequency (MF), 0.5 mT modulation amplitude (MA), 41 ms conversion time (CT), 41 ms time constant (TC) and 1024 points. Simulations of EPR spectra were conducted using the software EasySpin [19] and g-values are expressed relative to diphenylpicrylhydrazyl (DPPH) ($g = 2.0036$), which was used as an external standard.

Stopped-flow spectroscopy

Pre-steady-state kinetics of the oxidative and reductive half-reaction were studied using an Applied Photophysics SX20 (Leatherhead, UK) stopped-flow instrument with diode array and photo-multiplier (PMT) detection. All measurements were conducted in 65 mM sodium phosphate buffer, pH 7.5, using 20 µM of enzyme for the measurements with PMT and 40-60 µM for the diode array prescans in the single mixing mode. Reduced/oxidized enzyme was obtained using 1.2 equivalents of D-glucose/ferrocenium hexafluorophosphate as the wild-type AmPDH was present in the reduced state after purification and the mutant in the oxidized state. For the oxidative half-reaction, different concentrations of ferrocenium were used (25-300 µM). The reduction of the FAD was studied by addition of D-glucose (0.1-5 mM). All concentrations are given after mixing. Time traces at 462 nm were fit to a single exponential function using the Pro Data Viewer Software (Applied Photophysics), standard deviation was calculated from at least 3 measurements. Obtained k_{obs}-values were plotted against the substrate concentration and the apparent bimolecular rate constant (k_{app}) was obtained from the slope.

Differential scanning calorimetry (DSC)

DSC measurements were conducted as described in Hofbauer et al., 2012 [20] using 16 µM of AmPDH and variant H103Y in 65 mM sodium phosphate buffer, pH 7.5. For data analysis and conversion the Microcal Origin 7.0 software was used. Heat capacity (C_p) was expressed in kcal mol^{-1} K^{-1} (1 cal = 4.184 J). Data points were fitted to non-two-state equilibrium-unfolding models by the Lavenberg/Marquardt (LM) non-linear least square method.

*Thermo*FAD

Unfolding of the proteins was also followed by the increased emission of fluorescence of the FAD cofactor upon thermal denaturation [21]. Around 2 µl of concentrated protein were diluted with selected buffers to a final concentration of 16 µM in a final volume of 25 µl. Applied buffers were: 100 mM sodium acetate buffer, pH 3, 4 and 5; 100 mM sodium phosphate buffer pH 6, 7 and 8. The samples were heated in steps of 0.5 °C from 20 to 95 °C in a MyiQ Real-Time PCR cycler (BioRad) and fluorescence data were recorded. The T_m value was obtained as the maximum of the first derivative of the sigmoid curve [22] and represents the mean value of two independent experiments.

Chemical denaturation followed by fluorescence spectroscopy

Guanidinium hydrochloride (GdnHCl) was used for chemical denaturation of the wild-type AmPDH and variant H103Y. The changes in intrinsic tryptophan emission were followed by fluorescence spectroscopy. 0.8 µM AmPDH and H103Y in 65 mM sodium phosphate buffer, pH 7.5, were incubated with increasing concentrations of GdnHCl (0-6.5 M) for 18 h at room temperature. The excitation wavelength was set to 295 nm, an emission wavelength scan was conducted with a PerkinElmer Enspire plate reader from 320 to 400 nm at room temperature. The fraction of unfolded protein α was calculated for each GdnHCl concentration according to $\alpha=(F_N-F)/(F_N-F_U)$. F_N is the fluorescence emission maximum of the protein in the native, unfolded state, F_U the fluorescence emission maximum at the completely unfolded state. F represents the emission maximum at a defined GdnHCl concentration. The free enthalpy, ΔG^0, was determined according to ΔG_0 = -RTln$K$ = -RTln[α/(1-α)] where R is the gas constant, T is the absolute temperature and K is the equilibrium constant. m is the slope of the linear curve $\Delta G^0 = \Delta G^0_{H2O}-(m*[\text{GdnHCl}]) = m*(c_m-[\text{GdnHCl}]$, c_m is the concentration of GdnHCl with $K = 1$.

Long-term stability studies

Dilutions of AmPDH and variant H103Y in 65 mM sodium phosphate buffer were incubated in an Eppendorf tube at different temperatures and the remaining enzymatic activity was determined regularly over 35 weeks (4 °C, 21 °C, 30 °C) and 24 h (40 °C and 50 °C) in duplicates.

Results and discussion

The mechanism of the formation and the impact of a covalent FAD-linkage on enzyme catalysis were subject of several studies [3]. However, the effects of the removal of the covalent bond are very diverse in the flavoproteins investigated so far. PDH is a flavoprotein dehydrogenase with a covalently bound FAD, which is rather rare. Therefore the impact of the disruption of the covalent bond on catalysis as well as on the conformational and thermal stability were studied in the mutant H103Y and compared to the wild-type protein.

Overall structural and enzymatic activity

Figure 1A depicts the far-UV ECD spectra [23] of wild-type AmPDH and the variant H103Y. Both spectra are very similar showing two minima at 208 and 222 nm suggesting dominating α-helical structures, which nicely reflect the known crystal structure of AmPDH. The almost identical spectra of wild-type and variant protein clearly demonstrate that the exchange of histidine 103 had no effect on the overall fold and only provoked localized structural changes. Thus the covalent FAD to protein linkage is not a prerequisite for proper folding of PDH.

The mutation of histidine 103 to tyrosine was previously shown to have a negative effect on steady-state kinetic parameters of AmPDH. The catalytic efficiencies towards sugar substrates and electron acceptors decreased substantially [16]. However, these findings could not be explained satisfactorily. This actually motivated us to the present study. In the beginning the pH dependence of PDH activity was tested using the standard assay with ferrocenium hexafluorophosphate and D-glucose at 30 °C and buffers from pH 2.5 to 10 (Figure 2). Both AmPDH and variant H103Y exhibited maximum activity around pH 9. The wild-type enzyme showed higher relative activity than the mutant H103Y from pH 2.5 to 8.5. At pH > 8.5 the mutant was more active. Interestingly, at pH 6 the wild-type flavoprotein shows about 20% higher activity in sodium phosphate buffer compared to citrate buffer, whereas there was no impact on the variant.

Since the variant H103Y is still catalytically active, it must (noncovalently) bind a redox-active FAD-cofactor. This has been further confirmed by the stopped-flow and EPR measurements shown below and allows the conclusion that the mutation did not cause drastic alterations of the active site geometry (which was also suggested by the ECD data). In the closely related GMC-member POx, the overall crystal structure as well as the active site of mutant H167A was found to be nearly identical to the wild-type [15]. A similar result was obtained for the flavoprotein vanillyl-alcohol oxidase (VAO). A comparison of the crystal structure of mutant H422A with the wild-type gave a root mean square deviation for all C-α atoms of only 0.27 Å. The active site architecture was similar to the wild-type, even an identical substrate-binding-mode could be observed [24]. In contrast to that finding, mutant H46A in alditol oxidase, also member of the VAO family of flavoproteins, was expressed in a partially insoluble state and did not bind FAD at all. Therefore the authors supposed that folding and the (active site) structure were impaired [25]. Chito-oligosaccharide oxidase from *Fusarium graminearum* contains a very rare double-covalent FAD-linkage. A disruption of both covalent bonds (H94A/C154A) drastically diminished the expression levels, supporting the role of covalent flavin linkages in protein stability. The expression of the single mutants yielded similar expression levels as the wild-type [26]. These observations of representatives of different superfamilies do not allow to distinguish a clear trend or a reason for the structural integrity determinants of these non-covalent flavoproteins mutants. Factors that have a large influence are the expression host, the geometry of the (substituted) amino acid that covalently binds the FAD in the active site and the choice of the replacing amino acid.

Oxidative and reductive half reaction

To identify the rate-limiting step in the reaction catalyzed by PDH, stopped-flow experiments of the reductive and oxidative half-reaction of the wild-type and mutant H103Y at 30 °C were conducted. For a first impression of the changes occurring, spectral scans using diode array detection were performed. For calculation of rate constants measurements at 462 nm were performed.

Figure 3A depicts the spectral changes of wild-type AmPDH upon addition of D-glucose. It was interesting to see that the purified recombinant protein existed in a mixed oxidation state (FAD/$FADH_2$) (compare with Figure 5A). During the reaction the absorbance around the maxima at 372 nm and 462 nm rapidly decreased (Figure 3A). The reaction was monophasic and the time traces at 462 nm could be fitted by a single-exponential function (Figure 3B). Upon plotting the resulting k_{obs}-values *versus* the glucose concentration an apparent bimolecular rate constant of $(1.1 \pm 0.03) \times 10^5\ M^{-1}\ s^{-1}$ could be calculated.

Performing the same experiment with the H103Y variant demonstrated that the mutation significantly decelerated the two-electron transfer reaction from glucose to the redox cofactor (Figure 4). The UV-vis spectrum of the purified recombinant variant was different from that of the wild-type protein. The two maxima typical for a flavoprotein were superimposed by a third maximum around 430 nm which might suggest the presence of a semiquinone radical (see below). Nevertheless, there was a clear monophasic reduction of the cofactor within the first 10 s (Figure 4B) that strictly depended on the sugar concentration. The reaction was about 800-times slower compared to the wild-type enzyme (i.e. k_{app}= (1.4 ±

0.09) × 10^2 M^{-1} s^{-1}. With both enzymes there was an additional small and very slow reduction of FAD cofactor when monitored at longer time frame, however this phase was independent of the glucose concentration (not shown).

For studying the oxidative half reaction (i.e. reoxidation of the redox cofactor by an artificial electron acceptor) ferrocenium hexafluorophosphate was used. In contrast to the reductive half-reaction the kinetics of reoxidation of $FADH_2$ by the artificial electron acceptor was similar (Figures 5 & 6). There was a clear linear dependence of the rate of absorbance increase at 462 nm from the concentration of ferrocenium hexafluorophosphate. The calculated apparent bimolecular rate constants were (4.9 ± 0.3) × 10^5 M^{-1} s^{-1} (wild-type) and (8.1 ± 0.1) × 10^5 M^{-1} s^{-1} (H103Y). During this transition the absorbance increase at 462 nm was more pronounced than that at 360 nm (Figure 5A).

This monophasic fast reoxidation reaction was followed by a further slow transition. After prolonged reaction time in the mutant H103Y the absorbance at 462 nm was blue-shifted and peak at 430 nm emerged (see inset to Figure 6A, spectrum C). This spectrum resembles the first spectrum observed during reduction of variant H103Y by D-glucose (Figure 4A) and might suggest the formation of a semiquinone state of the prosthetic group. This intermediate cannot be physiologically relevant as it emerges after several seconds of incubation. A neutral semiquinone species is reported to exhibit absorbance in the range of 580 to 620 nm, whereas the anionic form shows characteristic absorbance at 380 nm and around 400 nm [27]. The appearance of such a spectral intermediate (anionic semiquinone) was reported for wild-type AmPDH, indicated by shoulders around 395 and 495 nm [4]. It has to be mentioned that maxima at 625 nm and around 330 to 350 nm are due to the absorbance of the electron acceptor ferrocenium hexafluorophosphate.

The presented presteady-state investigations clearly demonstrated that the reductive half reaction is the main determinant for the catalytic efficiency of AmPDH. The reduction of the FAD was slowed down by about three orders of magnitude in the non-covalent FAD-bound mutant H103Y compared to wild-type PDH. One proposed function of the covalent FAD-bond is the maintenance of a high redox potential, as for non-covalently bound flavoproteins a much lower midpoint potential was observed [3]. Non-covalent mutants like H167A in POx [15], H422A in VAO [24] or H69A in cholesterol oxidase [28] showed a decrease in redox potential due to the amino acid replacement. A lower redox potential is accompanied by a decrease of reductive half reaction rates, as shown here for PDH mutant H103Y. This finding supports the theory that the covalent FAD attachment modulates the redox properties of flavoenzymes.

Surprisingly, the oxidative half-reaction occurs nearly two times faster in mutant H103Y than in the wild-type using ferrocenium hexafluorophosphate as the electron acceptor. A fivefold increase in oxygen reactivity was recently reported for this mutant [16]. In VAO, the same effect was observed. The rate of flavin reduction was decreased and the oxidative half-reaction occurred slightly faster in mutant H422A than in wild-type VAO [24].

Semiquinone radical formation

As outlined above there was evidence from UV-vis spectroscopy for the existence of a stable semiquinone radical in the resting state of H103Y variant of AmPDH (Figure 4A and inset to Figure 6A). This prompted us to use electron paramagnetic resonance (EPR) spectroscopy for identification of this paramagnetic species. Interestingly, both proteins (wild-type and mutant) unequivocally have a semiquinone radical in their stable resting state at pH 7.5.

The EPR spectrum of wild-type AmPDH is characterized by a peak of linewidth ΔB_{PP} = 1.43 mT and two shoulders at lower and higher magnetic field, separated by about 5 mT

(Figure 1B, black line). This spectrum is characteristic for an anionic semiquinone radical representing the interaction of the unpaired electron with two ^{14}N nitrogen atoms at position 5 and 10 in FAD (with the shoulders originating from the A_{zz} value of the ^{14}N coupling) [29]. The presence of the semiquinone anion radical in the resting state of wild-type AmPDH indicates an equilibrium of the oxidized form of the enzyme with its reduced forms.

The mutant H103Y AmPDH showed a similar EPR spectrum but with a smaller linewidth of ΔB_{PP} = 1.06 mT and adjacent shoulder peaks separated by ~4.5 mT (Figure 1B, grey line). The origin of this radical is also an anionic semiquinone indicating a higher mobility of the FAD due to a smaller linewidth. This correlates with the non-covalently bound FAD in the H103Y mutant and shows an equilibrium of the reduced enzyme with its oxidized forms. Simulations of both EPR spectra are shown in Figure 1B (red and blue line).

Thermal and conformational stability

Next we investigated the role of the FAD-protein linkage on the thermal and conformational stability. The thermostability of AmPDH and variant H103Y (in 65 mM sodium phosphate buffer pH 7.5) was investigated using differential scanning calorimetry (DSC). Figure 7 shows the thermograms of the two enzymes which show non-two-state unfolding for both the wild-type and the mutant. The wild-type enzyme shows two main transitions with T_m-values at 57.8 and 65.3 °C, respectively, which might reflect the consecutive melting of the two domains (i.e. a substrate binding domain and a cofactor binding domain [4]) of this flavoprotein. In the variant both transitions occur at lower temperatures (55.6 and 64 °C). In addition in both proteins there is a third smaller endotherm at 44.8 (44.1 °C) which might reflect the unfolding of present apoprotein. The endotherm is more pronounced in the mutant. The loss of the FAD cofactor is more likely to occur in the non-covalent variant than in the wild-type, which is also reflected by the calculated calorimetric enthalpies (areas under fitted curves) of the respective transitions. In wild-type PDH the calorimetric enthalpy for the first transition (11.4 ± 2.0 kcal/mol) reflecting the melting of the apoprotein is significantly smaller than the enthalpy for the corresponding transition in variant H103Y (43.5 ± 1.3 kcal/mol). By contrast, the calculated enthalpy of the second transition at around 56 °C in wild-type PDH (201.4 ± 8.9 kcal) is significantly larger than the enthalpy for the respective transition in variant H103Y (163.4 ± 2.6 kcal), which might suggest that this transition reflects the unfolding of the FAD-binding domain. Taking into account the error in calculation of enthalpies, the observed differences between wild-type protein and mutant in the transitions at 44 °C and 56 °C nicely compensate each other ($\Delta H_{\mathrm{apo}} = 32.1 \pm 3.3$ kcal; $\Delta H_{\mathrm{FAD\text{-}domain}} = 38.0 \pm 11.5$ kcal).

In order to assess the influence of pH on thermostability, *Thermo*FAD experiments using buffers with different pH were carried out. *Thermo*FAD was first described by Forneris et al. [21]. In this method, the intrinsic fluorescence of the FAD cofactor is used to assess the thermostability of a protein. The technique can be applied to flavoproteins with covalently as well as non-covalently attached flavin. In the native, folded state the fluorescence is quenched by the surrounding protein environment. With increasing temperature, the protein starts to unfold, the FAD is exposed to the solvent and the increase in fluorescence can be detected. The concentrated protein samples were diluted in sodium acetate or phosphate buffer (pH 3-8) and the fluorescence was measured at increasing temperatures. The determined T_{m} values were highly reproducible and revealed that both enzymes are most thermostable at pH 6 in sodium phosphate buffer with T_{m} values of 72 °C for the wild-type and 63.8 °C for variant H103Y (Figure 8). The difference in T_{m} between the wild-type and the mutant decreases with increasing pH. At acidic pH values the mutant is more destabilized than the wild-type protein. One might speculate whether the influence of pH on thermostability can be attributed to the protonation state of the histidine 103 in the wild-type which was replaced by a tyrosine in the variant.

Additionally, AmPDH and variant H103Y were incubated over several months to probe the long-term stability at 4 °C, room temperature (21 °C) and 30 °C in 65 mM sodium phosphate buffer. Residual activity was determined using the standard ferrocenium/D-glucose assay. The stability of the wild-type protein decreased with increasing incubation temperature, after 35 weeks 77%, 46% and 21%, respectively, of the activity remained. The variant H103Y showed a different behavior, 35 weeks of incubation at 4 °C increased the activity to 152%, whereas the residual activities after incubation at 21 °C and 30 °C were nearly identical with 27% and 28%.

The temperature stability at 40 °C and 50 °C was investigated over 24 hours. AmPDH and variant H103Y show similar stability at 40 °C with 81% and 83% residual activity, the activity dropped slowly for both enzymes (Figure 9). At 50 °C the wild-type protein is much more stable than the mutant with 63% vs. 2% residual activity after 24 h. Variant H103Y already reached its half-life after around 2.5 h of incubation, whereas wild-type AmPDH slowly lost activity.

In general, PDH is a very stable enzyme, the half-life at 4 °C is longer than one year. For the wild-type, the residual activity decreased gradually with increasing incubation temperature whereas the mutant showed a harsh drop of the residual activity. The increase in activity of mutant H103Y at 4 °C could be due to a loss of FAD cofactor upon freezing (after purification) and thawing incubation.

To study the conformational stability of PDH chemical unfolding with guanidine hydrochloride (GdnHCl) was performed monitoring changes of the intrinsic tryptophan fluorescence. Figure 10 shows the shift of the fluorescence emission maximum after incubation of wild-type AmPDH and the variant H103Y with increasing concentrations of GdnHCl. Unfolding started around 2 M GdnHCl and was completed around 5 M for the mutant and above 6 M for the wild-type protein. At first sight the obtained plots suggest a two-state unfolding, however with a broad transition range. Upon closer inspection it is evident that from 2.0 - 3.5 M GdnHCl a first unfolding event took place, which is more pronounced in variant H103Y. The variant H103Y showed a higher emission maximum at 0 M GdnHCl than the wild-type. This was also observed for mutant H69A in cholesterol oxidase [30].

From the plots of the change in free enthalpy (ΔG^0) *versus* the GdnHCl concentrations, $\Delta G^0_{\mathrm{H2O}}$ values of 19.25 ± 1.65 kJ mol^{-1} (wild-type protein) and 14.63 ± 0.24 kJ mol^{-1} (mutant) were calculated (Table 1). Thus, besides having a higher thermal stability, also the conformational stability of the wild-type protein is higher. This is also reflected by a higher c_m value (i.e. denaturant concentration required for midterm unfolding) in the wild-type protein (4.0 ± 0.07 M *versus* 3.7 ± 0.04 M). From the slope of the linear curve $\Delta G^0 = \Delta G^0_{\mathrm{H2O}} - (m*[\mathrm{GdnHCl}])$, *m* was calculated to be 4.8 ± 0.3 kJ mol^{-1} M^{-1} and 3.9 ± 0.0 kJ mol^{-1} M^{-1}. The *m*-value stands for the effectivity of the denaturant and is proportional to the number of groups in a protein. A single mutation of two otherwise identical proteins should not influence the *m*-value. However, in the present case the covalent attachment of the cofactor is affected. This could explain that the single mutation has significant impact on the overall protein stability. PDH possesses eight tryptophans out of 577 amino acids, mainly located in the outer shell of the protein. Therefore the changes in tryptophan fluorescence are maybe not fully indicative for global changes in protein structure, but a clear destabilizing effect of the non-covalently linked FAD cofactor in variant H103Y could be observed.

Summary and conclusions

In summary, it could be shown that the disruption of the FAD to protein covalent linkage does not impair the binding of the cofactor to the protein nor alter its overall secondary structure composition. The prosthetic group is still redox active. However, the reductive half-reaction was about by three orders of magnitude slower in the variant compared to the wild-type protein, whereas the impact on the oxidative half-reaction was relatively small. EPR spectroscopy unequivocally demonstrated the presence of semiquinone radicals in the resting state of both recombinant proteins and suggested a higher mobility of the cofactor in the variant. Moreover, disruption of the covalent linkage decreases the thermal and conformational stability of the protein.

In conclusion, the observed effects on catalysis can mostly be attributed to a decrease in the reduction potential of the cofactor and as a consequence in the decrease of the capacity of the mutant to oxidize glucose. In the wild-type protein the cofactor is tightly bound to the protein and supports the structural integrity and stability of PDH.

Acknowledgements

The authors thank Cindy Lorenz for technical assistance and Stefan Scheiblbrandner for helping with the stopped-flow measurements. This work was supported by the Austrian Science Fund FWF (grant P22094 to CKP), IK is a member of the doctoral program BioToP (Biomolecular Technology of Proteins) of the Austrian Science Fund (W1224).

References

[1] J. Volc, E. Kubátová, D.A. Wood, G. Daniel, Arch Microbiol 167 (1997) 119-125.

[2] C.K. Peterbauer, J. Volc, Applied Microbiology and Biotechnology 85 (2010) 837-848.

[3] D.P.H.M. Heuts, N.S. Scrutton, W.S. McIntire, M.W. Fraaije, FEBS Journal 276 (2009) 3405-3427.

[4] T.C. Tan, O. Spadiut, T. Wongnate, J. Sucharitakul, I. Krondorfer, C. Sygmund, D. Haltrich, P. Chaiyen, C.K. Peterbauer, C. Divne, PLoS One 8 (2013) e53567.

[5] P. Halada, C. Leitner, P. Sedmera, D. Haltrich, J. Volc, Analytical Biochemistry 314 (2003) 235-242.

[6] S.F. Mathews, Z.W. Chen, H.D. Bellamy, W.S. McIntire, Biochemistry® 30 (1991) 238-247.

[7] C.D. Reeve, M.A. Carver, D.J. Hopper, Biochemical Journal 269 (1990) 815-819.

[8] C.H. Huang, W.L. Lai, M.H. Lee, C.J. Chen, A. Vasella, Y.C. Tsai, S.H. Liaw, Journal of Biological Chemistry 280 (2005) 38831-38838.

[9] N.G.H. Leferink, D.P.H.M. Heuts, M.W. Fraaije, W.J.H. van Berkel, Archives of Biochemistry and Biophysics 474 (2008) 292-301.

[10] M.W. Fraaije, R.H.H. Van Den Heuvel, W.J.H. Van Berkel, A. Mattevi, Journal of Biological Chemistry 275 (2000) 38654-38658.

[11] J. Jin, H. Mazon, R.H.T. Van Den Heuvel, A.J. Heck, D.B. Janssen, M.W. Fraaije, FEBS Journal 275 (2008) 5191-5200.

[12] A. Hassan-Abdallah, R.C. Bruckner, G. Zhao, M.S. Jorns, Biochemistry 44 (2005) 6452-6462.

[13] M.B. McNeil, J.S. Clulow, N.M. Wilf, G.P.C. Salmond, P.C. Fineran, Journal of Biological Chemistry 287 (2012) 18418-18428.

[14] F. Tasca, L. Gorton, M. Kujawa, I. Patel, W. Harreither, C.K. Peterbauer, R. Ludwig, G. Nöll, Biosensors and Bioelectronics 25 (2010) 1710-1716.

[15] M. Kujawa, H. Ebner, C. Leitner, B.M. Hallberg, M. Prongjit, J. Sucharitakul, R. Ludwig, U. Rudsander, C. Peterbauer, P. Chaiyen, D. Haltrich, C. Divne, Journal of Biological Chemistry 281 (2006) 35104-35115.

[16] I. Krondorfer, K. Lipp, D. Brugger, P. Staudigl, C. Sygmund, D. Haltrich, C.K. Peterbauer, PLoS One 9 (2014) e91145.

[17] C. Sygmund, A. Gutmann, I. Krondorfer, M. Kujawa, A. Glieder, B. Pscheidt, D. Haltrich, C. Peterbauer, R. Kittl, Appl Microbiol Biotechnol 94 (2012) 695-704.

[18] P. Staudigl, I. Krondorfer, D. Haltrich, C.K. Peterbauer, Biomolecules 3 (2013) 535-552.

[19] S. Stoll, A. Schweiger, J Magn Reson 178 (2006) 42-55.

[20] S. Hofbauer, K. Gysel, G. Mlynek, J. Kostan, A. Hagmüller, H. Daims, P.G. Furtmüller, K. Djinović-Carugo, C. Obinger, Biochimica et Biophysica Acta - Proteins and Proteomics 1824 (2012) 1031-1038.

[21] F. Forneris, R. Orru, D. Bonivento, L.R. Chiarelli, A. Mattevi, FEBS Journal 276 (2009) 2833-2840.

[22] M.W. Pantoliano, E.C. Petrella, J.D. Kwasnoski, V.S. Lobanov, J. Myslik, E. Graf, T. Carver, E. Asel, B.A. Springer, P. Lane, F.R. Salemme, Journal of Biomolecular Screening 6 (2001) 429-440.

[23] S.M. Kelly, T.J. Jess, N.C. Price, Biochimica et Biophysica Acta - Proteins and Proteomics 1751 (2005) 119-139.

[24] M.W. Fraaije, R.H.H. Van Den Heuvel, W.J.H. Van Berkel, A. Mattevi, Journal of Biological Chemistry 274 (1999) 35514-35520.

[25] D.P.H.M. Heuts, E.W. Van Hellemond, D.B. Janssen, M.W. Fraaije, Journal of Biological Chemistry 282 (2007) 20283-20291.

[26] D.P.H.M. Heuts, R.T. Winter, G.E. Damsma, D.B. Janssen, M.W. Fraaije, Biochemical Journal 413 (2008) 175-183.

[27] P. Macheroux, Methods in molecular biology (Clifton, N.J.) 131 (1999) 1-7.

[28] L. Motteran, M.S. Pilone, G. Molla, S. Ghisla, L. Pollegioni, Journal of Biological Chemistry 276 (2001) 18024-18030.
[29] J.S. Hyde, L.E. Eriksson, A. Ehrenberg, Biochim Biophys Acta 222 (1970) 688-692.
[30] L. Caldinelli, S. Iametti, A. Barbiroli, F. Bonomi, D. Fessas, G. Molla, M.S. Pilone, L. Pollegioni, Journal of Biological Chemistry 280 (2005) 22572-22581.

Table 1. Thermodynamic parameters for GdnHCl-mediated unfolding followed by monitoring the intrinsic fluorescence of tryptophan (excitation 295 nm, emission 320-400 nm).

Thermodynamic parameter	AmPDH	AmPDH variant H103Y
$\Delta G^0_{\mathrm{H2O}}$ [kJ mol^{-1}]	19.25 ± 1.65	14.63 ± 0.24
m [kJ mol^{-1} M^{-1}]	4.80 ± 0.29	3.89 ± 0.00
c_m [M]	4.01 ± 0.07	3.74 ± 0.04

Figure legends

Figure 1. (A) Far-UV ECD spectra of 8 µM AmPDH (black) and H103YAmPDH (grey) in 65 mM sodium phosphate buffer pH 7.5. (B) Cw EPR spectra of wild-type AmPDH (black) and H103Y AmPDH mutant (grey) and their simulations (red, blue) recorded at room temperature at pH 7.5. Simulation parameters for wild-type AmPDH (red) are $g_{iso} = 2.0028$, A_{iso} (N^5) = 0.78 mT, A_{iso} (N^{10}) = 0.32 mT and for H103Y AmPDH $g_{iso} = 2.0028$, A_{iso} (N^5) = 0.63 mT, A_{iso} (N^{10}) = 0.34 mT.

Figure 2. Effect of pH on the overall activity of AmPDH (black) and AmPDH variant H103Y (white) with ferrocenium hexafluorophosphate and 25 mM D-glucose at 30 °C. Circles: citrate buffer; triangles: phosphate buffer; squares: borate buffer.

Figure 3. Reductive half-reaction of wild-type AmPDH followed by stopped-flow spectroscopy. (A) Spectral changes upon reduction of 60 µM AmPDH with 200 µM D-glucose at 30 °C. (B) Typical time trace and fit at 462 nm of the reaction between 21 µM AmPDH and 2.5 mM D-glucose at 30 °C. (C) Plot of the pseudo-first-order rate constants *versus* D-glucose concentration.

Figure 4. Reductive half-reaction of AmPDH variant H103Y followed by stopped-flow spectroscopy. (A) Spectral changes upon reduction of 40 µM mutant with 25 mM D-glucose at 30 °C. (B) Typical time trace and fit at 462 nm of the reaction between 21 µM AmPDH and 2.5 mM D-glucose at 30 °C. (C) Plot of the pseudo-first-order rate constants *versus* D-glucose concentration.

Figure 5. Oxidative half-reaction of AmPDH followed by stopped-flow spectroscopy. (A) Spectral changes of oxidation of 60 µM AmPDH by 200 µM ferrocenium hexafluorophosphate at 30 °C. (B) Typical time trace and fit at 462 nm of the reaction between 21 µM AmPDH with 100 µM ferrocenium hexafluorophosphate at 30 °C. (C) Plot of pseuodo-first-order rate constants *versus* ferrocenium concentration.

Figure 6. Oxidative half-reaction of AmPDH mutant H103Y followed by stopped-flow spectroscopy. (A) Spectral changes of oxidation of 60 µM AmPDH variant H103Y by 200 µM ferrocenium hexafluorophosphate at 30 °C. Inset: reduced state (a), oxidized state (b) and spectrum observed after prolonged measurement of 50 s (c). (B) Typical time trace and fit at 462 nm of the reaction between 21 µM AmPDH variant H103Y with 100 µM ferrocenium hexafluorophosphate at 30 °C. (C) Plot of pseudo-first-order rate constants *versus* ferrocenium concentration.

Figure 7. Thermostability of AmPDH and AmPDH variant H103Y determined by differential scanning calorimetry in 65 mM sodium phosphate buffer pH 7.5. Black lines: original data. Red lines: fits of t endotherms to a non-two-state transition model.

Figure 8. Plot of T_m values of wild-type AmPDH (black) and variant H103Y (white) determined by *Thermo*FAD at different pH values in 100 mM sodium acetate buffer (pH 3-5) or 100 mM sodium phosphate buffer (pH 6-8).

Figure 9. Residual activity of AmPDH (black) and AmPDH variant H103Y (white) after incubation at 40 °C (circles) and 50 °C (triangles) in 65 mM sodium phosphate buffer pH 7.5. Activity was determined using the standard ferrocenium/D-glucose assay.

Figure 10. GdnHCl mediated unfolding of AmPDH (black) and AmPDH variant H103Y (white) followed by fluorescence spectroscopy (excitation 295 nm). 800 nM of protein was incubated around 18 h with GdnHCl concentrations from 0-6.5 M in 65 mM sodium phosphate buffer pH 7.5. The fluorescence emission maximum was plotted against the GdnHCl concentrations.

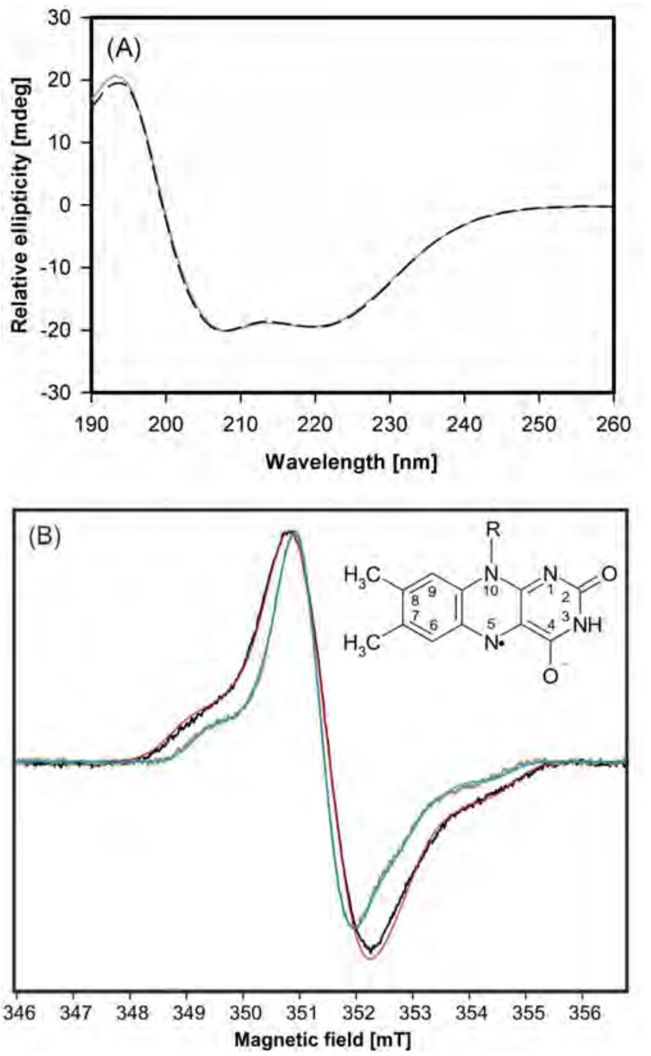
(A)
Relative ellipticity [mdeg]
30
20
10
0
-10
-20
-30
190
200
210
220
230
240
250
260
Wavelength [nm]
(B)
R
H3C
H3C
N
N
O
NH
N•
O−
1
2
3
4
5
6
7
8
9
10
346
347
348
349
350
351
352
353
354
355
356
Magnetic field [mT]

Figure 1.

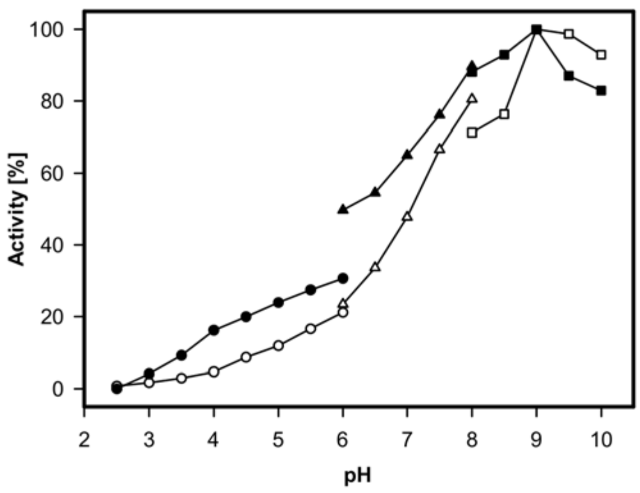

Figure 2.

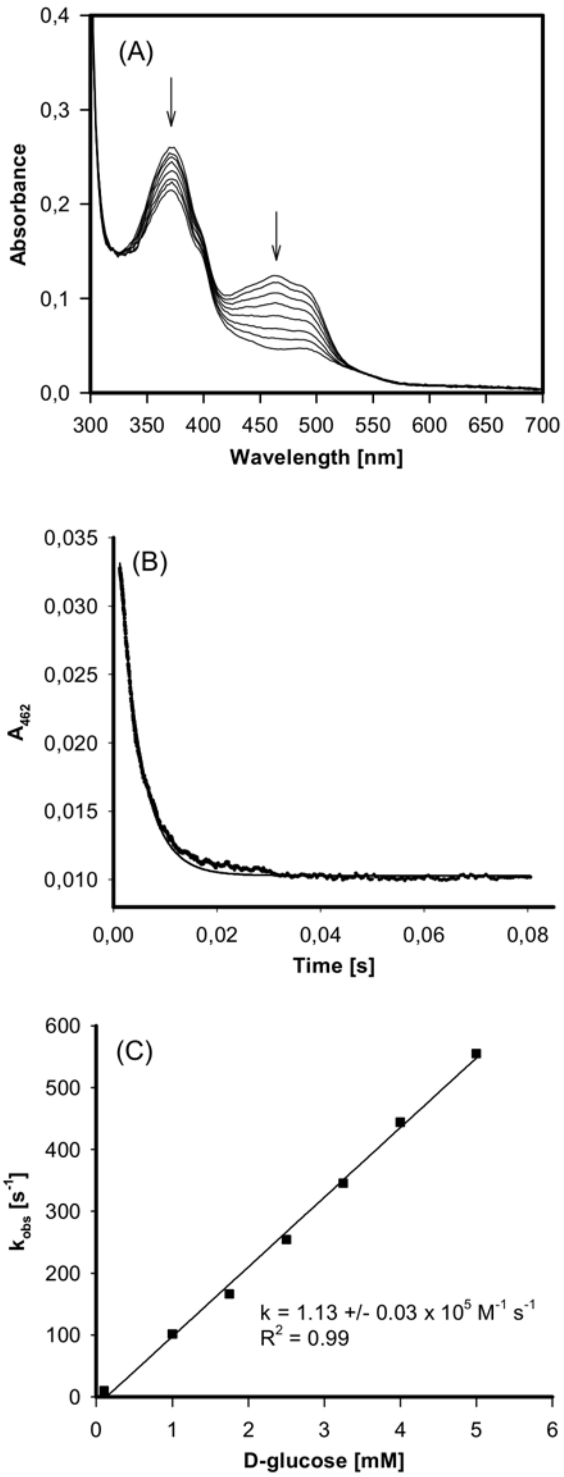
(A)
0,4
0,3
0,2
0,1
0,0
Absorbance
300
350
400
450
500
550
600
650
700
Wavelength [nm]
(B)
0,035
0,030
0,025
0,020
0,015
0,010
A_{462}
0,00
0,02
0,04
0,06
0,08
Time [s]
(C)
600
500
400
300
200
100
0
k_{obs} [s^{-1}]
k = 1.13 +/- 0.03 x 10^5 M^{-1} s^{-1}
R^2 = 0.99
0
1
2
3
4
5
6
D-glucose [mM]

Figure 3.

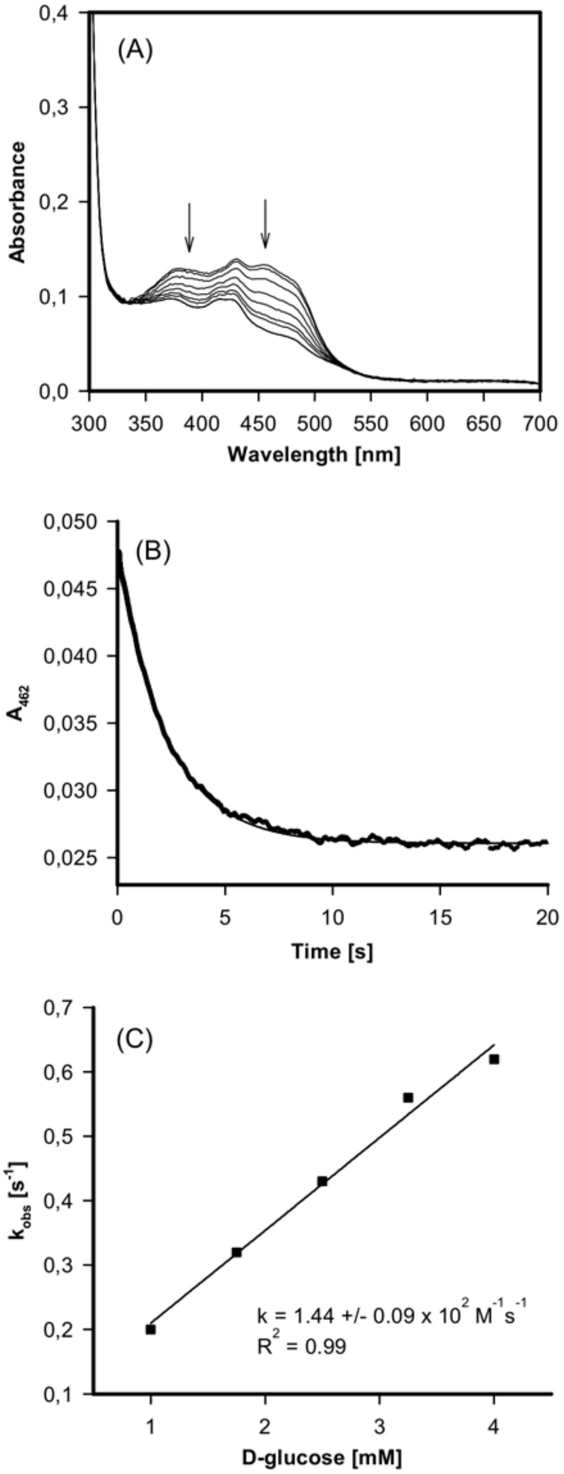
(A)
Absorbance
0,0
0,1
0,2
0,3
0,4
300
350
400
450
500
550
600
650
700
Wavelength [nm]
(B)
A_{462}
0,025
0,030
0,035
0,040
0,045
0,050
0
5
10
15
20
Time [s]
(C)
k_{obs} [s^{-1}]
0,1
0,2
0,3
0,4
0,5
0,6
0,7
1
2
3
4
D-glucose [mM]
k = 1.44 +/- 0.09 x 10^2 $M^{-1}s^{-1}$
R^2 = 0.99

Figure 4.

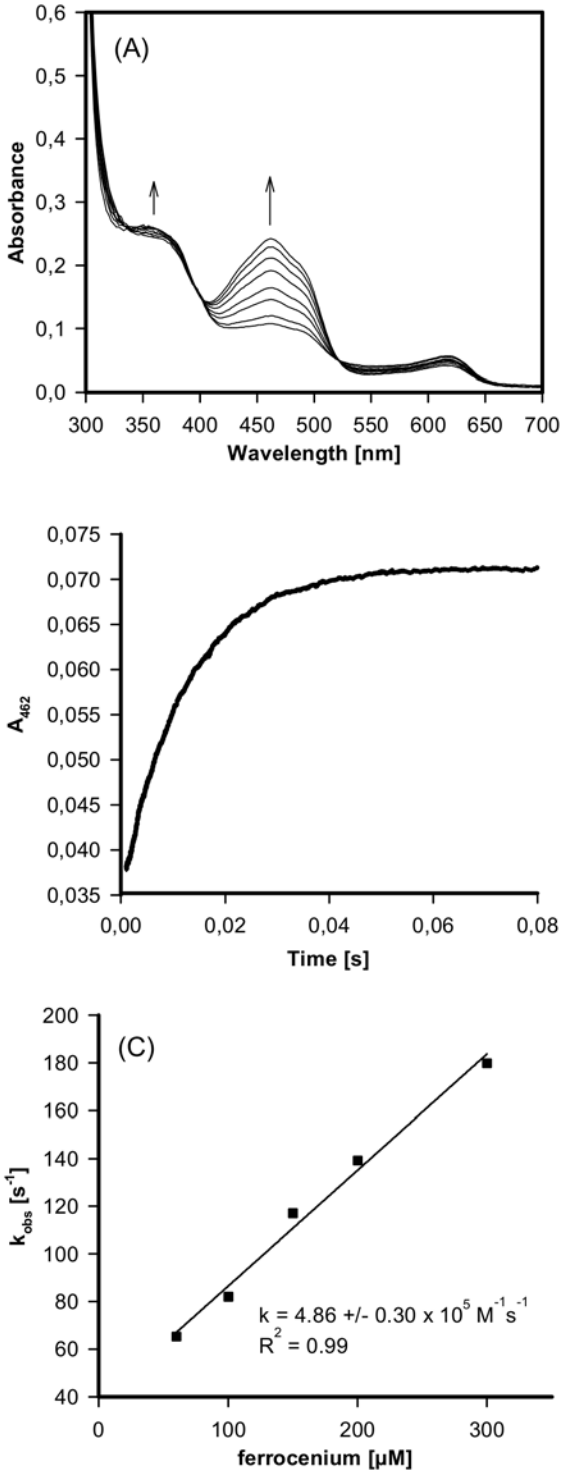
(A)
Absorbance
Wavelength [nm]
0,0
0,1
0,2
0,3
0,4
0,5
0,6
300
350
400
450
500
550
600
650
700
A_{462}
Time [s]
0,035
0,040
0,045
0,050
0,055
0,060
0,065
0,070
0,075
0,00
0,02
0,04
0,06
0,08
(C)
k_{obs} [s^{-1}]
ferrocenium [µM]
40
60
80
100
120
140
160
180
200
0
100
200
300
k = 4.86 +/- 0.30 x 10^5 $M^{-1}s^{-1}$
R^2 = 0.99

Figure 5.

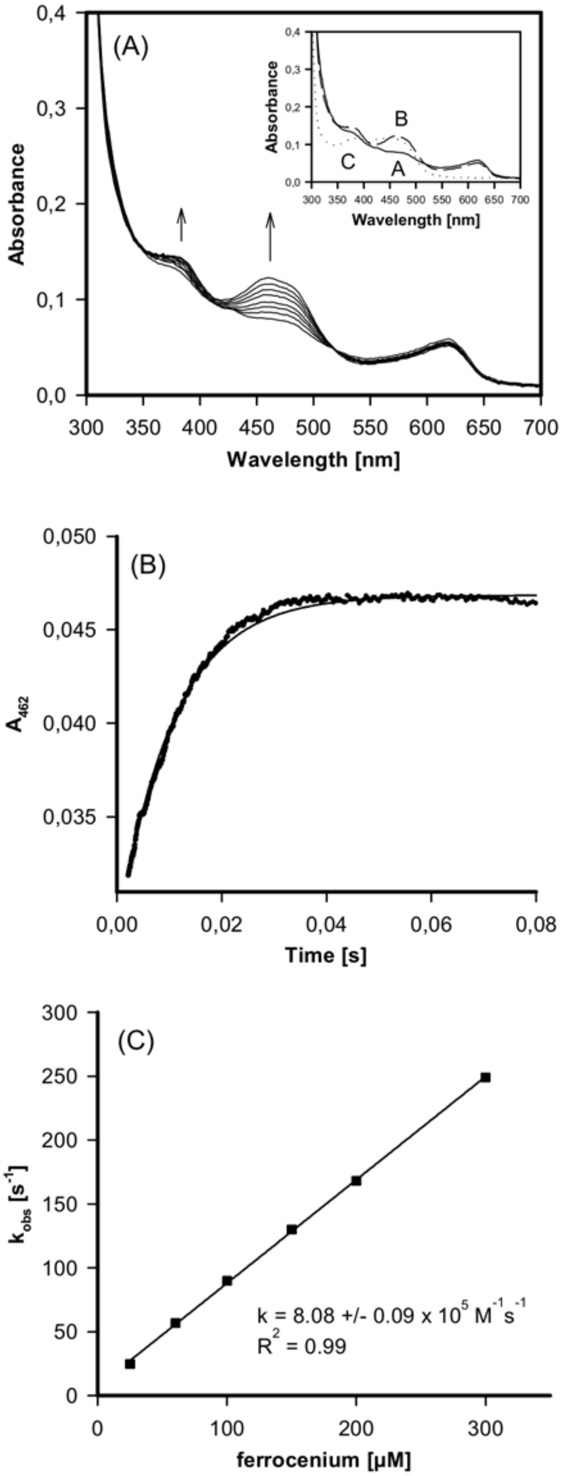
(A)
Absorbance
Wavelength [nm]
0,0
0,1
0,2
0,3
0,4
300
350
400
450
500
550
600
650
700
B
C
A
(B)
A_{462}
Time [s]
0,035
0,040
0,045
0,050
0,00
0,02
0,04
0,06
0,08
(C)
k_{obs} [s^{-1}]
ferrocenium [µM]
k = 8.08 +/- 0.09 x 10^5 $M^{-1}s^{-1}$
R^2 = 0.99
0
50
100
150
200
250
300

Figure 6.

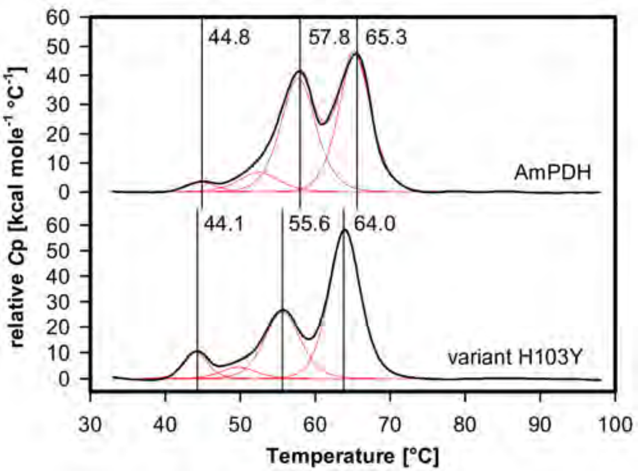
relative Cp [kcal mole^{-1} °C^{-1}]
60
50
40
30
20
10
0
44.8
57.8
65.3
AmPDH
44.1
55.6
64.0
variant H103Y
30
40
50
60
70
80
90
100
Temperature [°C]

Figure 7.

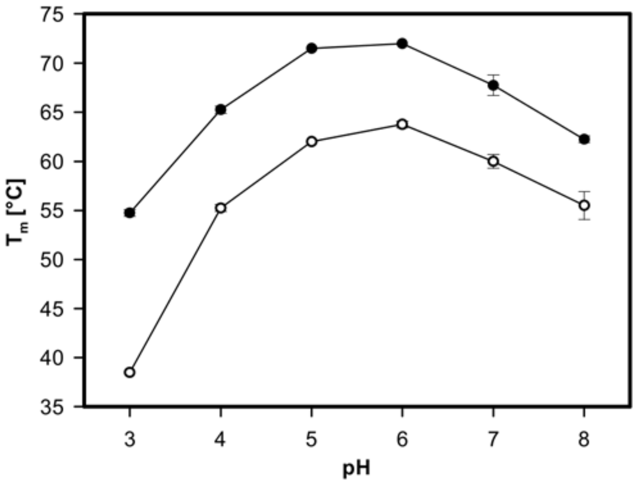

Figure 8.

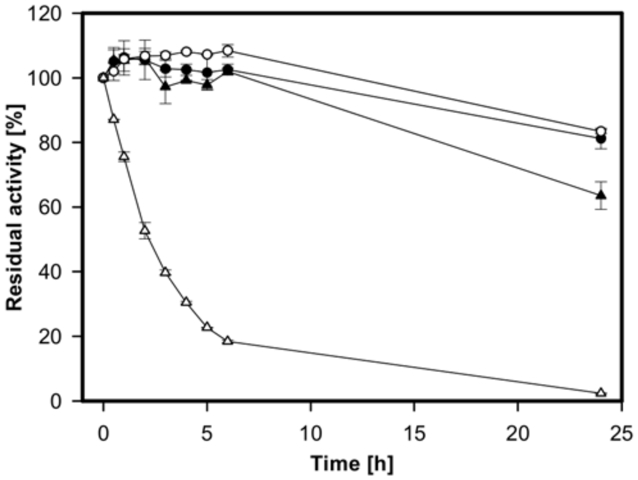

Figure 9.

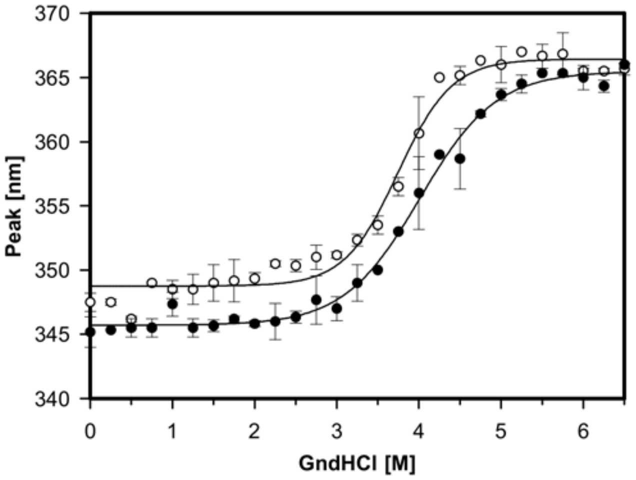

Figure 10.

Chapter 4. Characterization and engineering of GMC oxidoreductases

Paper VI

Semi-rational engineering of cellobiose dehydrogenase for improved hydrogen peroxide production.

Christoph Sygmund, Paul Santner, **Iris Krondorfer**, Clemens K. Peterbauer, Miguel Alcalde, Gibson S. Nyanhongo, Georg M. Guebitz and Roland Ludwig

Microbial Cell Factories (2013) 12: 38.

Paper VII

Convenient microtiter-plate-based activity assays for flavin-dependent oxidoreductases.

Dagmar Brugger, **Iris Krondorfer**, Kawah Zahma, Thomas Stoisser, Juan M. Bolivar, Bernd Nidetzky, Clemens K. Peterbauer and Dietmar Haltrich

Biotechnology Journal (2014) DOI: 10.1002/biot.201300336.

Paper VI

Sygmund *et al. Microbial Cell Factories* 2013, **12**:38
http://www.microbialcellfactories.com/content/12/1/38

MICROBIAL CELL FACTORIES

RESEARCH **Open Access**

Semi-rational engineering of cellobiose dehydrogenase for improved hydrogen peroxide production

Christoph Sygmund[1], Paul Santner[1], Iris Krondorfer[1], Clemens K Peterbauer[1], Miguel Alcalde[2], Gibson S Nyanhongo[3], Georg M Guebitz[3] and Roland Ludwig[1*]

Abstract

Background: The ability of fungal cellobiose dehydrogenase (CDH) to generate H_2O_2 *in-situ* is highly interesting for biotechnological applications like cotton bleaching, laundry detergents or antimicrobial functionalization of medical devices. CDH's ability to directly use polysaccharide derived mono- and oligosaccharides as substrates is a considerable advantage compared to other oxidases such as glucose oxidase which are limited to monosaccharides. However CDH's low activity with oxygen as electron acceptor hampers its industrial use for H_2O_2 production. A CDH variant with increased oxygen reactivity is therefore of high importance for biotechnological application. Uniform expression levels and an easy to use screening assay is a necessity to facilitate screening for CDH variants with increased oxygen turnover.

Results: A uniform production and secretion of active *Myriococcum thermophilum* CDH was obtained by using *Saccharomyces cerevisiae* as expression host. It was found that the native secretory leader sequence of the *cdh* gene gives a 3 times higher expression than the prepro leader of the yeast α-mating factor. The homogeneity of the expression in 96-well deep-well plates was good (variation coefficient <15%). A high-throughput screening assay was developed to explore saturation mutagenesis libraries of *cdh* for improved H_2O_2 production. A 4.5-fold increase for variant N700S over the parent enzyme was found. For production, N700S was expressed in *P. pastoris* and purified to homogeneity. Characterization revealed that not only the k_{cat} for oxygen turnover was increased in N700S (4.5-fold), but also substrate turnover. A 3-fold increase of the k_{cat} for cellobiose with alternative electron acceptors indicates that mutation N700S influences the oxidative- and reductive FAD half-reaction.

Conclusions: Site-directed mutagenesis and directed evolution of CDH is simplified by the use of *S. cerevisiae* instead of the high-yield-host *P. pastoris* due to easier handling and higher transformation efficiencies with autonomous plasmids. Twelve clones which exhibited an increased H_2O_2 production in the subsequent screening were all found to carry the same amino acid exchange in the *cdh* gene (N700S). The sensitive location of the five targeted amino acid positions in the active site of CDH explains the high rate of variants with decreased or entirely abolished activity. The discovery of only one beneficial exchange indicates that a dehydrogenase's oxygen turnover is a complex phenomenon and the increase therefore not an easy target for protein engineering.

---

* Correspondence: roland.ludwig@boku.ac.at
[1] Vienna Institute of Biotechnology, Department of Food Sciences and Technology, BOKU-University of Natural Resources and Life Sciences, Vienna, Austria
Full list of author information is available at the end of the article

BioMed Central

© 2013 Sygmund et al.; licensee BioMed Central Ltd. This is an Open Access article distributed under the terms of the Creative Commons Attribution License (http://creativecommons.org/licenses/by/2.0), which permits unrestricted use, distribution, and reproduction in any medium, provided the original work is properly cited.

Background

The extracellular fungal flavocytochrome cellobiose dehydrogenase (CDH, EC 1.1.99.18) is secreted by wood-degrading, phytopathogenic and saprotrophic fungi [1]. The widespread appearance implies an important function of CDH in the process of wood degradation [2-5]. It is a monomeric protein consisting of two domains [6,7], which oxidizes several carbohydrates at the flavodehydrogenase domain carrying an FAD cofactor. A smaller, heme *b* containing cytochrome domain is connected via a flexible linker. A typical CDH consists of approximately 800 amino acids. In some ascomycetous CDHs, like the one from *Myriococcum thermophilum* (828 aa) used in this study, a family 1 carbohydrate binding module (CBM1) is additionally attached to the C-terminus. The molecular mass ranges from 85 up to 101 kDa depending on the degree of glycosylation, which can account for up to 20% of the molecular mass [8,9]. Basidiomycetous CDHs show a high specificity for cellobiose and cello-oligosaccharides, whereas some ascomycetous CDHs like *M. thermophilum* CDH have a broader substrate specificity and oxidize also other mono-, di- and oligosaccharides, albeit with lower catalytic efficiency [1,5,9,10]. During the reductive half-reaction the FAD cofactor oxidizes suitable carbohydrates at the anomeric C1 atom into intermediary lactones, which hydrolyze spontaneously to the corresponding aldonic acids (Figure 1). Re-oxidation of the FAD can be performed by either two-electron acceptors (quinones, 2,6-dichloroindophenol, phenoxazine- and phenothiazine dyes) or by one-electron acceptors (polysaccharide monooxygenases, cytochrome *c*, ferricyanide and ferrocenium) or very slowly by oxygen [3,4,9].

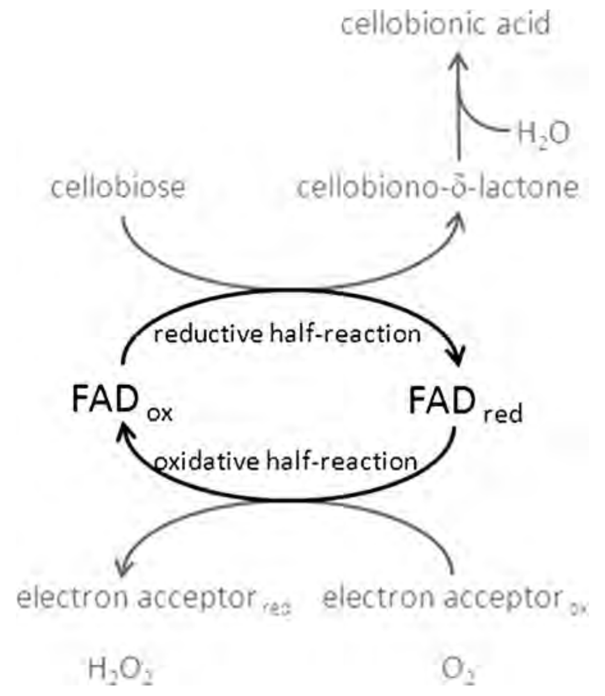

Figure 1 ***Half-reactions of the FAD cofactor in the flavodehydrogenase domain of CDH.*** In the reductive half-reaction the oxidized FAD is reduced by e.g. cellobiose, which is converted into the 1,5-lactone before it spontaneously hydrolyzes in the aqueous reaction medium to the aldonic acid. The reduced FAD is regenerated in the oxidative half-reaction by electron acceptors or, very slowly, by oxygen.

Due to its versatile properties CDH has been applied in biosensors for the detection of lactose, glucose and catecholamines, in enzymatic biofuel cells as anode catalyst [8,11], for the production of lactobionic acid [12-14], as well as in biodegradation [15] and bioremediation [16]. A more recent proposed application of CDH has been the *in situ* production of H_2O_2 for cotton bleaching [10,17,18]. CDH has the potential to replace the currently used mixture of H_2O_2 and NaOCl, which causes damage to the cotton fibres, forms toxic by-products and consumes large amounts of energy and water. In the proposed eco-friendly bleaching system, CDH produces the reactive oxygen species. The suitability of CDH for this approach was demonstrated [18]. In contrast to other proposed biocatalysts like choline oxidase [19] or glucose oxidase [20] CDH can produce H_2O_2 by oxidation of a wide range of carbohydrates (cellulose and cellodextrins, galactomannans, lactose, maltose or glucose) which occur in the process (e.g. from starch desizing), are added or generated by cellulolytic enzymes [10]. Similarly, the potential of CDH for medical application was recently demonstrated [21,22]. The main drawback of CDH for these applications is its relatively slow H_2O_2 production rate compared to oxidases. CDH with increased oxygen reactivity would combine the mentioned advantages with an increased H_2O_2 production. Such a CDH would be very attractive for the pulp & paper industry, cotton-bleaching, consumer applications like laundry detergents or antimicrobial functionalization of medical devices, e.g., catheters.

The modulation of the oxygen reactivity in flavoenzymes is currently an active field of research. However, no definite guidelines exist on how to change a dehydrogenase into an oxidase or vice versa [23,24]. It has been shown that the protein matrix surrounding the flavin cofactor (FAD or FMN) has a great effect on the oxygen reactivity [25]. Therefore, semi-rational protein engineering, which targets amino acid residues in the catalytic-site in close vicinity to the FAD by saturation mutagenesis, was the applied strategy to increase the oxygen reactivity of CDH. Several saturation mutagenesis libraries of the *M. thermophilum cdh* gene for five target residues close to the FAD were constructed by the sequence overlap extension (SOE) method and functionally expressed in *S. cerevisiae*. A robust and easy to use high-throughput screening (HTS) assay was established to select CDH variants for improved

H_2O_2 production. Finally, the mutated *cdh* gene was recombinantly expressed in *P. pastoris* to prepare sufficient amounts of the CDH variant for kinetic characterization and evaluation of the assay.

Results and discussion

Expression of *M. thermophilum* CDH in *S. cerevisiae*

CDH is a secretory glycosylated fungal protein, and expression has so far only been successful in eukaryotic expression systems. During the last years, *P. pastoris* was established as the standard expression system for CDH [5,26-28]. Although it is a powerful host for recombinant protein production it is not considered as the preferred host organism for protein engineering by directed evolution. The lack of reliable episomal vectors along with modest transformation efficiencies, preclude in most of the cases the use of this yeast for such approaches. Indeed, no reports of semi-rational engineering or directed evolution of CDHs are published. Even the possibility to express the sole flavodehydrogenase domain of CDH in the prokaryotic expression system *E. coli* [29] has not triggered engineering studies. This can be explained by the essential role of the cytochrome domain for many applications [8,10,15]. So far, heterologous expression of a full length CDH can only be achieved in eukaryotic expression hosts. Therefore, one goal of this study was to establish *S. cerevisiae* as eukaryotic expression system for CDH, which would allow screening for improved variants of full length CDH. *S. cerevisiae* is one of the most successfully used host organisms for directed evolution of eukaryotic proteins due to high transformation efficiencies, easy genetic manipulation and secretion of the target proteins [30,31]. There are several reports in literature where the expression level of the target protein could be increased by the exchange of the native secretory leader sequence with the α-factor prepro leader from *S. cerevisiae*, even subjecting the corresponding fusion gene to several rounds of evolution for improved secretion [32-35].

Therefore we evaluated in a preliminary experiment the influence of the signal sequence on the expression level of CDH in *S. cerevisiae*. Two nucleotide sequences coding for *M. thermophilum* CDH (*r*CDH) with different signal sequences were cloned into pJRoC30 for expression under the control of the GAL1 promoter. Plasmid pJRoC30-*Mt*CDH-nat encodes the full length CDH including its native secretory leader. In plasmid pJRoC30-*Mt*CDH-α the native signal sequence was replaced by the α-factor prepro leader. The resulting expression vectors were transformed into chemical competent *S. cerevisiae* cells. Ninety-six colonies of each transformation were picked and cultivated in 96-well deep-well plates. After 120 h of induction, supernatants were tested for CDH activity with the (2,6-dichloroindophenol) DCIP assay. The construct with the native secretory leader (0.05 U mL^{-1}) showed on average a 3.1 times higher DCIP activity compared to the construct with the α-factor prepro leader (0.016 U mL^{-1}). To test the uniformity of the expression levels in the 96-well deep-well plates the coefficient of variation was calculated (Figure 2). Both constructs showed a variation below 15% which is acceptable for screening mutant libraries [36]. However, due to the higher expression levels, the expression cassette employing the native secretory leader was selected for further studies.

Library construction and high-throughput screening (HTS)

A comparative (homology) model of CDH from *M. thermophilum* was constructed using the crystal structure of the *Phanerochaete chrysosporium* flavodehydrogenase domain as template (PDB accession code 1KDG, Figure 3). The local alignment of the sequences (see Additional file 1) has a sequence identity of 39% for the modeled flavodehydrogenase sequence (positions 251 – 829), whereas the overall sequence identity is only 35%. The obtained model was carefully tested by local and global model quality check programs. Five amino acids in the catalytic-site close to the FAD were selected for saturation mutagenesis. Three amino acids (G323, A322 and L324) interact with FAD's isoalloxazine ring system and are in close vicinity of the C4a-N5 locus, which is proposed to be important for the reduction of molecular oxygen in FAD-dependent oxidases. Two amino acids (N700 and H701) are part of the catalytic subsite close to the isoalloxazine ring and fully conserved among CDHs. It was anticipated that mutations of H701, the general base, leads in case of any substitution to inactive variants which can be used to evaluate the mutagenesis method. Degenerated codons of the NNS type were used. The corresponding mutant libraries were double screened for CDH activity and expression with the DCIP-based assay and for H_2O_2 production with the ABTS-HRP coupled assay. The ABTS-HRP coupled assay was derived from a published method [18] by switching leucocrystal violet by ABTS and splitting the reaction into a H_2O_2 generating part and, after thermal deactivation of the enzyme variants, a colorimetric detection reaction. The DCIP-based assay showed that a large number of mutations at the selected positions result in inactive CDH variants: 55% at G323, 80% at A322, 34% at L324, 29% at N700 and 99% at H701. This demonstrates the importance of the targeted amino acids for enzymatic activity although folding and stability could also be affected. Amino acid H701 corresponds in terms of position to H689 in *P. chrysosporium* CDH which has been proposed to act as catalytic base [7]. Its importance in the catalytic machinery is reflected by the highest number of inactive variants.

During the first screening round twelve variants at position N700 and seven variants at position G232 were selected due to an increased H_2O_2 production and subjected

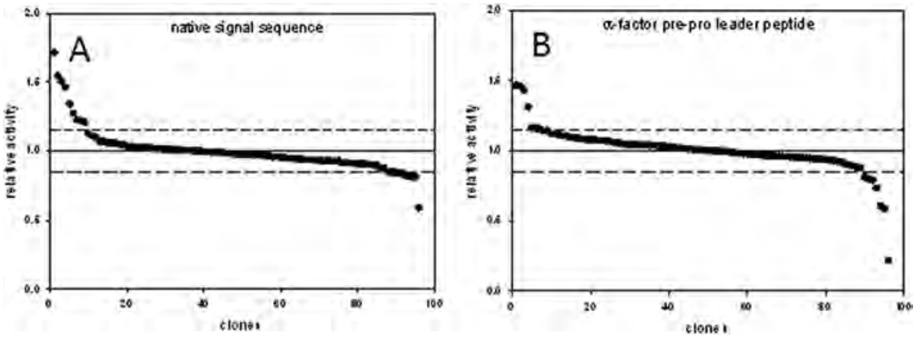

Figure 2 Landscapes of CDH expression levels. Dashed lines indicate the variation coefficient. *S. cerevisiae* cells were transformed with plasmid pJRoC30-MtCDH-nat (**A**) and pJROC30-MtCDH-α (**B**). 96 individual colonies of each transformation were cultivated under inducing conditions. Centrifuged supernatants were used for the DCIP-based assay.

to a re-screening. The increased H_2O_2 production could be confirmed for all N700 variants in the re-screening while the G232 variants turned out to be false positives. The twelve re-screened variants of position N700 showed an increased DCIP activity (~4 times) as well as an increased H_2O_2 production (~5 times) compared to *r*CDH. The sequencing results showed that all of them carried the mutation N700S. The amino acid serine was encoded by any of the 3 possible codons TCT, TCA and AGT, which demonstrates the good performance of the site-saturation mutagenesis method and the reliability of the screening assay.

Production and purification of *M. thermophilum* CDH variant N700S in *P. pastoris*

Although expression levels of CDH in *S. cerevisiae* (0.05 U/mL) were sufficient to perform the screening assay, they were low compared to reported expression levels of CDH using its standard recombinant expression host *P. pastoris*. Therefore we decided to use *P. pastoris* as production host for fermentation to obtain high amounts of CDH for protein purification. The mutation N700S was introduced into the *P. pastoris* expression plasmid pPIC*Mt*CDH by a two-step mutagenesis approach. The resulting plasmid was transformed into electro-competent *P. pastoris* cells. The enzyme was produced with a PCR verified clone in a 7-L stirred and aerated bioreactor. The volumetric CDH activity in the culture supernatant was measured with the DCIP assay and reached a maximum value of 1800 U L^{-1} after 123 h. The recombinant enzyme was purified to apparent homogeneity using a two-step purification protocol (Table 1). Although only the purest fractions were pooled, 75% of the total activity was recovered. The homogeneous preparation consisted of 690 mg CDH (Figure 4A) with a specific DCIP activity of 8 U mg^{-1} and a high absorbance ratio A_{420}/A_{280} of 0.54, which was calculated from the UV/Vis absorption spectrum (Figure 4B) and is an indicator for the purity of the CDH sample [1]. The spectrum shows the typical increase of CDH's *b*-type heme α- and β-band at 562 and 533 nm, respectively, the red-shift from 421 to 429 nm of the heme's Soret-band and the decrease of the FAD signal in the range of 450 – 500 nm upon reduction of CDH with a carbohydrate substrate.

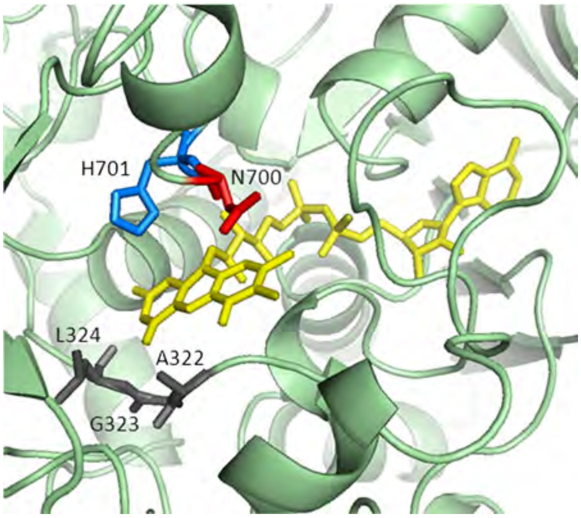

Figure 3 Model of *M. thermophilum* CDH (template: *P. chrysosporium* CDH structure 1KDG). The active site with the FAD cofactor (yellow) and five mutated amino acid positions A322, G323, L324 (grey), N700 (red) and H701 (catalytic base, blue) are highlighted.

Oxygen reactivity

The O_2 consumption rates of variant N700S and *r*CDH were determined at 30°C using a fluorescence-based fiber optic sensor. This sensor does not consume O_2 like a Clark-type electrode, which considerably reduces the oxygen concentration in small reaction volumes and therefore introduces a bias. Both enzymes were applied at the same protein concentration (0.18 mg mL^{-1}). Variant N700S consumed all O_2 present in the 1.9 mL microreactor (2.3 μmol) in 100 min, whereas the unmodified *r*CDH took 420 min (Figure 5). This increased oxygen reactivity

Table 1 Purification scheme of CDH variant N700S

Purification step	Total activity (U)	Total protein (mg)	Specific activity (U mg^{-1})	Yield (%)	Purification (fold)
Culture supernatant	7380	3360	2.2	100	1
Phenyl-Sepharose	5980	950	6.3	81	2.9
Q-Source	5540	690	8.0	75	3.6

was also verified by the stopped ABTS assay in cuvettes. While the fluorescence-based fiber optic sensor measures the decrease in oxygen concentration, the stopped ABTS assay indirectly detects the produced H_2O_2. One milligram of *r*CDH produced 0.028 µmol H_2O_2 per minute while variant N700S produced 0.127 µmol H_2O_2 per minute. Both methods showed that N700S converts O_2 to H_2O_2 about 4.2 to 4.5 times faster than *r*CDH.

Kinetic characterization of variant N700S

Initial rates of substrate turnover were recorded over a substrate range of 0.003 to 10 mM cellobiose for variant N700S and *r*CDH using DCIP, 1,4-benzoquinone and oxygen as electron acceptor. Kinetic data are summarized in Table 2. The catalytic constant (k_{cat}) for cellobiose increased significantly for variant N700S compared to *r*CDH. Without more detailed kinetic measurements it is difficult to discriminate if the mutation increases the rate of the reductive half-reaction (the oxidation of cellobiose and the concomitant reduction of FAD to $FADH_2$) or increases the rate of $FADH_2$ oxidation by electron acceptors in the oxidative half reaction. The increase of k_{cat} was nearly identical for the two-electron acceptors DCIP (3.0-fold) and 1,4-benzoquinone (3.1-fold) but higher for oxygen (4.5-fold). The K_M values for cellobiose increased for N700S when compared to *r*CDH with DCIP (2.9-fold), 1,4-benzoquinone (2.5-fold) and oxygen (2.0-fold). The increased K_M is most probably a kinetic effect and not due to changed affinities for the electron acceptors, which have no known binding site. The catalytic efficiencies (k_{cat}/K_M) for variant N700S and *r*CDH are similar for DCIP and 1,4-benzoquinone, but for oxygen the catalytic efficiency of N700S is 2.4-fold higher than for *r*CDH. These data indicate that part of the increased substrate turnover comes from a faster reductive half-reaction, but in the case of oxygen also a faster oxidative half-raction is influencing the overall velocity. In conclusion, position N700 seems to influence both: substrate and oxygen turnover. In the homology model of *M. thermophilum* CDH (Figure 2) the amino acid N700 corresponds to the position of amino acid N688 in *P. chrysosporium*. This asparagine residue is positioned between the catalytic subsite *C* and the binding subsite *B* and with only minor positional changes in the cellobiose molecule it may interact with either of the subsites, thereby influencing substrate binding or catalysis. Due to the close vicinity to the catalytic base H689 it might also influence its proton abstracting properties. The comparative model of variant N700S shows that the serine side chain can easily flip its orientation between both subsites. To fully elucidate the influence of the mutation on the reaction mechanism more elaborate steady-state and presteady-state experiments are needed. The high substrate concentrations used in technological processes, which are much higher than the K_M value of the CDH variant for cellobiose, ensures a 4.5-fold increased turnover of the co-substrate O_2. Under such conditions

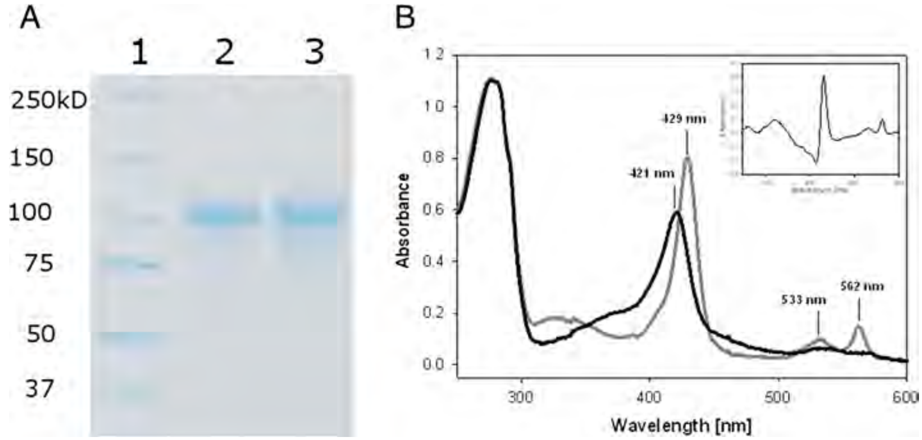

Figure 4 Verification of protein purity. A. SDS-PAGE of CDHs expressed in *P. pastoris* after purification. Lane 1, molecular mass marker; lane 2, *r*CDH; lane 3, variant N700S. **B**. Absorption spectra of the CDH variant N700S. The black line shows the oxidized state and the grey line the reduced form. The difference spectrum (red-ox) is shown in the inset.

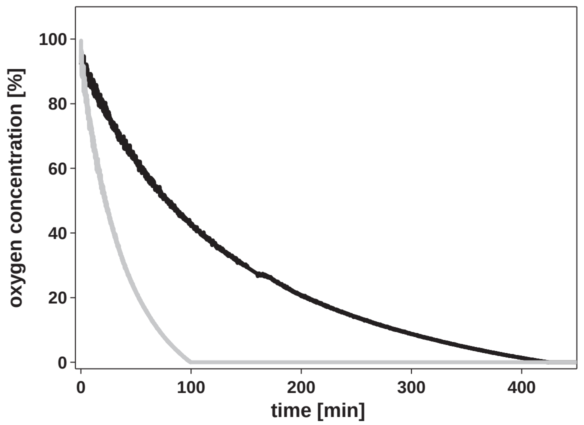

Figure 5 Measurement of the oxygen consumption rate of *r*CDH (grey line) and N700S (black line). Reactions were performed in a sealed microreactor containing 30 mM cellobiose in 100 mM McIlvaine buffer, pH 6.0. The decrease of the O_2 concentration was followed by an inert, luminescent sensor. An excess activity of catalase was added to disproportionate H_2O_2.

the obtained variant can be employed in 4–5 times lower amounts than the wild-type CDH to obtain the same amount of H_2O_2.

Conclusions

S. cerevisiae along with *E. coli* are the most successfully used host organisms for laboratory evolution and semi-rational protein engineering. The ease of genetic manipulation and its high transformation efficiencies due to the ability to maintain autonomously replicating plasmids facilitate the construction of mutant libraries. The successful expression of CDH under the control of the GAL1 promoter in *S. cerevisiae* offers a possibility to easily produce and screen for genetically engineered CDH variants and maybe also other mutated fungal oxidoreductases, which are needed for various biotechnological applications. The developed HTS assay can be easily adapted for other oxidase (H_2O_2 forming) activities. For production of selected variants *P. pastoris* is, however, the more efficient expression host.

The fact that most mutations at the selected positions resulted in inactive or less active CDH variants demonstrates that changes in the vicinity of the flavin have a tremendous impact on enzymatic activity. Out of the five selected amino acids only one mutation resulted in an increased H_2O_2 production. Further research towards an higher oxygen reactivity of CDH is definitely required for even more efficient cotton bleaching, laundry detergents or antimicrobial functionalization of medical devices.

Table 2 Apparent kinetic constants of *r*CDH and variant N700S

		Cellobiose		
Electron acceptor	Enzyme	K_m (μM)	k_{cat} (s^{-1})	k_{cat}/K_m (M^{-1} s^{-1})
DCIP	*r*CDH	11.4 ± 0.7	4.1 ± 0.1	360000
	N700S	33 ± 1	12.4 ± 0.6	375000
1,4-benzoquinone	*r*CDH	22 ± 1	4.3 ± 0.1	185000
	N700S	56 ± 2	13.4 ± 0.5	240000
oxygen	*r*CDH	37 ± 3	0.042 ± 0.003	1100
	N700S	73 ± 6	0.19 ± 0.01	2600

Kinetic constants for cellobiose were determined with DCIP, 1,4-benzoquinone and oxygen as electron acceptors at pH 6.0 and 30°C.

Methods

Chemicals and vectors

Chemicals were purchased from Sigma, Fluka, Roth or VWR and were of the highest purity available. Primers (the nucleotide sequences are shown in Table 3) were obtained from VBC Biotech (Vienna, Austria). Restriction enzymes and T4-ligase were purchased from Fermentas, Phusion polymerase from New England Biolabs and the yeast expression vector pPICZαA from Invitrogen. The uracil independent and ampicillin resistance shuttle vector pJRoC30 was obtained from the Department of Biocatalysis (CSIC, Spain). Recombinant CDH (*r*CDH) was produced as published [10].

Strains and media

The protease deficient *S. cerevisiae* strain BJ5465 was from LGC Promochem (Barcelona, Spain). SC drop-out plates (synthetic complete) contained 6.7 g L^{-1} yeast nitrogen base (YNB) without amino acids, 1.92 g L^{-1} yeast synthetic drop-out medium supplement without uracil, 2% (w/v) glucose, 25 mg L^{-1} chloramphenicol and 20 g L^{-1} agar. For the preparation of liquid minimal medium the agar was omitted and glucose was replaced by raffinose. The SG/R-CAA expression medium [37] contained 5 g L^{-1} casein hydrolysate, 9.67 g L^{-1} NaH_2PO_4, 6.77 g L^{-1} Na_2HPO_4, 2% (w/v) raffinose, 2% (w/v) galactose, 0.5% (w/v) glucose and 3.35% YNB. *P. pastoris* X-33 is a component of the EasySelect *Pichia* Expression Kit from Invitrogen. *P. pastoris* transformants were grown on YPD plates (10 g L^{-1} yeast extract, 20 g L^{-1} peptone, 10 g L^{-1} glucose and 100 mg L^{-1} zeocin) and the Basal Salts Medium (Invitrogen) was used for fermentation. The chemically competent *E. coli* strain NEB 5-alpha was purchased from New England Biolabs and used for maintenance and propagation of plasmids. *E. coli* cells were cultivated in Low Salt LB-medium (10 g L^{-1} peptone from casein, 5 g L^{-1} yeast extract, 5 g L^{-1} NaCl and 25 mg L^{-1} zeocin).

CDH expression in *S. cerevisiae*

The published plasmid pMt1 [10] was used as template for the amplification of *M. thermophilum* CDH cDNA with

Table 3 Nucleotide sequences of primers where N is A/T/G/C and S is C/G

Primer name	Sequence (from 5′ to 3′)
5MT-*Bam*HI	TATGGATCCATGAGAACTTCTTCTAGACTTATCG
5MT-*Xho*HI	TATCTCGAGCAGAATAACGTTCCAAACACC
3MT-*Xho*HI	TATCTCGAGTTACAAACATTGAGAGTACC
5MT-G323X	AGTCAATGCTNNSCTTTGGTTCAAGCC
3MT-G323X	TTGAACCAAAGSNNAGCATTGACTGCG
5MT-A322X	TACCGCAGTCAATNNSGGTCTTTGGTTCAAGC
3MT-A322X	AACCAAAGACCAGCSNNGACTGCGGTACCTCC
5MT-L324X	AGTCAATGCTGGTNNSTGGTTCAAGCCATATTCTTTGG
3MT-L324X	ACCAGCATTGACTGCGGTACCSNNACCAGCAT
5MT-N700X	TCCTTCTAACAGACGTTCTNNSCACTGGATGGGTACTAAC
3MT-N700X	CCAGTGSNNAGAACGTCTGTTAG
5MT-H701X	AGACGTTCTAACNNSTGGATGGGTAC
3MT-H701X	GTACCCATCCASNNGTTAGAACGTCT
5MT-N700S	CAGACGTTCTTCTCACTGGATGGGTAC
3MT-N700S	AGAACGTCTGTTAGAAGGAGAC

two different forward primers (5MT-*Bam*HI and 5MT-*Xho*Ifw) and the reverse primer 3MT-*Xho*I. The resulting nucleotide sequences encoded CDH with and without its native secretory leader sequence. The PCR amplicons were digested with the respective restriction enzymes and ligated into the equally treated shuttle vector pJRoC30 under the control of the GAL1 promotor. The resulting plasmid pJRoC30-*Mt*CDH-nat encoded for the native secretory leader whereas in plasmid pJROC30-*Mt*CDH-α it was replaced by the α-factor prepro leader peptide of *S. cerevisiae*. Both plasmids were transformed into competent *S. cerevisiae* cells using the yeast transformation kit (Sigma). Transformed cells were plated on SC drop-out plates and incubated for 4 days at 30°C. From each transformation 96 colonies were picked and cultured in a 96-well deep-well plate (Ritter) containing 100 μL of minimal media per well. These master plates were sealed with Breathe -Easy film (Diversified Biotech) to prevent evaporation and incubated in a shaking incubator (480 rpm) at 25°C and a relative humidity of 80%. After 48 h, 500 μL of expression medium SG/R-CAA were added to each well and the plates were incubated for additional 120 h. The cultivation was stopped by centrifugation for 5 min at 3000 × g. From each well 50 μL of clear culture supernatant were transferred from the master plate to 96-well plate assays using a pipetting robot (Janus, Perkin Elmer). The volumetric activity was measured with the DCIP-based assay.

Preparation of libraries and HT-screening

A comparative (homology) model of *M. thermophilum* CDH based on the template of *P. chrysosporium* CDH (1KDG, [7]) was used to select positions for mutagenesis. The model was calculated by the Swiss-Model protein structure homology modeling server [38] accessible via the ExPASy web server and checked by using the ANOLEA mean force potential [39], the GROMOS empirical force field energy [40], the composite scoring function QMEAN [41] and a stereochemistry check [42]. Five amino acids located in close vicinity of the FAD cofactor (A322, G323, L324, N700 and H701) were selected for site-saturation mutagenesis. The plasmid pJRoC30-*Mt*CDH-nat was used as template for the site-saturation PCRs, which allowed the construction of *cdh* libraries containing all possible codons at the targeted position. Randomized NNS codons were used to reduce the bias of the genetic code. Mutants were prepared by the sequence overlap extension method [43]. Two complementary mutagenic oligonucleotide primers were designed for each of the 5 target positions (Table 3). The primers were used together with the flanking primers RMLC-sense and RMLN-antisense [44] to amplify two DNA fragments with overlapping ends. In a subsequent fusion PCR these fragments were assembled. PCR products of the mutated *cdh* gene and flanking regions homologous to the vector were purified by electrophoresis, mixed with the *Xho*I and *Bam*HI linearized vector pJRoC30 (ratio PCR product:vector = 4:1) and transformed into competent cells using the yeast transformation kit. For each of the five target positions a library of 352 clones was screened. Individual clones were picked and cultured under the above-mentioned conditions. Four wells per plate were inoculated with *S. cerevisiae* transformed with pJRoC30-*Mt*CDH-nat as a positive control, 2 wells were inoculated with *S. cerevisiae* transformed with empty pJRoC30 as a negative control and 2 wells were not inoculated at all. After 168 h of incubation the culture supernatants were subjected to the DCIP-based screening assay. Therefore, 50 μL of each well were transferred from the master plate to two replica plates. 150 μL of the respective assay mixture (DCIP-based assay and ABTS-based assay) were added by the liquid-handling-robot. Variants with increased H_2O_2 production were selected for rescreening. Each of the selected variants was used to inoculate four wells of a new cultivation plate, which was incubated and screened as described above. Exchanges in the nucleotide sequence of approved hits were checked by sequencing. Therefore, colony PCRs were performed using the primers RMLC-sense and RMLN-antisense and the amplified fragments were sent for sequencing.

HTS assays for enzymatic activity and H_2O_2 production

CDH activity was measured by following the time-dependent reduction of 300 μM 2,6-dichloroindophenol (DCIP) at a wavelength of 520 nm ($\varepsilon_{520} = 6.8$ mM^{-1} cm^{-1}) in 100 mM McIlvaine buffer, pH 5.5, containing 30 mM cellobiose. The reaction was started by adding 150 μL of the DCIP-based assay solution to 50 μL sample in the well and followed in a temperature controlled plate reader at 30°C for 5 min.

H_2O_2 production was measured by a modified 2,2′-azino-bis(3ethylbenzthiazoline-6-sulfonate) (ABTS)-based assay. Originally, this assay quantifies the production of H_2O_2 by oxidases through the oxidation of ABTS in the presence of horseradish peroxidase. The formation of the green ABTS cation radical is followed spectrophotometrically at 420 nm ($\varepsilon_{420} = 36$ mM^{-1} cm^{-1}). However, because CDH can reduce the oxidized ABTS cation radical (like other electron acceptors), which would interfere with the assay, a modification was applied. First, 50 μL of a reaction mixture containing 60 mM cellobiose in 100 mM McIlvaine (citrate-phosphate) buffer, pH 5.5, was added to 50 μL of the sample for the production of H_2O_2. The reaction mixture was incubated at 30°C for 4 h before CDH was inactivated at 90°C for 10 min. This procedure does not influence the H_2O_2 concentration. The colorimetric reaction was started by the addition of 100 μL of ABTS reagent containing 2 mM ABTS and 5.7 U mL^{-1} peroxidase in 100 mM McIlvaine buffer, pH 5.5. The increase in absorbance was followed by a temperature controlled plate reader at 30°C for 5 min. The stoichiometry for this reaction is two since for one mol of H_2O_2 two mol of the green ABTS cation radical are formed. The enzymatic activity is given in units (U), which corresponds to the production of 1 μmol cellobionic acid or 1 μmol H_2O_2 per min.

Heterologous production of variant N700S in *P. pastoris*

The plasmid pPIC*Mt*CDH was used as template for the generation of mutant N700S by a two-step mutagenesis approach using PCR and *Dpn*I [45]. The sequences of the used primers 5*Mt*-N700S and 3*Mt*-N700S are given in Table 3. The mutation was confirmed by sequencing (LGC Genomics, Berlin, Germany). The *Sac*I linearized expression plasmid was transformed into electrocompetent X-33 cells and transformants were selected on YPD zeocin plates (1 mg L^{-1}). The integration of the gene was verified by colony PCR. A positive transformant was selected for production in a 7-L fermenter according to Harreither et al. [27].

Protein purification

The CDH variant N700S was purified by a hydrophobic interaction chromatography (HIC) and anion exchange chromatography (AIEX) according to a published procedure [10]. The purification was monitored by determination of total protein and activity. The purity of the enzyme preparation was verified by SDS-PAGE. The homogeneous CDH solution was sterile filtered, aliquoted and stored at −80°C for characterization.

Molecular properties

SDS-PAGE was carried out using Mini-PROTEAN TGX precast gradient gels (4 – 15%) and Bio-Safe Coomassie for staining (Bio-Rad Laboratories). Unstained Precision Plus Protein Standard was used for mass determination. All procedures were done according to the manufacturer's recommendations (Bio-Rad Laboratories). The spectra of homogeneously purified N700S were recorded at room temperature from 250 to 600 nm in both the oxidized and reduced state using a U-3000 Hitachi spectrometer (Tokyo, Japan). Spectra were recorded before and shortly after the addition of lactose to the cuvette. The oxidized spectrum was used for determining the purity represented by the ratio of A_{420}/A_{280}.

Oxygen consumption rates

A luminescence-based fiber optic sensor (PreSens GmbH, Regensburg, Germany) was used to measure O_2 consumption rates. Oxygen-saturated 100 mM McIlvaine buffer (oxygen concentration ~1200 μM), pH 6.0, containing 30 mM cellobiose was magnetically stirred in a gas-tight, temperature controlled (30°C) glass vial sealed by a septum (total volume 1870 μL). The reaction was started by adding 100 μL of enzyme solution (3.6 mg mL^{-1}) through a cannula.

Kinetic measurements

CDH activity was assayed using 2,6-dichloroindophenol (DCIP, $\varepsilon_{520} = 6.8$ mM^{-1} cm^{-1}) or 1,4-benzoquinone ($\varepsilon_{290} =$ 2.224 mM^{-1} cm^{-1}) as electron acceptors. The reactions were followed for 180 sec at 30°C in a Lambda 35 UV/Vis spectrophotometer. To assay CDH activity with oxygen as electron acceptor the modified ABTS assay described above was used. The reaction mixture for the production of H_2O_2 contained varying cellobiose concentrations (0.003 – 10 mM) dissolved in 100 mM McIlvaine buffer, pH 6.0, and 0.025 mg mL^{-1} *r*CDH or 0.01 mg mL^{-1} of N700S. The reaction mixtures were incubated at 30°C and heat inactivated for 5 minutes at 90°C. The color reaction was started by the addition of 100 μL ABTS reagent. Catalytic constants were calculated using nonlinear least-squares regression by fitting the observed data to the Michaelis-Menten equation (Sigma Plot 11, Systat Software, Chicago, IL, USA). The protein concentration in fermentation and electrophoresis samples as well as of purified enzyme preparations was determined by Bradford's method using bovine serum albumin as standard and a prefabricated assay from Bio-Rad Laboratories (Hercules, CA).

Additional file

Additional file 1: Local alignment (Clustal X) of *M. thermophilum* and *P. chrysosporium* flavodehydrogenase domains. Selected positions for mutagenesis are indicated with arrows.

Competing interests

The authors declare that they have no competing interests.

Authors' contributions

CS and RL planned the study and developed the scheme for high-throughput screening and enzyme characterization. MA selected the expression vector, strains and optimized yeast cultivations. PS and IK carried out the construction and screening of the site-saturation libraries, conducted the *P. pastoris* fermentation and purification of N700S. GG and GN measured the oxygen consumption and interpreted the data. CS wrote the first draft of the manuscript. MA and GG revised the manuscript. RL and CP coordinated the study, verified and interpreted results and revised the final manuscript. All authors have read and approved the final manuscript.

Acknowledgements

The authors thank the European Commission (FP7 243529-2-COTTONBLEACH) for financial support. CKP thanks the Austrian Science Fund (FWF) for financial support (grant P22094). IK is a member of the doctoral program BioToP (Biomolecular Technology of Proteins) of the Austrian Science Fund (FWF; W1224). MA thanks the Spanish Government for financial support (BIO2010-19697).

Author details

[1]Vienna Institute of Biotechnology, Department of Food Sciences and Technology, BOKU-University of Natural Resources and Life Sciences, Vienna, Austria. [2]Department of Biocatalysis, Institute of Catalysis, CSIC, 28049 Madrid, Spain. [3]Institute of Environmental Biotechnology, University of Natural Resources and Life Sciences, Vienna, Austria.

Received: 18 February 2013 Accepted: 14 April 2013
Published: 23 April 2013

References

1. Harreither W, Sygmund C, Augustin M, Narciso M, Rabinovich ML, Gorton L, Haltrich D, Ludwig R: **Catalytic properties and classification of cellobiose dehydrogenases from ascomycetes.** *Appl Environ Microbiol* 2011, **77:**1804–1815.
2. Beeson WT, Phillips CM, Cate JHD, Marletta MA: **Oxidative cleavage of cellulose by fungal copper-dependent polysaccharide monooxygenases.** *J Am Chem Soc* 2012, **134:**890–892.
3. Langston JA, Shaghasi T, Abbate E, Xu F, Vlasenko E, Sweeney MD: **Oxidoreductive cellulose depolymerization by the enzymes cellobiose dehydrogenase and glycoside hydrolase 61.** *Appl Environ Microbiol* 2011, **77:**7007–7015.
4. Phillips CM, Beeson WT, Cate JH, Marletta MA: **Cellobiose dehydrogenase and a copper-dependent polysaccharide monooxygenase potentiate cellulose degradation by *Neurospora crassa*.** *ACS Chem Biol* 2011, **6:**1399–1406.
5. Sygmund C, Kracher D, Scheibelbrandner S, Zahma K, Felice AK, Kittl R, Harreither W, Ludwig R: **Charecterization of the two *Neurospora crassa* cellobiose dehydrogenases and their connection to oxidative cellulose degradation.** *Appl Environ Microbiol* 2012, **78:**6161–6171.
6. Hallberg BM, Bergfors T, Baeckbro K, Pettersson G, Henriksson G, Divne C: **A new scaffold for binding haem in the cytochrome domain of the extracellular flavocytochrome cellobiose dehydrogenase.** *Structure* 2000, **8:**79–88.
7. Hallberg MB, Henriksson G, Pettersson G, Divne C: **Crystal structure of the flavoprotein domain of the extracellular flavocytochrome cellobiose dehydrogenase.** *J Mol Biol* 2002, **315:**421–434.
8. Ludwig R, Ortiz R, Schulz C, Harreither W, Sygmund C, Gorton L: **Cellobiose dehydrogenase modified electrodes: advances by materials science and biochemical engineering.** *Anal Bioanal Chem* 2013, **405:**3637–3658.
9. Zámocký M, Ludwig R, Peterbauer C, Hallberg BM, Divne C, Nicholls P, Haltrich D: **Cellobiose dehydrogenase - A flavocytochrome from wood-degrading, phytopathogenic and saprotropic fungi.** *Curr Protein Pept Sci* 2006, **7:**255–280.
10. Flitsch A, Prasetyo EN, Sygmund C, Ludwig R, Nyanhongo GS, Guebitz GM: **Cellulose oxidation and bleaching processes based on recombinant *Myriococcum thermophilum* cellobiose dehydrogenase.** *Enzyme Microb Technol* 2013, **52:**60–67.
11. Ludwig R, Harreither W, Tasca F, Gorton L: **Cellobiose dehydrogenase: a versatile catalyst for electrochemical applications.** *Chemphyschem* 2010, **11:**2674–2697.
12. Ludwig R, Ozga M, Zámocky M, Peterbauer C, Kulbe KD, Haltrich D: **Continuous enzymatic regeneration of electron acceptors used by flavoenzymes: Cellobiose dehydrogenase-catalyzed production of labtobionic acid as an example.** *Biocatal Biotransformation* 2004, **22:**97–104.
13. Van Hecke W, Ludwig R, Dewulf J, Auly M, Messiaen T, Haltrich D, Van Langenhove H: **Bubble-free oxygenation of a bi-enzymatic system: effect on biocatalyst stability.** *Biotechnol Bioeng* 2009, **102:**122–131.
14. Van Hecke W, Ludwig R, Dewulf J, Haltrich D, Van Langenhove H: **Green oxidation of renewable carbohydrates: lactobionic acid production as an example.** *Commun Agric Appl Biol Sci* 2008, **73:**9–13.
15. Ciullini I, Tilli S, Scozzafava A, Briganti F: **Fungal laccase, cellobiose dehydrogenase, and chemical mediators: combined actions for the decolorization of different classes of textile dyes.** *Bioresour Technol* 2008, **99:**7003–7010.
16. Cameron MD, Aust SD: **Cellobiose dehydrogenase - An extracellular fungal flavocytochrome.** *Enzyme Microb Technol* 2001, **28:**129–138.
17. Pricelius S, Ludwig R, Lant N, Haltrich D, Guebitz GM: **Substrate specificity of *Myriococcum thermophilum* cellobiose dehydrogenase on mono-, oligo-, and polysaccharides related to *in situ* production of H_2O_2.** *Appl Microbiol Biotechnol* 2009, **85:**75–83.
18. Pricelius S, Ludwig R, Lant NJ, Haltrich D, Guebitz GM: ***In situ* generation of hydrogen peroxide by carbohydrate oxidase and cellobiose dehydrogenase for bleaching purposes.** *Biotechnol J* 2010, **6:**224–230.
19. Ribitsch D, Karl W, Wehrschütz-Sigl E, Tutz S, Remler P, Weber HJ, Gruber K, Stehr R, Bessler C, Hoven N, *et al*: **Heterologous expression and characterization of choline oxidase from the soil bacterium *Arthrobacter nicotianae*.** *Appl Microbiol Biotechnol* 2009, **81:**875–886.
20. Tzanov T, Costa SA, Gübitz GM, Cavaco-Paulo A: **Hydrogen peroxide generation with immobilized glucose oxidase for textile bleaching.** *J Biotechnol* 2002, **93:**87–94.
21. Nyanhongo GS, Sygmund C, Ludwig R, Prasetyo EN, Guebitz GM: **An antioxidant regenerating system for continuous quenching of free radicals in chronic wounds.** *Eur J Pharm Biopharm* 2013.
22. Nyanhongo GS, Sygmund C, Ludwig R, Prasetyo EN, Guebitz GM: **Synthesis of multifunctional bioresponsive polymers for the management of chronic wounds.** *J Biomed Mater Res B Appl Biomater* 2013, **83:**396–404.
23. Chaiyen P, Fraaije MW, Mattevi A: **The enigmatic reaction of flavins with oxygen.** *Trends Biochem Sci* 2012, **37:**373–380.
24. Mattevi A: **To be or not to be an oxidase: challenging the oxygen reactivity of flavoenzymes.** *Trends Biochem Sci* 2006, **31:**276–283.
25. McDonald CA, Fagan RL, Collard F, Monnier VM, Palfey BA: **Oxygen reactivity in flavoenzymes: context matters.** *J Am Chem Soc* 2011, **133:**16809–16811.
26. Bey M, Berrin JG, Poidevin L, Sigoillot JC: **Heterologous expression of *Pycnoporus cinnabarinus* cellobiose dehydrogenase in *Pichia pastoris* and involvement in saccharification processes.** *Microb Cell Fact* 2011, **10:**113.
27. Harreither W, Felice AKG, Paukner R, Gorton L, Ludwig R, Sygmund C: **Recombinantly produced cellobiose dehydrogenase from *Corynascus thermophilus* for glucose biosensors and biofuel cells.** *Biotechnol J* 2012, **7:**1359–1366.
28. Zhang R, Fan Z, Kasuga T: **Expression of cellobiose dehydrogenase from *Neurospora crassa* in *Pichia pastoris* and its purification and characterization.** *Protein Expr Purif* 2011, **75:**63–69.
29. Desriani, Ferri S, Sode K: **Functional expression of *Phanerochaete chrysosporium* cellobiose dehydrogenase flavin domain in *Escherichia coli*.** *Biotechnol Lett* 2010, **32:**855–859.
30. Alcalde M: **Mutagenesis protocols in *Saccharomyces cerevisiae* by in vivo overlap extension.** *Methods Mol Biol* 2010, **634:**3–14.
31. Gonzalez-Perez D, Garcia-Ruiz E, Alcalde M: ***Saccharomyces cerevisiae* in directed evolution: an efficient tool to improve enzymes.** *Bioeng Bugs* 2012, **3:**172–177.
32. Brake AJ: **α-Factor leader-directed secretion of heterologous proteins from yeast.** In *Methods Enzymol. Volume 185.* Edited by David VG. Waltham: Academic Press; 1990:408–421.
33. Camarero S, Pardo I, Cañas AI, Molina P, Record E, Martínez AT, Martínez MJ, Alcalde M: **Engineering platforms for directed evolution of laccase from *Pycnoporus cinnabarinus*.** *Appl Environ Microbiol* 2012, **78:**1370–1384.
34. Garcia-Ruiz E, Gonzalez-Perez D, Ruiz-Duenas FJ, Martinez AT, Alcalde M: **Directed evolution of a temperature-, peroxide- and alkaline pH-tolerant versatile peroxidase.** *Biochem J* 2012, **441:**487–498.
35. Mate D, Garcia-Burgos C, Garcia-Ruiz E, Ballesteros AO, Camarero S, Alcalde M: **Laboratory evolution of high-redox potential laccases.** *Chem Biol* 2010, **17:**1030–1041.
36. Arnold F, Georgiou G: *Directed Enzyme Evolution: screening and selection methods*, Methods in Molecular Biology. Totowa, New Jersey: Humana Press; 2003:231.

37. Bowley DR, Labrijn AF, Zwick MB, Burton DR: **Antigen selection from an HIV-1 immune antibody library displayed on yeast yields many novel antibodies compared to selection from the same library displayed on phage.** *Protein Eng Des Sel* 2007, **20:**81–90.
38. Arnold K, Bordoli L, Kopp J, Schwede T: **The SWISS-MODEL workspace: a web-based environment for protein structure homology modelling.** *Bioinformatics* 2006, **22:**195–201.
39. Melo F, Feytmans E: **Assessing protein structures with a non-local atomic interaction energy.** *J Mol Biol* 1998, **277:**1141–1152.
40. Christen M, Hünenberger PH, Bakowies D, Baron R, Bürgi R, Geerke DP, Heinz TN, Kastenholz MA, Kräutler V, Oostenbrink C, *et al*: **The GROMOS software for biomolecular simulation: GROMOS05.** *J Comput Chem* 2005, **26:**1719–1751.
41. Benkert P, Tosatto SCE, Schomburg D: **QMEAN: a comprehensive scoring function for model quality assessment.** *Proteins* 2008, **71:**261–277.
42. Laskowski RA, MacArthur MW, Moss DS, Thornton JM: **PROCHECK: a program to check the stereochemical quality of protein structures.** *J Appl Crystallogr* 1993, **26:**283–291.
43. Ho SN, Hunt HD, Horton RM, Pullen JK, Pease LR: **Site-directed mutagenesis by overlap extension using the polymerase chain reaction.** *Gene* 1989, **77:**51–59.
44. Garcia-Ruiz E, Mate D, Ballesteros A, Martinez AT, Alcalde M: **Evolving thermostability in mutant libraries of ligninolytic oxidoreductases expressed in yeast.** *Microb Cell Fact* 2010, **9:**17.
45. Li S, Wilkinson MF: **Site-directed mutagene sis: a two-step method using PCR and *Dpn*I.** *Biotechniques* 1997, **23:**588–590.

doi:10.1186/1475-2859-12-38
Cite this article as: Sygmund *et al.*: Semi-rational engineering of cellobiose dehydrogenase for improved hydrogen peroxide production. *Microbial Cell Factories* 2013 **12**:38.

Submit your next manuscript to BioMed Central and take full advantage of:

- **Convenient online submission**
- **Thorough peer review**
- **No space constraints or color figure charges**
- **Immediate publication on acceptance**
- **Inclusion in PubMed, CAS, Scopus and Google Scholar**
- **Research which is freely available for redistribution**

Submit your manuscript at
www.biomedcentral.com/submit

BioMed Central

Paper VII

Biotechnology Journal
www.biotechnology-journal.com

Biotechnol. J. 2014, 9

DOI 10.1002/biot.201300336

Research Article

Convenient microtiter plate-based, oxygen-independent activity assays for flavin-dependent oxidoreductases based on different redox dyes

Dagmar Brugger[1], Iris Krondorfer[1], Kawah Zahma[1], Thomas Stoisser[2], Juan M. Bolivar[2], Bernd Nidetzky[2], Clemens K. Peterbauer[1] and Dietmar Haltrich[1]

[1] Food Biotechnology Laboratory, BOKU University of Natural Resources and Life Sciences, Vienna, Austria
[2] Institute of Biotechnology and Biochemical Engineering, Graz University of Technology, Graz, Austria

Received 31 JUL 2013
Revised 01 NOV 2013
Accepted 17 DEC 2013
Accepted article online 19 DEC 2013

Flavin-dependent oxidoreductases are increasingly recognized as important biocatalysts for various industrial applications. In order to identify novel activities and to improve these enzymes in engineering approaches, suitable screening methods are necessary. We developed novel microtiter-plate-based assays for flavin-dependent oxidases and dehydrogenases using redox dyes as electron acceptors for these enzymes. 2,6-dichlorophenol-indophenol, methylene green, and thionine show absorption changes between their oxidized and reduced forms in the visible range, making it easy to judge visually changes in activity. A sample set of enzymes containing both flavoprotein oxidases and dehydrogenases – pyranose 2-oxidase, pyranose dehydrogenase, cellobiose dehydrogenase, D-amino acid oxidase, and L-lactate oxidase – was selected. Assays for these enzymes are based on a direct enzymatic reduction of the redox dyes and not on the coupled detection of a reaction product as in the frequently used assays based on hydrogen peroxide formation. The different flavoproteins show low Michaelis constants with these electron acceptor substrates, and therefore these dyes need to be added in only low concentrations to assure substrate saturation. In conclusion, these electron acceptors are useful in selective, reliable and cheap MTP-based screening assays for a range of flavin-dependent oxidoreductases, and offer a robust method for library screening, which could find applications in enzyme engineering programs.

Keywords: 2,6-dichlorophenol-indophenol · flavin-dependent oxidoreductases · high-throughput screening · methylene green · thionine

1 Introduction

Oxidation of various organic substrates by enzymes is an area in biocatalysis that has attracted considerable interest, since the chemical industry is in search of greener alternatives to those currently used industrial processes. A limited number of enzymes can be used for these biocatalytic oxidation reactions, including dehydrogenases, oxidases, peroxidases, and monooxygenases [1, 2]. Flavin-dependent oxidoreductases are of significant importance in this area, and several enzymes of this group are currently employed as biocatalysts [3]. This is partly because of the ability of flavin-dependent oxidoreductases to react directly with molecular oxygen thus avoiding other cofactors, cosubstrates or metal catalyst for oxidation reactions, but also for the enormous catalytic versatilities that have been shown by flavin oxidoreductases. An additional area of interest for flavoenzymes is electrochemistry, where suitable enzymes can be applied in biosensors or for biofuel cell applications. Here, dehydrogenases that lack oxygen reactivity are favorable since a

---

Correspondence: Prof. Dietmar Haltrich, Department für Lebensmittelwissenschaften und -technologie, Universität für Bodenkultur, Muthgasse 18, A-1190 Wien, Austria
E-mail: dietmar.haltrich@boku.ac.at

Abbreviations: CDH, cellobiose dehydrogenase; **DAAO**, D-amino acid oxidase; **DCPIP**, 2,6-dichlorophenol-indophenol; **FAD**, flavin adenine dinucleotide; **LOx**, L-lactate oxidase; **MG**, methylene green; **MTP**, microtiter plates; **Thi**, thionine; **PDH**, pyranose dehydrogenase; **POx**, pyranose 2-oxidase

© 2014 The Authors. Biotechnology Journal published by Wiley-VCH Verlag GmbH & Co. KGaA, Weinheim.
This is an open access article under the terms of the Creative Commons Attribution License, which permits use, distribution and reproduction in any medium, provided the original work is properly cited.

futile reaction of the electrode-bound enzymes with oxygen will result in hydrogen peroxide formation, which can impede stability of the biocatalyst. Recently, several new flavin-containing oxidoreductases have been introduced to this area in addition to commonly used glucose oxidases, yet there is wide interest in the identification of novel enzymes for these above-mentioned applications [4, 5]. For example, it has been proposed that, based on genome sequence data, many attractive and so far unknown flavoproteins can still be obtained from nature [3].

Flavin-dependent oxidoreductases show a reaction mechanism consisting typically of two half-reactions [6]. In the reductive half-reaction an electron donor substrate (e.g. a sugar or an amino acid) is oxidized, while the flavin is reduced (reactions 1 or 2).

$$E - FAD + S \rightarrow E - FADH_2 + P \quad (1)$$

$$E - FMN + S \rightarrow E - FMNH_2 + P \quad (2)$$

In the ensuing oxidative half-reaction the reduced flavin is re-oxidized by the second substrate oxygen, yielding the oxidized prosthetic group and H_2O_2 (shown for reduced $FADH_2$ in reaction 3), or by alternative electron acceptors such as quinones, redox dyes, or chelated metal ions [7]. The two-electron redox systems of the redox dyes DCPIP, thionine (Thi), and methylene green (MG) are shown in reactions 4–6, with the phenothiazines MG and Thi showing an oxidized cationic dye-form and a colorless reduced leuco-form [8, 9]

$$FADH_2 + O_2 \rightarrow FAD + H_2O_2 \quad (3)$$

$$DCPIP + 2e^- + 2H^+ \rightarrow DCPIH_2 \quad (4)$$

$$Thi^+ + 2e^- + H^+ \rightarrow ThiH \quad (5)$$

$$MG^+ + 2e^- + H^+ \rightarrow MGH \quad (6)$$

It was the aim of our work to test whether redox dyes that are frequently used in biosensor applications to transport electrons from the prosthetic group of an oxidoreductase can also be used as colorimetric substrates in microtiter plate (MTP)-based active assays for flavin-dependent oxidoreductases.

2 Materials and methods

2.1 Chemicals

All chemicals were of the highest purity commercially available. Lactose monohydrate, α-D-glucose monohydrate and dipotassium hydrogen phosphate anhydrous were purchased from Lactan (Graz, Austria). 2,6-dichlorophenol-indophenol (DCPIP), MG, Thi, sodium dithionite, D-methionine, L-(+)-lactic acid, and all other chemicals were obtained from Sigma-Aldrich (Vienna, Austria) unless otherwise stated.

2.2 Enzymes

Pyranose 2-oxidase (POx, EC 1.1.3.10) from *Trametes multicolor*, pyranose dehydrogenase (PDH, EC 1.1.99.29) from *Agaricus meleagris*, cellobiose dehydrogenase (CDH, EC 1.1.99.18) from *Neurospora crassa*, D-amino acid oxidase (DAAO, EC 1.4.3.3) from *Trigonopsis variabilis*, and L-lactate oxidase (LOx, EC 1.13.12.4) from *Aerococcus viridans* were prepared and purified to apparent homogeneity as described previously [7, 10–13].

2.3 Screening for electron acceptors

The following electron acceptors were tested for their reactivity with 0.1 U *Tm*POx and 100 mM D-glucose in 50 mM phosphate buffer pH 6.5: DCPIP (150 μM), methylene blue (15 μM), MG (25 μM), celestine blue (75 μM), Meldola's blue (50 μM), Thi (20 μM), toluidine blue (15 μM), reactive blue 2 (160 μM), direct red 81 (80 μM), acid orange 74 (150 μM), sudan orange (100 μM), malachite oxalate green (8 μM), $K_3[Cr(CN)_6]$ (12 mM), and $K_3[Fe(CN)_6]$ (1 mM). The different reactions were followed on a U-3000 spectrophotometer (Hitachi, Tokyo, Japan).

2.4 Spectral properties of redox dyes

Electron acceptor stock solutions were prepared as follows: DCPIP was dissolved in a small amount of ethanol over low heat and then adjusted to the desired concentration (3 mM) with reverse osmosis water; MG and Thi stock solutions (0.5 and 1 mM, respectively) were prepared in reverse osmosis water. Spectra of the selected redox dyes DCPIP (70 μM), MG (25 μM), and Thi (20 μM) were measured in 50 mM phosphate buffer (pH 6.5), and these dyes were reduced by adding sodium dithionite ($Na_2S_2O_4$). The changes in the absorption spectra were recorded with a U-3000 spectrophotometer (Hitachi) in the range from 400 to 800 nm. To investigate the pH dependence of the spectral properties of the electron acceptors DCPIP, MG, and Thi, absorbance spectra were recorded in the range of pH 3.0–9.0 in steps of 1.0 pH unit by using the following buffers: 50 mM citrate buffer (pH 3.0–5.0), 50 mM phosphate buffer (pH 5.0–8.0), and 50 mM Tris buffer (8.0–9.0). The concentration of the redox dyes was 70 μM for DCPIP, 25 μM for MG, and 20 μM for Thi.

2.5 Microtiter plate activity assays

MTP assays were performed in standard 96-well plates. Each well contained 100 μL of the assay mixture, which was composed of the electron acceptor (450 μM DCPIP, 75 μM MG, or 100 μM Thi), varying activities of purified

© 2014 The Authors. Biotechnology Journal published by Wiley-VCH Verlag GmbH & Co. KGaA, Weinheim

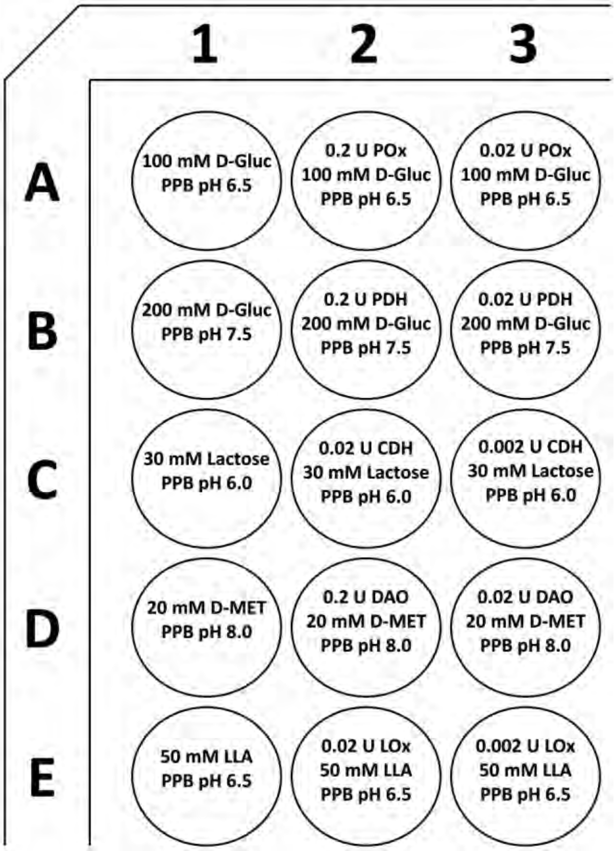

	1	2	3
A	100 mM D-Gluc PPB pH 6.5	0.2 U POx 100 mM D-Gluc PPB pH 6.5	0.02 U POx 100 mM D-Gluc PPB pH 6.5
B	200 mM D-Gluc PPB pH 7.5	0.2 U PDH 200 mM D-Gluc PPB pH 7.5	0.02 U PDH 200 mM D-Gluc PPB pH 7.5
C	30 mM Lactose PPB pH 6.0	0.02 U CDH 30 mM Lactose PPB pH 6.0	0.002 U CDH 30 mM Lactose PPB pH 6.0
D	20 mM D-MET PPB pH 8.0	0.2 U DAO 20 mM D-MET PPB pH 8.0	0.02 U DAO 20 mM D-MET PPB pH 8.0
E	50 mM LLA PPB pH 6.5	0.02 U LOx 50 mM LLA PPB pH 6.5	0.002 U LOx 50 mM LLA PPB pH 6.5

Figure 1. Compositions of the reaction mixtures used in the microtiter plate assays shown in Fig. 3, each well contained additionally 450 µM DCPIP, 75 µM MG, or 100 µM Thi as indicated. These dye concentrations were selected so that changes in the absorption can be detected by eye, which is not possible when higher concentrations are used. The first column represents the negative control (no enzyme added). Line A: POx, pyranose 2-oxidase from *Trametes multicolor*; B: PDH, pyranose dehydrogenase from *Agaricus meleagris*; C: CDH, cellobiose dehydrogenase from *Neurospora crassa*; D: DAAO, D-amino acid oxidase from *Trigonopsis variabilis*; E: LOx, L-lactate oxidase from *Aerococcus viridans*. PPB, phosphate buffer; D-Gluc, D-glucose; D-MET, D-methionine; LLA, L-lactic acid.

POx, PDH, CDH, DAAO, or LOx (0.2, 0.02, or 0.002 U), 50 mM phosphate buffer and the appropriate substrate (D-glucose for POx and PDH, lactose for CDH, D-methionine for DAAO, and L-lactic acid for LOx). The individual composition of the reaction mixtures for the respective wells is shown in Fig. 1, with the first column of the 96-well plate representing the negative control (no enzyme added). Electron acceptor reduction was followed at room temperature (22°C) at 520 nm for DCPIP, 655 nm for MG, and 600 nm for Thi using the Microplate reader Sunrise[a] (Tecan, Austria). The relative absorption change was calculated according to Eq. (7).

$$\text{electron acceptor absorption change (\%)} = \frac{A_t}{A_0} \times 100 \quad (7)$$

where A_0 is the initial electron acceptor absorption and A_t is the absorption measured at the time point t. The absorption change in percentage was plotted versus time.

In addition, realistic enzyme samples were employed in the MTP-based assays, using two different samples and expression systems. Crude, intracellular extracts of *Escherichia coli* were used as a source of POx, and culture supernatants of *Pichia pastoris* were the source of recombinant CDH. POx was recombinantly produced in *E. coli* as reported in ref. [14], while CDH was obtained from shaken flask cultures of *P. pastoris* basically as described by Sygmund [15], however, omitting the trace element solution from the medium. The following reaction mixtures were analyzed as negative controls: (i) cell lysates of *E. coli* BL21 Star DE3 harboring the pET21d$^+$ expression vector without the POx gene, D-glucose and dye; (ii) dye and substrate without enzyme; (iii) dye and enzyme without substrate. The MTP set-up was as described above, and the total volume per well was increased to maximally 200 µL, depending on the amount/activity of protein applied.

2.6 Steady-state kinetic measurements

Apparent steady-state kinetic constants for the two-electron, two-proton acceptor DCPIP and the 2-e$^-$, 1-H$^+$ acceptors MG and Thi were determined at room temperature (22°C) for POx, PDH, CDH, DAAO, and LOx. Initial rates of the DCPIP assay were recorded at 520 nm, where the pH dependence of the spectral properties of DCPIP is least pronounced. A molar extinction coefficient $\varepsilon_{520\ \text{nm}}$ of 6.8 mM^{-1} cm^{-1} was used for pH values below 6.5, whereas a value of 6.6 mM^{-1} cm^{-1} was used when the pH was above 6.5 [16]. The reaction in the MG assay was followed at 655 nm and the corresponding molar extinction coefficient ε_{655} was 46.6 mM^{-1} cm^{-1}. Initial rates of the reduction of Thi were recorded at 600 nm and a molar extinction coefficient ε_{600} of 55.4 mM^{-1} cm^{-1} was applied. Although Thi does not strictly obey Lambert–Beer's law [17], for the small concentration range that was employed in these experiments the absorption is linearly dependent on the Thi concentration. The molar extinction coefficients for MG and Thi were determined experimentally at pH 6.5 from the slope of the regression line of various electron acceptor concentrations versus their absorption intensity at 655 and 600 nm for MG and Thi, respectively (data not shown).

Kinetic constants were calculated by nonlinear least-square regression, fitting the data to the Henri-Michaelis-Menten or Hill equation (Sigma Plot 11, Systat Software). The path length of the quartz cuvettes used was varied between 3 and 10 mm depending on the electron acceptor concentration used so that the initial absorption value did not exceed a value of 2.0.

© 2014 The Authors. Biotechnology Journal published by Wiley-VCH Verlag GmbH & Co. KGaA, Weinheim

2.6.1 2,6-dichlorophenol-indophenol

Initial rates of reduction of DCPIP were followed at 520 nm. The reaction mixtures for the determination of the apparent steady-state kinetic constants contained varied concentrations of DCPIP (0.0075 to maximally 1.2 mM), substrate in saturating concentrations (100 mM D-glucose for POx, 200 mM D-glucose for PDH, 30 mM lactose for CDH, 200 mM D-methionine for DAAO, and 200 mM L-lactic acid for LOx), 50 mM phosphate buffer (pH 6.5 for POx and LOx, pH 7.5 for PDH, pH 6.0 for CDH, and pH 8.0 DAAO) and a suitable amount of the respective enzyme (POx, PDH, CDH, DAAO, and LOx).

2.6.2 Methylene green

Initial rates of the reduction of MG were recorded at 655 nm, and the assay mixtures contained varied MG concentrations (0.003–0.2 mM), while all other conditions were as for DCPIP.

2.6.3 Thionine

For the determination of initial rates of the reduction of Thi absorption changes were recorded at 600 nm. Thi concentrations were varied from 0.001 to maximally 0.3 mM. All other conditions were as with DCPIP.

3 Results

3.1 Screening for suitable electron acceptors

We performed an initial screening for suitable electron acceptors that show a visible color change in reasonable time, using the flavoenzyme POx since it was previously shown that this enzyme reduces a wide range of different quinones, redox dyes, and complexed metal ions [7]. The electron acceptors that were tested in this screening included DCPIP, methylene blue, MG, celestine blue, Meldola's blue, Thi, toluidine blue, reactive blue 2, direct red 81, acid orange 74, sudan orange, malachite oxalate green, $K_3[Cr(CN)_6]$, and $K_3[Fe(CN)_6]$. Quinones were not included because of the possibility of polymerization at higher pH values [18]. Some of these potential electron acceptors did not show any reaction in the POx-catalyzed reaction (e.g. reactive blue 2, direct red 81 or $K_3[Cr(CN)_6]$) while other showed very slow color changes under the initial screening conditions (e.g. malachite oxalate green). Based on this initial screening we selected DCPIP, MG, and Thi as the most promising electron acceptors (redox dyes) since they reacted directly with POx, and showed distinct color changes that are clearly visible even by eye within a short reaction period.

3.2 Spectral properties of the selected redox dyes

Absorption changes of DCPIP, MG, and Thi are shown in Fig. 2 for the reduction by $Na_2S_2O_4$ at pH 6.5. For DCPIP and Thi the maximal change in absorption between the oxidized and reduced states was recorded at 600 nm, and a color shift from blue and purple (oxidized state) to colorless (completely reduced state) could be observed for DCPIP and Thi, respectively. MG is turquoise-colored in the oxidized form and shows an absorption maximum at 655 nm, while the reduced form is again colorless. To investigate the dependence of the DCPIP, MG, and Thi spectra on the pH value, their absorption profiles were recorded in the range of pH 4.0–9.0. The absorbance of Thi and MG are pH-independent (data not shown), while the spectral properties of DCPIP show a strong pH dependency [16]. Since the lowest effect of the pH was observed at 520 nm, this wavelength was used for further experiments.

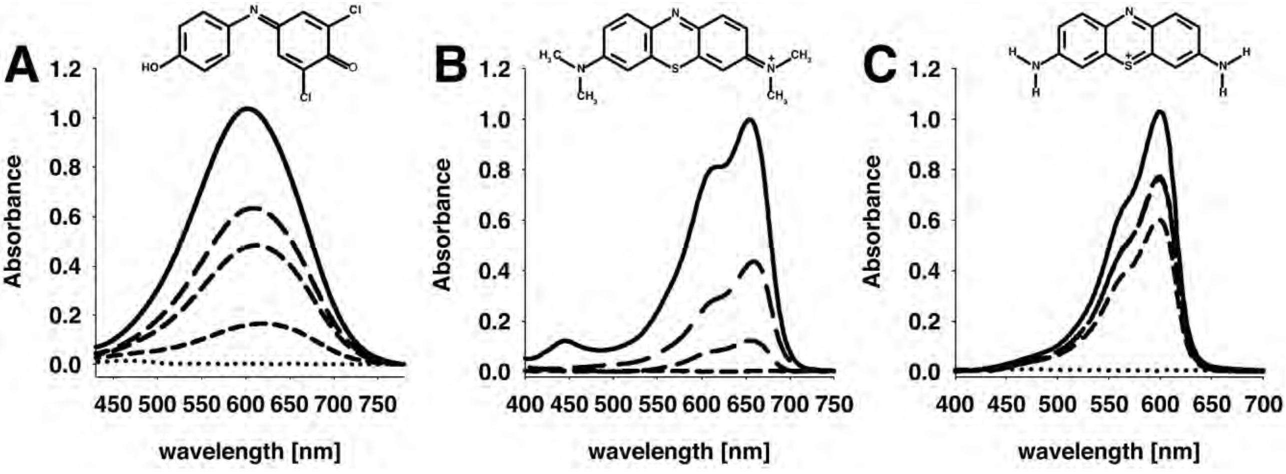

Figure 2. Absorption spectra of (**A**) 70 µM DCPIP, (**B**) 25 µM MG and (**C**) 20 µM thionine in 50 mM phosphate buffer (pH 6.5) of the oxidized state (solid line) and the (partly) reduced state (discontinuous lines). Sodium dithionite was added stepwise until complete reduction was attained. Spectra were obtained in 10-mm quartz cuvettes, and the concentration of the dyes was chosen so that the maximum absorption value was 1.

© 2014 The Authors. Biotechnology Journal published by Wiley-VCH Verlag GmbH & Co. KGaA, Weinheim

3.3 Microtiter plate assay

The reduction of DCPIP, MG, and Thi by the sample enzymes in the presence of a suitable electron-donor substrate is shown in Fig. 3 by characteristic color changes. Each well of the 96-well MTP contained the respective electron acceptor (DCPIP, MG, or Thi), varying activities of one of the flavoenzymes POx, PDH, CDH, DAAO, or LOx plus the appropriate electron donor substrate. The different assay conditions are shown in Fig. 1, in which the first column of the 96-well MTP represents the negative control (no enzyme added). All five tested flavin-dependent

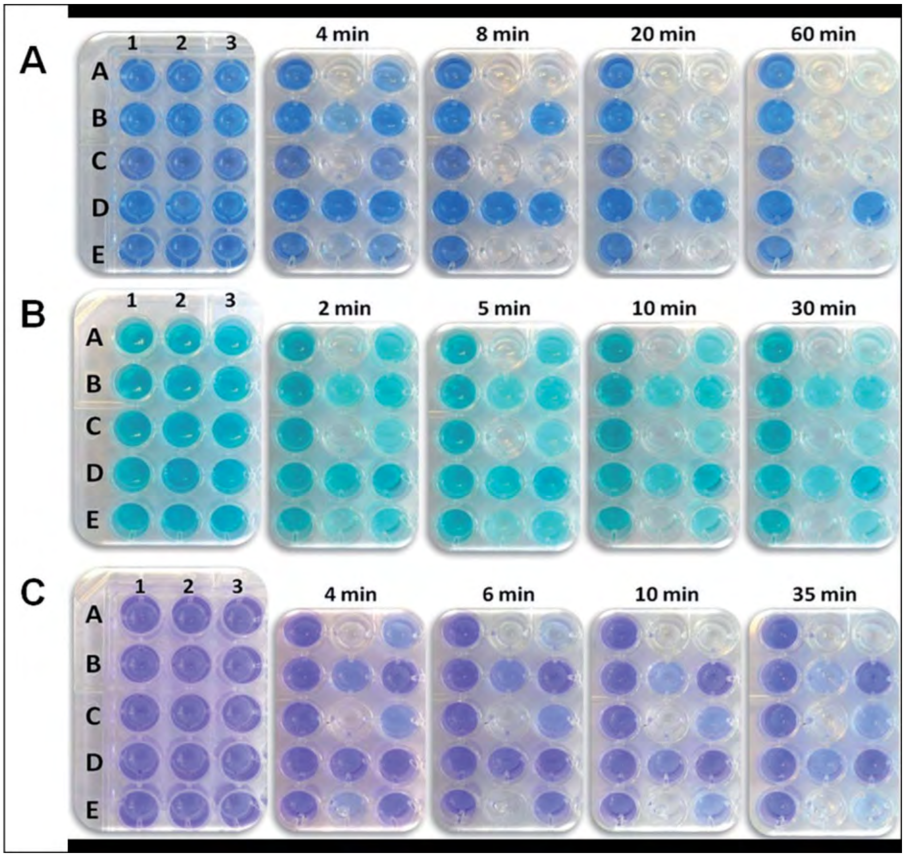

Figure 3. Microtiter-plate-based activity assays using (**A**) DCPIP, (**B**) MG, or (**C**) Thi as indicators for the activity of various flavoenzymes. The composition of the individual assay mixtures per well is as given in Fig 1. The plates to the far left show the beginning of the reaction at 0 min.

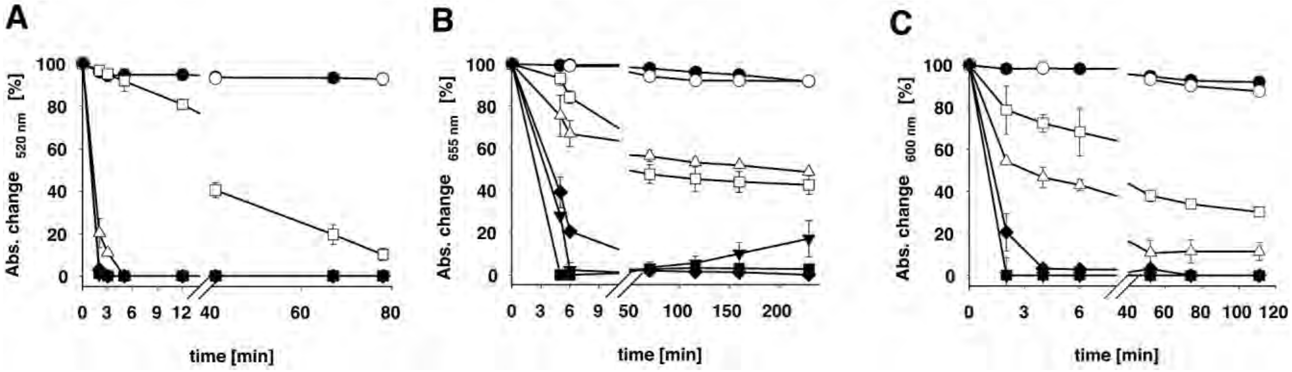

Figure 4. Time course of the absorption change of (**A**) DCPIP, (**B**) methylene green, or (**C**) thionine when reacting with different flavoenzymes and the appropriate enzyme substrate. The activity stated is the total activity added per well. Absorbance values were measured directly in 96-well plates by using a microplate reader. Data presented are the mean of duplicate independent measurements ± the standard deviation shown by the error bars. Symbols: ●, negative control I, no enzyme added; ○, negative control II, no substrate added; ▼, pyranose 2-oxidase from *Trametes multicolor* (0.2 U); △, pyranose dehydrogenase from *Agaricus meleagris* (0.2 U); ■, cellobiose dehydrogenase from *Neurospora crassa* (0.02 U); □, D-amino acid oxidase from *Trigonopsis variabilis* (0.2 U); ◆, L-lactate oxidase from *Aerococcus viridans* (0.02 U).

© 2014 The Authors. Biotechnology Journal published by Wiley-VCH Verlag GmbH & Co. KGaA, Weinheim

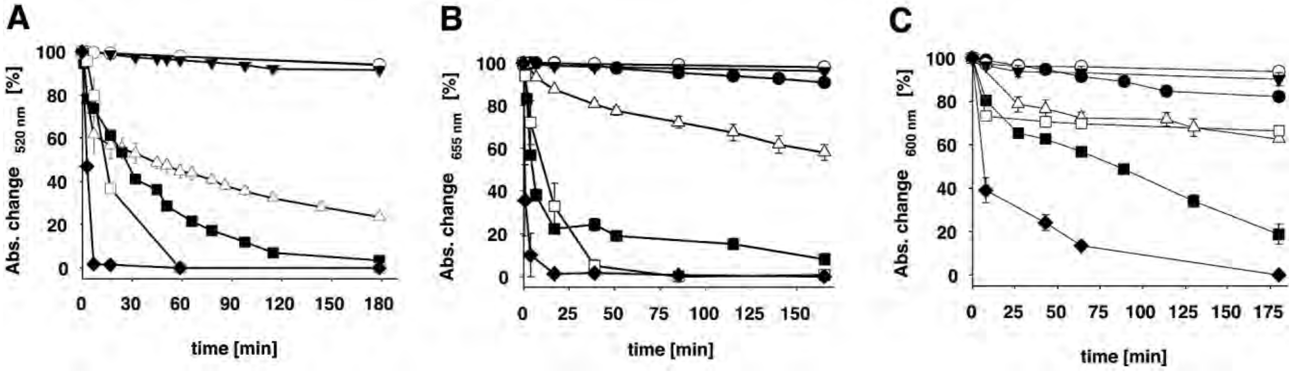

Figure 5. Time course of the absorption change of (**A**) DCPIP, (**B**) methylene green, or (**C**) thionine when reacting with cell lysates of *E. coli* expressing POx or clear supernatant of *P. pastoris* expressing CDH; D-glucose and lactose were used as the respective substrates. The activities stated are the total activity added per well. Data presented are the mean of duplicate independent measurements ± the standard deviation shown by the error bars.
Symbols: ●, negative control I, cell lysates of *E. coli* carrying the pET21d$^+$ expression vector without the POx gene; ○, negative control II, no enzyme added; ▼, negative control III, clear *P. pastoris* supernatant containing 0.01 U cellobiose dehydrogenase from *Neurospora crassa* without addition of the electron donor (sugar) substrate; △ and ■, cell lysates of *E. coli* expressing pyranose 2-oxidase from *Trametes multicolor* (0.002 and 0.01 U); □ and ◆, clear supernatant of *P. pastoris* containing cellobiose dehydrogenase from *Neurospora crassa* (0.002 and 0.01 U).

enzymes show discoloration of the redox dye within 1 h, even with the lowest activities tested. This color change and differences in intensities can be judged easily by eye. Some of these colorimetric changes could be observed rapidly within the first minutes of the reaction, even when using only low activities of 0.002 U per well, e.g. for CDH and LOx.

The absorbance changes over time, calculated according to Eq. (7), for the reduction of DCPIP, MG, and Thi are shown in Fig. 4. Again, the absorbance changes resulting from the reduction of the redox dyes by the tested flavoenzymes can be conveniently measured on a microtiter plate reader and give significant results for the activity ranges chosen within a reasonable time of less than 60 min. After approximately 1 h the slow re-oxidation of MG by air could be observed for the system POx/glucose, presumably because glucose was completely oxidized at this point. This slight re-oxidation of the reduced form by oxygen is also known from the blue bottle experiment using methylene blue, a compound that is structurally related to MG [19, 20]. This re-oxidation was not observed for the other two redox dyes used.

In addition, we used two different realistic enzyme samples as typically employed in enzyme engineering approaches, cell lysates of *E. coli* overexpressing POx from *T. multicolor* and culture supernatants of *P. pastoris* cultivations, in which CDH from *N. crassa* was extracellularly expressed (Fig. 5). Even low activities of only 2 and 10 mU per well gave absorbance changes over time that could be clearly distinguished from the reaction blanks. When using these low enzyme activities, DCPIP and MG gave unambiguous results with 3 h, while Thi proved to be less sensitive and only the higher of the two enzyme activities (10 mU per well) could be clearly identified within the reaction time of 3 h (Fig. 5).

3.4 Catalytic constants

The apparent steady-state kinetic constants were measured for the 2-e$^-$, 2-H$^+$ acceptor DCPIP (used in varying concentrations of 7.5 µM to maximal 1.2 mM while the second electron-donor substrate was held constant in saturating concentrations) and the 2-e$^-$, 1-H$^+$ acceptors MG (3.0–200 µM) and Thi (1.0–300 µM). Kinetic data are summarized in Table 1. The five investigated flavoproteins show very low apparent Michaelis constants mostly in the micromolar range for these redox dyes. The five flavoenzymes differ significantly in their catalytic constants k_{cat} and catalytic efficiencies k_{cat}/K_m for these electron acceptors, with the lowest efficiencies found for DAAO and PDH. This is also evident from Fig. 3 and 4, where the slowest change in color/decrease in absorbance is observed for these two enzymes.

4 Discussion

Rapid, convenient, and reliable colorimetric assays are a prerequisite for different approaches in enzyme development, ranging from screening of mutational libraries to the identification of novel enzymes from metagenomic libraries. Typically, large numbers of samples have to be evaluated by activity-based assays in these approaches, and microassays are preferred for this purpose because they facilitate rapid screening of numerous samples and substantially reduce reagent consumption. When screening for flavin-dependent oxidases the second reaction product, hydrogen peroxide, is frequently detected in a second, enzyme-coupled reaction. Here, chromogenic substrates such as 4-aminoantipyrine together with a suitable phenolic compound [21], *o*-dianisidine [22],

© 2014 The Authors. Biotechnology Journal published by Wiley-VCH Verlag GmbH & Co. KGaA, Weinheim

Table 1. Kinetic properties of *Tm*POx, *Am*PDH, *Nc*CDH, *Tv*DAAO, and *Av*LOx with DCPIP, methylene green and thionine as electron acceptors and D-glucose as saturating substrate for POx and PDH, lactose for CDH, D-methionine for DAAO and L-lactic acid for LOx[a)]

Enzyme	DCPIP			Methylene green			Thionine			Oxygen			Refs.
	K_M (mM)	k_{cat} (s^{-1})	k_{cat}/K_M $(mM^{-1}\ s^{-1})$	K_M (mM)	k_{cat} (s^{-1})	k_{cat}/K_M $(mM^{-1}\ s^{-1})$	K_M (mM)	k_{cat} (s^{-1})	k_{cat}/K_M $(mM^{-1}\ s^{-1})$	K_M (mM)	k_{cat} (s^{-1})	k_{cat}/K_M $(mM^{-1}\ s^{-1})$	
POx	1.88 ± 0.15	70 ± 4	38	0.12 ± 0.01	1.63 ± 0.10	13	0.20 ± 0.01	4.2 ± 0.1	24	0.090	71	790	[7]
PDH	0.66 ± 0.07	2.7 ± 0.13	4.1	0.14 ± 0.01	0.34 ± 0.08	2.5	0.12 ± 0.01	0.25 ± 0.01	2.1	nd	nd	nd	–
CDH	0.037 ± 0.001	3.7 ± 0.04	99	0.042 ± 0.003	15.1 ± 0.4	360	0.014 ± 0.001	7.2 ± 0.1	511	nd	nd	nd	–
DAAO	0.031 ± 0.002	0.033 ± 0.001	1.0	0.062 ± 0.006	0.190 ± 0.008	3.0	0.032 ± 0.005	0.161 ± 0.004	5.0	0.755 ± 0.076	229 ± 12	303	[35]
LOx	1.60 ± 0.15	189 ± 11	118	0.14 ± 0.01	3.0 ± 0.2	22	0.11 ± 0.003	1.30 ± 0.05	12	0.83 ± 0.03	140 ± 1	167	[13]

a) Published data for the kinetic constants with oxygen are given, for the flavoprotein dehydrogenases these data are not available. Data presented are the mean of triplicate independent measurements ± the standard deviation.

or 2,2′-azinobis(3-ethylbenzthiazoline)-6-sulfonic acid (ABTS) [23, 24] are used together with horseradish peroxidase or another suitable peroxidase. Obviously, these approaches cannot be used for flavin-dependent dehydrogenases since these only show negligible activity with oxygen. Various quinones are often used directly as an electron acceptor by a number of flavin-dependent oxidoreductases. A drawback for the use of quinones in screening assays, however, is that the redox reaction can only be followed in the UV range, which makes the use of special and rather expensive MTP necessary. Furthermore, quinones can give confounded results due to their spontaneous oxidative side reactions in the alkaline pH range [18]. Recently, ferricyanide was used in a high-throughput screening assay that is based on the formation of Prussian Blue, but it was shown that this assay is highly specific for CDH while other flavin-dependent carbohydrate oxidoreductases (glucose oxidase, PDH) do not show similar reactions [25].

It was the aim of our work to test whether mediators that are used in enzyme-based biosensors [26] can also be used as convenient colorimetric substrates in MTP-based activity assays used for high-throughput screening of flavin-dependent oxidoreductases. To this end, we initially tested 14 different compounds that are often employed as redox mediators in biosensors, mainly various phenothiazine derivatives, for their ability to directly react with the flavin adenine dinucleotide (FAD)-dependent enzyme POx. Based on rapid direct enzyme-catalyzed reduction of the mediators and clear color changes we selected DCPIP, MG, and Thi, which show distinct absorption changes between their oxidized and reduced forms in the visible range, as the most promising substrates in these assays for further characterization. These three redox dyes are direct substrates (electron acceptors) for various flavin-dependent oxidoreductases, both oxidases and true dehydrogenases. These studied flavin-dependent oxidoreductases belong to three different enzyme superfamily of flavoproteins (POx, PDH, and CDH are members of the glucose-methanol-choline (GMC) oxidoreductase family; DAAO belongs to the glutathione reductase family [27] and L-LOx to the L-α-hydroxy acid oxidase family [28]). They all contain covalently or non-covalently bound FAD or flavin mononucleotide (FMN): monomeric PDH and each subunit of the homotetramer POx bind one FAD covalently [29, 30], homodimeric DAAO [31], and the flavin domain of the monomeric flavocytochrome CDH [32] contain one non-covalently bound FAD, whereas each subunit of the homotetramer LOx binds one FMN non-covalently [33].

All five tested enzymes (POx from *T. multicolor*, PDH from *A. meleagris*, CDH from *N. crassa*, DAAO from *T. variabilis*, LOx from *A. viridans*) reacted rapidly and efficiently with these electron acceptors so that decolorization of the dye in the MTP was visible within few minutes. This is also expressed by the high apparent catalytic con-

© 2014 The Authors. Biotechnology Journal published by Wiley-VCH Verlag GmbH & Co. KGaA, Weinheim

stants k_{cat} determined for these electron acceptors in presence of an excess of the respective electron donor substrates, which were found to range from 0.033 to 189 s^{-1}. This indicates that the selected redox dyes might be useful for activity assays of a wide range of different flavin-dependent oxidoreductases. Furthermore, the apparent Michaelis constants of all tested enzymes were typically found to be in the micromolar range for these three electron acceptors, indicating that only low concentrations have to be used to the assays to assure substrate saturation and hence maximum reaction velocities. Another clear advantage of these dyes for activity assays is that they react directly with the enzymes to be tested in contrast to frequently used assays that are based on a second, enzyme-coupled assay such as the ones that are frequently used for the detection of the reaction product hydrogen peroxide as this will also reduced costs for these assays; these dyes are cheap and there are no extra costs for additional reagents and enzymes. The reduced forms of the redox dyes were stable in the presence of oxygen in these assays, and only MG showed some slight re-oxidation by oxygen after a prolonged incubation period and once the electron donor substrate was exhausted from the reaction mixture. This should however not interfere with MTP-based screening. Furthermore, MG and Thi did not show a pH dependence of their absorption properties, and this will make their application in enzyme activity assays possible even over a wide pH range. The proposed method might be useful in the primary screening for desired enzyme activities of libraries. To avoid a potential bias in the screening, i.e. identification of variants showing improved activities only with these specific electron acceptors and not with the specific electron donor substrates that often are of interest in an enzyme improvement program ("you get what you screen for" [34]), two or more electron acceptors can be used in the library screening for specific activities, which will be possible because of the ease of application. In conclusion, the activity assays based on the electron acceptors DCPIP, MG, and Thi offer a rapid, robust and cheap method for screening of a large number of samples, which could find applications in enzyme engineering programs of flavin-dependent oxidoreductases or identification of novel enzyme activities from metagenomic libraries, to name a few examples.

This work was supported by BOKU University of Natural Resources and Life Sciences (BOKU Doc Program) and by the Austrian Science Fund (FWF), Doctoral Programme BioToP–Biomolecular Technology of Proteins (FWF W1224) and individual project P22094 (to CKP), which is gratefully acknowledged. We thank Wolfgang Graschopf for his help and support.

The authors declare no financial or commercial conflict of interest.

5 References

[1] Hollmann, F., Arends, I. W. C. E., Bühler, K., Schallmey, A., Bühler, B., Enzyme-mediated oxidations for the chemist. *Green Chem.* 2011, *13*, 226–265.

[2] Monti, D., Ottolina, G., Carrea, G., Riva, S., Redox reactions catalyzed by isolated enzymes. *Chem. Rev.* 2011, *111*, 4111–4140.

[3] Winter, R. T., Fraaije, M. W., Applications of flavoprotein oxidases in organic synthesis: Novel reactivities that go beyond amine and alcohol oxidations. *Curr. Org. Chem.* 2012, *16*, 2542–2550.

[4] Shao, M., Zafar, M. N., Falk, M., Ludwig, R. et al., Optimization of a membraneless glucose/oxygen enzymatic fuel cell based on a bioanode with high coulombic efficiency and current density. *ChemPhysChem* 2013, *14*, 2260–2269.

[5] Ludwig, R., Ortiz, R., Schulz, C., Harreither, W. et al., Cellobiose dehydrogenase modified electrodes: Advances by materials science and biochemical engineering. *Anal. Bioanal. Chem.* 2013, *405*, 3637–3658.

[6] Dijkman, W. P., de Gonzalo, G., Mattevi, A., Fraaije, M. W., Flavoprotein oxidases: Classification and applications. *Appl. Microbiol. Biotechnol.* 2013, *97*, 5177–5188.

[7] Leitner, C., Volc, J., Haltrich, D., Purification and characterization of pyranose oxidase from the white rot fungus *Trametes multicolor*. *Appl. Environ. Microbiol.* 2001, *67*, 3636–3644.

[8] Akkermans, R. P., Roberts, S. L., Marken, F., Coles, B. A. et al., Methylene green voltammetry in aqueous solution: Studies using thermal, microwave, laser, or ultrasonic activation at platinum electrodes. *J. Phys. Chem. B* 1999, *103*, 9987–9995.

[9] Wondrak, G. T., NQO1-activated phenothiazinium redox cyclers for the targeted bioreductive induction of cancer cell apoptosis. *Free Rad. Biol. Med.* 2007, *43*, 178–190.

[10] Sygmund, C., Kittl, R., Volc, J., Halada, P. et al., Characterization of pyranose dehydrogenase from *Agaricus meleagris* and its application in the C-2 specific conversion of D-galactose. *J. Biotechnol.* 2008, *133*, 334–342.

[11] Nidetzky, B., Stability and stabilization of D-amino acid oxidase from the yeast *Trigonopsis variabilis*. *Biochem. Soc. Trans.* 2007, *35*, 1588–1592.

[12] Sygmund, C., Kracher, D., Scheiblbrandner, S., Zahma, K. et al., Characterization of the two *Neurospora crassa* cellobiose dehydrogenases and their connection to oxidative cellulose degradation. *Appl. Environ. Microbiol.* 2012, *78*, 6161–6171.

[13] Unterweger, B., Stoisser, T., Leitgeb, S., Birner-Grünberger, R., Nidetzky, B., Engineering of *Aerococcus viridans* L-lactate oxidase for site-specific PEGylation: Characterization and selective bioorthogonal modification of a S218C mutant. *Bioconj. Chem.* 2012, *23*, 1406–1414.

[14] Spadiut, O., Radakovits, K., Pisanelli, I., Salaheddin, C. et al., A thermostable triple mutant of pyranose 2-oxidase from *Trametes multicolor* with improved properties for biotechnological applications. *Biotechnol. J.* 2009, *4*, 525–534.

[15] Sygmund, C., Santner, P., Krondorfer, I., Peterbauer, C. K. et al., Semi-rational engineering of cellobiose dehydrogenase for improved hydrogen peroxide production. *Microb. Cell Fact.* 2013, *12*, 38.

[16] Baminger, U., Subramaniam, S. S., Renganathan, V., Haltrich, D., Purification and characterization of cellobiose dehydrogenase from the plant pathogen *Sclerotium* (*Athelia*) *rolfsii*. *Appl. Environ. Microbiol.* 2001, *67*, 1766–1774.

[17] Rabinowitch, E., Epstein, L. F., Polymerization of dyestuffs in solution: Thionine and methylene blue. *J. Am. Chem. Soc.* 1941, *63*, 69–78.

[18] Frébortová, J., Fraaije, M. W., Galuszka, P., Sebela, M. et al., Catalytic reaction of cytokinin dehydrogenase: Preference for quinones as electron acceptors. *Biochem. J.* 2004, *380*, 121–130.

© 2014 The Authors. Biotechnology Journal published by Wiley-VCH Verlag GmbH & Co. KGaA, Weinheim

[19] Cook, A. G., Toliver, R. M., Willams, J. E., The blue bottle experiment revisited: How blue? How sweet? *J. Chem. Educ*. 1994, *71*, 160–161.

[20] Azmat, R., Ahmed, S., Qureshi, S., Vali Mohammed, F., Uddin, F., Aerobic oxidation of D-glucose by methylene green in alkaline aqueous solution by visible spectrophotometry. *J. Appl. Sci*. 2006, *6*, 2784–2788.

[21] Ribitsch, D., Winkler, S., Gruber, K., Karl, W. et al., Engineering of choline oxidase from *Arthrobacter nicotianae* for potential use as biological bleach in detergents. *Appl. Microbiol. Biotechnol*. 2010, *87*, 1743–1752.

[22] Gabler, M., Hensel, M., Fischer, L., Detection and substrate selectivity of new microbial D-amino acid oxidases. *Enzyme Microb. Technol*. 2000, *27*, 605–611.

[23] Spadiut, O., Brugger, D., Coman, V., Haltrich, D. et al., Engineered pyranose 2-oxidase: Efficiently turning sugars into electrical energy. *Electroanalysis* 2010, *22*, 813–820.

[24] Salaheddin, C., Spadiut, O., Ludwig, R., Tan, T. C. et al., Probing active-site residues of pyranose 2-oxidase from *Trametes multicolor* by semi-rational protein design. *Biotechnol. J*. 2009, *4*, 535–543.

[25] Vasilchenko, L. G., Ludwig, R., Yershevich, O. P., Haltrich, D. et al., High-throughput screening for cellobiose dehydrogenases by Prussian Blue in situ formation. *Biotechnol. J.* 2012, *7*, 919–930.

[26] Privett, B. J., Shim, J. H., Schoenfisch, M. H., Electrochemical sensors. *Anal. Chem.* 2008, *80*, 4499–4571.

[27] Caldinelli, L., Iametti, S., Barbiroli, A., Bonomi, F. et al., Unfolding intermediate in the peroxisomal flavoprotein D-amino acid oxidase. *J. Biol. Chem.* 2004, *279*, 28426–28434.

[28] Maeda-Yorita, K., Aki, K., Sagai, H., Misaki, H. et al., L-Lactate oxidase and L-lactate monooxygenase: Mechanistic variations on a common structural theme. *Biochimie* 1995, *77*, 631–642.

[29] Tan, T. C., Spadiut, O., Wongnate, T., Sucharitakul, J. et al., The 1.6-Å crystal structure of pyranose dehydrogenase from *Agaricus meleagris* rationalizes substrate specificity and reveals a flavin intermediate. *PLoS ONE* 2013, *8*, e53567.

[30] Hallberg, M. B., Leitner, C., Haltrich, D., Divne, C., Crystal structure of the 270 kDa homotetrameric lignin-degrading enzyme pyranose 2-oxidase. *J. Mol. Biol*. 2004, *341*, 781–796.

[31] Pilone, M. S., D-Amino acid oxidase: New findings. *Cell. Mol. Life Sci*. 2000, *57*, 1732–1747.

[32] Zamocky, M., Ludwig, R., Peterbauer, C., Hallberg, B. M. et al., Cellobiose dehydrogenase – a flavocytochrome from wood-degrading, phytopathogenic and saprotropic fungi. *Curr. Protein Pept. Sci.* 2006, *7*, 255–280.

[33] Li, S. J., Umena, Y., Yorita, K., Matsuoka, T. et al., Crystallographic study on the interaction of L-lactate oxidase with pyruvate at 1.9 Å resolution. *Biochem. Biophys. Res. Comm*. 2007, *358*, 1002–1007.

[34] Schmidt-Dannert, C., Arnold, F. H., Directed evolution of industrial enzymes. *Trends Biotechnol*. 1999, *17*, 135–136.

[35] Trampitsch, C., Slavica, A., Riethorst, W., Nidetzky, B., Reaction of *Trigonopsis variabilis* D-amino acid oxidase with 2,6-dichloroindophenol: Kinetic characterisation and development of an oxygen-independent assay of the enzyme activity. *J. Mol. Cat. B: Enzymatic* 2005, *32*, 271–278.

© 2014 The Authors. Biotechnology Journal published by Wiley-VCH Verlag GmbH & Co. KGaA, Weinheim

Acknowledgements

Zuerst möchte mich bei Priv.-Doz. Dr. Clemens K. Peterbauer für seine unkomplizierte, humorvolle und kollegiale Betreuung bedanken, besonders für die stets rasche Korrektur diverser Arbeiten und Publikationen. Weiters bedanke ich mich bei Univ.-Prof. Dr. Dietmar Haltrich und Dr. Roland Ludwig für zahlreiche Ratschläge und tatkräftige Unterstützung bei kniffligen Aufgabenstellungen. Auch Dr. Roman Kittl und Dr. Christoph Sygmund möchte ich danken dass sie immer ein offenes Ohr für die Herausforderungen des Laboralltags hatten und wesentlich zu deren Bewältigung beigetragen haben.

Ich bedanke mich bei Univ.-Prof. Dr. Christian Obinger, Univ.-Prof. Dr. Paul G. Furtmüller, DI Stefan Hofbauer, Dr. Katharina Pirker und DI Monika Soudi für die Hilfe und gute Zusammenarbeit bei tiefergehenden biochemischen Fragestellungen. Besonders bedanken möchte ich mich bei Dr. Christa Jakopitsch aber auch bei allen PIs und Kollegen des Doktorandenkollegs „BioToP“ für die anspruchsvolle und interessante Ausbildung und den wissenschaftlichen Input. Dem Wissenschaftsfonds Österreich (FWF) danke ich für die Finanzierung dieser Arbeit.

Meinen Freunden und Kollegen danke ich herzlich für ihre tatkräftige Hilfe in diversen Belangen, besonders meinen „Nachbarn“ im Büro die schon für viele heitere Momente gesorgt haben. Dr. Petra Staudigl, DI Regina Paukner, Cindy Lorenz und DI Dagmar Brugger danke ich im Besonderen, ihr wart für mich Freundin, Lehrerin, Erfolgscoach und Psychologin in einer Person. Danke auch an Mag. Katharina Lipp, die im Zuge ihrer Masterarbeit einen wesentlichen Anteil am Gelingen vieler Experimente hat.

Mein besonderer Dank gilt meinen Eltern für ihre uneingeschränkte Unterstützung und Fürsorge. Zuletzt möchte ich dem wichtigsten Menschen danken, Peter du hast immer an mich geglaubt und mich ermutigt. Du bist meine starke Schulter zum Anlehnen und mein Rückhalt, dafür danke ich dir von Herzen.